



HAL
open science

Understanding regional climate variability for solar energy development in West Africa.

Derrick Kwadwo Danso

► **To cite this version:**

Derrick Kwadwo Danso. Understanding regional climate variability for solar energy development in West Africa.. Climatology. Université Grenoble Alpes [2020-..]; Université Félix Houphouët-Boigny (Abidjan, Côte d'Ivoire), 2021. English. NNT : 2021GRALU015 . tel-03293671

HAL Id: tel-03293671

<https://theses.hal.science/tel-03293671>

Submitted on 21 Jul 2021

HAL is a multi-disciplinary open access archive for the deposit and dissemination of scientific research documents, whether they are published or not. The documents may come from teaching and research institutions in France or abroad, or from public or private research centers.

L'archive ouverte pluridisciplinaire **HAL**, est destinée au dépôt et à la diffusion de documents scientifiques de niveau recherche, publiés ou non, émanant des établissements d'enseignement et de recherche français ou étrangers, des laboratoires publics ou privés.

THÈSE

Pour obtenir le grade de

DOCTEUR DE L'UNIVERSITE GRENOBLE ALPES

**préparée dans le cadre d'une cotutelle entre
l'Université Grenoble Alpes et l'Université Félix
Houphouët Boigny**

Spécialité : **Océan, Atmosphère, Hydrologie**

Arrêté ministériel : le 6 janvier 2005 – 25 mai 2016

Présentée par

Derrick Kwadwo DANSO

Thèse dirigée par **Sandrine ANQUETIN**

codirigée par **Arona DIEDHIOU** et **Arsène Toka KOBEA**

préparée au sein des laboratoires **Institut des Géosciences de
l'Environnement (IGE)** et **Laboratoire des Sciences de la Matière,
de l'Environnement et de l'Energie Solaire (LASMES)**

dans les Écoles Doctorales **Sciences de la Terre, de
l'Environnement et des Planètes (STEP)** et **Sciences de
Structures de la Matière et Technologie (SSMT)**

Understanding regional climate variability for solar energy development in West Africa

Thèse soutenue publiquement le **1 Juin 2021**,
devant le jury composé de :

Madame Gaëlle UZU

Directrice de Recherche, IRD, IGE, Présidente

Monsieur Peter KNIPPERTZ

Professeur, Karlsruhe Institute of Technology, Rapporteur

Monsieur Cyrille FLAMMANT

Directeur de Recherche, CNRS, LATMOS, Rapporteur

Monsieur Leonard Kofitse AMEKUDZI

Professeur, Physics Department, KNUST, Examineur

Monsieur Philippe BLANC

Professeur, Centre O.I.E., MINES ParisTech, Examineur

Madame Sandrine ANQUETIN

Directrice de Recherche, CNRS, IGE, Directrice de thèse

Monsieur Arona DIEDHIOU

Directeur de Recherche, IRD, IGE, Co-directeur de thèse

Monsieur Arsène Toka, KOBEA

Professeur, LASMES (UFHB), Co-directeur de thèse



"Prediction is very difficult, especially about the future."

Niels Bohr

Acknowledgements

Firstly, I wish to use this opportunity to thank all the reviewers and members of the jury for accepting to evaluate my thesis.

Throughout these three years of PhD, I have been assisted by many people and in so many ways. I would like to use this opportunity to recognize and thank all the people who supported and inspired me throughout this wonderful journey.

First of all, I thank God for making this journey possible and for the numerous blessings he has showered on my life.

This PhD would not have been possible without my amazing advisors: Sandrine, Arona, and Arsène. It has been a real pleasure working with you guys, and I will like to say a few words of appreciation to you.

To Sandrine, I want to say thank you for your supervision and support throughout this work. Throughout the thesis, you have always been available to discuss my work and kind to advise me on various things. Our weekly meetings (which was your initiative) enabled me to carry out this research in the best possible way. I have been very lucky to work with you as my PhD supervisor, and I hope to continue working with you in the future. A special thank you again, for helping me with my abstract and extended summary in French (unfortunately, my French is still not good enough).

To Arona, as I said three years ago during my Master's thesis, you are the best. You have been supportive in many ways since I first met you in 2017. Your expert ideas and experience have been essential to this work. You continue to inspire me every day, and I am thankful to you for believing in me.

To Arsène, I am very grateful for your kindness and readiness to assist me during my stays in Abidjan. Despite your busy schedule, you still found enough time to discuss my work and help me with all administrative procedures.

I wish to express my gratitude to the members of my thesis follow-up committee: Hubert, Nathalie, and Damien. It was a real pleasure interacting with you during the

annual CT meetings. Your advice and contributions were essential for the success of this thesis.

A big thank you to Christophe, who also advised me on my work many times during this thesis. Your constructive comments and critique of my work pushed me to even improve. Not forgetting Benoit and Baptiste, my MSc supervisors, who I continued to work with during the last three years. You guys have influenced me positively in my ability to work on complex research problems. I appreciate the numerous and insightful discussions we have had and your continued support since 2017.

Because of the nature of the thesis, I frequently moved between Abidjan and Grenoble. During these travels, I met some incredible people that I would like to thank. Firstly, I wish to thank Bamba and Stella for kindly receiving me when I first arrived in Abidjan. I say thank you to Francis for receiving me upon my arrival in Grenoble, and to Adeline and Sandrine for showing me around the lab. I also say thanks to the administrative and information service staff at IGE for facilitating my first and subsequent arrivals, as well as my other trips for missions abroad. I also want to say thanks to the ED STEP for facilitating my joint-supervision and registration at UGA. I also want to express my appreciation to everyone at IGE. I especially thank all members of the HMCIS team at IGE. A special mention to team leader Brice for his kindness and support on countless occasions. I thank Gilles, who I shared an office with for most of this thesis, for being helpful to me at many different times.

I want to thank everyone at LASMES for their kind reception during all my stays in Abidjan. To Evelyne and Kouakou, with who I worked a lot and collaborated on some articles, I say thank you so much for your incredible contributions to my thesis. I am grateful to Bamba for his encouragement and positivity at all times. To Stella, Madina, Salomon (Oga), Regis, Vicky, Zouzoua, and all my colleagues at LASMES, I say a very big thank you for all the times we spent together. I will forever cherish those moments.

To my former WASCAL colleagues and friends especially Thierry, Shari, and Peter, thank you for following my PhD and providing me feedback at various points throughout this journey. Also, to Larbi, Charles, and Pato, thank you for your wonderful friendship. I cannot forget Yves and Junior for all the football matches we played together.

Finally, to a very special person in my life, my mom, thank you for your encouragement and prayers that have kept me going throughout all these years.

Abstract

Since Paris Agreement in 2015, interest in projects dealing with solar photovoltaic energy development and its implementation in West Africa has risen tremendously. Nevertheless, a notable drawback to this development in the region is the intense cloud cover which reduces incoming solar radiation when present and causes fluctuations in solar power production. Understanding the occurrence of clouds and their impacts on the incoming solar radiation is important for developing strategies to manage solar power generation. However, our understanding of clouds in West Africa is still relatively low. This is further complicated by the possible future impacts of climate change on the physical factors that control solar power generation in the region. Thus, this thesis seeks to address the following questions:

1. How frequently and in what synoptic conditions do clouds occur and evolve in West Africa?
2. What are the effects of the occurrence and evolution of clouds on the incoming solar radiation?
3. How will climate change affect solar power generation and its atmospheric drivers?

A climatology of various cloud types over West Africa is first created using reanalysis data and satellite-based observations. In general, cloud cover in West Africa is characterized by a south-north gradient, with the southern areas cloudiest at all times. During the rainy season, the cloud coverage is between 70% and 80% over southern West Africa. High- and mid-level clouds occur throughout the year over the entire region. However, low clouds, with distinct seasonal and spatial variations, are primarily confined to the south in the dry season but intensify and extend northward in the rainy season. South of 15° N, at least one cloud type is present at all times, and the simultaneous occurrence of all cloud types is frequent. In contrast, the areas north of 15° N are characterized by the frequent occurrence of cloudless sky conditions.

Afterward, the synoptic conditions in which low clouds occur are investigated. The results showed that during the rainy season, low cloud occurrences are characterized by a strong moisture flux dominated by a significant amount of background moisture and strong southwesterly winds blowing from the Gulf of Guinea. Furthermore, low cloud occurrence is preceded by a significant reduction of the air temperature in the lower atmosphere. Moisture flux is weaker in the dry season; however, the background moisture level plays an important role in the occurrence of low clouds in the region.

Next, the direct impacts of cloud occurrence on the quantity and variability of incoming solar radiation are quantified. The results showed that attenuation of solar radiation is greatest during the summer months over the whole region. In August, about 55% of solar radiation is lost on average over southern West Africa, while between 20% and 35% is lost over the Sahel area and northern parts of the region. In terms of the variability, the study revealed that in the dry season, the sub-daily evolution of the incoming solar radiation does not change much from one year to the other. On the other hand, the radiation received during the rainy season is associated with higher uncertainty.

Finally, the impacts of climate change on future solar power potential and its drivers are investigated with a suite of CMIP6 climate models. The results showed a decrease in the solar power generation over the entire West Africa region, with most of the models projecting about a 20% reduction over southern West Africa in the second part of the 21st century. All models project a decrease in surface solar radiation and an increase in the near-surface air temperature. However, the projected reduction of the future solar power potential is predominantly due to the decrease of the surface solar radiation rather than the temperature increase. These results contribute directly to the ongoing feasibility assessments of long-term solar energy projects and have direct implications for the siting of solar farms in the region.

Résumé

Après la COP21 en 2015, les projets de déploiement d'infrastructures photovoltaïques pour l'électrification de l'Afrique de l'Ouest (AO) augmentent significativement. Néanmoins, la couverture nuageuse demeure une limite dans ce déploiement massif. Ainsi, il est important de mieux comprendre pour mieux anticiper la présence des nuages et leurs impacts sur le rayonnement solaire pour mettre en œuvre des stratégies de gestion de production d'énergie solaire adaptées et durables. Notre compréhension sur la variabilité spatio-temporelle des nuages en AO reste encore limitée. Ces enjeux sont exacerbés dans un contexte d'évolution climatique dans la mesure où il est nécessaire de bien anticiper les impacts futurs possibles sur les facteurs physiques qui contrôlent la production d'énergie solaire dans la région. Ainsi, cette thèse s'est attachée à répondre aux questions suivantes:

1. Quelles sont les échelles de variabilité spatio-temporelle des nuages en AO et quelles sont les conditions synoptiques associées?
2. Quelles sont les signatures des nuages sur le rayonnement solaire net au sol?
3. Comment le changement climatique affectera-t-il la production d'énergie solaire et pourquoi?

Une climatologie des différents types de nuages au-dessus de l'AO a d'abord été créée en utilisant les réanalyses ERA5 et des observations par satellite. Les résultats montrent que la couverture nuageuse est caractérisée par un gradient sud-nord, les zones méridionales étant les plus nuageuses. Pendant la saison des pluies, les nuages couvrent 70 à 80% de la région sud de l'AO. Les nuages bas sont principalement localisés au sud pendant la saison sèche, mais s'intensifient et s'étendent vers le nord pendant la saison des pluies. Au sud de 15° N, au moins un type de nuage est présent à tout moment, et la présence simultanée de tous les types de nuages est fréquente.

Puis, les conditions synoptiques dans lesquelles se produisent les nuages bas ont été étudiées. Les résultats montrent que pendant la saison des pluies, les occurrences de ces nuages sont caractérisées par un flux de sud-ouest dominé par une quantité

importante d'humidité venant du Golfe de Guinée. La formation des nuages bas est précédée d'une réduction significative de la température de l'air dans la basse atmosphère. Le flux d'humidité est plus faible pendant la saison sèche; cependant, le niveau d'humidité de fond joue un rôle important dans l'apparition de ces nuages dans la région.

Les impacts directs de l'apparition des nuages sur la quantité et la variabilité du rayonnement solaire entrant sont quantifiés. L'atténuation du rayonnement solaire est la plus importante pendant les mois d'été dans toute la région. En août, environ 55% du rayonnement solaire est absorbé par la couverture nuageuse en moyenne sur le sud de l'AO, tandis qu'entre 20 et 35% est perdu sur la zone du Sahel et les parties nord de la région. L'étude a révélé également qu'en saison sèche, l'évolution infra-journalière du rayonnement solaire entrant ne change pas beaucoup d'une année à l'autre. En revanche, le rayonnement reçu pendant la saison des pluies est associé à une plus grande incertitude.

Enfin, les impacts du changement climatique sur la production future d'énergie solaire sont étudiés à l'aide de quatre modèles climatiques CMIP6. Les résultats montrent une diminution de la production d'énergie solaire en AO, la plupart des modèles prévoyant une réduction d'environ 20% dans le sud de l'AO au cours de la deuxième partie du 21^e siècle. Tous les modèles projettent une diminution du rayonnement solaire de surface et une augmentation de la température de l'air à la surface. Cependant, la réduction prévue de la production future d'énergie solaire est principalement liée à la diminution du rayonnement solaire de surface plutôt qu'à l'augmentation de la température. Ces résultats contribuent directement aux études de faisabilité d'implantation des fermes solaires dans la région.

Contents

Acknowledgements	ii
Abstract	iv
Résumé	vi
Résumé étendu	xii
1 Introduction	1
1.1 In the race toward a sustainable world: The role of the energy sector	1
1.1.1 Global climate change and energy	1
1.1.2 Responses to the warming climate	3
1.1.3 Reducing emissions in the energy sector: The Paris Agreement	3
1.1.4 West Africa’s commitments: Aftermath of the Paris Agreement	4
1.2 Solar energy in West Africa	4
1.3 Meteorological factors for planning and developing solar energy	7
1.3.1 Uncertainties related to cloud cover	7
1.3.2 Other factors	9
1.3.3 Key open questions	9
1.4 Summary of research goals	10
1.5 Thesis outline	11
2 Research framework	13
2.1 Region of interest	14
2.2 Data sources	17
2.2.1 Surface-based observations	18
2.2.2 Model reanalyses data	19
2.2.3 Satellite-based observations	21
2.2.4 Global Climate Models (GCMs)	23
2.3 Data evaluation	24

2.3.1	Evaluation of ERA5 and CERES cloud fractions and occurrence frequencies	24
2.3.2	Evaluation of ERA5 surface incoming radiation	29
2.3.3	Evaluation of CMIP6 historical simulations	30
3	Occurrence and spatiotemporal variability of clouds in West Africa	36
3.1	Chapter overview	36
3.1.1	Contributions	37
3.2	Article: Spatio-temporal variability of cloud cover types in West Africa with a satellite-based and reanalysis data	39
3.3	Introduction	40
3.4	Datasets and methods	42
3.4.1	Datasets	42
3.4.2	Methods	44
3.5	Cloud cover variability	46
3.5.1	Seasonal evolution of cloud cover	46
3.5.2	Diurnal evolution of the cloud cover types	49
3.6	Cloud occurrence frequency in West Africa	52
3.6.1	General occurrence frequency	52
3.6.2	Low-level cloud cover occurrence as a function of fractional coverage	56
3.6.3	Solitary occurrence of cloud types	58
3.7	Summary and conclusions	60
4	Synoptic conditions related to clouds occurrence in West Africa	63
4.1	Chapter overview	63
4.1.1	Contributions	64
4.2	Article: Daytime low-level clouds in West Africa – occurrence, associated drivers and shortwave radiation attenuation	66
4.3	Introduction	67
4.4	Data	69
4.5	Methods	70
4.5.1	Identification of low-level clouds occurrence	70
4.5.2	Identification of synoptic conditions during LLC occurrence	72
4.5.3	Determination of cloud shortwave attenuation effects	74
4.6	Temporal distribution of occurrence of daytime low-level clouds	74
4.7	Synoptic conditions related to the occurrence of daytime low-level clouds	78
4.7.1	Atmospheric circulation and moisture flux	79

4.7.2	Surface heat fluxes	82
4.8	Attenuation of incoming shortwave radiation during LLC occurrence	85
4.9	Conclusions	88
5	Impacts of clouds on the availability and variability of the solar resource in West Africa	90
5.1	Chapter overview	90
5.1.1	Contributions	91
5.2	Article: Cloudiness information services for solar energy management in West Africa	92
5.3	Introduction	93
5.4	Materials and methods	95
5.4.1	Data	95
5.4.2	Methodology	97
5.5	Results and discussion	100
5.5.1	Variability of received surface solar radiation	100
5.5.2	Attenuation of incoming solar radiation by clouds	101
5.5.3	Dependence of cloud radiation attenuation of cloud fraction	105
5.5.4	Multi-timescale persistence of sky conditions	106
5.6	Summary and Conclusions	111
6	The future of solar energy in West Africa: Impacts of climate change	113
6.1	Chapter overview	113
6.1.1	Contributions	114
6.2	Article: Potential climate change impacts on solar photovoltaic energy and its atmospheric drivers in West Africa	115
6.3	Introduction	116
6.4	Data and methodology	117
6.4.1	Study area	117
6.4.2	Data	118
6.4.3	Estimation of changes in potential solar PVP generation	119
6.5	Changes in future solar PVP generation	120
6.6	Drivers of projected changes in solar PVP	124
6.6.1	Surface irradiance and near-surface air temperature	124
6.6.2	Cloudiness and aerosols	125
6.7	Discussion and conclusion	131
7	Conclusion	134

7.1	Summary and implications of main outcomes of thesis	134
7.1.1	The frequency and evolution of clouds in West Africa	135
7.1.2	Synoptic drivers of cloud occurrence in West Africa	136
7.1.3	Effects of clouds on the incoming shortwave radiation	138
7.1.4	Impacts of climate change on solar energy and its drivers	139
7.2	Future research directions	140
7.2.1	Improving cloud climatology	140
7.2.2	Extension to aerosols	141
7.2.3	CMIP6 models' uncertainties	142
7.2.4	Developing and managing solar energy	143
Appendices		145
A Additional information on CMIP6 models		145
A.1	Model configurations	145
A.2	Seasonal evaluation of models	147
B Supplementary information for article 2		152
B.1	Vertical profiles of cloud hydrometeor content during LLC occurrence	152
B.2	Specific humidity associated with LLC occurrence and potential tem- perature before and after low-level cloud formation	154
C Supplementary information for article 4		156
C.1	Projected changes in air temperature and surface solar irradiance in West Africa	156

Résumé étendu

Préambule

Ces recherches doctorales ont été menées en co-tutelle entre l'Université Houphouët Boigny à Abidjan (Côte d'Ivoire) et l'Université Grenoble Alpes (France). Dans ce cadre, le manuscrit de thèse, écrit en anglais, doit alors être précédé d'un résumé étendu en français.

Dans les pages qui suivent, je propose donc une synthèse des principaux résultats présentés plus en détail dans les chapitres 2 à 6 ; certaines des figures, présentées dans ces parties plus détaillées sont reprises ici pour faciliter la lecture.

Contexte

Depuis l'accord de Paris en 2015, l'intérêt pour les projets traitant du développement et de la mise en œuvre de centrales solaire en Afrique de l'Ouest (AO) s'est intensifié dans toute la région. Cet intérêt est non seulement dû à la nécessité de satisfaire la demande croissante d'électricité de manière durable, mais aussi dû à l'abondance de la ressource solaire dans cette région. Cependant, le développement et la mise en œuvre à grande échelle de l'énergie solaire en AO sont encore incertains, principalement en raison de certaines barrières climatiques. Le rayonnement solaire reçu à la surface de la terre est contrôlé par l'évolution de certaines variables liées au climat, telles que les nuages et la poussière. Ces deux paramètres sont abondamment présents dans la région. Les nuages, en particulier, peuvent fortement diminuer le rayonnement solaire incident et donc la production d'énergie solaire, lorsqu'ils sont présents (Bartlett et al., 1998; Hartmann, 1993). De plus, la variation sub-horaire de la nébulosité est partiellement gouvernée par l'irradiation solaire de surface (et l'énergie produite) (Engeland et al., 2017). Il est donc nécessaire de documenter leur occurrence et leur évolution dans la région ainsi que leurs impacts quantitatifs sur le rayonnement solaire incident.

En général, la météorologie de l'AO est assez complexe, avec des caractéristiques climatiques contrastées dans les différentes zones. Par exemple, plus de 80% des pluies de la saison humide dans la zone sahélienne (nord de l'AO) sont dues aux systèmes convectifs de mésoéchelles (MCS) se déplaçant d'est en ouest (Klein et al., 2020). Cependant, la zone guinéenne présente une situation différente i) une convection locale essentiellement gouvernée par l'état de la surface continentale, ii) des nuages de basse couche associés au flux d'humidité du Golfe de Guinée, et iii) des nuages convectifs profonds advectés d'est en ouest (Adler et al., 2011; Maranan et al., 2018; Sassen et al., 2009). Ces systèmes nuageux sont principalement à l'origine de la variabilité de la réflectivité atmosphérique qui contrôle la quantité d'irradiation de surface reçue dans la région. Ils ne sont cependant pas suffisamment bien compris, probablement lié au manque d'observations dans la région. De plus, les résultats des précédents modèles de circulation générale du climat (GCM) reproduisent mal les systèmes nuageux dans cette région, en particulier les nuages convectifs de basse altitude (Hannak et al., 2017). Cela s'explique généralement par le manque de représentation adéquate des processus dans la couche limite atmosphérique et des gradients terre-océan qui déterminent l'apparition et l'évolution des systèmes nuageux dans la région.

Par conséquent, il est nécessaire de mieux comprendre la variabilité spatio-temporelle de ces nuages en s'appuyant sur une base de données de long terme. Une climatologie de ces nuages aiderait à préciser leur occurrence et leur variabilité régionales. L'impact quantitatif des nuages sur le rayonnement solaire incident est inconnu dans la plupart des régions de l'Afrique de l'Ouest. Néanmoins, le changement climatique peut affecter leurs propriétés radiatives microphysiques (comme la teneur en eau des nuages) ou d'autres facteurs qui peuvent influencer la quantité de rayonnement solaire incident et la production d'énergie solaire. Cependant, très peu d'études (par exemple, Dajuma et al. (2016) and Sawadogo et al. (2020)) ont tenté de traiter ces questions importantes, essentielles pour toute étude de faisabilité d'un projet d'énergie solaire durable à long terme dans la région. Par conséquent, de nombreuses questions restent encore ouvertes et l'absence d'élément de réponse fragilise les projets d'implantation de système de production d'énergie solaire dans la région.

Les travaux menés dans ce travail de thèse contribue à apporter quelques éléments de réponses notamment en s'attachant à répondre aux questions suivantes :

1. Quelles sont les échelles de variabilité spatio-temporelle des nuages en Afrique de l'Ouest et quelles sont les conditions synoptiques associées ?

2. Quelles sont les signatures des nuages sur le rayonnement solaire net au sol ?
3. Comment le changement climatique affectera-t-il la production d'énergie solaire et pourquoi ?

Ensembles de données

Une synthèse du Chapitre 2 est proposée dans cette section.

Le principal ensemble de données utilisé dans cette étude est la cinquième génération de la réanalyse du climat mondial (ERA5) du Centre européen pour les prévisions météorologiques à moyen terme (CEPMMT) (Hersbach et al., 2020). Elle est produite sur une grille régulière de résolution spatiale relativement élevée d'environ 30 km à une résolution temporelle d'une heure. ERA5 fournit des distributions bidimensionnelles (2D) de la fraction des nuages sur des couches stratifiées simples dans l'atmosphère. Quatre types de couverture nuageuse sont proposés dans ERA5 sur la base d'une partition de l'atmosphère, à savoir la couverture nuageuse de basse altitude (LCC), la couverture nuageuse de moyenne altitude (MCC), la couverture nuageuse de haute altitude (HCC) et la couverture nuageuse totale (TCC). TCC intègre tous les nuages depuis la surface jusqu'au sommet de la troposphère. LCC fait référence à tous les nuages présents depuis le niveau de la surface jusqu'à environ 2 km d'altitude dans l'atmosphère (Forbes, 2017). MCC et HCC se réfèrent respectivement à tous les nuages présents de 2 km à environ 6,4 km et de 6,4 km au sommet de la troposphère. ERA5 fournit également le rayonnement de courte longueur d'onde descendant en surface (également connu sous le nom de rayonnement solaire global ou rayonnement à onde courte).

Les autres variables ERA5 utilisées comprennent l'humidité spécifique, les composantes zonales et méridiennes du vent, et les flux de chaleur sensible et latent en surface. Pour cette étude, 10 années (de 2006 à 2015) sont considérées ; seules les périodes diurnes sont prises en compte dans la mesure où l'objectif à terme concerne l'évaluation de la ressource climatique pour la production d'énergie solaire.

La fraction nuageuse fournie par ERA5 et le rayonnement solaire global ont d'abord été évalués en utilisant conjointement des observations de surface (Galle et al., 2018; Lott et al., 2001) et des observations satellitaires (Mace et al., 2006). L'évaluation a montré que ERA5 est capable de reproduire raisonnablement la nébulosité (Figure 1) et le rayonnement solaire incident (Figure 2) en AO. La ré-analyse ERA5 a également été comparée au produit synoptique des nuages et du système d'énergie radiatif de la Terre (CERES) (Rutan et al., 2015).

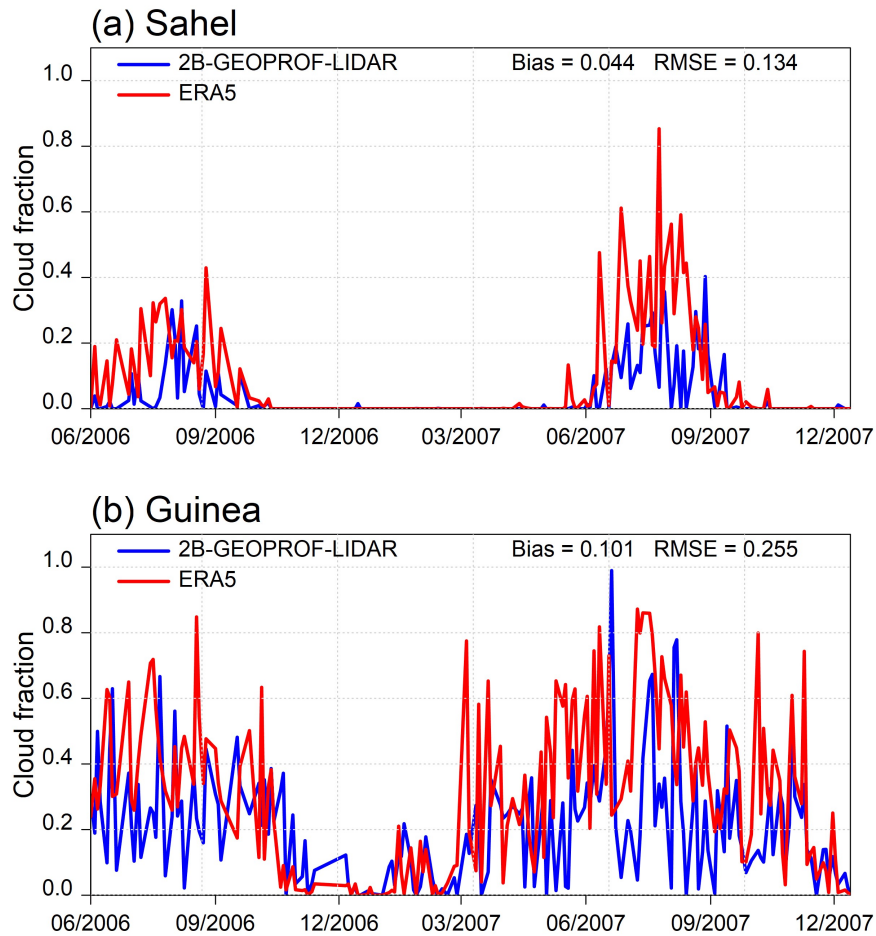


Figure 1: Fraction diurne de la couverture nuageuse de basse couche reproduite dans les réanalyses ERA5 et comparées avec l’observation 2B-GEOPROF-LIDAR pour les régions (a) du Sahel et (b) de la Guinée en Afrique de l’Ouest, et pour la période de juin 2006 à décembre 2007.

Dans le chapitre 6, quatre modèles de circulation générale (GCM) (Table 1) participant à la phase 6 du projet d’intercomparaison des modèles couplés (CMIP6) (Eyring et al., 2016) sont utilisés pour étudier les impacts du changement climatique sur la production d’énergie solaire en AO. Pour cela, les runs historiques et les projections futures (ScenarioMIP) (O’Neill et al., 2016) sont utilisés. Dans le ScenarioMIP, les projections sont basées sur un ensemble de scénarios d’émissions et d’utilisation des terres basés sur les trajectoires de développements socio-économiques (SSP) (O’Neill et al., 2014) et les trajectoires de concentration représentative (RCP). Ici, le scénario SSP5-8.5, un des plus pessimistes est utilisé comme le scénario futur présumé selon lequel les impacts du changement climatique sur la production potentielle d’énergie solaire seront évalués. Il scénarise des tendances de démographie croissante, dans une économie à forte intensité énergétique basée sur les combustibles

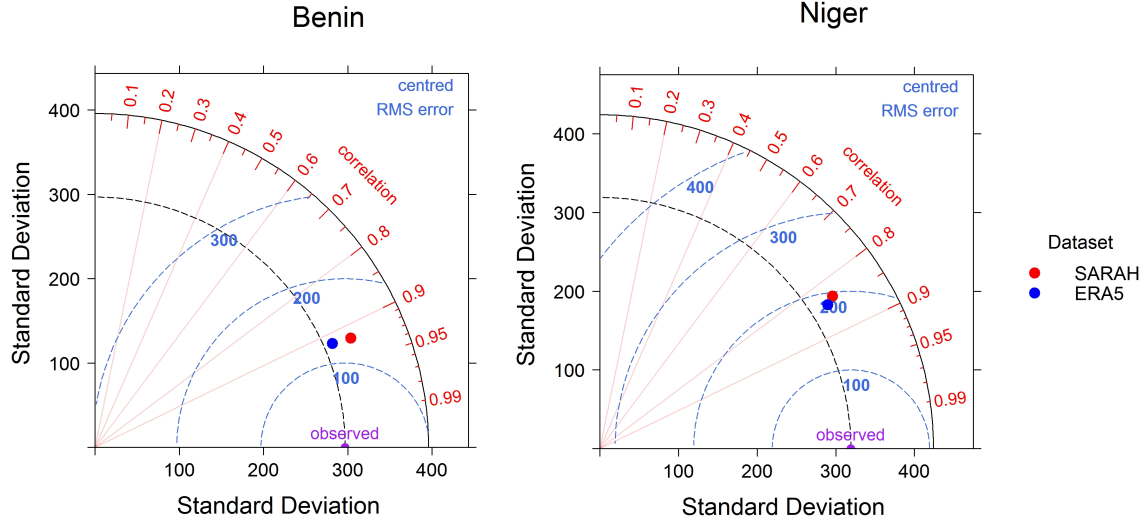


Figure 2: Les diagrammes de Taylor montrant l'évaluation de l'ERA5 (et du SARAH) avec les observations de surface des observatoires AMMA-CATCH.

fossiles (Meinshausen et al., 2020).

Table 1: Sélection de GCM pour étudier les impacts du changement climatique sur le potentiel d'énergie solaire en Afrique de l'Ouest.

Model	Institute	Country	Reference
AWI-CM-1-1-MR	Alfred Wegener Institute, Helmholtz Centre for Polar and Marine Research	Germany	Semmler et al. (2020)
EC-Earth3	EC-Earth	European Consortium	Wyser et al. (2020)
MPI-ESM1-2-HR	Max Planck Institute	Germany	Müller et al. (2018)
MRI-ESM2-0	Meteorological Research Institute	Japan	Yukimoto et al. (2019)

Les résultats historiques des GCM ont été évalués à l'aide du produit CERES. Les sorties des modèles GCM ont ensuite été corrigées afin de réduire leurs biais par rapport aux données observées (Figure 3).

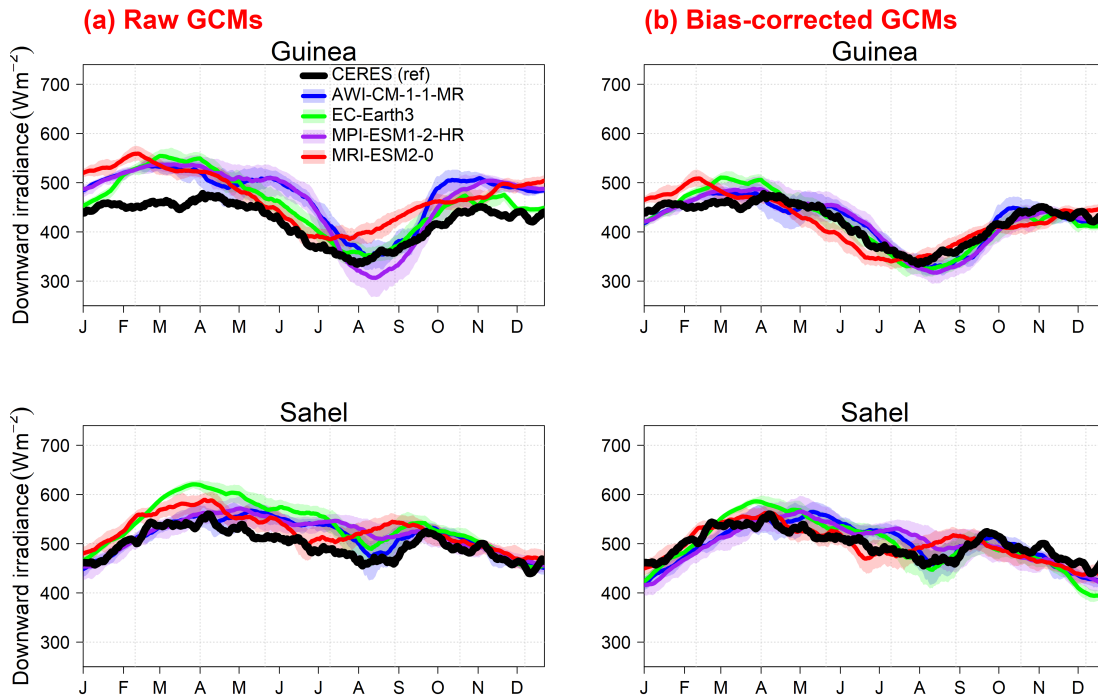


Figure 3: Cycle annuel moyen du rayonnement incident à la surface pour les régions de Guinée (haut) et du Sahel (bas). Comparaison entre les sorties des 4 GCM (AWI ; EC-Earth ; MPI et MRI) avec les observations CERES. (a) les moyennes d'ensemble brutes des GCM et (b) les moyennes d'ensemble des GCM corrigées. L'enveloppe pour chaque GCM représente la variabilité (fourchette maximale et minimale) entre les différents membres de l'ensemble.

La fréquence et l'évolution des nuages en Afrique de l'Ouest

Dans cette section, je résume succinctement le Chapitre 3, lui-même constitué de l'article publié dans le journal *Quarterly Journal of the Royal Meteorological Society* (Danso et al., 2019).

La variabilité et la fréquence d'occurrence de la couverture nuageuse ont été calculées pour l'ensemble de l'Afrique de l'Ouest pour chacune des quatre saisons de l'hémisphère nord, à savoir DJF (décembre, janvier, février), MAM (mars, avril, mai), JJA (juin, juillet, août) et SON (septembre, octobre, novembre). ERA5 et CERES ont été utilisés pour calculer ces variables et les comparer. Toutefois, seuls les résultats s'appuyant sur les réanalyses ERA5 sont présentés dans ce résumé étendu (les lecteurs sont invités à se reporter au Chapitre 3 pour plus de détails).

Les résultats de cette analyse montrent que la couverture nuageuse varie fortement dans le temps et sur l'ensemble de la région (Figure 4). Globalement,

la couverture nuageuse en AO est caractérisée par un gradient sud-nord, les zones méridionales proches de la côte guinéenne étant toujours les plus nuageuses. Les points d'altitude élevés comme les hautes terres de Guinée et du Nigeria sont également soumises à une nébulosité intense plus fréquente que dans les autres régions. Comme attendu, on observe également que la nébulosité totale est la plus intense au cœur de la saison de mousson (JJA). Pendant cette période, la nébulosité totale moyenne se situe entre 70 et 80 % autour de la côte guinéenne et moins de 50 % au Sahel et au nord de AO. Pendant les autres saisons, la nébulosité totale moyenne reste faible.

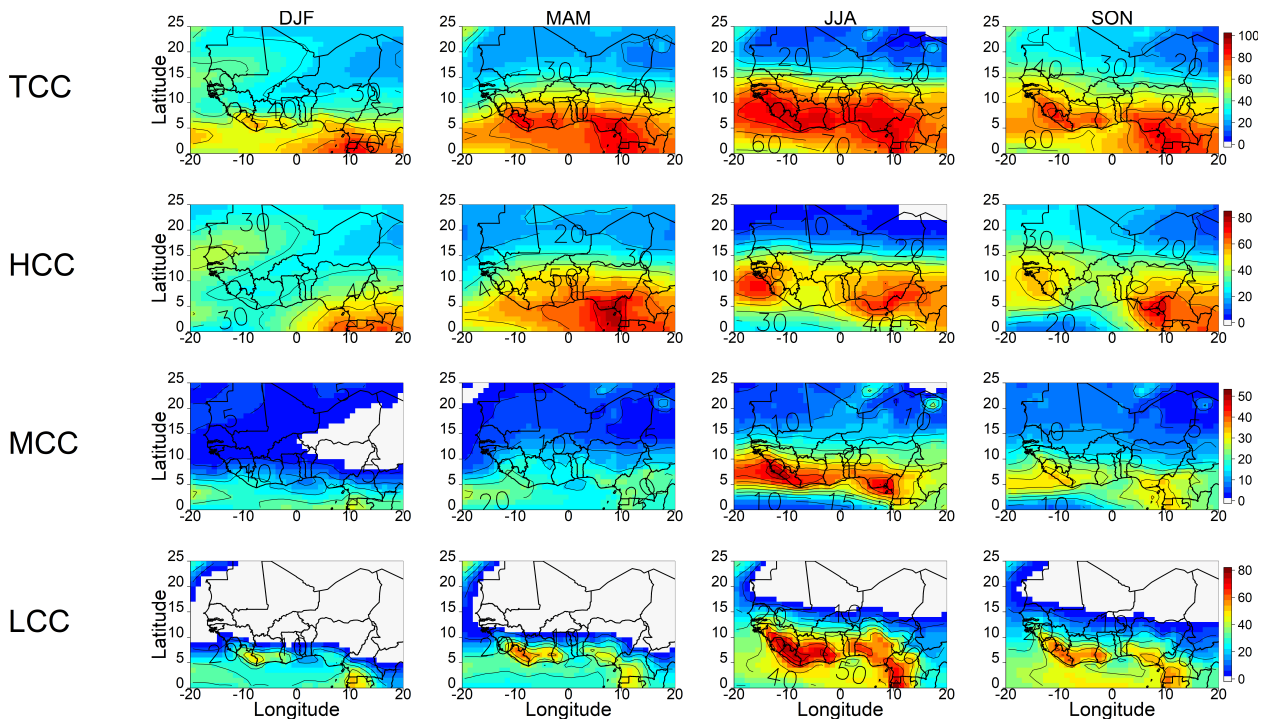


Figure 4: Évolutions saisonnières moyennes de la couverture nuageuse totale (TCC), des nuages de haute altitude (HLC), de moyenne altitude (MLC) et de basse couche (LLC) en pourcentage à partir des réanalyses ERA5. Les valeurs moyennes des fractions de nuages indiquées ici sont calculées à partir des valeurs horaires diurnes (0600 UTC à 1700 UTC) pour une période de 10 ans (2006-2015).

On s'est également intéressé à analyser l'occurrence des différents types de nuages, nuages de basse couche, de moyenne altitude et des nuages de haute altitude. Les principaux résultats sont repris ci-dessous :

- Les nuages bas présentent une variabilité saisonnière et spatiale particulière au regard des autres types de nuages. Pendant la saison sèche (DJF), ces nuages se trouvent principalement autour de la côte guinéenne mais s'intensifient et s'étendent vers le nord dans la région sahélienne pendant la saison des pluies.

Leur évolution saisonnière semble suivre les déplacements saisonniers de la ZCIT. Ces nuages ont également un cycle diurne distinct en toutes saisons dans la partie sud de la ZCIT. Dans la région du Sahel, ils se produisent généralement lors de la période de mousson (JJA) avec un cycle diurne marqué.

- Les nuages hauts et de moyenne altitude sont présents dans toute la région quelque soit la saison mais s'intensifient pendant la période de mousson (JJA), en particulier autour de la côte guinéenne. Les variations diurnes de ces deux types de nuages sont relativement plus faibles que celles observées pour les nuages bas.

Une climatologie similaire a été réalisée en utilisant les données du CERES (Figure 5) :

- L'évolution de la nébulosité totale est bien corrélée avec celle obtenue avec les données ERA5. Une couverture nuageuse plus importante (plus de 40 %) est observée sur les régions océaniques et côtières de l'AO pendant la saison sèche (DJF), tandis que les zones terrestres intérieures présentent des fractions de couverture nuageuse plus faibles. La couverture nuageuse s'intensifie et s'étend vers le nord pendant la saison humide (JJA).
- L'occurrence spatiale et temporelle des nuages haut (HLC) et de moyenne altitude (MLC) obtenue à partir des données CERES est similaire à celle obtenue avec les réanalyses ERA5 sur la région, ces deux types de nuages étant omniprésents sur la majorité de la région tout au long de l'année, cette présence se renforçant pendant la saison de mousson. Cependant, les capteurs passifs des satellites ne sont pas en mesure de détecter les nuages élevés optiquement fins, entraînant très probablement une sous-estimation de la fraction nuageuse de ce type de nuage.
- Pendant les saisons DJF et MAM, les données CERES ne présentent pas une variabilité spatiale bien marquée des nuages bas entre les régions guinéenne (sud) et sahélo-saharienne (nord). Néanmoins et de façon inattendue, les données CERES présentent une occurrence de ces nuages sur la région du Sahel/Sahara (jusqu'à environ 20 %) pendant toute l'année, laissant présager que les nuages bas (par exemple les systèmes convectifs peu profonds) se produisent rarement sur ces régions sauf au cœur de la saison de mousson (Bouniol et al., 2012). Les observations passives par satellite restituent parfois la présence de poussière du désert du Sahara comme des nuages bas (Loeb et al., 2018), et pourraient donc expliquer la présence de ces nuages sur le nord de l'Afrique de l'Ouest pendant la saison sèche. De plus, les capteurs des satellites pas-

sifs ne sont pas capables de détecter les nuages bas lorsqu'il y a des nuages superposés. Cela conduit à une sous-estimation de leur occurrence, comme le montrent les zones indiquées par des cases blanches.

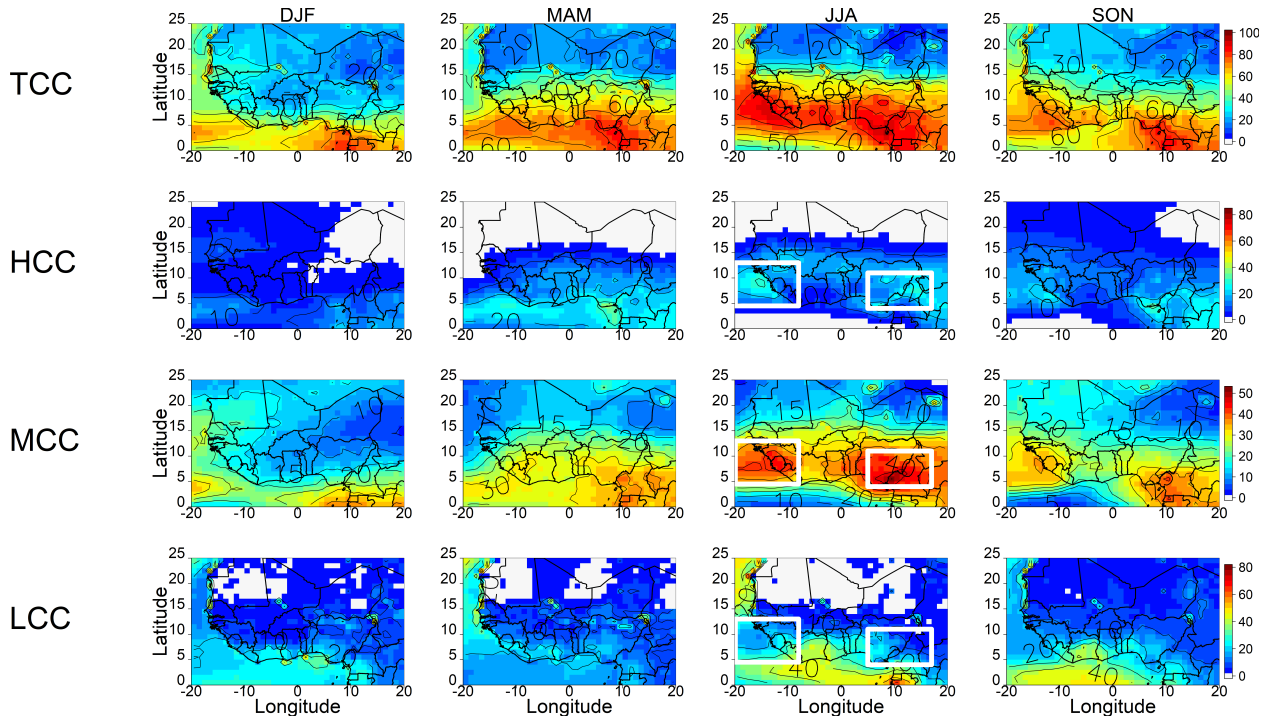


Figure 5: Évolutions saisonnières moyennes de la couverture nuageuse totale (TCC), des nuages de haute altitude (HCC), de moyenne altitude (MLC) et de basse couche (LCC) en pourcentage à partir des observations satellite CERES. Les valeurs moyennes des fractions de nuages indiquées sont calculées à partir des valeurs horaires diurnes (0600 UTC à 1700 UTC) pour une période de 10 ans (2006-2015). Les rectangles blancs indiquent les zones où les nuages de haute altitude (HCC) et de moyenne altitude (MLC) empêchent le capteur du satellite de détecter les nuages de basse couche.

L'évolution diurne des nuages dans la région a également été étudiée à l'aide des deux jeux de données (Figure 6). Au sud de la latitude 15° N, il existe en permanence au moins un type de nuage. La fréquence d'occurrence de la présence simultanée des trois types de nuages est plus élevée dans ces régions. Les nuages bas sont également fréquents dans ces zones, en particulier autour des régions côtières de l'AO. La fréquence d'apparition de nuages dans la basse atmosphère, qui entraînent une perte importante de rayonnement incident, se situe entre 10 et 20 % autour de la côte de Guinée pendant la saison humide (JJA). D'autre part, toutes les zones situées au nord de la latitude 10° N sont caractérisées par une occurrence élevée de situation de ciel clair, soit sans nuage.

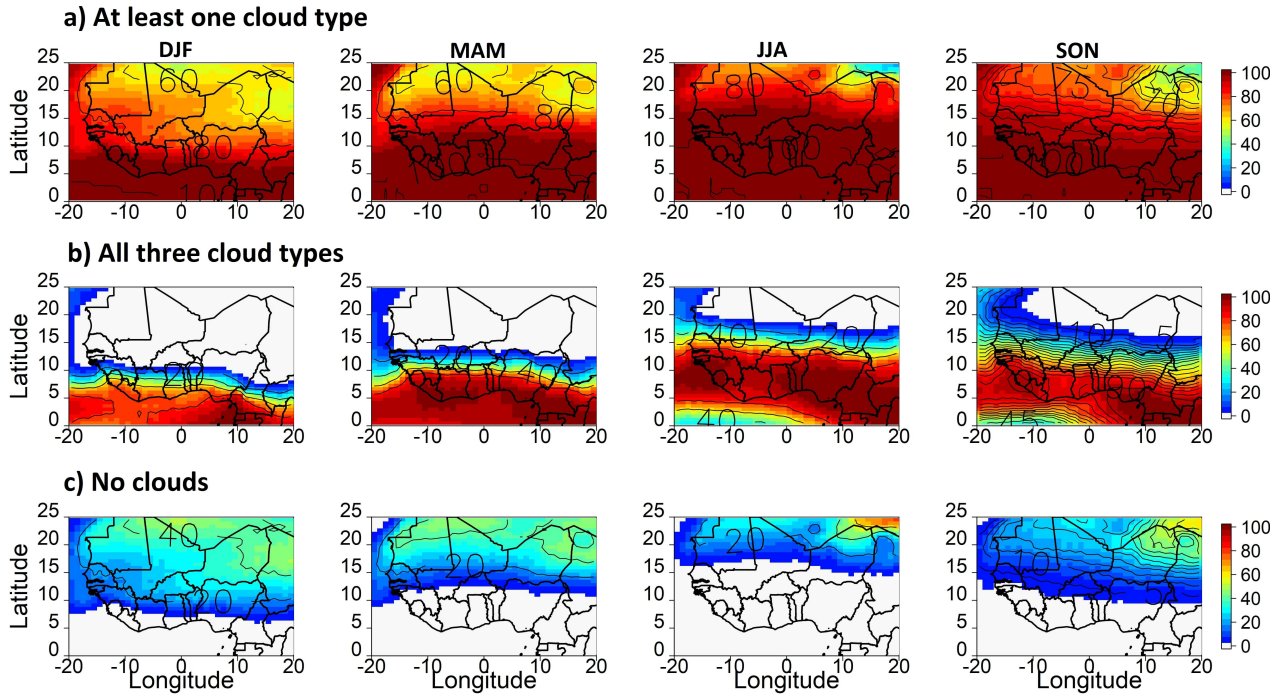


Figure 6: A partir des réanalyses ERA5, fréquence d’occurrence saisonnière pour (a) au moins un type de nuage présent, (b) les trois types de nuages simultanément et (c) aucune présence de nuage.

Ces résultats ont des implications directes sur l’implantation des fermes solaires dans la région. Par exemple, compte tenu des effets radiatifs élevés des nuages bas sur le rayonnement incident (Bouniol et al., 2012), on peut décider d’implanter de grandes fermes solaires loin de la côte guinéenne. En effet, compte tenu de la fréquente présence simultanée des trois types de nuages, les centrales solaires PV situées en Guinée seront alors susceptibles de beaucoup moins produire pendant ces périodes. Ceci est particulièrement vrai pendant la saison de mousson en raison de l’intensification des nuages et de l’augmentation de la fréquence d’apparition simultanée des trois types de nuages. La région du Sahel et les parties nord de l’AO peuvent sembler favorables à l’implantation de grandes fermes solaires en raison de la couverture et de la fréquence d’occurrence relativement faibles des nuages. Cependant, ces régions sont soumises à des événements de particules de poussière provenant du désert du Sahara, qui peuvent réduire drastiquement le rayonnement et également se déposer sur les panneaux solaires, réduisant ainsi la production d’électricité. Rappelons néanmoins que ces situations particulières de poussière n’ont pas été directement analysées dans ce travail.

Facteurs synoptiques de l'apparition des nuages en Afrique de l'Ouest

Dans cette section, je présente les principaux résultats du Chapitre 4, constitué de l'article publié dans le journal *Earth System Dynamics* (Danso et al., 2020a).

Suite aux résultats précédents, nous nous sommes attachés à identifier les processus synoptiques qui déclenchent et maintiennent la présence des nuages. Pour cela, nous avons ciblé notre étude uniquement sur les nuages bas (LLC) présents en journée en raison de leur impact significatif sur le rayonnement solaire incident par rapport aux nuages de moyenne et haute altitude. Avec les données ERA5, trois classes de couverture nuageuse de basse couche ont été définies puis analysées : situation sans LLC (qui ne peut pas être assimilée à une situation de ciel clair car ces situations peuvent présenter des couvertures nuageuses de moyenne ou haute altitude), classe 1 et classe 2. Les classes 1 et 2 correspondent à des situations où la fraction nuageuse des nuages de basse couche (LLC) est faible (jusqu'à 50 % pour la classe 1) et importante (plus de 50 % pour la classe 2), et ce pour deux fenêtres sous-régionales, les régions de Guinée et du Sahel en AO (Figure 7).

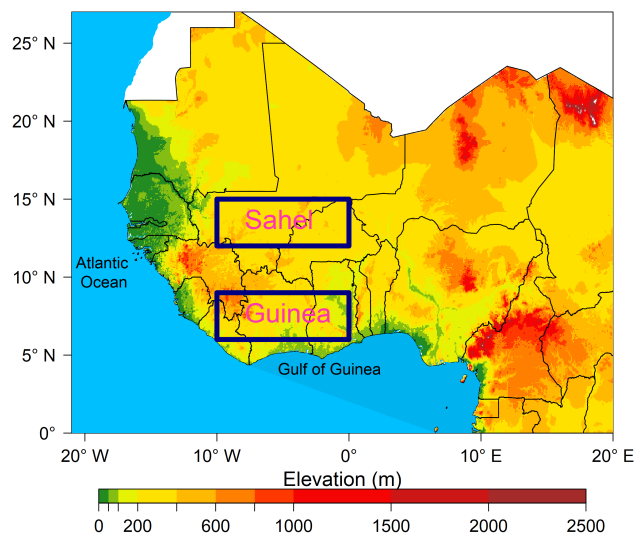


Figure 7: Carte de l'Afrique de l'Ouest présentant les deux sous-régions sélectionnées (rectangles bleu foncé) utilisées pour l'identification des situations de nuages de basse couche (LLC). Le nom indiqué pour chaque fenêtre est basé sur la zone climatique correspondante.

Figure 8, les résultats montrent que la présence des trois classes de couverture nuageuse dans les régions de Guinée et du Sahel de l'AO est marquée par des variations saisonnières significatives :

- En Guinée, les situations sans LLC sont très rares et ne se produisent que pendant la saison sèche (DJF). En revanche, la présence de LLC est détectable tous les mois dans cette zone. Les situations de LLC associée à la classe 1 (faible fraction nuageuse) présentent un cycle saisonnier marqué avec des occurrences plus élevées pendant les saisons sèches et plus faibles en saison humide (JJAS). Inversement, les situations de LLC associée à la classe 2 (fraction nuageuse significative) sont plus fréquentes en période humide (JJAS). Cette période est associée à un flux d'humidité en provenance du Golfe de Guinée (Thorncroft et al., 2011) et à l'advection d'air froid qui favorise la formation de nuages bas sur la région pendant cette période, comme le montrent Adler et al. (2019).
- Au Sahel, les situations sans LLC sont fréquentes, se produisant chaque mois sauf en août lorsque la mousson est pleinement développée sur la région sahélienne de l'Afrique de l'Ouest. De même, les situations de LLC associée à la classe 1 (faible fraction nuageuse) sont fréquentes tout au long de l'année, mais les occurrences les plus fortes se produisent de juillet à octobre et les plus faibles pendant la saison sèche. Les situations de LLC associée à la classe 2 (fraction nuageuse significative) sont marquées par une forte signature saisonnière, se produisant seulement de juillet à octobre avec un pic distinct en août lorsque la zone de convergence intertropicale (ZCIT) est localisée à sa latitude la plus septentrionale sur l'AO (Nicholson, 2018). Cette période coïncide également avec la pluviosité maximale sur la région du Sahel (Nicholson, 2013) et suggère un lien étroit entre l'occurrence de ces situations et la pluviosité sahélienne.

Figure 9, on note que dans les deux sous-régions (Guinée, Sahel), les situations sans LLC ne présentent pas de variations diurnes très marquées. Dès que des LLC sont présents (Classes 1 ou 2), alors leur occurrence semble être marquée par le cycle diurne :

- En Guinée, le nombre de situations de LLC associée à la classe 1 est faible en début de matinée mais augmente progressivement tout au long de la journée jusqu'en fin d'après-midi. Au contraire, le nombre de situations de LLC associée à la classe 2 est élevé en début de matinée et diminue tout au long de la journée jusqu'en fin d'après-midi. Le pic du début de la matinée pour ces situations de classe 2 pourrait être le résultat de la contribution des résidus des nuages nocturnes de type stratus de basse altitude qui persistent longtemps dans la journée (Kalthoff et al., 2018). Ces nuages ont généralement une couverture fractionnée importante lors de leur apparition pendant la nuit (van der Linden et al., 2015) mais se dissipent pendant la journée (Kalthoff et al.,

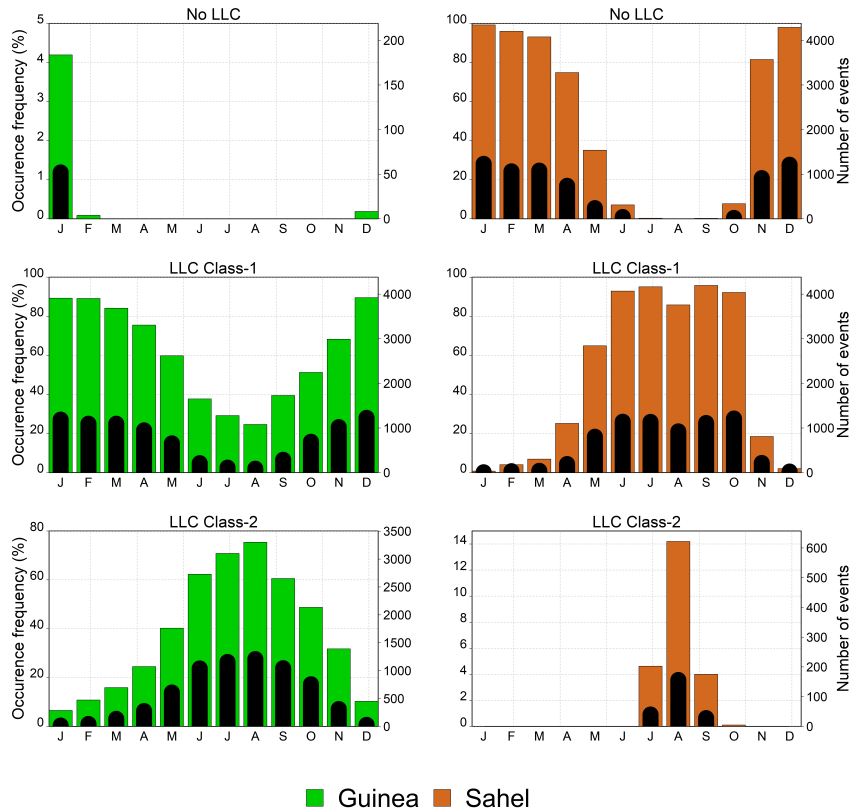


Figure 8: Distribution mensuelle de la fréquence d'occurrence des événements horaires pour les trois classes de LLC pendant la journée dans les régions de Guinée (barre verte) et du Sahel (barre orange), telles qu'elles sont définies dans la Figure 7. Les barres noires représentent la distribution des occurrences des événements qui durent au moins six heures consécutives (leurs valeurs réelles ont été multipliées par un facteur 4 pour améliorer la lisibilité de la figure).

2018). Les évolutions des occurrences des situations associées aux classes 1 ou 2 pourraient donc être liées à la dissipation progressive de ces nuages nocturnes pendant la journée.

- Au Sahel, le nombre de situations de LLC associée à la classe 1 ne présentent pas de cycle diurne particulier. En revanche, le nombre de situations de LLC associées à la classe 2 est fortement marqué par le cycle diurne, où l'on observe une fréquence d'occurrence plus élevée en fin de matinée et en milieu de journée et des valeurs plus faibles en début de matinée et en fin d'après-midi. Cette tendance semble être contrôlée par des processus de surface tels que le chauffage solaire diurne continental (Mallet et al., 2009). De plus, elle pourrait être liée à l'apparition de MCS profonds dont les parties convectives seraient considérées comme des nuages bas si elles se trouvent dans les 2 km les plus bas de l'atmosphère. Ces MCS présentent une évolution assez similaire (à la

fois saisonnière et diurne) à la classe 2 dans cette région de l’Afrique de l’Ouest (Vizy & Cook, 2019).

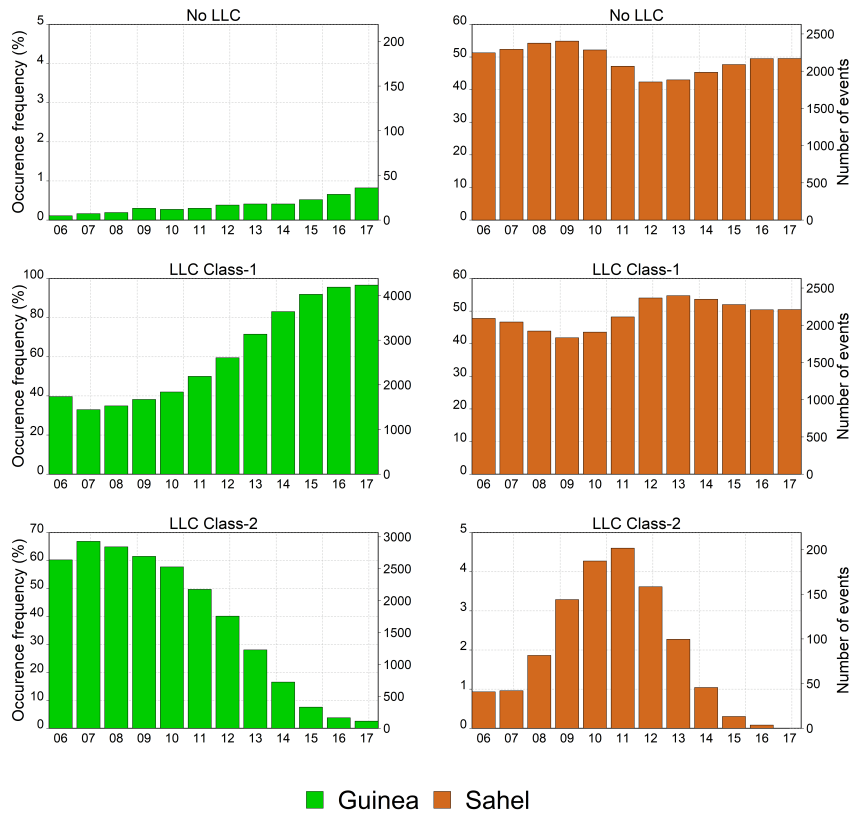


Figure 9: Evolution diurne de la fréquence d’occurrence des trois classes de LLC pendant la journée dans les deux sous-régions d’intérêt (Guinée et Sahel), telles qu’elles sont définies dans la Figure 7.

La circulation atmosphérique régionale et le flux d’humidité ont été analysés pour ces trois classes (sans LLC , classe 1, classe2),. Pour cela, une approche composite a été utilisée afin de produire des résultats robustes basés sur un grand nombre de situations. Par ailleurs, pour mener à bien cette analyse à l’échelle régionale, nous nous sommes attachés à ne retenir que les situations qui présentaient une durée suffisamment longue ; ainsi seules les situations durant au moins six heures consécutives ont été retenues dans chacune des classes. Une analyse composite du flux d’humidité et du vent à 950 hPa a été effectuée ainsi que pour les flux de chaleur de surface et la température de l’air dans les 2 premiers km de l’atmosphère.

Pendant la saison humide (JAS), dans les deux régions (Figure 10), l’occurrence des situations de LLC associées aux classes 1 et 2 est liée à un flux d’humidité élevé dominé par de forts vents du sud-ouest (flux d’humidité positif) provenant du golfe de Guinée. Le flux d’humidité est plus important pour les situations associées à la classe 2 que ceux associées à la classe 1 (quelque soit la sous-région). Cependant,

le flux d'humidité est plus intense pour les situations LLC au Sahel en termes de pénétration dans les terres.

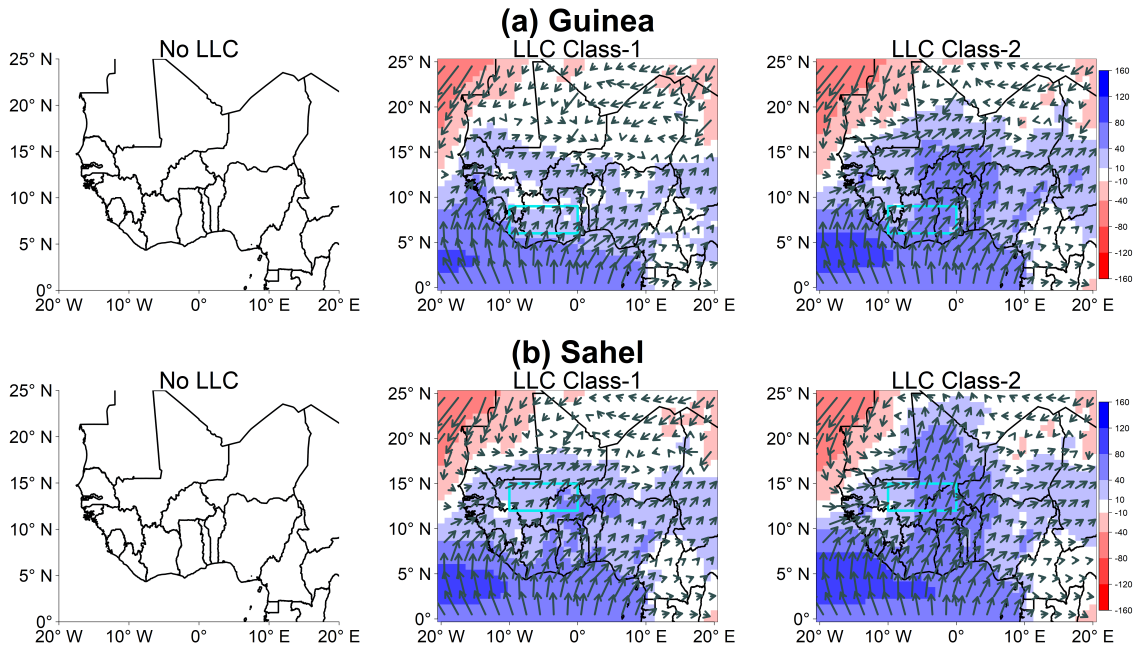


Figure 10: Composites du flux d'humidité 950 hPa (couleurs, $\text{g kg}^{-1} \text{m s}^{-1}$) et du vent (vecteurs, m s^{-1}) sur l'AO pour les trois classes d'occurrence de LLC dans les sous-régions Guinée (en haut) et Sahel (en bas) pendant la saison humide (JAS) de 2006 à 2015. Seules les occurrences d'au moins six heures consécutives sont prises en compte. La moyenne des vecteurs vent est calculée sur 2 points de grille dans les directions x et y. Aucun événement de la classe sans LLC (No LLC) n'a été extrait dans ces deux sous-régions pendant cette saison.

Pendant la saison sèche (DJF), dans les deux régions (Figure 11), les situations atmosphériques sans LLC sont caractérisées par des vents secs provenant du nord-est qui inhibent la formation de LLC. L'apparition de situations associées à la classe 1 en Guinée et au Sahel est caractérisée par des vents du sud le long de la côte sud mais qui ne pénètrent pas dans les deux sous-régions étudiées. Néanmoins, les situations atmosphériques de types classe 1 ou 2 sont associées à une humidité spécifique importante (vrai pour les deux saisons), contrairement aux situations sans LLC qui présentent une très faible humidité spécifique dans l'atmosphère (Figure 12). Ceci est en accord avec Babic et al. (2019b) qui montrent que la différence la plus nette entre les situations de LLC et sans LLC réside dans l'humidité spécifique, suggérant que l'humidité de fond peut jouer un rôle crucial dans la formation et le maintien de nuages de basse couche en AO. Par ailleurs, les situations LLC associées à la classe 1 pendant la saison sèche au Sahel (DJF) sont liées à des anomalies positives d'humidité spécifique qui semblent avoir été transportées sur le

continent depuis l'Atlantique Nord (non montré). Les situations LLC associées à la classe 2 en Guinée sont associées à un flux d'humidité beaucoup plus important dans la région ainsi qu'à une anomalie positive d'humidité spécifique à l'intérieur et autour de la fenêtre (non montré).

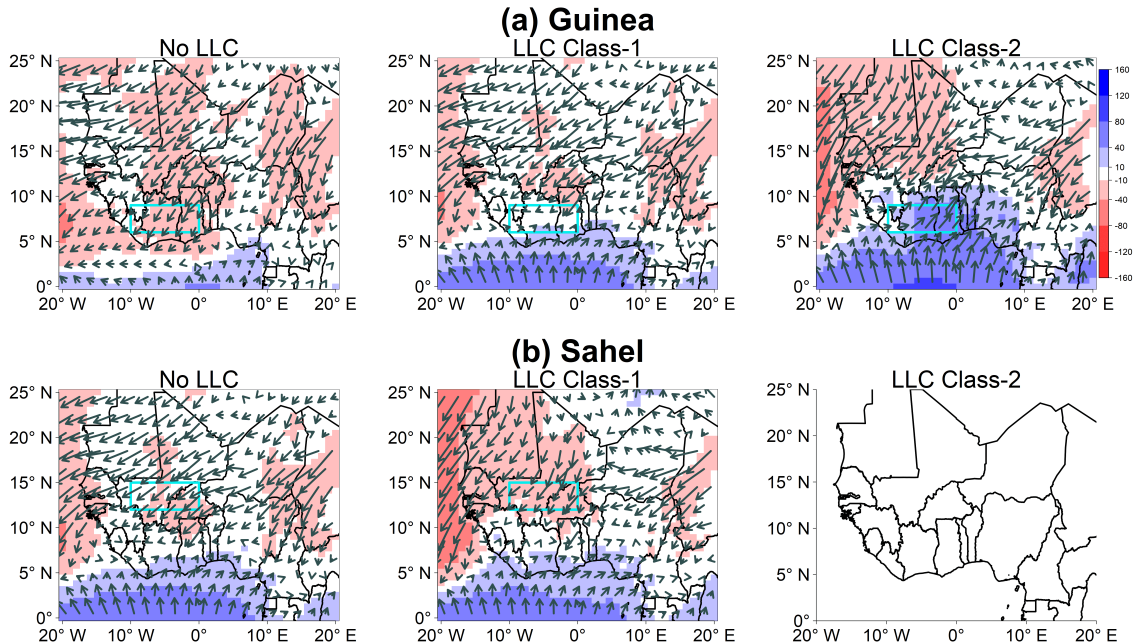


Figure 11: Idem que pour la Figure 10 mais pour la saison sèche (DJF). Aucun événement de la classe 2 n'a été extrait dans la zone du Sahel pendant cette saison.

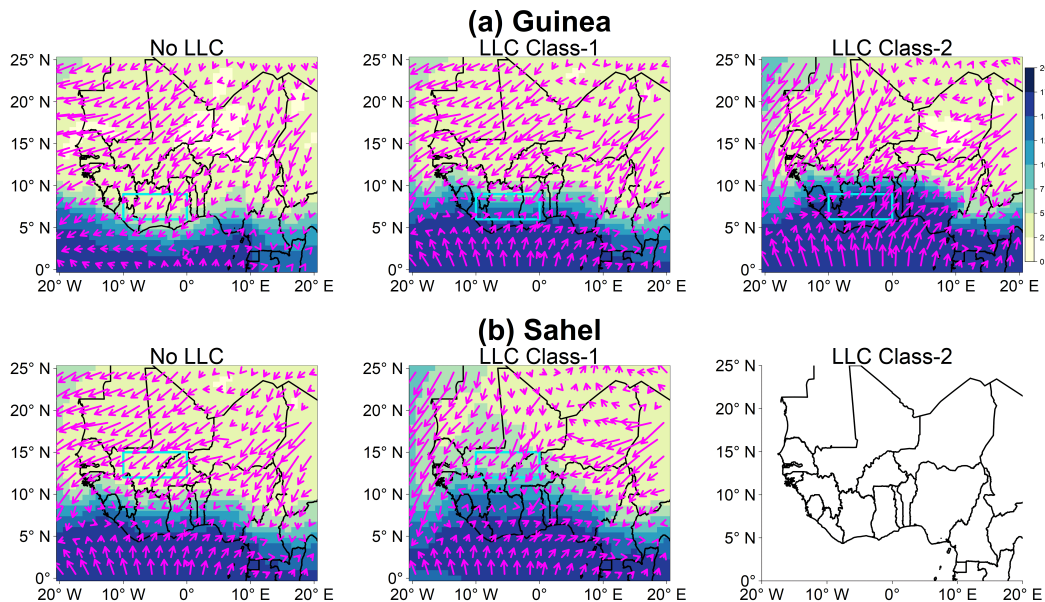


Figure 12: Idem que la Figure 11 mais pour l'humidité spécifique (couleurs, g kg^{-1}) et du vent (vecteurs, m s^{-1}).

Nous avons analysé le flux d’humidité composite (à 950 hPa) de la première heure juste avant l’événement LLC ($1h_{Before}LLC$) et de la première heure juste après la disparition de la situation de LLC ($1h_{After}LLC$), ainsi que la différence entre ces deux périodes. Ceci est illustré pour la classe 2 pendant la saison humide JAS dans les deux sous-régions Guinée et Sahel (Figure 13). Dans ces deux régions, le flux d’humidité pendant $1h_{Before}LLC$ est plus important que $1h_{After}LLC$ et il y a une différence significative entre les deux périodes, comme le montre la Figure 13. Ceci est également vrai pour les composites d’humidité spécifique uniquement (voir pour plus de détails le Chapitre 4).

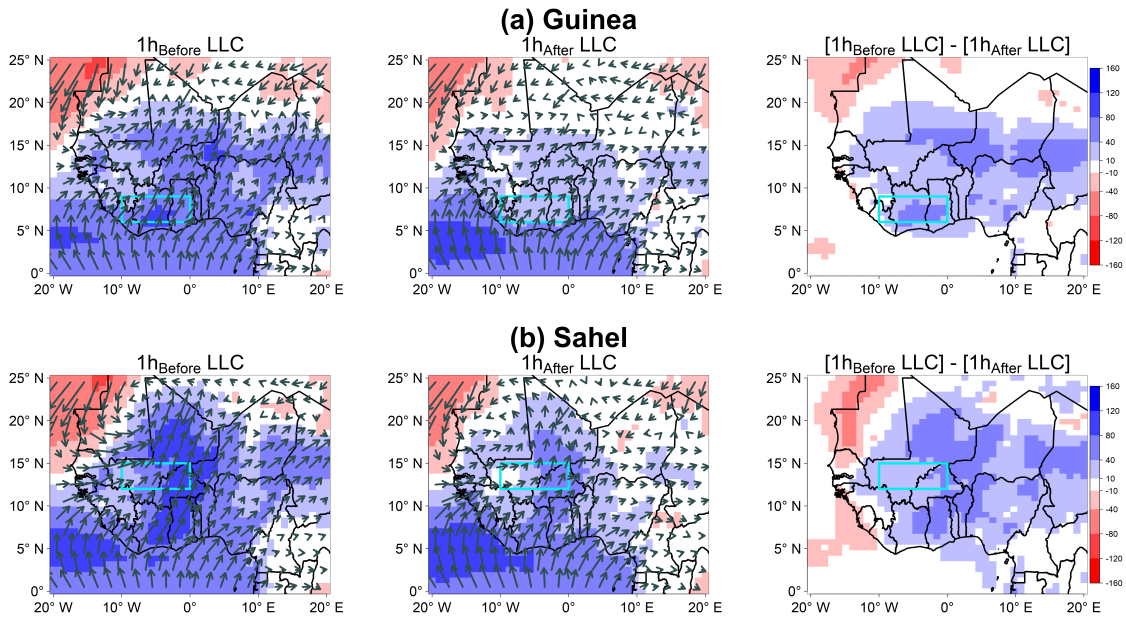


Figure 13: Cartes composites du flux d’humidité 950 hPa (couleurs, g kg^{-1}) et du vent (vecteurs, m s^{-1}) sur l’AO pour l’heure précédant l’occurrence d’une situation associée à la classe 2 ($1h_{Before}LLC$) et après sa disparition ($1h_{After}LLC$) et la différence entre les deux périodes pendant la saison humide (JAS) de 2006 à 2015. La moyenne des vecteurs vent est calculée sur 2 points de grille dans les directions méridionale et zonale.

Pendant $1h_{Before}LLC$, la vapeur d’eau associée au flux d’humidité est probablement refroidie par l’advection d’air froid dans la région qui conduit à la saturation et, par conséquent, à la formation de nuages de basse couche. En effet, le profil vertical de la température potentielle dans la basse atmosphère pendant les deux périodes montre une forte diminution de la température juste avant l’apparition de la situation de LLC et une augmentation après sa disparition (Figure 14). Cette baisse de température peut être une indication du refroidissement causé par l’advection d’air froid, comme le montrent Babic et al. (2019b). Dans la région de Guinée, des études ont montré que le refroidissement par l’advection horizontale de l’air froid provenant

du Golfe de Guinée contribue de manière significative à la formation de nuages de basse couche (par exemple, Adler et al. (2019) and Babic et al. (2019b)). Dans la région du Sahel, l'advection de l'air humide peut être cruciale pour la formation de nuages de basse couche comme le suggèrent Parker et al. (2005). Cependant, avant la formation de ces nuages dans la région du Sahel, un refroidissement peut se mettre en place, dû à l'advection méridionale (Marsham et al., 2013) ainsi qu'à l'advection d'air froid provenant de l'Atlantique Nord, ce qui pourrait expliquer la forte réduction de température pendant $1h_{Before}LLC$.

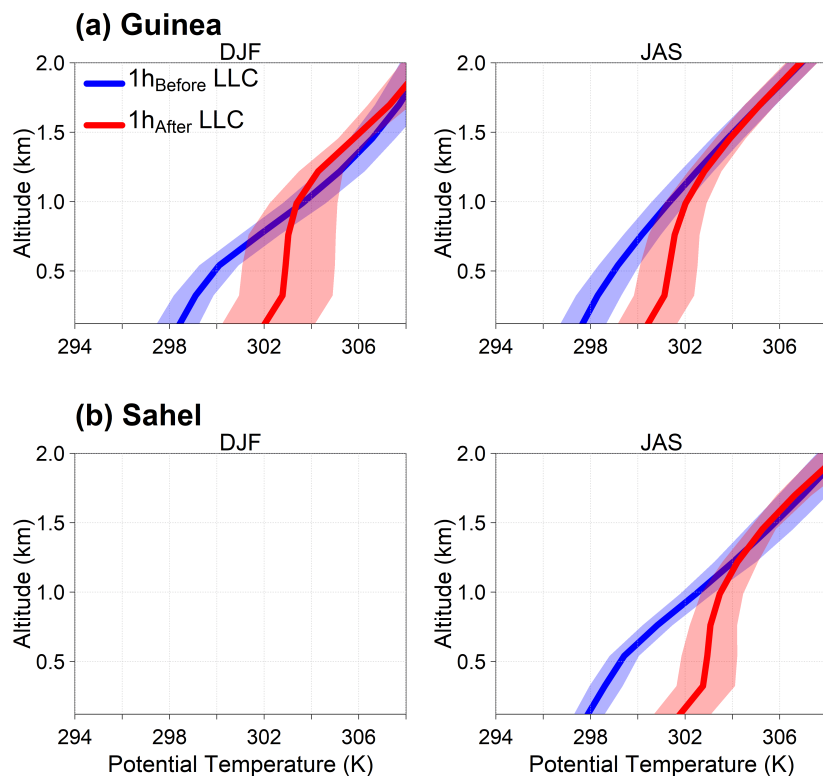


Figure 14: Profil vertical de la température potentielle moyenne (ligne solide) sur les 2 premiers km de l'atmosphère, calculée pour les deux sous-régions (Guinée et Sahel) pour toutes les "heures" précédant l'apparition d'une situation associées à la classe 2 et toutes les "heures" suivant sa disparition. Les régions ombrées représentent les 10e et 90e quantiles. Aucune situation de LLC associée à la classe 2 n'a été extraite dans la zone du Sahel pendant la saison sèche (DJF).

Pendant la saison sèche, le flux d'humidité lors de l'apparition des nuages de basse couche n'est pas aussi fort que pendant la saison des pluies. Cependant, l'humidité de fond joue un rôle important dans l'apparition des nuages (voir Chapitre 4). En étudiant ces processus à la fois pour la saison humide et la saison sèche, cette étude s'inscrit dans le prolongement des études antérieures menées en AO qui ne portaient que sur la saison de mousson.

Persistance des nuages et effets du rayonnement incident à ondes courtes

Les principaux résultats détaillés dans le Chapitre 5 sont présentés dans cette section. Ils sont publiés dans le numéro special “Towards Inclusive and Operational Weather and Climate Services to Strengthen Resilience to Climate Change” de la revue *Atmosphere* (Danso et al., 2020b).

On s’intéresse ici à examiner comment notre compréhension sur l’apparition et l’évolution des nuages peut être directement utilisée pour développer une gestion optimale des fermes solaires. Il s’agit donc de transformer une connaissance académique en service climatique, dédié au secteur socio-économique.

Nous avons déterminé quantitativement les effets des nuages sur le rayonnement solaire incident. Pour ce faire, nous avons utilisé l’atténuation du rayonnement à courte longueur d’onde des nuages (CRA_{SW}^{\downarrow}), définie comme la quantité de rayonnement solaire incident perdue par absorption ou réflexion par les nuages. Elle est estimée par la différence entre le rayonnement à courte longueur d’onde de surface dans des conditions de ciel clair (SW^{\downarrow} dans $W m^{-2}$) et le flux de rayonnement à courte longueur d’onde de surface de ciel clair (SW_{CS}^{\downarrow} dans $W m^{-2}$). SW_{CS}^{\downarrow} est calculé pour les mêmes conditions atmosphériques de température, d’humidité, d’ozone, de gaz à l’état de traces et d’aérosols que le SW^{\downarrow} correspondant (avec nuages), mais en supposant qu’il n’y a pas de nuages. Par conséquent, CRA_{SW}^{\downarrow} ne tient compte que des effets des nuages sur le rayonnement solaire incident, mais pas des aérosols. Pour éliminer l’influence du moment de la journée et donc l’effet de l’angle d’élévation solaire sur le calcul de la valeur moyenne CRA_{SW}^{\downarrow} , nous exprimons l’atténuation du rayonnement (CRA_{SW}^{\downarrow}) en pourcentage de la valeur SW_{CS}^{\downarrow} . CRA_{SW}^{\downarrow} a été calculé sur diverses sous-régions en Afrique de l’Ouest lorsque des nuages sont présents (c’est-à-dire que la fraction totale des nuages n’est pas nulle). Pour un type de nuage particulier (LLC, MLC, ou HLC) l’atténuation CRA_{SW}^{\downarrow} est calculée en utilisant la même procédure et les mêmes hypothèses, mais uniquement lorsque ce type de nuage est présent et que les autres nuages sont absents. À partir de là, il a été possible de déterminer la relation entre la fraction nuageuse du type de nuage considéré et son atténuation CRA_{SW}^{\downarrow} associée.

Dans toutes les zones explorées, l’atténuation moyenne du rayonnement solaire incident par les nuages est la plus élevée en été, de juillet à octobre, ce qui correspond au cœur de la saison de mousson dans la région (Figure 15). Pendant cette période, l’AO est soumise à un flux d’humidité en provenance du golfe de Guinée qui augmente la couverture nuageuse, intensifiant ainsi l’atténuation du ray-

onnement solaire incident qui, à son tour, entraîne une diminution de la production d'énergie solaire. L'atténuation maximale se produit en août lorsque la zone de convergence intertropicale (ZCIT) est à sa position la plus septentrionale en AO. En revanche, de très faibles atténuations sont observées de décembre à février, lorsque la plus grande partie de l'Afrique de l'Ouest est soumise à des conditions climatiques sèches. L'évolution de l'atténuation du rayonnement CRA_{SW}^{\downarrow} suit naturellement l'évolution annuelle des nuages dans la région telle qu'elle est présentée sur la Figure 4.

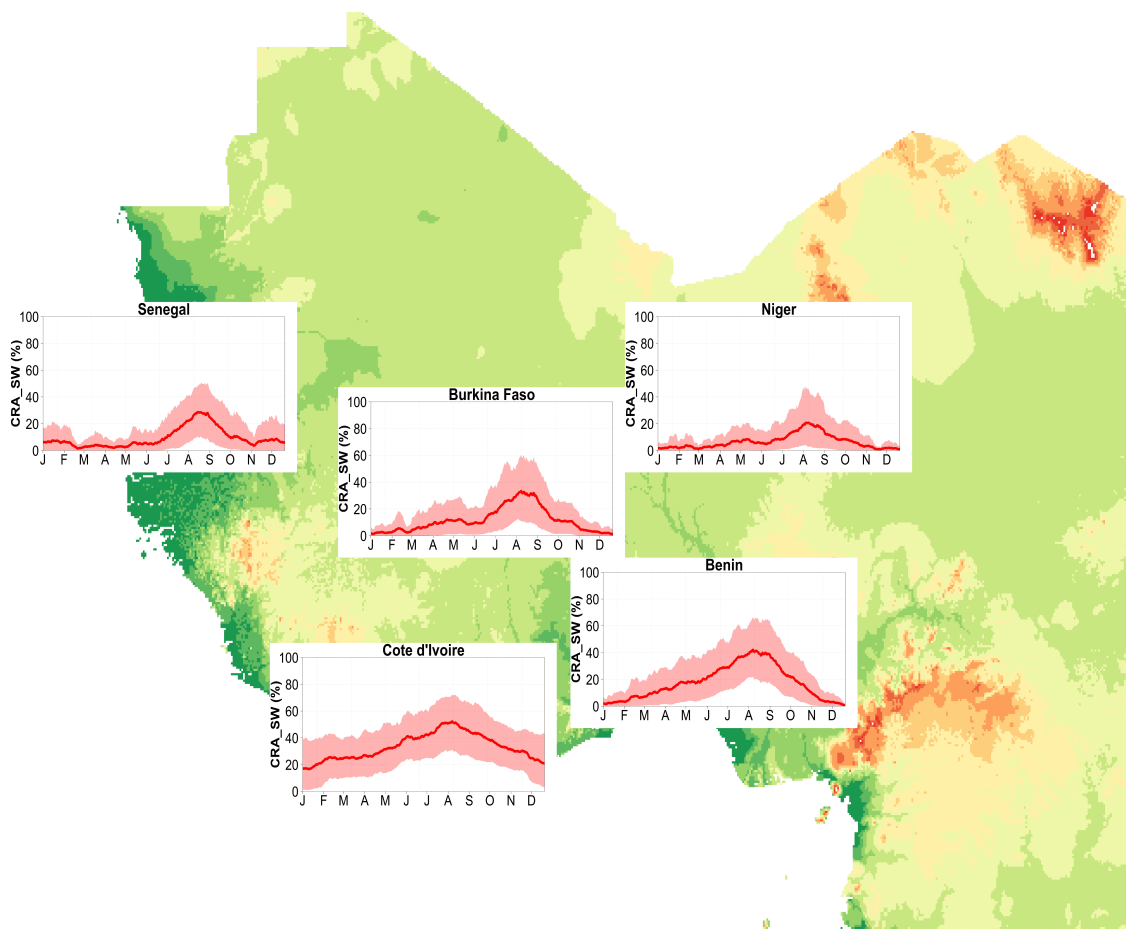


Figure 15: Cycle annuel moyen (courbe solide) de l'atténuation du rayonnement à courte longueur d'ondes courtes, due à la présence de nuages en Afrique de l'Ouest. Les régions ombrées correspondent aux 10^e et 90^e quantiles.

Bien que toutes les régions affichent des cycles annuels similaires, l'atténuation du rayonnement solaire incident (CRA_{SW}^{\downarrow}) est la plus élevée dans la partie sud de l'AO. Pour tous les mois, la moyenne CRA_{SW}^{\downarrow} est plus élevée en Côte d'Ivoire et au Bénin que dans toutes les autres sous-régions explorées. En août, environ 55 % et 40 % du rayonnement solaire entrant sont perdus en moyenne à cause des nuages en Côte d'Ivoire et au Bénin respectivement, contre environ 20 %, 30 % et 35 %

au Niger, au Sénégal et au Burkina Faso. D'autre part, l'atténuation moyenne est d'environ 5 % ou moins dans toutes les régions en janvier, sauf en Côte d'Ivoire où environ 20 % du rayonnement solaire incident est perdu. De plus, l'atténuation CRA_{SW}^\downarrow pendant les mois d'été est associée à une grande variabilité dans toutes les zones (la région ombragée représentant les 10^e et 90^e quantiles). Cela pourrait être dû à un degré élevé de variation des propriétés optiques (telles que l'épaisseur optique des nuages) des différents systèmes nuageux qui se produisent dans la région, mais ce point doit faire l'objet d'analyses plus approfondies.

Le coefficient de corrélation (R) entre la fraction nuageuse pour chaque type de nuages (LLC, MLC, HLC) et l'atténuation CRA_{SW}^\downarrow associée est présenté dans le Table 2. Pour les cinq sous-régions sélectionnées, l'atténuation CRA_{SW}^\downarrow présente une forte corrélation avec la fraction nuageuse des nuages de basse couche (LLC) et de moyenne altitude (MLC). Ainsi, une fraction nuageuse plus importante (plus petite) de LLC ou de MLC conduit à une atténuation plus importante (plus faible) du rayonnement solaire incident. Par contre, l'atténuation CRA_{SW}^\downarrow semble moins impactée par la des nuages de haute altitude (HLC). Cela est probablement dû à la faible épaisseur optique des nuages HLC, qui permet à une grande partie du rayonnement solaire incident de passer à travers avec une très faible atténuation.

Table 2: Relation entre la fraction des nuages et l'atténuation du rayonnement à ondes courtes des nuages pour les différents types de nuages dans les cinq fenêtres sélectionnées.

Region	R (CRA_{SW}^\downarrow vs. fraction de nuage)		
	<i>HLC</i>	<i>MLC</i>	<i>LLC</i>
Senegal	0.59	0.94	0.93
Burkina Faso	0.53	0.93	0.99
Niger	0.5	0.92	0.91
Benin	0.45	0.93	0.96
Cote d'Ivoire	0.72	0.97	0.92

Compte tenu de la forte corrélation positive entre la fraction nuageuse et CRA_{SW}^\downarrow pour les nuages de basse couche (LLC) et de moyenne altitude (MLC), nous analysons leur occurrence et leur persistance sur l'ensemble de l'AO. Cette information est utile pour qualifier la fiabilité de la production d'électricité solaire à partir de centrales solaires dans cette région.

La Figure 16 montre la fréquence annuelle moyenne d'occurrence des nuages de basse couche, LLC, de moyenne altitude, MLC, et des conditions de ciel clair qui persistent sur des durées de 2 à plus de 6h (soit sur toute la journée).

On ne s'intéresse ici qu'aux situations où la fraction nuageuse de ces deux types de nuages (LLC, MLC) est élevée (au moins 50 %). Globalement, les situations nuageuses qui persistent pendant plusieurs heures sont plus fréquentes dans le sud de l'AO (au sud de la latitude 10° N), en particulier autour des zones côtières. L'occurrence des situations de nuageuse de basse couche persistant pendant exactement deux heures consécutives est de l'ordre de 30 à 50 % du temps dans une année en moyenne. Sur ces mêmes régions, les nuages de basse couche peuvent persister pendant plusieurs heures consécutives (plus de 2 heures) pour un nombre important de fois dans l'année, allant jusqu'à environ 5 à 15 % de cas au cours desquels ces nuages persistent pendant plus de six heures consécutives. Cela signifie que pendant environ 18 à 55 jours dans une année, en moyenne, le rayonnement solaire reçu à la surface sera bien inférieur à la moyenne attendue pendant au moins plus de la moitié du temps au cours de chaque jour. De même, les nuages de moyenne altitude, MLC, persistent pendant exactement deux heures consécutives pendant environ 8 à 16 % du temps au cours d'une année, en moyenne. Ces nuages présentent également des durées de persistance qui vont bien au-delà de ces 2 heures, et ce pour un grand nombre de jours dans une année.

Les régions sahéliennes et septentrionales de l'AO (au nord de la latitude 10° N) sont caractérisées par une fréquence élevée de conditions de ciel sans nuage. Sans nuage, seule une petite fraction du rayonnement solaire incident sera atténuée en raison des autres constituants atmosphériques (vapeur d'eau, gaz à l'état de traces, ozone, etc.). C'est un cas idéal pour les gestionnaires de fermes solaires photovoltaïques, car le rayonnement solaire sera maximal conduisant à une production d'énergie optimale. Au nord du Niger, du Mali et de la Mauritanie, par exemple, le ciel sans nuage peut persister pendant plus de six heures consécutives, soit environ 30 % du temps au cours d'une année, en moyenne. Ces régions sont toutefois caractérisées par une forte concentration de particules de poussière qui pourraient réduire considérablement le rayonnement solaire incident. Cette question de l'influence de la poussière sur le rayonnement solaire entrant n'est cependant pas abordée dans cette étude.

Pour la gestion globale des installations photovoltaïques, il est également nécessaire de caractériser le rayonnement solaire de surface reçu (comme utilisable ou non utilisable) et la persistance associée pour chaque seuil d'énergie reçue. Nous avons donc divisé le rayonnement de surface reçu en trois seuils, à savoir "Low" ($SW^\downarrow < 100$), "Moderate" ($100 \leq SW^\downarrow \leq 500$), et "High" ($SW^\downarrow > 500$). Ces seuils ont été choisis arbitrairement. Avec un seul panneau photovoltaïque, le seuil "Low" conduira à une très faible production d'électricité, considérée comme non utilisable, tandis que les autres seuils conduiront à des productions relativement plus élevées

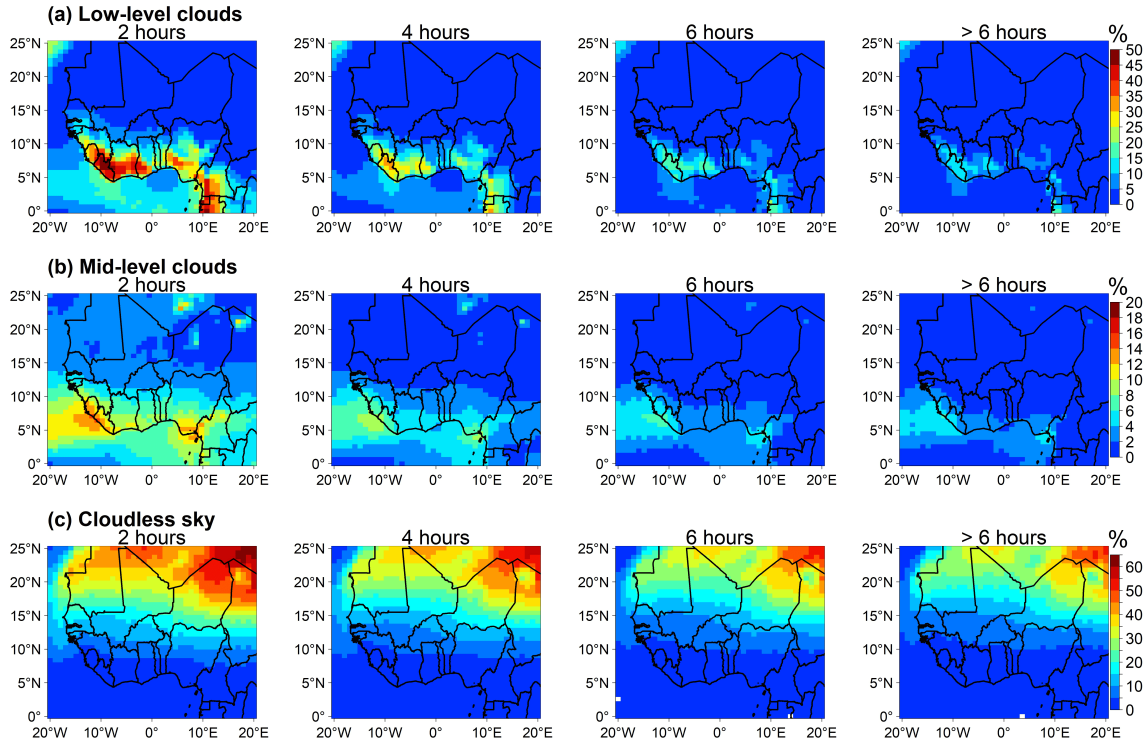


Figure 16: Distribution spatiale de la fréquence d'occurrence (a) de la nébulosité à basse altitude (LLC), (b) de la nébulosité à moyenne altitude (MLC) et (c) des conditions de ciel sans nuage qui persistent pendant plusieurs heures en Afrique de l'Ouest. Seules les occurrences de LLC et MLC avec une couverture d'au moins 50 % sont prises en compte.

et donc exploitables.

Malgré des conditions nuageuses persistantes dans certaines parties de la région Ouest Africaine, les périodes de rayonnement de surface extrêmement faible ne durent pas longtemps sur l'ensemble de la région (Figure 17). D'autre part, les événements persistants "Moderate" et "High" SW^\downarrow sont plus fréquents en toutes saisons. Les événements persistants "High" SW^\downarrow dominent au Niger et au Bénin, pour toutes saisons. Par exemple, pendant la saison humide (JJA) au Niger, le seuil "High" SW^\downarrow peut persister jusqu'à trois heures consécutives pendant environ 45 % du temps. De même, pendant la saison sèche (DJF) et l'intersaison (MAM) en Côte d'Ivoire, les seuils "High" persistants SW^\downarrow sont plus fréquents. Cependant, les situations où les seuils moderate persistent, sont plus importantes pendant la saison humide (JJA) en Côte d'Ivoire, ce qui est probablement le résultat de l'intensification de la couverture nuageuse sur la région pendant cette période. Par conséquent, la production d'énergie solaire pendant cette saison en Côte d'Ivoire sera modérée pendant des périodes prolongées. Les centrales solaires devront donc être

surdimensionnées pour compenser la réduction de la production. Il est intéressant de voir que la fréquence des événements persistants "Low" SW^\downarrow en Côte d'Ivoire est très faible en toutes saisons, indépendamment de la couverture nuageuse intense dans la partie sud de l'AO. Par conséquent, la production d'énergie solaire extrêmement faible ne se prolongera pas sur de longues périodes.

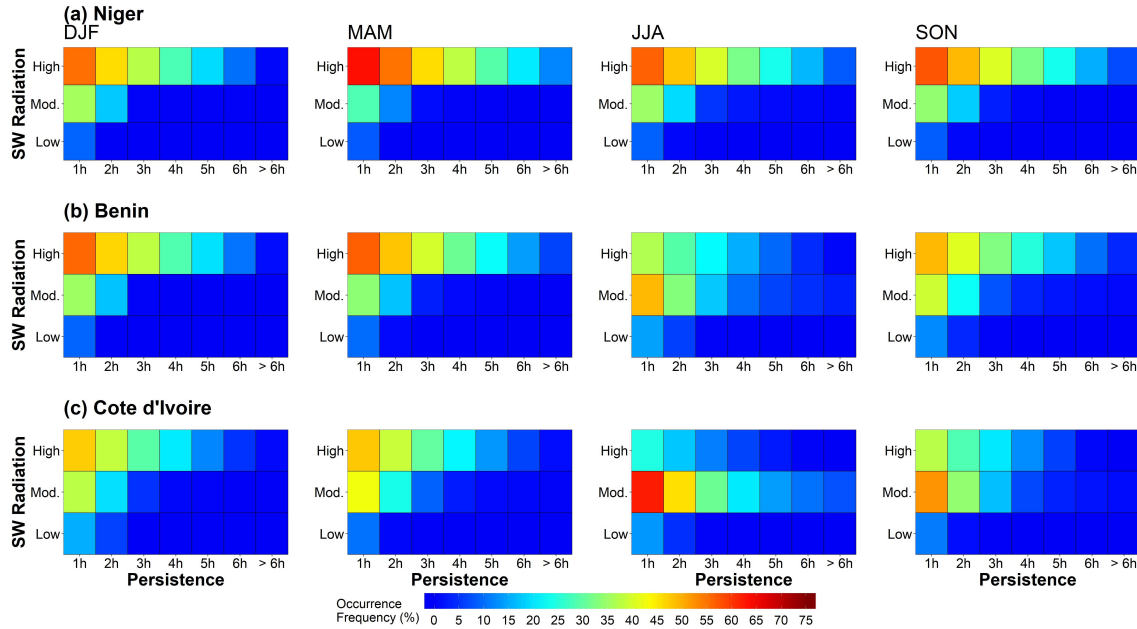


Figure 17: Fréquence moyenne saisonnière d'occurrence des rayonnements de surface *Low* ($SW^\downarrow < 100$), *Moderate* ($100 \leq SW^\downarrow \leq 500$), et *High* ($SW^\downarrow > 500$) qui persiste pendant plusieurs heures dans les sous-régions (a) du Niger, (b) du Bénin et (c) de la Côte d'Ivoire pour toutes les saisons.

En règle générale, la fréquence élevée des événements persistants "High" SW^\downarrow identifiée sur la région ouest africaine pourrait être considérée comme favorable au développement de l'énergie solaire. Cependant, ce résultat peut être interprété de différentes manières selon le type et la taille (capacité) de la centrale photovoltaïque. Pour les petits systèmes photovoltaïques hors réseau sans stockage sur batterie, certaines demandes jusqu'à un certain nombre d'heures (par exemple, 3 heures) d'alimentation électrique (comme le pompage de l'eau dans un foyer ou un immeuble de bureaux) peuvent être effectuées fréquemment pendant la saison. Certaines de ces demandes en électricité (par exemple, le pompage de l'eau) ne sont pas effectuées tous les jours, et il est donc nécessaire de programmer les périodes où elles seront effectuées. Cette activité de programmation peut nécessiter de comprendre également la propagation de ces événements persistants de "High" SW^\downarrow pendant la saison. Cette question dépasse toutefois le cadre de cette étude, mais doit être étudiée. D'autre part, pour les grandes centrales photovoltaïques (connectées ou pas au réseau), les événements persistants de type "High" SW^\downarrow peuvent entraîner

une production d'électricité excessive, en particulier pendant les heures creuses. Cet excédent sera perdu à moins qu'il n'y ait une installation de stockage (par exemple, une batterie) pour stocker temporairement cette énergie excédentaire produite.

Impacts du changement climatique sur l'énergie solaire et ses moteurs

Cette section reprend les éléments significatifs du Chapitre 6.

Cette partie de la thèse explore l'intérêt et la pertinence des informations fournies par les modèles climatiques pour évaluer le potentiel futur de la production d'énergie solaire. Pour cela, nous avons utilisé les sorties de modèles de quatre modèles climatiques de l'exercice CMIP6 pour la période historique et leurs projections dans le cadre de la trajectoire SSP5-8.5. Les résultats de simulation de la période historique ont d'abord été évalués à l'aide des observations du satellite CERES. Une correction des biais quantiles-quantiles a été appliquée pour réduire les biais des modèles climatiques. La production potentielle d'énergie solaire sur l'AO, pour la période historique et pour les périodes futures, a été estimée à l'aide des sorties du modèle corrigées du biais. La série chronologique de la production d'énergie solaire (PVP) a été estimée à l'aide d'un modèle simple qui utilise l'irradiation de la surface et la température comme données d'entrée (Perpiñan et al., 2007). Les contributions individuelles de l'irradiance solaire (I_s) et de la température de l'air (T_a) aux changements futurs de la PVP sont également estimées. Pour ce faire, nous avons calculé la production future de PVP, en gardant l'une ou l'autre de ces variables (I_s et T_a) identique à celle de la période historique (c'est-à-dire en utilisant sa série chronologique historique) tandis que la série chronologique future de l'autre variable est utilisée.

Le calcul de la production d'énergie solaire pour la période historique et les périodes futures basées sur le scénario SSP5-8.5 nous a permis de déterminer les impacts possibles du changement climatique sur les futurs projets d'énergie solaire dans la région. Dans le proche avenir (Figure 18a), tous les modèles s'accordent sur la distribution spatiale du changement attendu de la PVP solaire sur l'AO. La PVP solaire diminuera jusqu'à -7 % dans la région, le sud de l'AO connaissant une diminution plus importante que la partie nord. Ceci est vrai pour tous les modèles ; cependant, le modèle MRI-ESM présente une diminution légèrement plus faible de la PVP solaire pour la période à venir. De même, les quatre modèles s'accordent généralement sur la distribution spatiale de la variation de la PVP solaire dans la seconde moitié du 21^e siècle (Figure 18b). Tous les modèles (sauf MRI-

ESM) montrent un net gradient sud-nord ; le sud de l'AO présentant une plus forte diminution de la PVP solaire dans le futur lointain. En effet, la PVP solaire peut diminuer jusqu'à environ -20 % à certains endroits de la côte guinéenne. L'ampleur de ce changement vu par MRI-ESM est cependant nettement plus faible que pour les autres modèles.

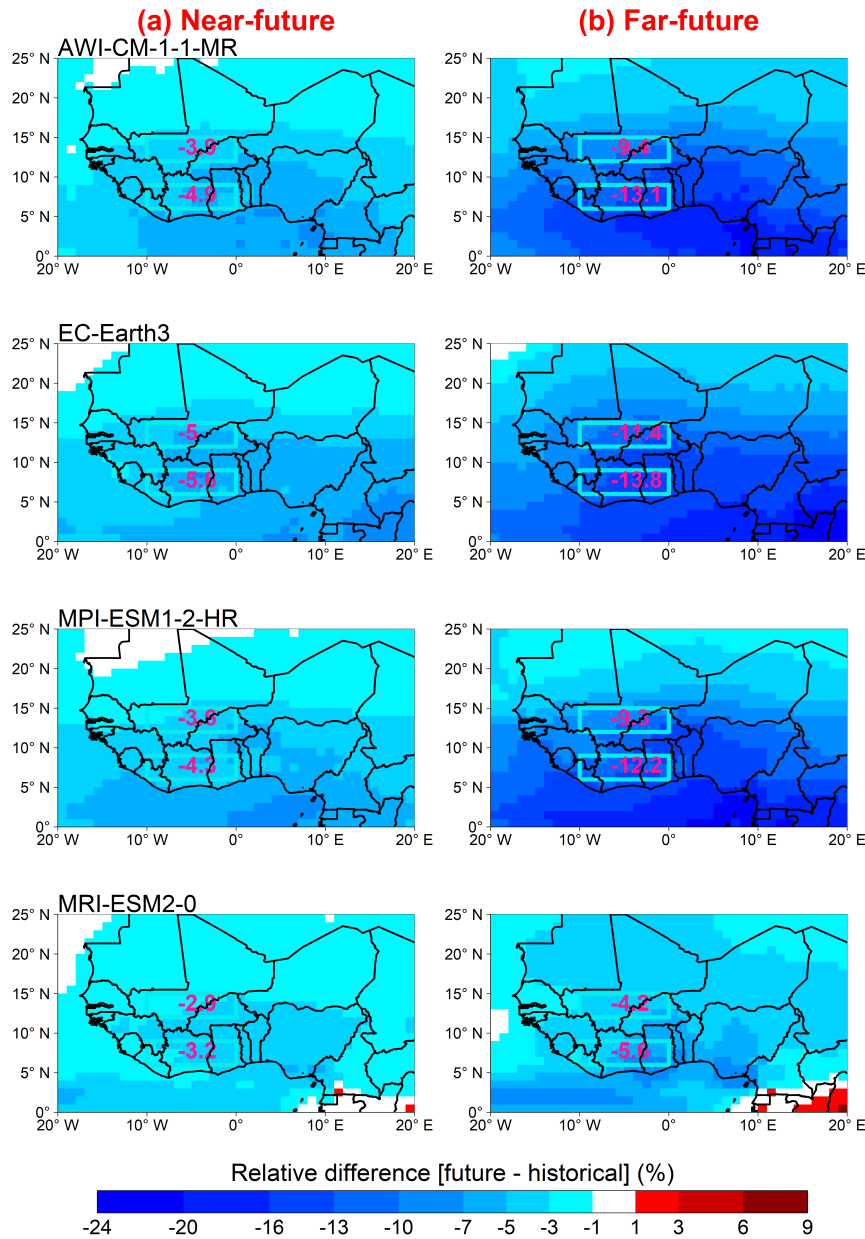


Figure 18: Par rapport à la période historique (1980-2014), variation de la production potentielle d'électricité solaire photovoltaïque annuelle moyenne (%) pour les périodes a) 2015 – 2049, nommée futur proche, et b) 2050 – 2084 référencée comme futur lointain pour quatre modèles CMIP6 dans le cadre du SSP5-8.5. La moyenne d'ensemble de chaque modèle est utilisée pour le calcul. Les valeurs indiquées en rose sont les changements moyens pour les sous-régions Guinée et Sahel.

Indépendamment de cette différence entre MRI-ESM et les autres modèles, en particulier pendant les mois d'été en futur lointain, les quatre GCM anticipent tous des tendances significatives à la baisse de la production de PVP solaire dans les régions de la Guinée et du Sahel (voir Chapitre 6). Les modèles AWI-CM, EC-Earth et MPI-ESM présentent toutefois des tendances à la baisse relativement plus prononcées que le MRI-ESM. En outre, la tendance à la baisse dans la fenêtre de la Guinée est légèrement plus marquée que dans la région du Sahel, et ce pour tous les modèles.

Quelque soit la fenêtre de projection (proche futur ; futur lointain), la réduction du potentiel d'énergie solaire sera la plus marquée pendant les mois d'été (Figure 19). Dans le futur lointain, le changement de la production d'énergie solaire PVP est principalement négatif tout au long de l'année, avec, comme précédemment indiqué, des diminutions plus importantes pendant les mois d'été dans les deux régions. En Guinée, la diminution de la PVP solaire moyenne en été atteint environ -40 % pour AWI-CM et MPI-ESM et -30 % pour EC-Earth. MRI-ESM, cependant, montre des diminutions significativement plus faibles de la PVP solaire future (entre -10 et 0 %) et de légères augmentations dans certains cas. Cela est également vrai pour la région du Sahel où les trois autres modèles s'accordent sur le signe et l'ampleur de la variation du PVP solaire tout au long de l'année. Il est important de noter les fortes valeurs négatives dans l'intervalle de confiance de -90 % pendant l'été pouvant atteindre environ -60 %, sauf pour MRI-ESM. En général, la réduction prévue de la production d'énergie solaire est importante et pourrait avoir des implications critiques pour la durabilité à long terme des projets proposés s'ils ne sont pas développés stratégiquement en tenant compte des effets possibles du changement climatique.

Bien que la température de l'air proche de la surface augmente considérablement à l'avenir, elle n'entraînera pas de changement significatif du potentiel d'énergie solaire sur l'ensemble de la région (Figure 20b). Cependant, l'irradiation à la surface, qui devrait diminuer, sera la cause principale des changements futurs du potentiel d'énergie solaire dans toute la région (Figure 20a).

La diminution prévue de l'irradiation à la surface est principalement due aux raisons suivantes :

- En général, tous les modèles prévoient une augmentation de la trajectoire de l'eau liquide du nuage (Figure 21). Ceci augmentera à son tour l'albédo des nuages dans la région, entraînant une diminution du rayonnement solaire incident.

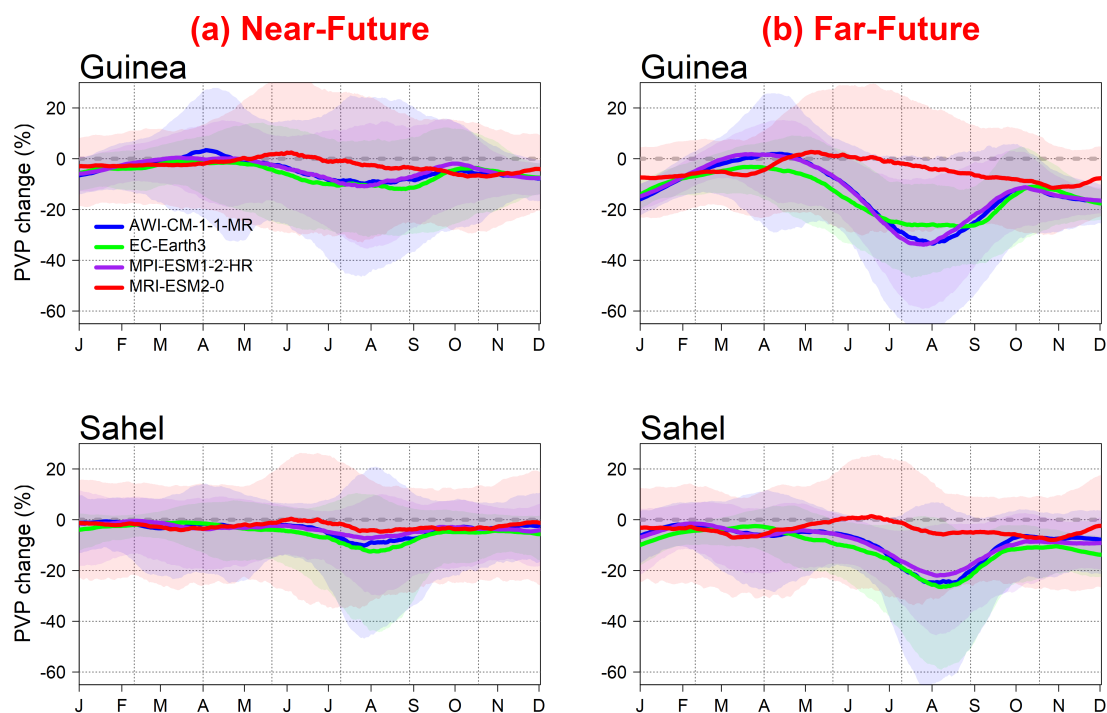


Figure 19: Changements relatifs du cycle annuel moyen de la production d'électricité solaire photovoltaïque (courbes solides) dans les sous-régions Guinée et Sahel en Afrique de l'Ouest. Les zones ombrées indiquent les 95^e et 5^e percentiles interannuels.

- La charge d'aérosols devrait également augmenter à l'avenir, ce qui renforcera les effets directs et indirects des aérosols. Cela semble avoir une influence significative sur le rayonnement solaire incident dans la région (Figure 22).

Ces résultats sont nouveaux à bien des égards. Tout d'abord, l'utilisation du CMIP6 pour évaluer les impacts du changement climatique sur le potentiel d'énergie solaire est unique dans la région. Les résultats obtenus montrent une diminution plus importante du potentiel d'énergie solaire par rapport aux études précédentes, qui étaient basées sur les sorties des modèles CMIP5. En outre, il s'agit de la première étude dans la région contribue à l'évaluation des changements de certains des facteurs (i.e. aérosols, l'eau des nuages) qui influencent les facteurs de production d'énergie solaire.

Conclusion et perspectives

Sont reprises ici les principales conclusions et perspectives, détaillées dans le dernier chapitre du manuscrit.

Les résultats de cette étude ont des implications directes sur l'implantation

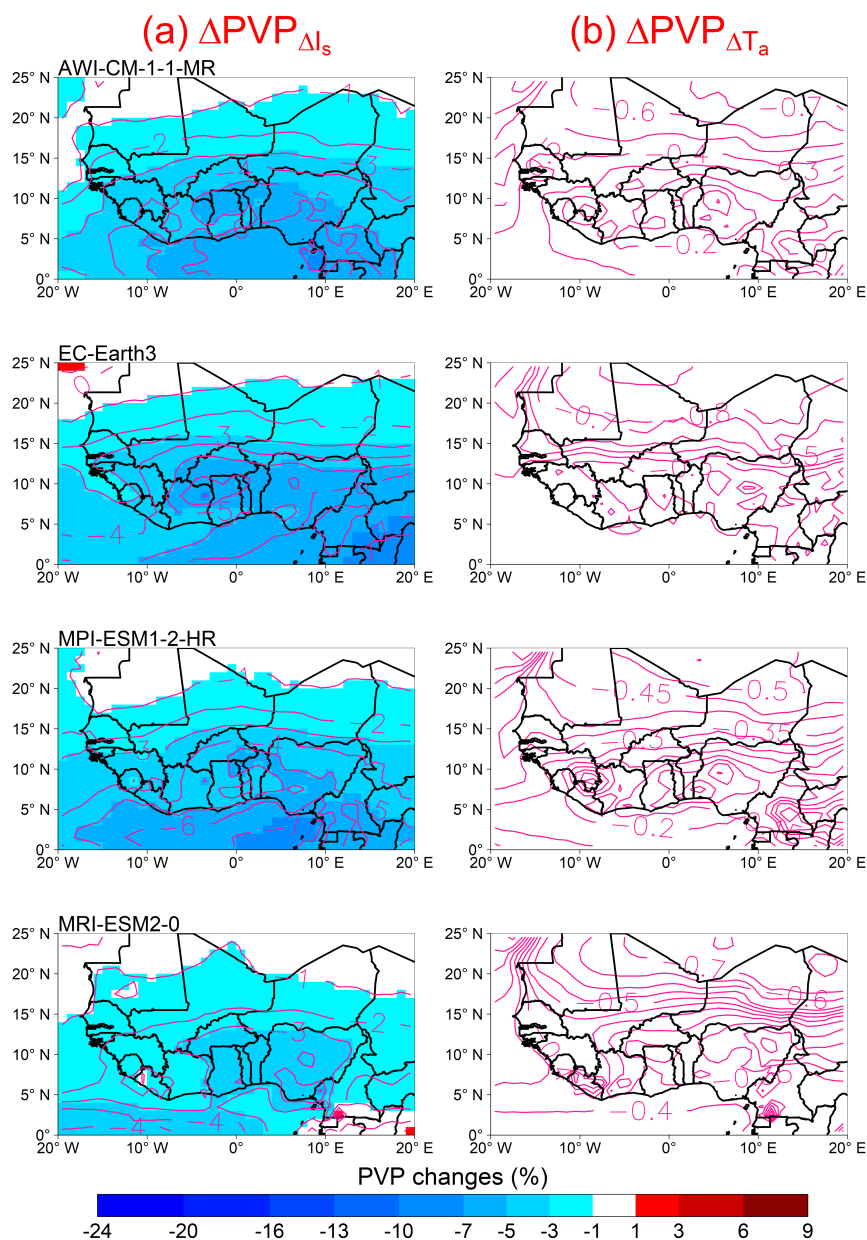


Figure 20: Par rapport à la période historique (1980-2014), variation de la production potentielle d'électricité solaire photovoltaïque annuelle moyenne (%) en tenant compte des changements projetés en période futur lointain (2050 - 2084) (a) de l'irradiation de la surface et (b) de la température de l'air proche de la surface pour quatre modèles CMIP6 dans le cadre du SSP5-8.5. Les courbes de niveau indiquent des valeurs de changement annuel moyen. La moyenne d'ensemble de chaque modèle est utilisée pour le calcul.

des fermes solaires dans la région ouest africaine. Par exemple, compte tenu des effets radiatifs élevés des nuages bas sur le rayonnement incident à courtes longueurs d'onde, les gestionnaires des fermes solaires pourraient décider d'installer ces systèmes de production électrique loin de la côte guinéenne, compte tenu de la persis-

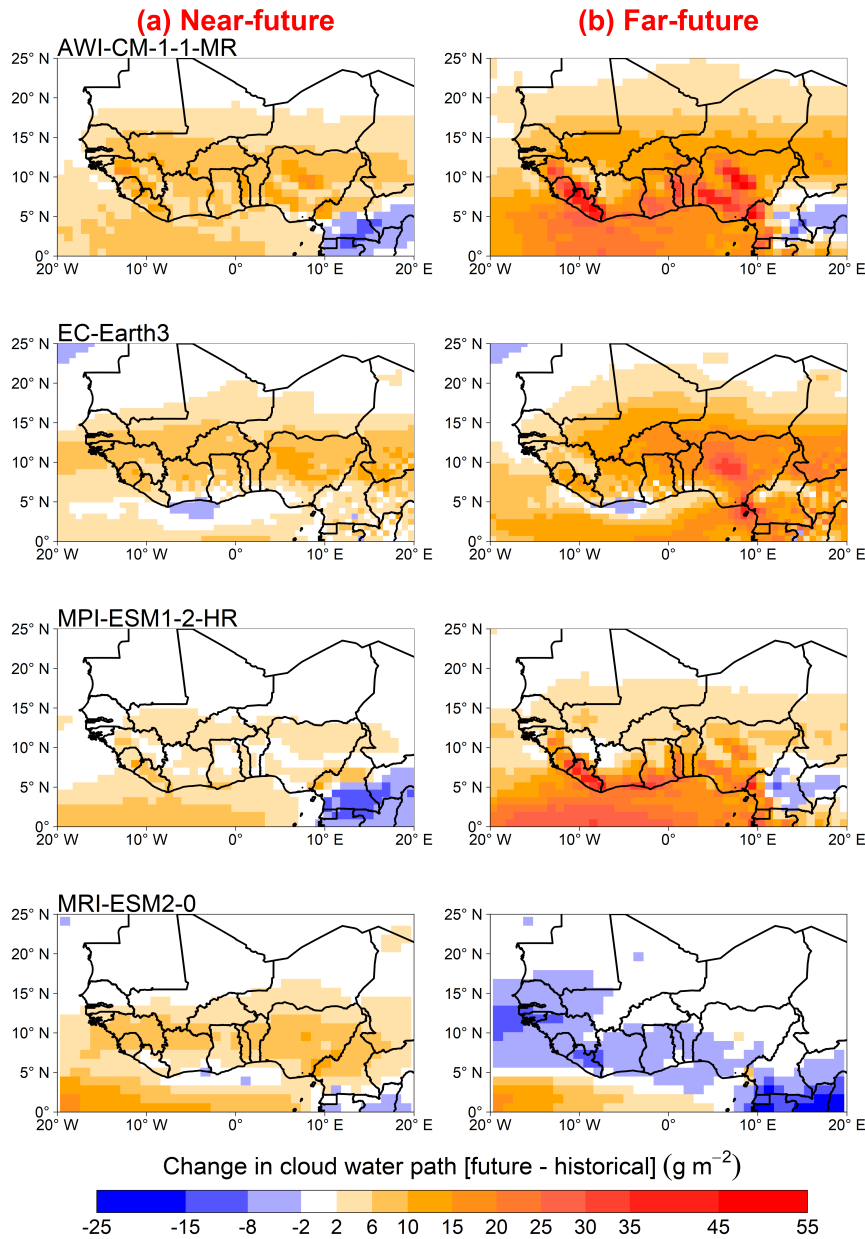


Figure 21: Différence moyenne annuelle (futur moins historique) de l'eau liquide des nuages pour (a) la période de futur proche (2015 - 2049) et (b) la période de futur lointain (2050 - 2084) pour quatre modèles CMIP6 dans le cadre du SSP5-8.5.

tance de ces nuages dans cette région. Associé à une occurrence simultanée des trois types de nuages (LLC, MLC, HLC), ces installations photovoltaïques solaires localisées dans cette région seraient susceptibles de produire un très faible pourcentage de leurs capacités nominales pendant de longues périodes. Ceci est particulièrement vrai pendant la saison humide, de mousson, en raison de l'intensification des nuages et de l'augmentation de la fréquence d'apparition simultanée des trois types de nuages. La région du Sahel et les parties nord de l'AO semblent plus favor-

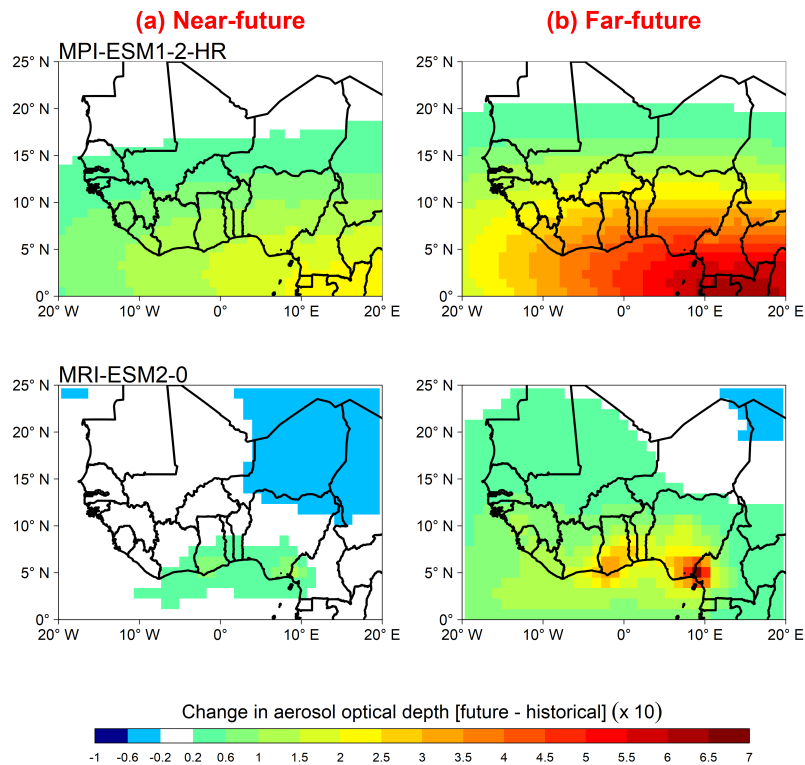


Figure 22: Différence moyenne annuelle (futur moins historique) de l'épaisseur optique à 550nm pour (a) la période de futur proche (2015 - 2049) et (b) la période de futur lointain (2050 - 2084) pour quatre modèles CMIP6 dans le cadre du SSP5-8.5.

ables à l'implantation de grandes fermes solaires en raison de la faible fréquence d'occurrence des nuages et de leurs couvertures sur cette région. Cependant, ces régions sont soumises à d'autres facteurs impactants la production énergétique solaire, notamment les particules de poussière provenant du désert du Sahara, qui peuvent bloquer le rayonnement et se déposer sur les panneaux solaires réduisant ainsi la production d'électricité. Cette problématique n'a pas été directement abordée dans cette étude.

Des perspective d'amélioration directe de l'étude pourrait être d'utiliser les observations de surface qui restent encore très parcimonieuses en AO. Un enjeu pourrait donc être de proposer des cadres nécessaires pour acquérir, sur le long terme, des observations de surface et des propriétés des nuages dans cette région.

D'une manière plus directe, d'autres produits de données disponibles pourraient être comparés aux résultats de notre étude. Certaines mesures de campagnes de terrain disponibles pourraient également être intégrées dans les systèmes de prévision afin d'améliorer les prévisions dans des produits comme ERA5. Elles pourraient également être utilisées pour évaluer les observations par satellite ou les résultats des simulations de modèles climatiques.

Les types de nuages dans les réanalyses ERA5 (et CERES) sont classés par catégories à l'aide de couches stratifiées. Cela signifie que tous les nuages qui se produisent dans une couche donnée (par exemple, à basse altitude) sont classés comme un seul type de nuage. Bien que cette approche soit commune à la plupart des modèles et produits satellites, elle peut conduire à un mélange de différents systèmes de nuages à considérer comme un seul type. Comme les systèmes nuageux d'une même catégorie pourraient avoir des propriétés radiatives différentes, les études futures pourraient étendre ce travail en isolant les différents systèmes, en développant leur climatologie et en estimant leurs propriétés radiatives.

Ces travaux ont fourni des informations importantes sur l'occurrence des nuages et la manière dont ils affectent le rayonnement de surface. Cependant, les aérosols ont également des impacts critiques sur le rayonnement incident et l'efficacité des panneaux solaires. Une amélioration possible de l'étude consistera donc à déterminer les effets radiatifs combinés des nuages et des aérosols sur le rayonnement solaire incident. Cela permettrait d'obtenir une représentation globale plus complète des impacts de l'atmosphère sur l'irradiation à la surface et proposerait donc ainsi un cadre plus intégré pour toutes études de planification et de mise en oeuvre de fermes solaires. On pourrait également envisager de développer une climatologie et de déterminer les effets radiatifs des différents types d'aérosols dans la région.

Une autre perspective importante de ce travail consisterait à quantifier les incertitudes associées aux scénarios des projections futures sur la production électrique solaire. En effet, dans ce travail, nous nous sommes limités à la seule trajectoire SSP5-8.5. Bien entendu, d'autres trajectoires de développement sont proposées par la communauté internationale, et nous disposons des sorties de modèles CMPI6. Des études futures pourraient alors comparer les projections basées sur d'autres voies de développement plus optimistes que celle choisie dans le cadre de cette thèse. Une telle étude aiderait, si besoin est, à démontrer l'apport d'une démarche plus sobre en énergie carbonée sur le développement socio-économique de populations aujourd'hui très vulnérables et donc qu'un développement durable à l'échelle planétaire n'est pas impossible.

Chapter 1

Introduction

1.1 In the race toward a sustainable world: The role of the energy sector

1.1.1 Global climate change and energy

It is a collective belief that human-induced global warming and its consequent changes in the climate, poses one of the greatest threats to life on earth. Since the late 19th century, the global average surface temperature has risen by approximately 1°C (Stocker et al., 2014). This warming is due to an increase in the concentration of greenhouse gases such as CO_2 , which trap heat near the surface of the earth. Increasing greenhouse gas concentrations are largely due to human activities and account for more than half of the observed global average temperature rise (Bindoff et al., 2013). The current warming rate is projected to increase further in the future if the historical anthropogenic greenhouse gas emission trends continue (IPCC, 2014).

Among the various anthropogenic activities, the energy sector is deemed the largest contributor to global greenhouse gas emissions (Bruckner et al., 2014), responsible for nearly two-thirds of all emissions (Figure 1.1). This is primarily due to the combustion of fossil fuels for various activities such as electricity generation and transportation, which consequently emits CO_2 into the atmosphere. According to a report by the International Energy Agency, global CO_2 emissions from the energy sector increased by 1.7 % in 2018 to reach a record high of 33.1 Gt CO_2 (IEA, 2019b). This rise in emissions was attributed to higher energy consumption largely due to economic and population growth around the world. The report also noted that, about half of increase in energy demand emerged from the power sector, in response

in higher electricity consumption. In the power sector, electricity generation from coal- and gas-fired power plants (i.e., conventional production methods) alone was responsible for 38 % of the total energy-related CO₂ emissions in 2018 (IEA, 2019b).

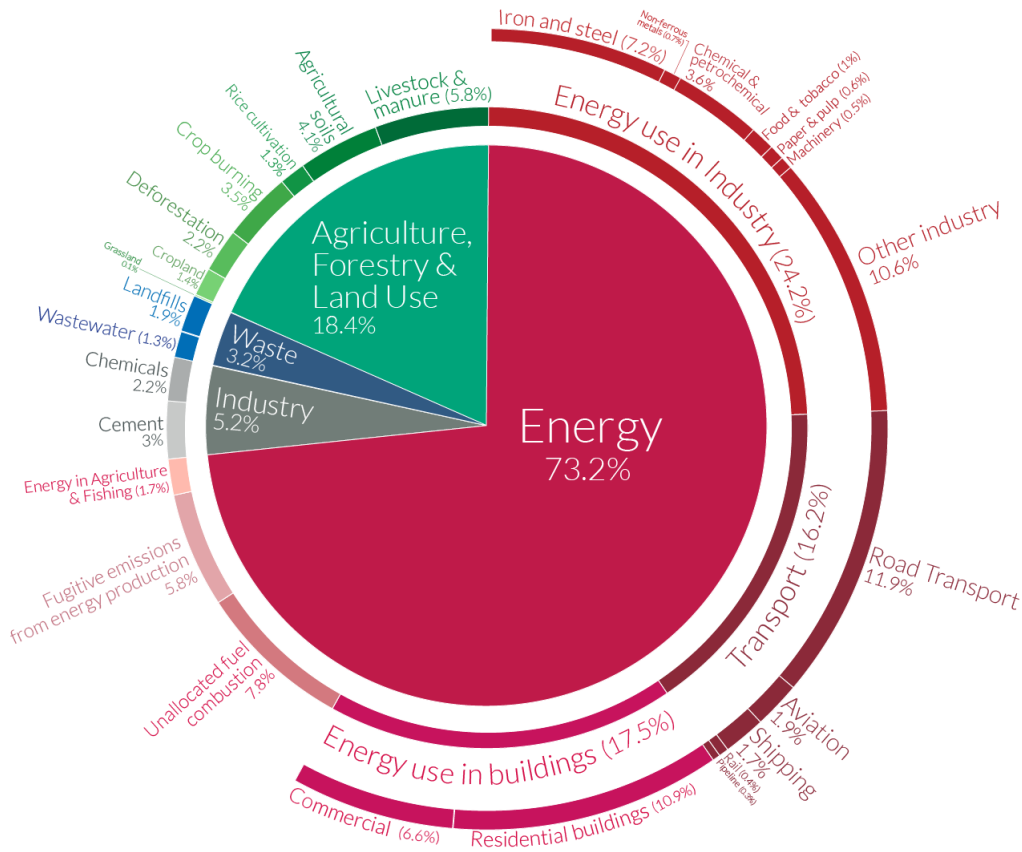


Figure 1.1: Global greenhouse gas emissions by sector. This is shown for the year 2016. Source: Climate Watch, the World Resources Institute (Ritchie, 2020).

The continuing economic growth and development around the world mean that demand for electricity will also increase (Bedi & Toshniwal, 2019). Using conventional methods to supply this expected increase in electricity demand will further escalate the concentration of greenhouse gases in the atmosphere. The world is already experiencing severe impacts of global warming such as rising sea levels, extreme climate events and water stress. These may intensify in the future if the global surface temperature rises further due to additional greenhouse gas emissions in the atmosphere. In addition, the impacts of global warming may lead to severe economic harm in the long-term (Wade & Jennings, 2016). In a nutshell, electricity generation is imperative if nations keep developing. However, how could nations develop in a more sustainable way without having to increase the concentration of greenhouse gases in a world that is already warming at an unprecedented rate?

1.1.2 Responses to the warming climate

To avoid severe climate change due to the warming of the earth's surface, major changes are required. Over the years, many decisions have been taken at the global scale as a response to the observed and projected global warming. As a first step to address the climate change problem, the United Nations Framework Convention on Climate Change (UNFCCC) was formed in 1992 by the United Nations. The goal of the convention was to prevent all human interferences with the climate system that are deemed dangerous (Bodansky, 1993). From the UNFCCC came the Kyoto Protocol, formed in 1997, which legally binds the world's most industrialized and developed countries to emission reduction targets (Böhringer, 2003).

On the back of experiencing one of the warmest decades on record, world leaders made the Paris Agreement in 2015 to combat climate change. The Paris Agreement aimed to limit the global temperature rise in the 21st century to no more than 2°C and further pursue efforts to limit the rise to a more ambitious target of 1.5°C . This ambitious target requires drastic changes, especially from the energy sector, to cut down greenhouse emissions.

1.1.3 Reducing emissions in the energy sector: The Paris Agreement

The 21st session of the Conference of Parties to the UNFCCC (COP21), which led to the negotiation of the Paris Agreement highlighted the need for drastic measures to limit global greenhouse emissions. In the energy sector, there was a general consensus that the world needs to significantly transform the way it produces and uses energy in order to have a chance to meet the 2°C warming limit of the agreement. Large shares of renewable electricity production such as wind energy and solar photovoltaic (PV) power, has to be integrated into power systems to meet the expected increase in electricity demand and to gradually limit production from the fossil-based conventional power plants (UNFCCC, 2015). The carbon capture technology (Wilberforce et al., 2019) was also touted as a possible way of directing extracting and reducing the concentrations of CO_2 in the atmosphere. The large-scale feasibility of such technology, however, remains uncertain.

The Paris Agreement requires all countries in the world to take actions to limit their emissions of greenhouse gases. However, due to the different situations and conditions in each country, the agreement provided the opportunity for each to submit their own Intended Nationally Determined Contributions (INDC) (Rogelj et al., 2016). Through these INDCs, all nations, including West African countries,

committed through the intended actions, to reduce greenhouse gas emissions.

1.1.4 West Africa’s commitments: Aftermath of the Paris Agreement

The greenhouse gas emission levels by countries in sub-Saharan Africa are just a tiny fraction of that of the industrialized countries (Arto & Dietzenbacher, 2014; Ritchie & Roser, 2017). Nevertheless, the "no boundary" nature of the impacts of global warming and climate change means that countries in West Africa (WA) are committed to decarbonizing their economies. In the power sector, countries in the region are committed to adopt a development strategy that will lead towards a decarbonization of the various national economies. Through the vision of the African Agenda 2063 (AU, 2015; DeGhetto et al., 2016), the shares of renewable electricity production will be significantly increased. Solar and wind power are projected to increase to 24 % and 6 % respectively by the end of 2040, a significant increase from their combined current contribution of less than 1 % (IEA, 2019a).

Many industries and countries in WA have already initiated renewable energy development projects since the 2015 Paris Agreement (Aliyu et al., 2018; Elum & Momodu, 2017; Ikejemba et al., 2017). Solar energy especially has received much attention in the WA region in the transition towards cleaner and sustainable electricity generation practices.

1.2 Solar energy in West Africa

The recent escalation of interest in developing solar power plants in WA is not only due to the need to satisfy increasing electricity demand in a sustainable way but also the abundance of the solar resource in the region. Solar radiation maps developed from long term observations (ESMAP, 2020) show that, the region receives a high amount of horizontal irradiation (Figure 1.2) and well as direct normal irradiation (Figure 1.3) for developing solar PV plants as well as concentrated solar power (CSP) systems respectively. There is a general recognition and consensus that, this potential can be developed on a large-scale to produce electricity in the region. In addition, investment in solar energy development in the region can be economically attractive.

As a result, some countries in WA form part of the largest solar markets in the whole of Africa (Tiyou, 2017). There are several active plans by the countries to develop the solar energy potential in the region. The plans for development range from large-capacity power plants that will feed into the electricity grid (Lee

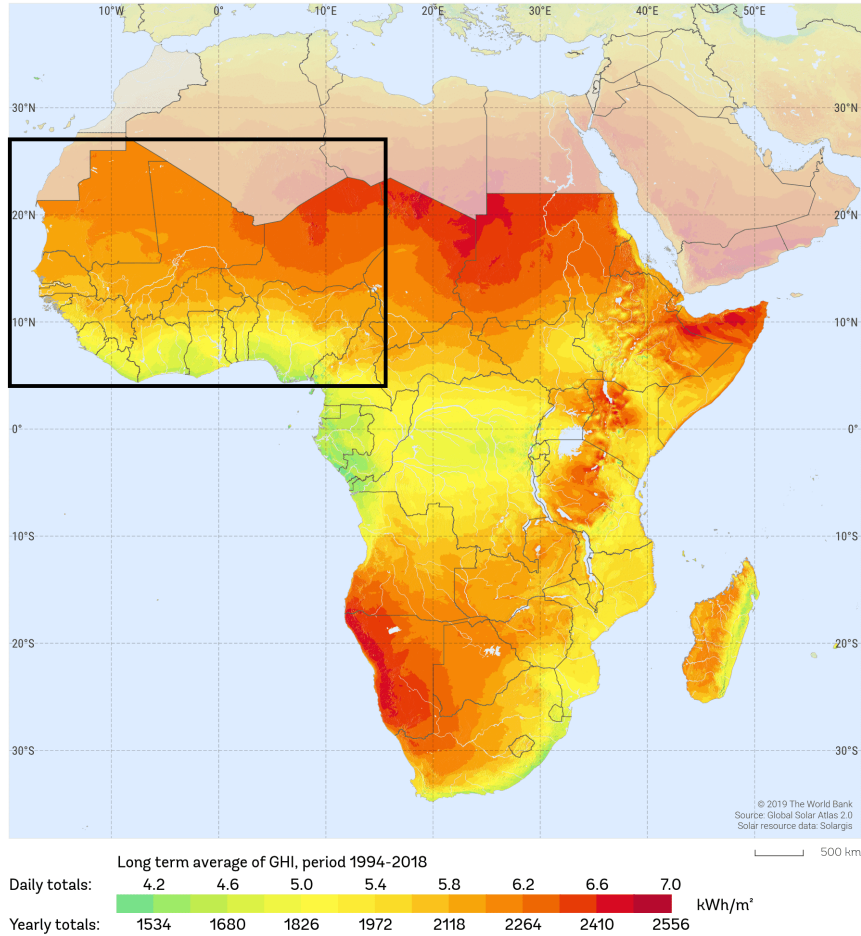


Figure 1.2: Climatology (1994 – 2018) of global horizontal irradiation (GHI) in sub-Saharan Africa. The black box shows the location of West Africa. *Source:* Global Solar Atlas, owned by the World Bank Group and provided by Solargis.

& Callaway, 2018; Mas’ud et al., 2016) to smaller scale solar projects such as off-grid rural solar electrification (Baurzhan & Jenkins, 2016; Moner-Girona et al., 2018; Odou et al., 2020) and rooftop solar power generation (Enongene et al., 2019; Kanteh Sakiliba et al., 2015). Countries like Burkina Faso and Ghana currently house some relatively large solar PV power plants in the region. For example, the 33 MW Zagtouli power plant in Burkina Faso is currently the largest operational solar PV plant in the region (Moner-Girona et al., 2017). In Ghana, there is a 20 MW total capacity for operational solar power generation and a 155 MW solar power project, which will be the largest single solar plant in Africa when completed, is currently underway (Kuwonu, 2016). There are many other projects that have been approved or being discussed in countries like Cote d’Ivoire, Nigeria and Senegal (e.g., MPEER (2014)).

Despite the high resource availability, the current investment in the develop-

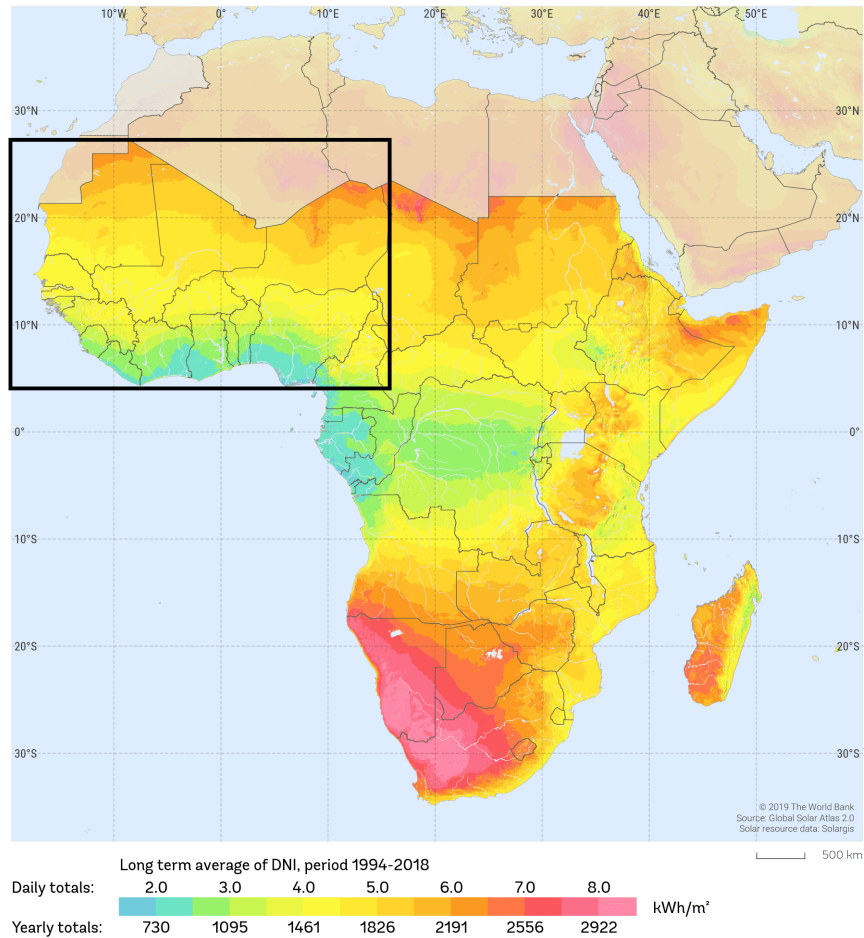


Figure 1.3: Climatology (1994 – 2018) of direct normal irradiation (DNI) in sub-Saharan Africa. The black box shows the location of West Africa. *Source:* Global Solar Atlas, owned by the World Bank Group and provided by Solargis.

ment of solar power is very low. Although expected to increase in the future (AU, 2015), the current development and contribution of solar power plants to total electricity generation in all of sub-Saharan Africa is very low (less than 1% as shown in Figure 1.4) (IEA, 2019a). This could be attributed to drawbacks from technical, economic or climate (meteorological) related challenges. Some of these challenges could be linked and lead to many uncertainties regarding solar power production in the region. The focus in this work will be on the climate related challenges and the associated uncertainties for solar energy development in WA.

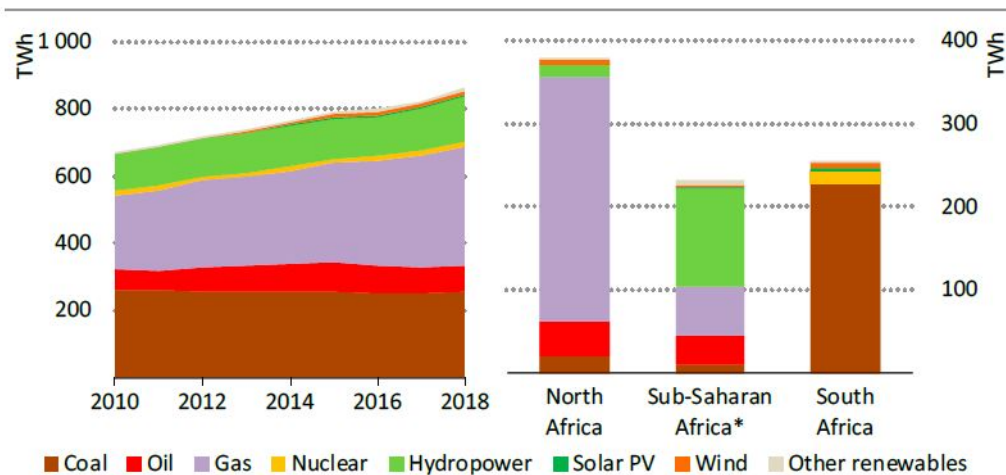


Figure 1.4: Electricity generation (TWh) by fuel type in Africa (left) and different regions of Africa (right) in 2018. *Source:* IEA (2019a) Africa Energy Outlook 2019. All rights reserved.

1.3 Meteorological factors for planning and developing solar energy

The solar radiation received on the earth’s surface is controlled by the evolution of some climate-related variables such as clouds and dust. Additionally, the power generated by solar PV panels is dependent on the air temperature (Dubey et al., 2013), humidity in the atmosphere (Ghazi & Ip, 2014), as well as dust accumulation (Bonkaney et al., 2017). It is important to understand the space-time evolution of these factors in order to make good decisions in the planning of large-scale solar energy development and implementation. The main focus of this thesis will be on clouds and, to a smaller extent, the impacts of changes in temperature on solar power production. In this section, issues of cloud cover and their related uncertainties in WA are introduced.

1.3.1 Uncertainties related to cloud cover

When present, clouds impact the energy budget of the earth by blocking part of the incoming shortwave radiation from the sun or the outgoing longwave radiation from the surface (Bartlett et al., 1998; Hartmann, 1993). The presence of clouds can lead to a significant decrease in the surface irradiance (black curve in Figure 1.5) and hence, the production of solar power from PV panels. Additionally, the sub-hourly variation of cloudiness is inherited partially by the surface solar irradiance (and the solar PV power produced) (Engeland et al., 2017). Thus, on a clear day, the profile of the received surface solar irradiance follows a smooth curve steadily increasing

from the morning to the afternoon and then decreasing afterward into the evening (red curve in Figure 1.5). However, on a cloudy day, the profile is intermittent with many fluctuations as illustrated in Figure 1.5. For grid-connected solar power plants, the fluctuations in power production present serious technical challenges to the managers of the electricity grid (Obi & Bass, 2016). It is therefore important to understand the nature of clouds and their impacts on the incoming solar irradiance to enable the successful integration of utility-scale solar power production in the grid.

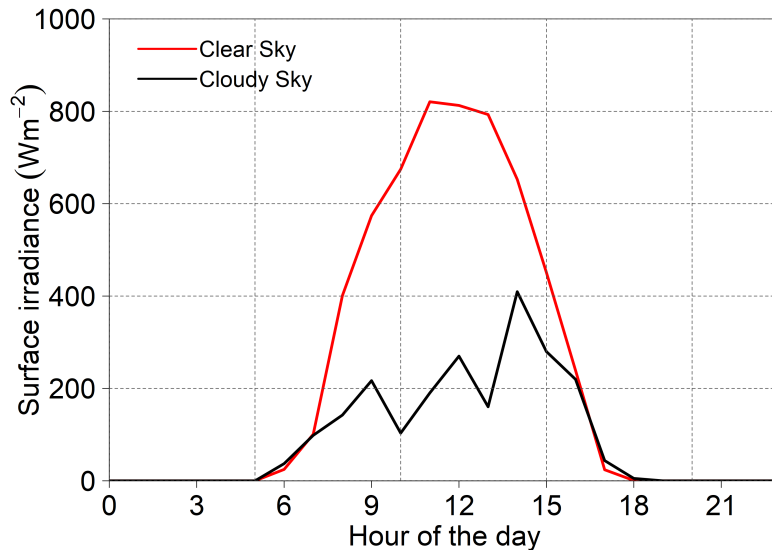


Figure 1.5: Typical profiles of surface solar irradiance in clear and cloudy conditions.

However, very few studies have in the past attempted to address this issue essential for any feasibility study of solar energy production in WA (Dajuma et al., 2016; Ohunakin et al., 2015). In general, the meteorology of the region is rather complex, with contrasting climate characteristics across the different zones. For example, over 80 % of rain during the wet season in the Sahelian zone (northern WA) is due to the mesoscale convective systems (MCS) advected from east to west (Klein et al., 2020). However, the Guinean zone (southern WA) conversely experiences i) local convection associated with the state of the continental surface, ii) low cloud layers associated with moisture flux from the Guinean Gulf, and iii) deep convected clouds advected from east to west (Adler et al., 2011; Maranan et al., 2018; Sassen et al., 2009).

These cloud systems mainly drive the variability of the atmospheric reflectivity that controls the amount of solar irradiance received in the region. They are, however, not well understood. To a large extent, this could be attributed to the lack of observations (Knippertz et al., 2015) in the region. Besides, previous Global Climate Models (GCMs) outputs poorly reproduce cloud systems in this region, in

particular the low-level convective clouds (Hannak et al., 2017). Usually, this is explained by the lack of proper representation of the processes in the atmospheric boundary layer as well as the land-ocean flux gradients that drive the occurrence and evolution of cloud systems in the region.

Consequently, a climatology of the occurrence and variability of clouds based on a long-term data record is still missing in the region. Furthermore, the quantitative impact of clouds on the incoming solar radiation is unknown in most areas in WA. Also, it is currently not clear how climate change will impact the atmospheric reflectivity and absorptivity of the region in the future. As a result, there are many open questions when discussing the variability of atmospheric reflectivity and/or absorptivity due to cloud cover and its potential impacts for utility-scale development of solar power in WA. This could partly explain why solar power development in the region is low despite the huge potential.

1.3.2 Other factors

Clouds mainly influence the incoming solar radiation but other climate-related variables can affect the efficiency of the solar PV cells or panels. Higher air temperature tends to reduce the conversion efficiency of PV cells (Furkan & Mehmet Emin, 2010; Omubo-Pepple et al., 2009; Zhang et al., 2015). Dust accumulation on PV panels is also known to reduce the power output and gradually leads to a degradation of the conversion efficiency of the PV cells (Sulaiman et al., 2011). With part of the Sahara Desert in WA, dust remains a significant source of technical challenge for solar power production. Dust in the atmosphere can also block a fraction of the incoming solar radiation, although their effect may not be as large as clouds (Highwood & Ryder, 2014; Solmon et al., 2012). Moreover, biomass burning activities in the region (and other remote areas) emit aerosol plumes in the sky, which also impacts the incoming solar radiation (Dajuma et al., 2020; Denjean et al., 2020). Additionally, some studies have found humidity can also affect the efficiency of solar PV cells (e.g., Rahman et al. (2015)).

1.3.3 Key open questions

The issues with the above challenges of climate-related variables pose serious open questions that are yet to be properly addressed. The presently low implementation of solar power in the region despite the high potential could partly be due to the many open questions. Some investors may be reluctant to massively invest in the solar energy potential of the region without a proper scientific investigation and documentation of the nature of the various climate-related challenges. Such docu-

mentation will be needed to assess the long-term feasibility and to prepare efficient management approaches to integrate large shares of solar power in the region. It could then help to alleviate the fears of the risks related to a massive investment in the development of solar power plants.

In such context, this work will seek to address some important scientific questions related to weather-related variables. The focus of this thesis will mainly be on cloud cover as it has the most significant influence on the atmospheric reflectivity and/or absorptivity that controls the incoming solar radiation. Clouds present the highest uncertainty because our understanding of the processes and drivers that trigger their occurrence and evolution in the region is still relatively low. This uncertainty is further compounded by the lack of long-term surface-based observation in the region.

The uncertainties associated with cloud cover, in addition to its influence on atmospheric reflectivity and/or absorptivity, lead us to the following questions that will be addressed in this PhD thesis:

1. How frequently and in what synoptic conditions do clouds occur and evolve in West Africa?
2. What are the effects of the occurrence and evolution of clouds on the incoming solar radiation?
3. How will climate change affect solar power generation and its atmospheric drivers?

1.4 Summary of research goals

Based on the background and research questions presented above, the goals of this thesis are summarized below. The organization of the thesis follows directly from these research goals:

- **How frequently and in what synoptic conditions do clouds occur and evolve in West Africa?**

For the first part of this question, the idea is to characterize the space-time occurrence and variability of different cloud types in WA. Here, the diurnal and seasonal variabilities of clouds will be investigated using a relatively long-term dataset. The focus will be on the entire region but also on contrasting areas to identify differences in cloud characteristics over the region. In the end, a climatology of clouds' occurrence and variability (diurnally and seasonally)

in the region will be presented.

The second part of the question will focus on low clouds and analyze the synoptic environments in which they occur. Various atmospheric processes will be analyzed to identify the drivers of low cloud occurrence. Additionally, the interaction of the low clouds with the earth's surface heat fluxes will be examined.

- **How will the presence of clouds affect, quantitatively, the amount and variability of the incoming solar irradiance?**

Here, the percentage of incoming solar radiation that is blocked from reaching the surface by clouds will be estimated. Furthermore, the variability of the received surface radiation will be analyzed and quantified. Also, the persistence of various sky conditions and different surface radiation classes will be quantified. This information is useful for the management of solar farms and will be provided as a climate service to stakeholders of solar energy development in WA.

- **In the future, how will climate change impact the main climate-related variables that control solar power production?**

The goal of the final part of this thesis is to assess the potential impacts of climate change on the future feasibility of solar energy generation in WA. Future projections of cloud cover and temperature will be used to assess the possible changes in the incoming radiation and the conversion efficiency of the solar PV cells, respectively.

1.5 Thesis outline

Chapter 2 will present a detailed research framework. Here, the study region, various datasets used, and their evaluation will be presented. The main results of this thesis will be presented in Chapters 3–6. Each of Chapters 3–6 will address, in that order, one of the four research questions outlined in section 1.4 above.

In collaboration with my advisors and other researchers, the results for the first three questions have already been published in three different scientific journals. My specific contribution to each of the three articles will be detailed at the beginning of the respective chapter. The main results of the final question will also be submitted for publication.

Chapter 7 will conclude the work with a summary of the main findings and

their implications for the solar energy sector in WA. Additionally, some directions for future work will be provided.

Chapter 2

Research framework

In a very general depiction, each of the research questions of this study will be answered by following four main steps as illustrated in Figure 2.1. It will first start with the delineation of the study area. Although the spatial domain of the study is WA, results of analysis over different areas in the region will be compared. The identification of various datasets and variables will be the next steps after which different computations and analysis will be carried out.

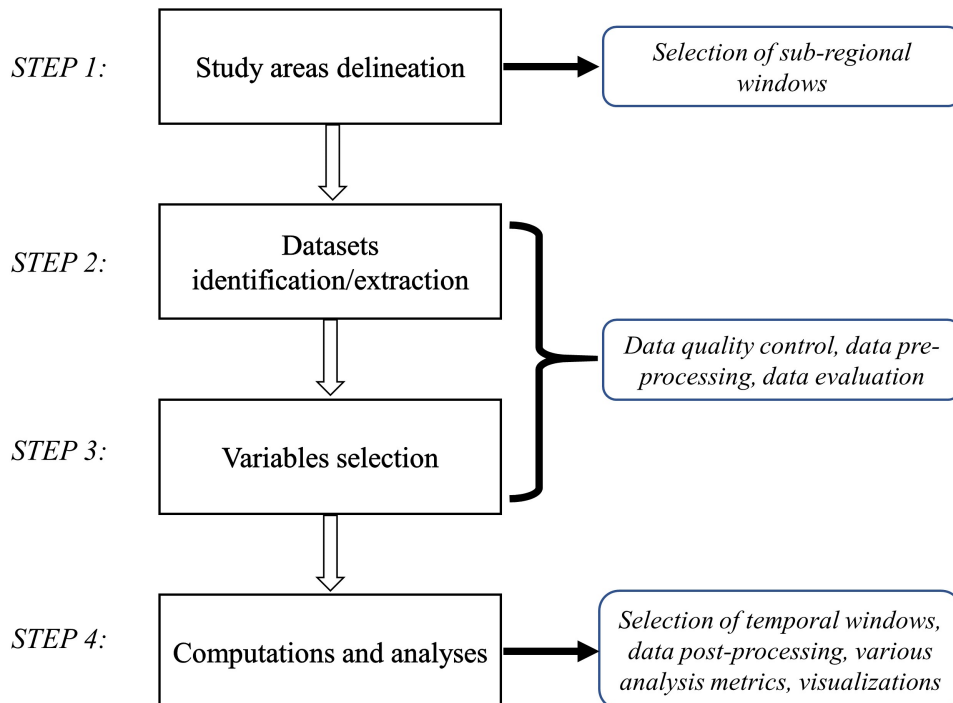


Figure 2.1: Universal 4-step approach to answer all research questions.

This "universal" approach will be followed to answer the research questions of this thesis; however, each question may entail a different approach throughout the steps.

This chapter will first present the study region of interest. The different concepts that will be explored to answer those questions in the study region will be introduced. Then the used data products will be presented. Their evaluation will finally be given.

2.1 Region of interest

The study is performed over mainland WA, with spatial boundaries from latitude 4° N to 25° N and longitude 20° W to 20° E (Figure 2.2). The WA region occupies an area over 6 000 000 km² at the western most part of Africa along the Atlantic Ocean. To the south, Benin, Cote d'Ivoire, Ghana, Nigeria, and Togo share a boundary with the Gulf of Guinea. The North Atlantic is the boundary of the western part of the region while Cameroon and Chad bound the eastern part. The northern countries of Mali, Mauritania, and Niger share boundaries with the parts of the Sahara Desert in North Africa. The majority of the WA region lies below 400 m (*a.s.l.*). However, there are also several highlands across the region, notably in the western part of the region in Guinea, the desert highlands in the northeastern part of the region, and some parts of northern Nigeria (Figure 2.2). Major land use and land cover types in WA include forestland, vegetations, wetlands, croplands, water bodies, and human settlements (Abiodun et al., 2012; Asenso Barnieh et al., 2020).

WA has a dual climate system comprised of wet and dry seasons. This is primarily controlled by the West African Monsoon (WAM) (Gu & Adler, 2004). The WAM is a major wind system that represents the interaction of two major migrating air masses. From November to February (winter time), hot and dry continental air mass blows from the Sahara Desert over most of WA due to the presence of a strengthened anticyclonic circulation. This northeasterly dry and dusty wind is known as the Harmattan. In the summer, the Harmattan is replaced by southwesterly monsoon winds that transport moisture from the Atlantic Ocean into the region. These moisture-laden air masses from the ocean feed the annual rainfall of the region (Nicholson, 2013). Depending on the region, the interannual variation of the WAM determines the difference between a year with sufficient rain and one with a drought (Fink et al., 2017).

Trade winds from the Northern and Southern hemispheres converge near the equator. At all times, the meeting point of these winds is a belt of variable width and stability called the Intertropical Convergence Zone (ITCZ). Over WA, it is locally called the Intertropical Discontinuity (ITD). It is the confluence region of the dry continental air mass from the Sahara and the moist monsoon air from the south Atlantic. The north and south movement of the ITD controls the amount

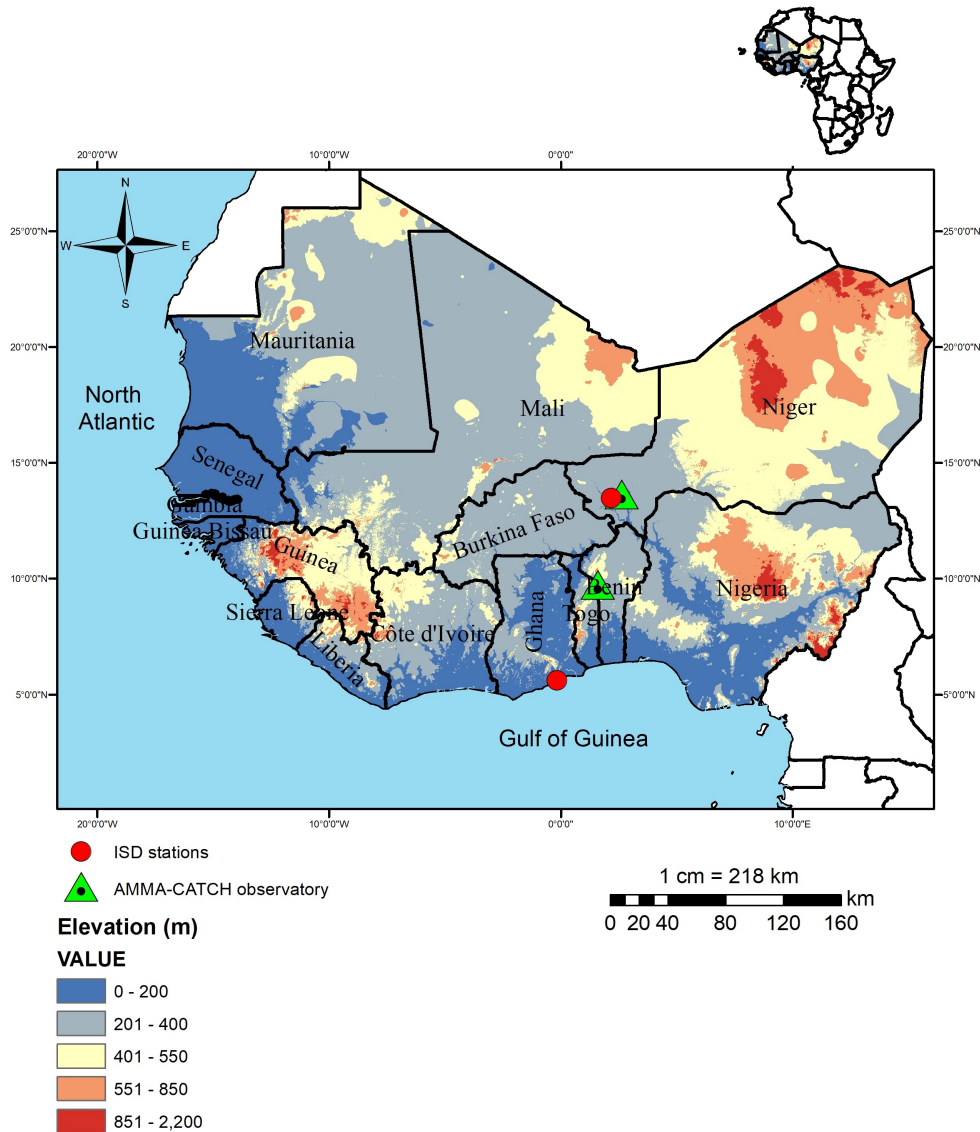


Figure 2.2: Elevation map of mainland West Africa, the study region. Also shown are the locations of some meteorological observation stations. Data from these stations are used for evaluation in this study.

and variability of rainfall in the region (Ferguson, 1985). Areas south of the ITD are characterized by rainfall in latitudinal belts of decreasing amounts while dry conditions are found in the north. The rainfall regime is characterized by latitudinal belts of decreasing rainfall and wet season length. These latitudinal belts of rainfall give rise to different climate zones (or vegetation zones) across the region (Fink et al., 2010a). North of 12.5° N is an arid climate zone named the Sahel. Near the Gulf of Guinea is the Guinean zone (or Guinea Coast), where the climate is mostly humid. Between the Sahel and the Guinea Coast, is the Sudanian zone with a sub-humid climate.

Most areas at the Guinea Coast receive abundant rainfall during the year with a short and less-marked dry season. Rainfall at higher latitudes is lower and is limited to a shorter wet season duration. Altitude modifies the latitudinal pattern of rainfall in some parts of WA with the high elevation areas of Guinea (Guinean Highlands) and Nigeria (Jos Plateau) receiving high rainfall amounts than lowlands of the same latitude (CILSS, 2016). Along the south-north gradient of decreasing rainfall, areas at the Guinea Coast records mean annual rainfall between 1200 mm to upwards of 2500 mm, while the Sahel region receives between 700 mm and 200 mm (Fink et al., 2017). Surface temperatures in the lowlands of WA are high throughout the year, with annual means usually above 18 °C. In the Sahel, maximum temperatures can reach above 40 °C (CILSS, 2016).

In this study, the focus will be on the whole of the WA region. However, special attention will also be given to some climate zones. A comparison of the cloud cover characteristics will be made for certain areas in the region. Details of the different areas that will be further analyzed, as well as the criteria for the selection of those areas, will be provided in the next chapters.

Over the study region, the cloud occurrence frequency and variability of various cloud types will be analyzed. Given an N number of data points of observations, the cloud occurrence frequency is simply defined as:

$$\text{cloud occurrence frequency} = \frac{n_{cld_events}}{N} \times 100 \quad (2.1)$$

where n_{cld_events} is the total number of cloudy events in the total number of data points. The occurrence frequency and variability will be computed over the entire WA region for each of the four northern hemispheric seasons, namely DJF (December, January, February), MAM (March, April, May), JJA (June, July, August), and SON (September, October, November). In general, DJF and JJA are considered as the dry and wet seasons, respectively. However, some past studies (e.g., Brooks and Legrand (2000), Frappart et al. (2009), Kucharski et al. (2013), and Lamprey (2008)) have used different seasonal classifications that correspond more to specific areas of WA. Nevertheless, they are not considered in this part of the study due to the focus of this study being on solar radiation rather than factors like precipitation, humidity, or temperature that have unique seasonal distributions in different areas of WA (Gbobaniyi et al., 2014; Sultan & Janicot, 2000). The seasonal variability will simply be a comparison of the mean cloud coverage for each of the seasons. Additionally, the diurnal variations of the different cloud types will be studied for each season in different areas across WA. This could help to understand the evolution and processes associated with cloudiness in the various climate zones over the

region.

2.2 Data sources

To study clouds' occurrence and characteristics, as well as their impact on the incoming solar radiation over the whole WA, a long-term database of observations over several locations is needed. However, WA is well known for its lack of surface observations of clouds (Knippertz et al., 2015), and to a large extent, this could explain the limited understanding of cloud systems in the region. There are a few surface-based observational databases of cloud properties from field campaigns including the African Monsoon Multidisciplinary Analysis – AMMA (Lebel et al., 2010; Redelsperger et al., 2006) and the Dynamics–Aerosol–Chemistry–Cloud Interactions in West Africa – DACCWA (Flamant et al., 2018; Knippertz et al., 2015) projects. Apart from the data collected during the AMMA field campaign, a number of observatories were set up within the project to collect basic climatological, hydrological, and ecological parameters in parts of WA to create a long-term database known as African Monsoon Multidisciplinary Analysis – Coupling the Tropical Atmosphere and the Hydrological Cycle Database (AMMA-CATCH DB) (Galle et al., 2018). There are also some cloud cover data from METAR reports (Lott et al., 2001) and deployed mobile facilities at weather stations (Miller & Slingo, 2007). These databases are usually deemed unsuitable for analyzing the long-term feasibility of solar energy over the region due to several factors. Chief among them is the fact that most of these databases (especially those from field campaigns) cover just a short period (a few weeks to about two months). Other databases are limited to only a single location over the entire WA while others provide a very coarse partitioning of cloud fraction. Additionally, there are many gaps in some of these databases.

Over a large domain like WA, there are opportunities to study the long-term solar energy feasibility with other data products such as model reanalyses, satellite-based observations, GCMs, etc. Although these databases have the advantages of covering extensive spatial domains and having longer temporal data records without gaps, they are often marred with errors and uncertainties that lead to doubts on their reliability (Hannak et al., 2017; Reichler & Kim, 2008; Shea et al., 2017). It is, therefore, necessary to know the range of those errors and uncertainties for each dataset before they are used for climate applications. The general consensus is that observations (surface-based observations followed by satellite-based observations) present far fewer uncertainties than other datasets (Amjad et al., 2020; Brisson et al., 2016). Thus, in this work, the different datasets will be evaluated with some of the available observational data records to ascertain the level of uncertainty presented

by each. In this section, all the datasets used in this study will be presented in detail.

2.2.1 Surface-based observations

Two main surface-based observations are used to evaluate the datasets used in this study: First is the Integrated Surface Hourly Database (ISD) archived on the National Climatic Data Center (NCDC) hierarchical data storage system (Lott et al., 2001). The ISD is a collection of surface hourly observations from nearly 20000 stations around the world spanning periods as early as 1900. It provides the common climate parameters such as surface temperature, precipitation, and humidity at each station and can be useful for global, regional, and local-scale analysis. It also provides a proxy for the total fraction of clouds in the atmosphere in the form of the Sky Cover (SKC) variable. The SKC variable is a coarse partitioning of cloud coverage into different classes of sky conditions. The main SKC classes in the ISD are defined as follows:

- CLR: Clear sky
- SCT: Scattered (1/8 to 4/8 oktas of the sky covered)
- BKN: Broken (5/8 to 7/8 oktas of the sky covered)
- OVC: Overcast (8/8 oktas)

The second surface-based observation is the high-quality measurements of surface downwelling shortwave radiation obtained from AMMA-CATCH DB. The AMMA-CATCH DB consists of surface measurements from some weather stations in Benin, Mali, and Niger. Surface solar irradiance is measured at 30-minute intervals from these AMMA-CATCH stations. Only data from Niger and Benin are used for the evaluation (Table 2.1). Mali is excluded due to a high percentage of missing data in the records.

Table 2.1: Details of AMMA-CATCH observation sites used for the evaluation of ERA5 data.

Station name	Longitude (°E)	Latitude (°N)	Start Date	End Date	Missing Data (%)
North Wankama	2.6337	13.6476	16/06/2005	09/06/2014	20.8
Nalohou	1.6046	9.7448	11/11/2005	01/01/2016	6.9

Both datasets are primarily used for evaluation. However, care must be taken when using these surface observations. Especially, comparing SKC information in

the ISD data to cloud fraction in other datasets can be ambiguous since the range-based definition of SKC could lead to a lot of uncertainties.

2.2.2 Model reanalyses data

The main dataset used for the majority of this study is the fifth generation of the European Centre for Medium-Range Weather Forecasts (ECMWF) Reanalysis of the global climate (ERA5) (Hersbach et al., 2020). ERA5 is produced using the ECMWF’s Integrated Forecast System (IFS) cycle *41r2* which also assimilates vast amounts of historical observation data from satellites and in-situ weather stations. It is the first reanalysis dataset produced as an operational service providing hourly estimates of a large number of essential atmospheric, surface, and oceanic climate variables including, but not limited to, rainfall, wind, pressure, air temperature, and sea surface temperature. The ERA5 data are produced on a regular grid at a relatively high spatial resolution of approximately 30 km. It resolves the atmosphere with 137 vertical levels from the surface to about 80 km (0.01 hPa) with 20 levels in the first 1 km of the atmosphere. Detailed information on the various schemes and model configuration used for ERA5 is provided in Hersbach et al. (2020).

ERA5 provides prognostic three-dimensional (*3D*) distributions of cloud properties including cloud fraction, cloud liquid water, and cloud ice water. These *3D* cloud variables are computed for each grid box at a subgrid-scale over all the model (or pressure) levels using the Tiedtke cloud scheme (Tiedtke, 1993) which is implemented in the ECMWF IFS. They are then used to produce diagnostically computed two-dimensional (*2D*) cloud fraction and vertically integrated hydrometeor content over single stratified layers in the atmosphere. The partitioning of the atmosphere results in four cloud cover types in ERA5 namely low-level cloud cover (LCC), mid-level cloud cover (MCC), high-level cloud cover (HCC), and total cloud cover (TCC). As shown in Figure 2.3 TCC integrates all clouds from the surface to the top of the troposphere. This is achieved in ERA5 using the maximum-random overlap assumptions (Barker, 2008; Jakob & Klein, 2000). LCC refers to all clouds integrated from the surface level to about 2 km altitude in the atmosphere (Forbes, 2017). MCC and HCC respectively refer to all clouds integrated from 2 km to about 6.4 km and from 6.4 km to the top of the troposphere.

ERA5 also provides the surface downwelling shortwave radiation (also known as the global solar radiation or shortwave radiation). It uses the “McRad” radiation scheme (Morcrette et al., 2008) to generate the shortwave radiation. The radiation scheme incorporates both the Monte Carlo Integration of the Independent Column Approximation – MCICA (Pincus et al., 2003) for representing the subgrid-scale

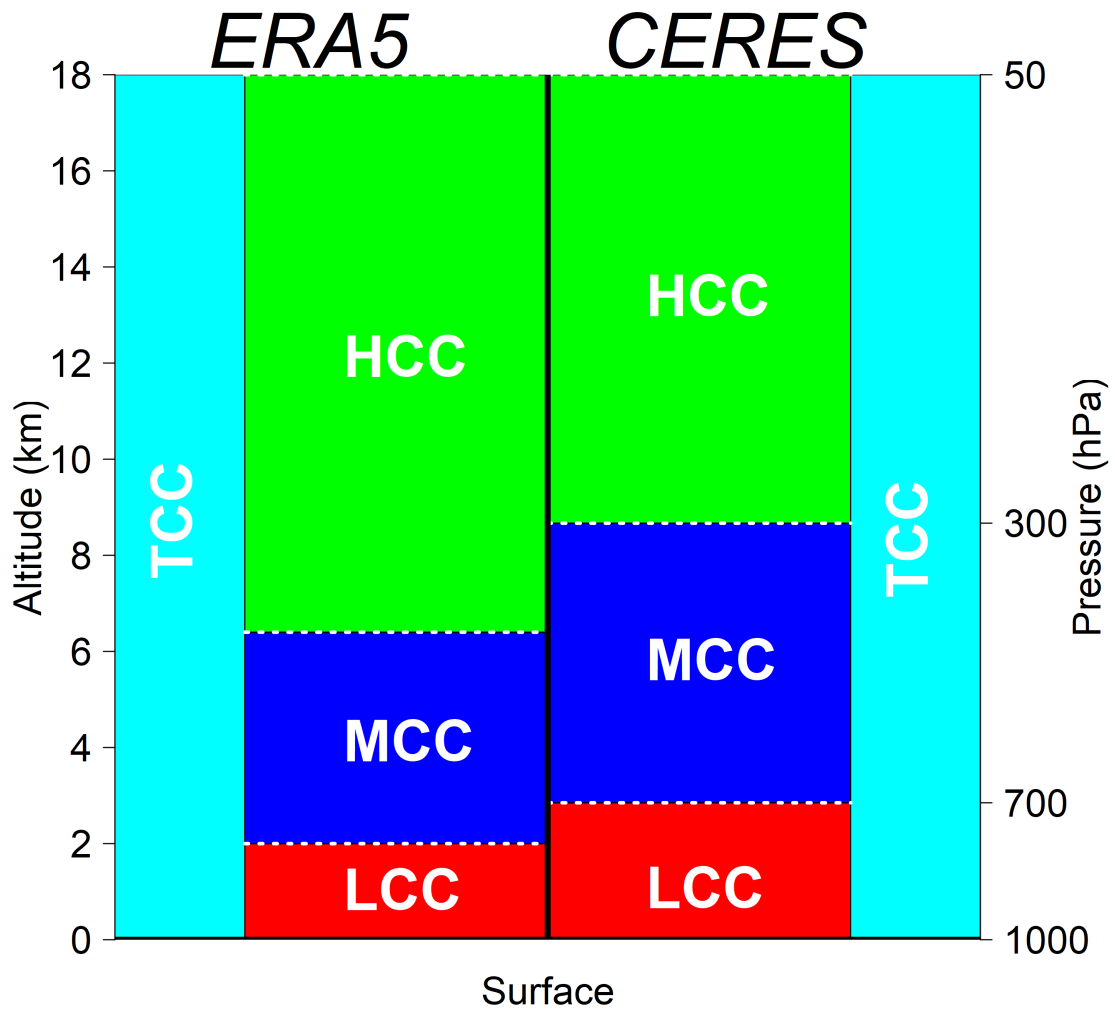


Figure 2.3: Definitions of different cloud types by their position in the atmosphere in the ERA5 and CERES SYN1deg products.

cloud structure and overlap and the Rapid Radiative Transfer Model – RRTMG (Iacono et al., 2008) for both the shortwave and longwave part of the radiation. At any point in time, shortwave radiation is an estimate of the amount of incoming solar radiation that reaches a horizontal plane on the Earth’s surface (C3S, 2017) after part of it is absorbed and/or reflected back to space by clouds and particles in the atmosphere. It consists of both the direct and diffuse components of solar radiation. This makes it the most important parameter for solar PV applications. In ERA5, this radiation parameter is accumulated over a duration. For the reanalysis, the accumulation period is over the 1 hour up to the validity date and time. The units are J m^{-2} . To convert to W m^{-2} , the accumulated values should be divided by the accumulation period expressed in seconds. The clear-sky surface downwelling shortwave radiation is also provided in ERA5. It is computed from the model radiation scheme using the same atmospheric conditions of temperature, humidity,

aerosols, ozone, and trace gases as the global solar radiation but assuming that there are no clouds.

Other ERA5 parameters such as specific humidity, eastward and northward components of the wind, and the surface heat fluxes are also used. Here, 10 years of data (from 2006 to 2015) will be analyzed. Since the analysis of cloud cover in the study is applied to the development of solar energy, only daytime hours will be considered in the various analyses that will be performed.

We also used the Modern-Era Retrospective analysis for Research and Applications, Version 2 – MERRA-2 (Gelaro et al., 2017). However, it was only used in the evaluation stage to provide an idea of ERA5’s relative performance to other reanalyses products.

2.2.3 Satellite-based observations

Satellite instruments at the top of the atmosphere measure radiant energy emitted and reflected by the earth’s surface. These measured radiances are then used as inputs for different algorithms to determine climatic variables such as the various cloud properties. In this section, a few satellite products used in the following chapters are introduced.

CERES

The Clouds and the Earth’s Radiant Energy System – CERES (Wielicki et al., 1996) instruments onboard the passive Terra and Aqua satellites provide observations of the earth’s emitted and reflected radiant energy. The CERES instruments have been in operation since 1999 and 2002 on the Terra and Aqua Moderate Resolution Imaging Spectroradiometer (MODIS) platforms respectively.

The CERES Synoptic product (hereinafter SYN1deg) provides Level 3 global hourly surface, atmosphere, and top of atmosphere radiant fluxes on a regular $1^\circ \times 1^\circ$ grid (Rutan et al., 2015). The SYN1deg product is intended to be used for applications that require cloud cover and radiation fluxes at a high temporal resolution (up to 1 hour). The atmospheric fluxes are provided at four pressure levels using a radiative transfer and inputs from the two MODIS platforms, geostationary (GEO) satellite data, and meteorological assimilation data from the Goddard Earth Observing System. Cloud properties are mostly derived from the MODIS instruments and multiple GEO visible and infrared imagers. Cloud properties retrieved with the MODIS sensor may be different from the GEO images. Thus, to ensure uniform cloud properties across all satellite data, each GEO instrument is calibrated

against the MODIS radiances (Doelling et al., 2013). The SYN1deg product also contains coincident aerosol properties used as input to compute the fluxes (Rutan et al., 2015). Further documentation on the inputs, calibrations, and radiation channels used to derive the product is available on the CERES project website (<http://ceres.larc.nasa.gov>).

The SYN1deg product provides cloud cover fractions for four different layers of the atmosphere: low, low-middle, high-middle, and high. These stratified layers are defined by the pressure at the cloud top height and thus leads to four cloud cover types namely: low cloud cover (surface to 700 hPa), low-middle cloud cover (700 hPa to 500 hPa), high-middle cloud cover (500 hPa to 300 hPa), and high cloud cover (upwards of 300 hPa). A single representative middle-level cloud cover is derived by simply summing the two middle-level cloud types as the SYN1deg product does not include overlap assumptions (Rutan et al., 2015). The total cloud cover is the vertically integrated cloud fractions over all the atmospheric layers. As shown in Figure 2.3, there are some differences in the cloud types provided by the SYN1deg and ERA5 products. As a result, care must be taken when comparing cloud fractions provided by these two products.

SYN1deg also provides surface radiant fluxes in the form of the downwelling shortwave radiation. This is computed using a distribution of cloud optical thickness estimated for each cloud layer (Barker, 1996; Oreopoulos & Barker, 1999) as an input for a two-stream radiative transfer model (Kato et al., 2005). The shortwave radiation is computed for different atmospheric states. The different atmospheric states include all-sky conditions, clear-sky (no cloud but include aerosols), pristine conditions (no cloud and no aerosol), and all-sky conditions but with no aerosol. The inputs for the radiation fluxes in various atmospheric states are described in Rutan et al. (2015). In this work, the all-sky and clear-sky shortwave radiation fluxes will be used for analysis. The advantages and challenges associated with the SYN1deg product will be presented in section 3.4.

The merged CloudSat and CALIPSO product (2B-GEOPROF-LIDAR)

The Cloud Profiling Radar (CPR) and Cloud-Aerosol Lidar with Orthogonal Polarization (CALIOP) are two active satellite instruments aboard CloudSat (Stephens et al., 2008) and Cloud-Aerosol Lidar and Infrared Pathfinder Satellite Observations (CALIPSO) (Winker et al., 2009). CloudSat and CALIPSO are two polar-orbiting satellites in the NASA A-Train constellation (Stephens et al., 2018) that cross the equator twice each day. Measurements from the two sensors are merged to form the 2B-GEOPROF-LIDAR product (Mace et al., 2009). With the ability of the CPR to

probe optically thick cloud layers and the ability of CALIOP to sense optically thin cloud layers and tops, the 2B-GEOPROF-LIDAR product provides a unique insight into the vertical distribution of clouds in the atmosphere. The 2B-GEOPROF-LIDAR product adopts the spatial resolution of the CPR with horizontal and vertical resolutions of approximately 1.4×1.8 km (along-track by across-track) and 250 m respectively (Mace et al., 2007).

The product provides Level-2 cloud fraction and hydrometeor content distribution in the atmosphere. Solar energy applications require continuous and high temporal resolution data. Therefore, the 2B-GEOPROF-LIDAR product may not be suitable for such applications given that it provides measurements twice daily at a given place (one in the night and one during the day). Besides, continuous measurements (i.e., everyday measurements) at the same location is highly unlikely. Therefore, the 2B-GEOPROF-LIDAR will primarily be used to evaluate other cloud products. The vertical distribution of the cloud fraction will be used for this purpose. It should however be noted that the CPR has challenges in determining clouds in the lowest 1 km of the atmosphere. CALIOP may be able to detect these clouds but its signal may be totally attenuated when there are optically overlying clouds.

SARAH-2 (Surface Radiation Data Set – Heliosat, Edition 2 (Pfeifroth et al., 2019)) surface solar irradiance data is also used for evaluation. SARAH-2 is available every hour at a high spatial resolution of $0.05^\circ \times 0.05^\circ$ and covers the region of 65° N to 65° S. Surface solar irradiance is derived from satellite observations of the visible channels of the Meteosat visible and infrared imager (MVIRI) and the Spinning Enhanced Visible and InfraRed Imager (SEVIRI) instruments onboard the geostationary Meteosat satellites. A detailed description of the SARAH data including the retrieval principles and algorithms is found in Mueller et al. (2015)

2.2.4 Global Climate Models (GCMs)

Four GCM ensembles (Table 2.2) participating in the Coupled Model Intercomparison Project Phase 6 (CMIP6) (Eyring et al., 2016) are used to investigate the impacts of climate change on solar energy production in WA. Details on the criteria for selecting the GCM's, the chosen future scenario, as well as for the sizes of the different GCM ensembles are given in Chapter 6. Both the historical outputs and the future projections under the Scenario Model Intercomparison Project (ScenarioMIP) (O'Neill et al., 2016) are used. In the ScenarioMIP, projections are driven by a set of emission and land use scenarios based on pathways of societal development, the shared socioeconomic pathways (SSP) (O'Neill et al., 2014; Riahi et al., 2017), and the Representative Concentration Pathways (RCP). Here, the SSP5-8.5 is used

as the presumptive future scenario under which the impacts of climate change on potential solar power production will be assessed. The SSP5-8.5 scenario envisions optimistic human development trends in a high energy-intensive, fossil-based economy (Meinshausen et al., 2020). The criteria for choosing the SSP5-8.5 is detailed in Chapter 6.

Table 2.2: Selected GCMs for investigating climate change impacts on solar energy potential in West Africa.

Model	Institute	Country	Reference
AWI-CM-1-1-MR	Alfred Wegener Institute, Helmholtz Centre for Polar and Marine Research	Germany	Semmler et al. (2020)
EC-Earth3	EC-Earth	European Consortium	Wyser et al. (2020)
MPI-ESM1-2-HR	Max Planck Institute	Germany	Müller et al. (2018)
MRI-ESM2-0	Meteorological Research Institute	Japan	Yukimoto et al. (2019)

The historical period will run from 1980 to 2014, while the projected period will be two 35-year periods from 2015 to 2084. For the periods considered, each of the model ensembles is available at a 3-hour temporal resolution with a nominal horizontal resolution of 100 km. The actual horizontal resolution slightly differs across the different GCMs. Further details regarding the different GCMs' configurations, physics schemes, and parameterizations are provided in Table A.1 of the Appendix A.

2.3 Data evaluation

2.3.1 Evaluation of ERA5 and CERES cloud fractions and occurrence frequencies

Observations from two ISD synoptic weather stations in WA, Niamey (13.482° N, 2.184° E) and Accra (5.605° N, 0.167° W) have been used to perform an evaluation of the ERA5 and CERES cloud cover datasets. Only these stations are used because it is observed that there are an extremely high percentage of missing values in other WA ISD stations. For the evaluation, only the dates and times in the two selected ISD station records without missing values are considered. Since ERA5 and CERES

are both gridded, we have selected the grid boxes within which the ISD stations are located.

In the ISD data, the SKC variable could be ‘compared’ with the TCC of ERA5 and CERES. Following the definitions of ISD, TCC values in ERA5 and CERES were assigned a particular SKC class. Therefore, cloud fractions in ERA5 and CERES were classified as follows:

- $TCC = 0\%$: CLR
- $0\% < TCC \leq 50\%$: SCT
- $50\% < TCC < 100\%$: BKN
- $TCC = 100\%$: OVC

Figure 2.4 presents the comparison between the frequencies (%) of SKC as classified in ERA5 and CERES datasets with the ISD observations. For frequency of ‘clear sky’ occurrences, ERA5 lies between ISD and CERES in all stations. ERA5 and CERES have a very good agreement with ISD for the SCT class in Accra but overestimates it by at least 15% in Niamey. For the BKN class, the frequency of ERA5 is very similar to ISD in Niamey but about 20% higher in Accra. In contrast, the frequency of the BKN class is similar to ISD in Accra but about 10% less in Niamey. In terms of the OVC class, ERA5 is similar to ISD in both stations. However, CERES overestimates the frequency by at least 10% in both stations.

Regardless of the differences, these results indicate a reasonable agreement between the surface observations (ISD) and ERA5 and CERES for some SKC classes. The discrepancies could be partly due to the uncertainties of comparing the gridded ERA5 and CERES data with the point ISD data. In any case, the magnitudes of the differences in the frequency of SKC classes between the datasets are not extreme. It should also be noted that the SKC classification used by the ISD is a very coarse partitioning of cloud fraction which is to be interpreted with care.

Given the coarse nature of ISD data, we further evaluated the occurrence of cloud cover in WA using satellite-based observations. Here, the emphasis will be on low clouds in the ERA5 dataset which will be significantly analyzed later in Chapter 4. The hourly ERA5 LCC is evaluated against the merged 2B-GEOPROF-LIDAR data.

Following the ERA5 definition, low-level clouds (LLC) are determined from the first 2 km above ground level in the 2B-GEOGROF-LIDAR product. Within these 2 km, there can be more than one cloud layer and the representative LLC fraction is computed with the maximum-random overlap rule (Geleyn & Hollingsworth,

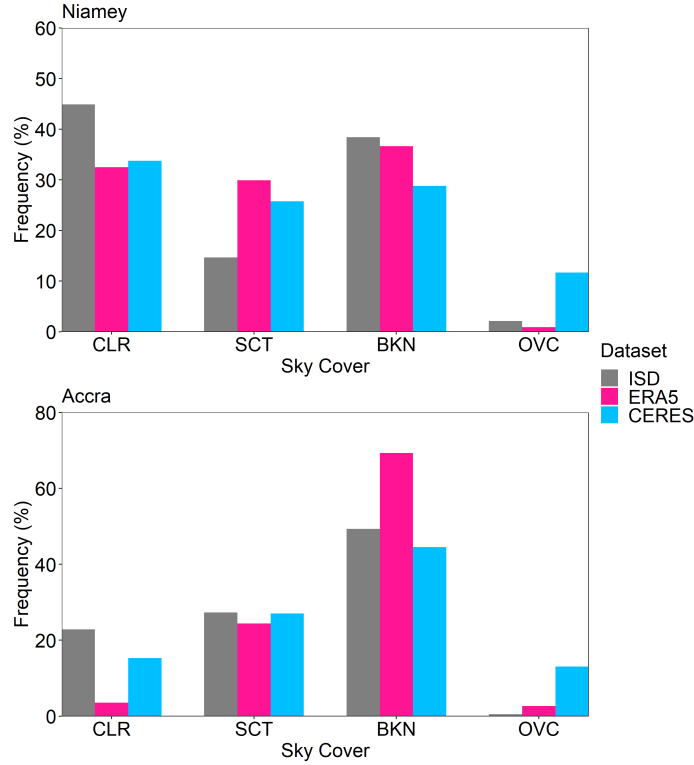


Figure 2.4: Evaluation of the occurrence of different sky cover classes in ERA5 and CERES with Integrated Surface Database (ISD) surface observations for 2 ground stations in West Africa for the 2006 – 2015 period.

1979) as shown in Equation 2.2:

$$CC_{i,j} = 1 - (1 - C_i) \prod_{k=i+1}^{j-1} \left[\frac{1 - \max(C_k, C_{k-1})}{1 - C_{k-1}} \right] \quad (2.2)$$

where, $CC_{i,j}$ is the total cloud fraction for layers i through j , k is the number of discretized atmospheric layers, C_i and C_k are the cloud fractions for the i^{th} and k^{th} layers respectively.

For this evaluation, six tracks of the 2B-GEOPROF-LIDAR product over WA are used (Figure 2.5). Only observations from the tracks passing through two spatial windows in the Guinean and Sahelian regions of WA are compared with ERA5.

The ERA5 cloud fractions are instantaneously generated at every hour of the day. However, the 2B-GEOPROF-LIDAR observations over the study area are not recorded exactly on the hour (e.g., on October 28, 2006 (Figure 2.6), the 2B-GEOPROF-LIDAR passed over whole WA in approximately 7 minutes from 14:08 to 14:15). In order to compare the ERA5 data with the satellite observations, the mean

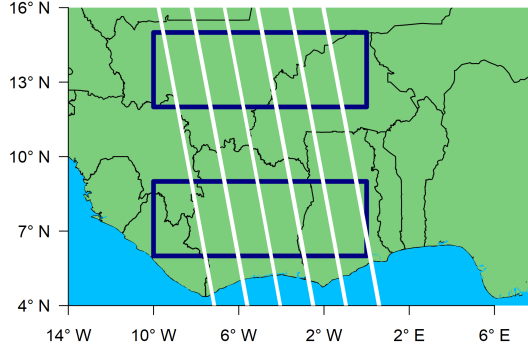


Figure 2.5: 2B-GEOPROF-LIDAR tracks (white lines) used for the evaluation of ERA5 cloud data. The two rectangular windows are the selected Guinean (south window) and Sahelian (north window) used for the evaluation.

cloud fraction of the two hours bounding the 2B-GEOPROF-LIDAR observation time (i.e., in this case 1400 and 1500 UTC, Figure 2.6c and d) are thus used. In the two selected windows, the closest grid points to the 2B-GEOPROF-LIDAR observation track are chosen from the ERA5 dataset for this evaluation. For the example shown in Figure 2.6, ERA5 is able to capture the latitudinal evolution of low clouds within the 7-minute observational time frame of the moving satellite over its track in WA. There are however some discrepancies, especially over the oceanic areas between 1°N and 4°N.

Since the satellite moves along its track over WA in approximately seven minutes, the time taken for the satellite to pass along its track within the Guinea or Sahel window will be much smaller. Therefore, the cloud fractions along the satellite track have been averaged to compare ERA5 with 2B-GEOPROF-LIDAR. The difference between the maximum and minimum longitude (latitude) along the track passing through each window is approximately 0.5° (3°). The mean bias and root mean square error (RMSE) between the observation data and ERA5 are then computed as follows:

$$Bias = \frac{1}{N} \sum_{i=1}^N (Y_{pred,i} - Y_{obs,i}) \quad (2.3)$$

$$RMSE = \sqrt{\frac{1}{N} \sum_{i=1}^N (Y_{pred,i} - Y_{obs,i})^2} \quad (2.4)$$

where, $Y_{obs,i}$ and $Y_{pred,i}$ are the i th observed and predicted values respectively and N is the number of data points.

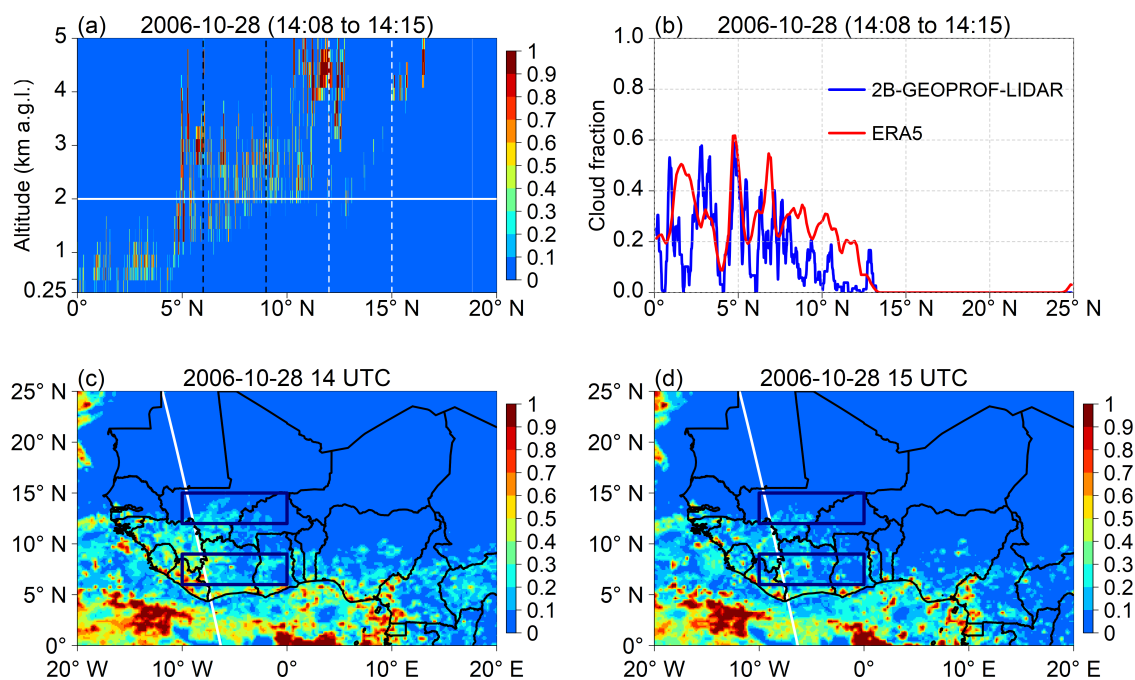


Figure 2.6: (a) 2B-GEOPROF-LIDAR vertical profile of cloud fraction, for a given daytime track over WA. Black and white dashed lines delineate the locations of the Guinea and Sahel windows used in this study respectively. All cloud structures below the solid white horizontal line, are considered as low clouds in our study. (b) Latitudinal cloud fraction seen along the 2B-GEOPROF-LIDAR track shown (blue) and the corresponding ERA5 closest grid point (red). Bottom: Corresponding ERA5 2D plots of LLC for the hours (c) preceding and (d) following the satellite observation time.

The occurrence frequencies of LLC are also compared. For this, LLC occurrence is divided into two classes (i.e., Class-1, when the LLC fraction is below 50% Class-2, when the LLC fraction exceeds 50%). Here, only the daytime tracks of satellite observations from June 2006 to December 2007 are used.

Figure 2.7 presents the comparison of LLC fraction (left column) and occurrence frequency (right column) of ERA5 and 2B-GEOPROF-LIDAR for the Sahel (upper row) and Guinea (lower row) windows. In terms of seasonality of the hourly LLC fraction, ERA5 captures the satellite observations well. It slightly overestimates the fraction in both regions with a bias of 0.044 and 0.101 in Sahel and Guinea respectively. It also presents low RMSE values of 0.134 and 0.255 in the Sahel and Guinea windows respectively. In terms of the occurrence frequency, ERA5 overestimates (underestimates) the occurrence of LLC Class-1 in the Sahel (Guinea) window by about 10%. The largest difference in occurrence frequency is obtained for LLC Class-2 in the Guinea region where ERA5 shows about 20% overestimation

in the occurrence frequency. This could be due to many reasons such as model related errors in the ERA5 product. It could also be due to the difficulty of the 2B-GEOPROF-LIDAR to detect low cloud structures below the lowest 1 km of the atmosphere. In WA, the lowest 1 km is where most of the frequent low-level stratiform cloud bases are found. These clouds tend to have large fractions (and are most likely LLC Class-2 in our definition) and thus, their non-detection by the satellite may have led to the low occurrence frequencies in the 2B-GEOPROF-LIDAR product as shown in Figure 2.7. In a nutshell, although the ERA5 hourly LLC data present some biases and deviations from the satellite observations, it also performs reasonably well in reproducing the LLC observations.

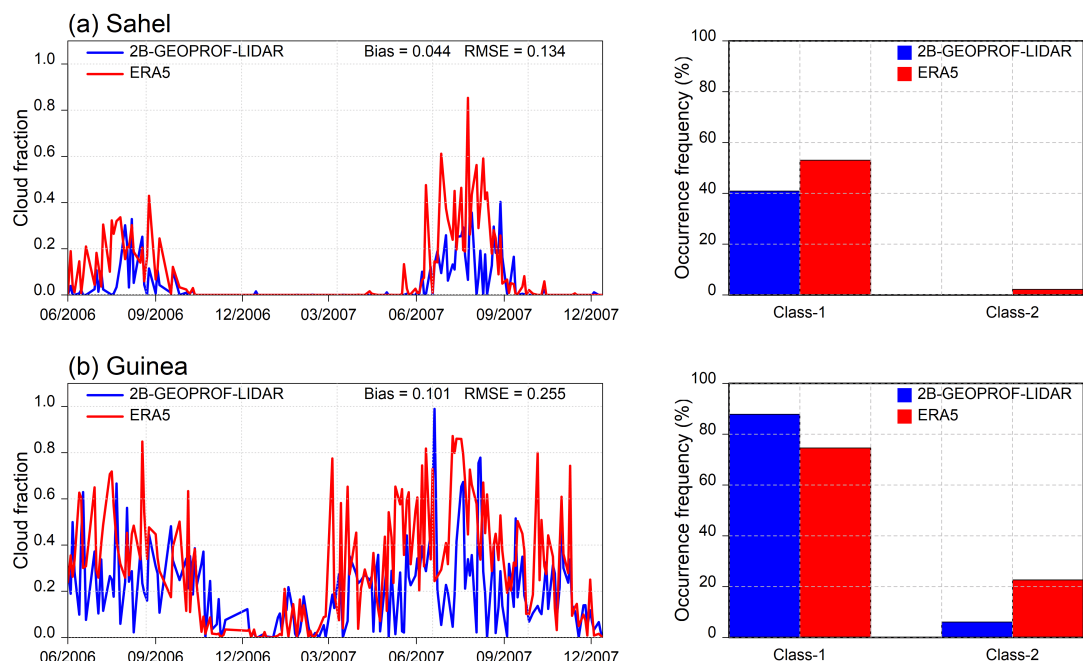


Figure 2.7: Evaluation of the daytime ERA5 LLC fraction (1st column) and occurrence frequency (2nd column) with the 2B-GEOPROF-LIDAR observation in the (a) Sahel and (b) Guinea windows. This evaluation is based on observations from June 2006 to December 2007.

2.3.2 Evaluation of ERA5 surface incoming radiation

The hourly ERA5 surface incoming irradiance is evaluated with surface observations obtained from the AMMA-CATCH DB. The hourly mean irradiances are computed for each station from the 30-minute measurements since the ERA5 irradiance data are hourly mean values. The evaluation is based on the period 2006 to 2015. Within this period, all missing records are excluded from the evaluation.

From the ERA5 data, the closest grid point to each station is then used for

the evaluation. Additionally, three other radiation products (SYN1deg, MERRA-2, and SARA2) are also evaluated in order to compare their relative performances with ERA5. The mean bias and RMSE (Equation 2.3 and Equation 2.4) between the observation data and all other datasets are computed (Table 2.3). The Taylor’s diagram (Taylor, 2001) is also used to show the correlation (R) with the observation, standard deviation, and RMSE of each dataset (Figure 2.8).

The evaluation shows that ERA5 overestimates the incoming irradiance with a bias of 20.17 W m^{-2} and 13.88 W m^{-2} in North Wankama and Nalohou respectively (Table 2.3). Against the ground observations, MERRA2 presents the smallest biases in both regions (1.19 W m^{-2} and -1.65 W m^{-2}) while SARA2 has the largest biases (23.84 W m^{-2} and 28.64 W m^{-2}). However, MERRA2 has the largest RMSE and least R at both observation sites (Figure 2.8a). ERA5 shows a good correlation with the surface observations with R of 0.96 and 0.93 in North Wankama and Nalohou respectively. All the four irradiance datasets correlate well (R values above 0.9 at both stations) with the surface observations as shown in the Taylor diagrams.

Table 2.3: Estimated mean bias (in W m^{-2}) against in-situ observations at the North Wankama and Nalohou observation sites.

	North Wankama	Nalohou
ERA5	20.17	13.88
MERRA-2	1.19	-1.65
SARA2	23.84	28.64
SYN1deg	4.15	7.3

It was suspected that the high correlations could be due to the ability of the various datasets to reproduce the seasonal cycle of irradiance. Therefore the time series was decomposed into its different components following West (1997). The seasonal component was subtracted from the other components, which were then summed together. The deseasonalized time series of the various datasets were then evaluated again. The results show that the correlations drop down when the seasonality is removed from the time series (Figure 2.8b), confirming the earlier hypothesis that the ERA5 and CERES datasets are able to reproduce the seasonal cycles of irradiance in the region.

2.3.3 Evaluation of CMIP6 historical simulations

The historical GCMs’ cloud cover and surface irradiance outputs are first evaluated using satellite observations. Here, the CERES SYN1deg is used as the observational reference to evaluate the CMIP6 GCM ensembles. From the raw 3-hourly GCM

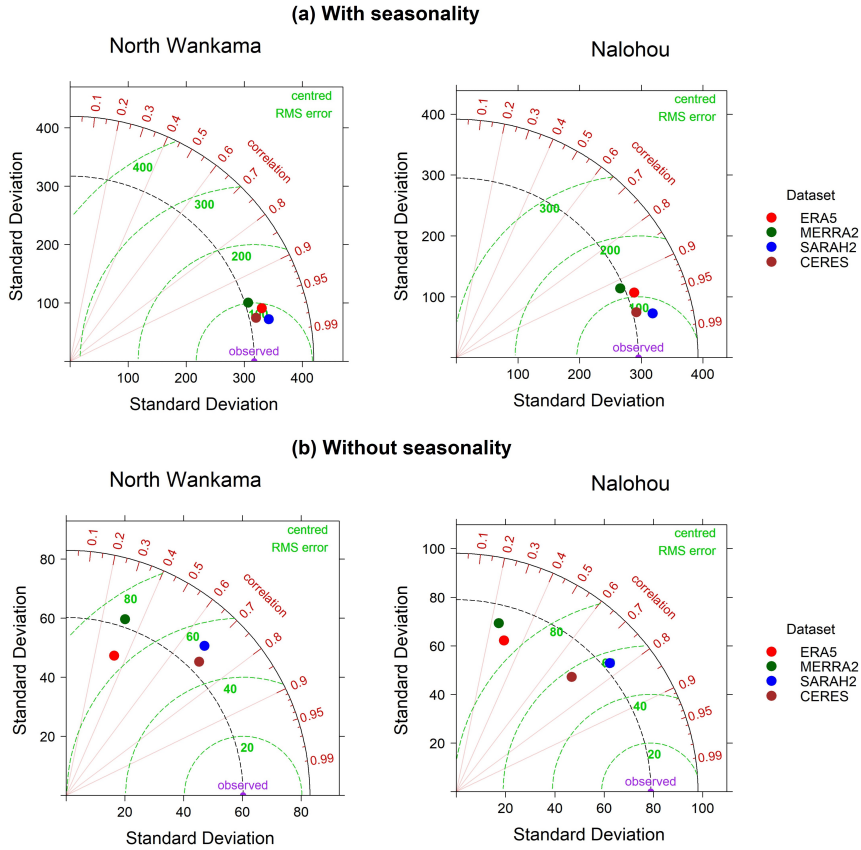


Figure 2.8: Taylor's diagrams showing evaluations of ERA5 (and other datasets) surface irradiance data with surface measurements at the North Wankama and Nalohou observation sites. Evaluation is made with (a) time series with seasonality and (b) deseasonalized time series.

outputs, the daily mean total cloudiness and solar irradiance are computed using only the daytime hours. The mean annual cycles of the ensemble mean of the different GCMs are then compared with the reference observation. The mean biases (Equation 2.3) and RMSE (Equation 2.4) are also computed. It should be noted that the entire historical period of the GCMs is not used for this evaluation. This is because the records for the reference data do not cover the entire historical period of the GCMs. Thus, the evaluation of the GCMs is only based on 14 years from 2001 to 2014.

GCM outputs are known to present biases (e.g., Hannak et al. (2017) and Tan et al. (2018)) that can lead to many uncertainties when used to perform impact studies. Therefore, bias correction methods are often applied to raw GCM outputs before they are used for impact studies (e.g., Fahad et al. (2018) and Lee et al. (2019)). These bias-correction techniques often lead to a significant reduction of model errors (Navarro-Racines et al., 2020). One of the most used methods for

correcting biases in stochastic variables such as cloudiness and irradiance is the quantile mapping approach (Déqué, 2007; Lavaysse et al., 2012; Piani et al., 2010). The quantile mapping approach, which assumes that both the observations and GCM intensity distribution are nearly approximated by the gamma distribution, removes systematic errors in the GCM outputs. It uses a transfer function (T) to adjust the cumulative distributive function (CDF) of the GCM (Q_m) to that of the observations (Q_o). Suppose CDFs of the observations and GCM are defined as f_o and f_m respectively, then:

$$T(f_m) = f_o \quad (2.5)$$

and the bias-corrected value of the GCM, Q_m^* will be given as:

$$Q_m^* = f_o^{-1}(f_m(Q_m)) \quad (2.6)$$

where, f_o^{-1} is the inverse CDF of the observations Q_o .

It is assumed that the biases in the historical simulations will be the same in the future period. Thus, the bias correction is carried out for both historical and future periods using the reference observation. The mean bias error and RMSE in the Guinean and Sahelian regions of WA are then estimated and compared for the raw and bias-corrected ensemble mean of the different GCMs (Figure 2.5).

Figure 2.9 presents a comparison of the mean annual cycles of total cloud area fraction between the GCM ensemble means and the observations in both Guinea and the Sahel. The raw GCM ensemble means present significant differences from the reference observations in both regions (Figure 2.9a). In the Guinea region, the GCMs predominantly underestimate cloud fraction from January to April. The AWI-CM-1-1-MR (hereafter AWI-CM) and MPI-ESM1-2-HR (hereafter MPI-ESM) further underestimate cloud cover through most of the rainy season (from April to September) and present a bimodal evolution in the annual cloudiness. This bimodal structure is absent in the observations and the other GCMs. It can therefore be directly linked to the underlying atmospheric component of the two models as they are similar in all aspects except in the ocean and sea-ice model components (see Appendix A). All models present the least difference from the reference observations from July to October. In the Sahel region, EC-Earth3 (hereafter EC-Earth) and MRI-ESM2-0 (hereafter MRI-ESM) present a peak in the cloudiness much earlier than the observations. It is interesting to note that the differences between the models and the observations are lowest during the actual peak of cloudiness in the Sahel region (in August) as shown in the observations.

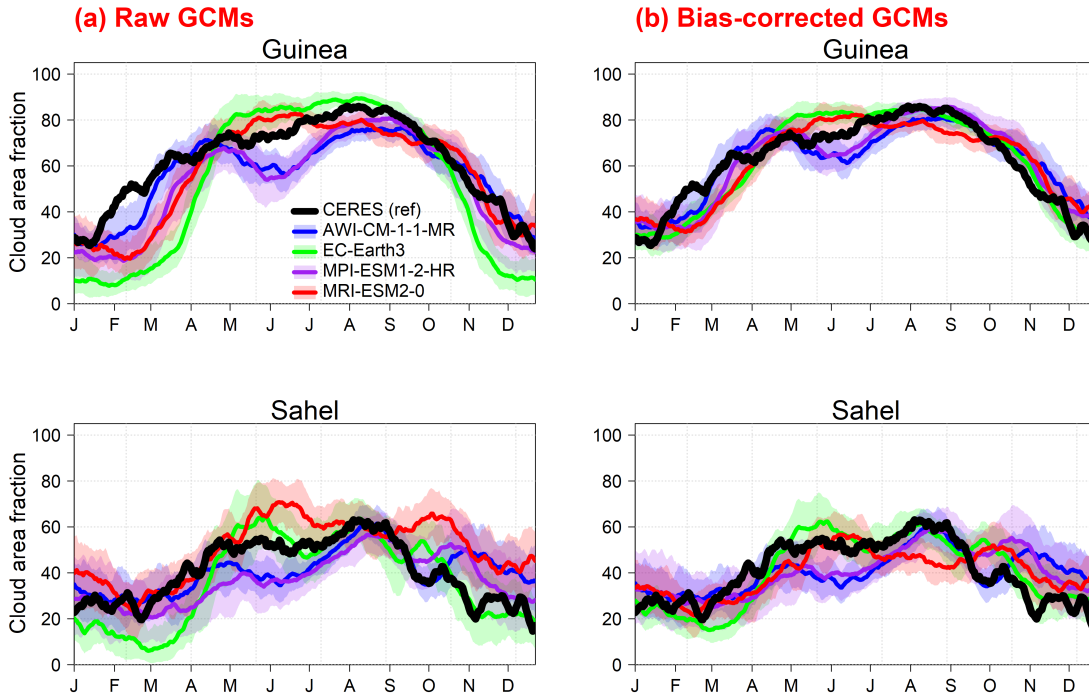


Figure 2.9: Comparison of the mean annual cycle of total cloudiness between CERES SYN1deg with the (a) raw GCM ensemble means and (b) bias-corrected GCM ensemble means in Guinea (top) and Sahel (bottom). The shaded region for each GCM represents the variability (maximum and minimum range) across the individual ensemble members of the GCM.

The application of quantile mapping to correct the raw GCMs leads to a substantial reduction of the models' cloud fraction biases in both Guinea and Sahel (Figure 2.9b). The reduction in model biases appears to be more efficient in the Guinea region than in the Sahel. Table 2.4 presents the values of the annual mean bias and RMSE calculated for both the raw and corrected GCMs ensemble mean cloud fractions. Further results on the evaluation of the CMIP6 GCMs' cloud fraction are provided in Appendix A.

Table 2.4: Annual mean bias and RMSE estimated for the raw and corrected (in bracket) GCMs' ensemble mean cloud fraction in the Guinea and Sahel regions.

Model	Bias (%)		RMSE (%)	
	<i>Guinea</i>	<i>Sahel</i>	<i>Guinea</i>	<i>Sahel</i>
AWI-CM-1-1-MR	-5.51 (-0.001)	0.32 (-0.002)	10.53 (9.1)	12.58 (12.86)
EC-Earth3	-10 (-0.004)	-4.1 (-0.004)	20.46 (8.59)	12.77 (10.27)
MPI-ESM1-2-HR	-9.71 (-0.002)	-3.38 (-0.003)	13.57 (8.61)	12.83 (12.34)
MRI-ESM2-0	-4.47 (-0.003)	10 (-0.003)	12.53 (10.16)	15.9 (11.98)

A comparison of the mean annual cycles of surface irradiances between the GCM ensemble means and the observations in both the Guinea and Sahel regions is presented in Figure 2.10. In both regions, the raw GCMs mostly overestimate the surface radiation (Figure 2.10a) throughout the year (except the MPI-ESM in Guinea during August). In most cases, the overestimation of surface radiation by the GCMs is consistent with the corresponding underestimation of cloud cover (Figure 2.9a) since clouds directly influence the amount of radiation that arrives at the earth's surface (Kasten & Czeplak, 1980; Wielicki et al., 1995).

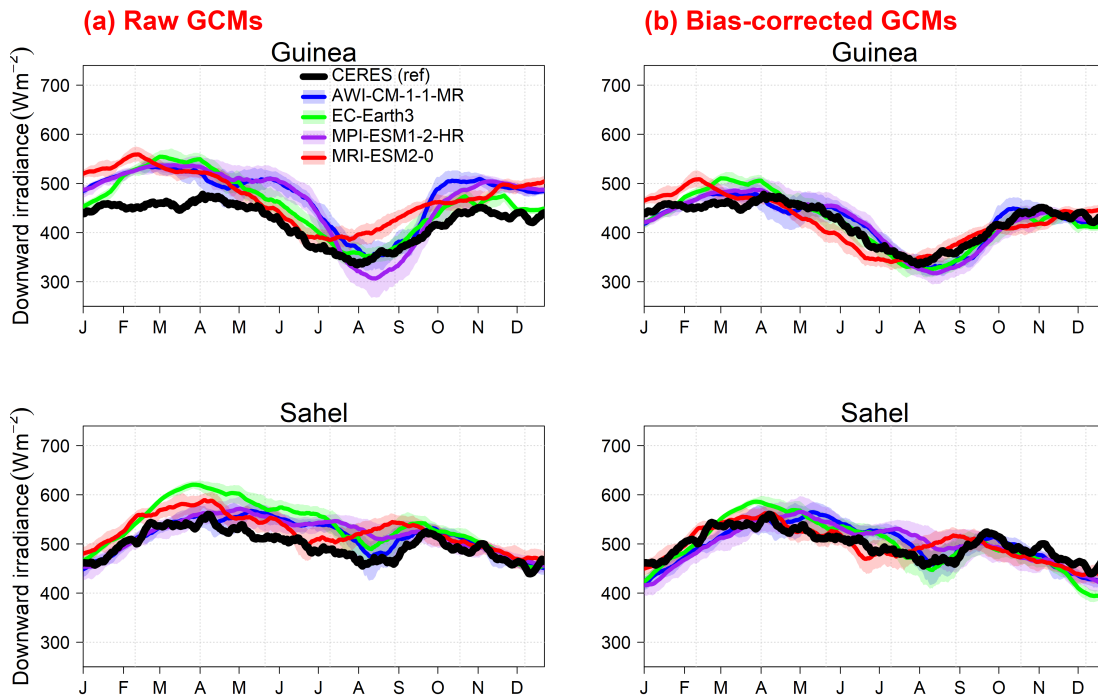


Figure 2.10: Same as Figure 2.9 but for surface irradiance.

However, there are instances where an underestimation (overestimation) of cloud fraction does not lead to an overestimation (underestimation) of the surface radiation. For example, during August in the Guinea region, the MPI-ESM underestimates both the cloud cover and the surface radiation. Moreover, the EC-Earth (and MRI-ESM from May to June) overestimates cloud cover during the wet season but does not lead to an underestimation of the surface radiation. In the Sahel region, the MRI-ESM notably overestimates cloud cover from May to July and from September to December but does not lead to an underestimation in the radiation. These inconsistencies could be explained by many factors. For example, higher cloud fraction will not necessarily lead to lower surface radiation as the radiation is influenced more by the water content in the clouds (Liou, 2002). Additionally, depending on the height of the cloud in the atmosphere and its corresponding water content, the effect on the surface downwelling radiation will be different. Thus, it

would be necessary to characterize the types of clouds simulated by the GCMs (by heights) as this could help to understand the different inconsistencies between the cloud cover and the corresponding surface radiation in the CMIP6 GCMs. However, such characterization would be challenging (in this study) as the model institutions usually provide only vertically integrated values of cloud properties.

Similar to the cloud cover, the application of quantile mapping leads to a significant reduction in the model deviations (Figure 2.10b). This is true for both regions; however, the reduction of deviations appears to be much higher in Guinea than in the Sahel. Table 2.5 presents the values of the annual mean bias and RMSE calculated for both the raw and corrected GCMs ensemble mean surface radiation.

Table 2.5: Same as Table 2.4 but for surface irradiance.

Model	Bias (W m^{-2})		RMSE (W m^{-2})	
	<i>Guinea</i>	<i>Sahel</i>	<i>Guinea</i>	<i>Sahel</i>
AWI-CM-1-1-MR	52.61 (-0.001)	16.65 (0.002)	59.61 (22.89)	31.81 (31)
EC-Earth3	35.68 (-0.002)	39.64 (-0.001)	46.75 (26.05)	50.21 (33.25)
MPI-ESM1-2-HR	45.52 (-0.003)	21.44 (-0.003)	59.62 (24.08)	36.35 (33.86)
MRI-ESM2-0	51.02 (0.001)	28.30 (-0.004)	58.78 (28.07)	38.65 (26.94)

Chapter 3

Occurrence and spatiotemporal variability of clouds in West Africa

3.1 Chapter overview

This chapter aims at answering the question “How frequently do different cloud types occur and evolve in WA?”.

For all feasibility studies involving large-scale solar power production, the question of the occurrence and evolution of cloudiness arises. It is necessary to characterize the occurrence of cloudy events and their variation during daytime hours across all seasons. This will help to have an idea of the periods during which solar power production is likely to be affected and subsequently, to develop effective management plans for operating grid-connected solar power plants.

In this chapter, space and time variability and occurrence frequency of clouds in WA are investigated using a state-of-the-art global reanalysis and a satellite-based observation product. The main novelty of the result in this chapter is that the cloud climatology is based on a long-term record of data. Additionally, the datasets used have not been previously analyzed to study cloudiness in WA. Another contribution from this work is a comparison of the nature of clouds in areas with contrasting climate regimes instead of focusing on a single location as done in previous studies.

The contents of the following chapter are from an article published in the **Quarterly Journal of the Royal Meteorological Society (QJRMS)** in 2019 (Danso et al., 2019).

3.1.1 Contributions

Concept and analysis framework

The conceptualization and analysis framework for this work has been determined by myself in collaboration with my advisors, Sandrine Anquetin, and Arona Diedhiou.

My specific contributions involved the identification of data products and delineation of the study areas. I first made an extensive search of different available data products that have multi-year records of cloud cover, cloud microphysical properties (cloud liquid and ice water contents), and the surface downwelling short-wave radiation. I presented the available datasets to my advisors who assisted in the final selection, after considering the strengths and weaknesses of each one in the context of the study objective. Although the analysis was performed over the whole of WA, I selected several areas in the region where a comparison of the different cloud characteristics was carried out. The regions were selected based on several criteria such as the inclusion of different climatic zones, proximity to the ocean, and the availability of surface observations to perform evaluations.

During the development of the analysis framework, we proposed a presentation of the seasonal variability and occurrence frequency of clouds based on the four seasons (DJF, MAM, JJA, and SON).

Data retrieval, processing and evaluation

After choosing the datasets, I retrieved them from their various repositories. I then performed different preprocessing on the data (extracting the study region boundaries, re-gridding, etc.). I incorporated some functions of Climate Data Operators – *cdo* (Schulzweida et al., 2006) and netCDF Operators – *nco* (Zender, 2008) in bash to perform this task. I then carried out an evaluation of the preprocessed datasets using synoptic observations as described in Chapter 2.

General methodology, visualizations and analysis

I used the *R* programming language and statistical software environment to compute occurrence frequencies, seasonal means, and diurnal cycles of cloud cover. I also used this tool to determine the probability distributions of three different cloud types.

All visualizations were made with *R*. Spatial maps were made with the help of the following *R* packages: *ncdf4* (Pierce, 2012), *raster* (Hijmans & van Etten, 2016), *rgdal* (Bivand et al., 2016), and *scales* (Wickham, 2016).

I contributed significantly to the interpretation of the figures and analysis

of the results. I particularly worked with Christophe Lavaysse (IGE) and Evelyne Touré (LAPA-MF) on the possible misrepresentation of dust as clouds in the satellite product.

Drafting and editing

I drafted the first version of the manuscript and edited it after integrating comments from all co-authors. After submission of the manuscript to QJRMS, I revised it after two rounds of reviews from two anonymous referees.

Presentations

I presented the results in this chapter at various conferences and seminars. Firstly, I made an internal presentation to my research teams at IGE in France and also at LAPA-MF in Cote d'Ivoire. I also presented this work during my participation in the European Research Course on Atmospheres (ERCA) 2019 in Grenoble, France. Some of the results were also presented at the SPSAS summer school in Sao Paulo, Brazil in July 2019 and the AGU 2019 Fall Meeting in San Francisco, USA.

3.2 Article: Spatio-temporal variability of cloud cover types in West Africa with a satellite-based and reanalysis data

Abstract: This study aims to understand and document the occurrence and variability of cloud cover types in West Africa (WA). Investigations are carried out with a 10-year hourly record of two cloud data products: CERES passive satellite observations and ERA5 reanalysis. The seasonal evolutions of high (HCC), middle (MCC), low (LCC) and total (TCC) cloud cover are examined. Both products agree on the seasonal and spatial occurrence of cloud cover, although CERES presents lower values of cloud fraction than ERA5 which is partly attributed to the inability of the satellite sensor to detect optically thin clouds in the atmosphere. Southern WA is found to be cloudier than other parts of the region in all seasons with mean TCC fractions of 70 % and 80 % for CERES and ERA5 respectively during the monsoon season. In all seasons, the presence of LCC over large areas of the Sahel/Sahara region is noted in the CERES product. This could be due to a possible misinterpretation of Saharan dust as low clouds which may have thus overestimated the occurrences and fractions of LCC over this region. Northern WA is associated with higher frequencies of no cloud occurrence events, unlike the south where cloudless skies are rarely observed. Furthermore, in southern WA, overcast conditions of LCC are observed for a significant number of times (up to 20 % of the time during the rainy season in CERES and 40 % in ERA5). The climatology of cloud cover presented in this study could be useful for the planning of solar energy projects.

Authors: Derrick Kwadwo Danso, Sandrine Anquetin, Arona Diedhiou, Christophe Lavaysse, Arsène Koba, N'Datchoh Evelyne Touré

3.3 Introduction

Clouds have an important influence on various aspects of the earth’s radiative balance. Their presence modulates the incoming solar and outgoing longwave radiation, surface temperature, and the earth’s atmospheric general circulation. Cloud-radiation interaction is also responsible for a large degree of uncertainty in global climate models (GCMs) (Dolinar et al., 2015; Soden & Held, 2006). A long-term observation of clouds is, therefore, necessary to understand the influence of clouds on the climate system. However, in West Africa (WA) a long-term observation of clouds is lacking, making it difficult to study the influence of clouds for many applications such as the ability to predict incoming surface solar radiation.

Cloud cover and its temporal evolution predominantly drive the variability of atmospheric reflectivity that determines the amount of solar radiation reaching the earth’s surface. Indeed, in a study by Supit and Van Kappel (1998), information on cloudiness was used to estimate surface solar radiation at locations where there were no radiation measurements. Clouds when present, reflect, scatter and transmit part of incoming solar radiation. Kasten and Czeplak (1980) found that the extent of reflection, scattering or transmission by clouds, depends on the type of cloud and its characteristics. Knowledge of the types and variability of clouds is thus very crucial to understand their effects on the different components of the earth’s radiative budget.

In general, the WA region has a complex cloud cover system which ranges from low layered clouds associated with moisture flux coming from the Gulf of Guinea (van der Linden et al., 2015), to deep mesoscale convective systems advected from east to west (Fink et al., 2010b; Schumacher & Houze Jr, 2006) and local convection associated with the state of the continental surface (Sylla et al., 2011). The interannual variability of these clouds has been found to be relatively small (Bouniol et al., 2012) but some systems are known to be associated with intraseasonal variation due to the intermittency of the African Easterly Wave (Söhne et al., 2008) or the variability of the Saharan Heat Low (Lavaysse et al., 2010). In the rainy season (JJAS), cloud systems’ occurrence in the region is greatly influenced by the West African Monsoon (WAM) (Klein et al., 2015) with the more frequent occurrence and patchier structures in the afternoon (Söhne et al., 2008). In the southern part of WA, there is a frequent occurrence of an extended cover of shallow low-level, non-precipitating stratiform clouds which often persist into the day, considerably reducing incoming surface solar radiation (Knippertz et al., 2011).

Part of these different cloud systems mainly drive the variability of atmospheric reflectivity but remains poorly studied due to lack of a long-term consistent

database of cloud cover observations. In addition, large differences exist between the different satellites, reanalysis and model datasets that are used in place of ground observations to study clouds in the region (Hill et al., 2016). The contribution of cloud cover to the radiation budget is thus not very well understood in several parts of the region. Few regional field campaigns such as the “African Monsoon Multidisciplinary Analysis” – AMMA (Redelsperger et al., 2006) and “Dynamics-Aerosol-Chemistry-Cloud Interactions in West Africa” – DACCIWA (Knippertz et al., 2015) have provided invaluable information on clouds in some parts of the region. Otherwise, ground-based observations of clouds are only available at the Atmospheric Radiation Measurement (ARM) Mobile Facility (AMF) site in Niamey, Niger (Miller & Slingo, 2007). Most studies dealing with the influence of clouds on solar radiation in WA have therefore been limited to Niamey, in the Sahel region (e.g. Bourgeois et al. (2018) and Bouniol et al. (2012)).

Bouniol et al. (2012) identified four cloud classes in the Niamey region: low-level clouds (bases below 3 km), mid-level clouds (bases between 3 km and 7 km), cirrus clouds (bases above 8 km) and deep convective systems. Mid-level clouds and anvil clouds (which are associated with deep convective systems) were found to have the largest impact on incoming solar radiation with radiative effects up to 150 W m^{-2} and 300 W m^{-2} respectively varying across months whereas cirrus clouds were found to have a minimal impact on solar radiation, reducing surface radiation up to about 50 W m^{-2} . Bourgeois et al. (2018), in a different study on the Niamey region, found that the cloud shortwave radiation effect ranges between -220 W m^{-2} and -20 W m^{-2} depending on the month and cloud properties. In some parts of southern WA, satellite observations have been used to show a large amount of incoming solar radiation is reflected back to space due to the presence of different cloud types (Hill et al., 2018).

The space-time variability of most of these cloud types and convection are not well understood and documented in several areas of the WA region, thus leaving many open key questions when dealing with the variability of atmospheric reflectivity due to cloud cover. Within this context, the present study aims to understand and document the climatology of cloud cover in the WA region. While previous studies such as Hill et al. (2016) and Hill et al. (2018) focus on cloud cover evolution in only southern WA, we first present a regional overview of cloud cover variability over the whole WA in general and then focus on the variability of these clouds in different climatic zones over the region. We intend to provide different scales of variability for different cloud cover type occurrences in the region which could be important for understanding different components of the earth’s radiation budget such as the amount of incoming surface solar radiation.

The paper is organized as follows: Section 3.4 provides a description of the datasets and methodology. Section 3.5 presents and discusses the results of cloud cover variability in the region while the occurrence frequencies of clouds are presented and discussed in Section 3.6. Conclusions are drawn in Section 3.7.

3.4 Datasets and methods

In this study, the time and space scales of variability of the cloud cover in WA are investigated from the perspective of evaluation of the solar energy resource. The present study, however, does not provide an evaluation of available solar energy resources. The cloud cover information come from both European Centre for Medium-Range Weather Forecasts (ECMWF) reanalysis – ERA5 (C3S, 2017) and passive remotely sensed observations of the Clouds and the Earth’s Radiant Energy System – CERES (Wielicki et al., 1996), both at hourly timescale for a period of 10 years from 2006 to 2015. The analysis in this study allows the comparison and thus the identification of differences between the two cloud cover data products, both of which have not yet been used to study cloud systems in the WA region. As detailed in section 2.3, the two datasets were first evaluated against synoptic in-situ observations of the Integrated Surface Database (ISD) (Lott et al., 2001) provided by the National Climatic Data Centre (NCDC). The evaluations revealed that differences in the magnitude of occurrence of sky cover classes between the synoptic in-situ observations and ERA5 and CERES are not so large (Figure 2.4 in section 2.3).

3.4.1 Datasets

Reanalysis data

Hourly cloud cover fraction data from ERA5 was extracted on a regular $1^\circ \times 1^\circ$ over WA. ECMWF’s Integrated Forecasting System (IFS), implements the Tiedtke cloud scheme (Tiedtke, 1993) to forecast a three-dimensional (3D) cloud fraction, cloud liquid water and cloud ice water for each grid box. These cloud variables are produced in CY41R2 of the ECMWF’s IFS and documented in Part IV of the IFS Documentation (available at <https://www.ecmwf.int/en/elibrary/16648-part-iv-physical-processes>).

ERA5 provides a 3D distribution of cloud cover parameters including cloud fraction, specific cloud liquid and ice water, prognostically computed at model levels as well as diagnostic cloud cover fractions on 2D single atmospheric layers (namely low-level, mid-level, high-level and total atmospheric column). The 2D cloud fraction variables include the total cloud cover fraction (TCC) which integrates all clouds from the surface level to the top of the atmosphere with overlap assump-

tions (Barker, 2008; Jakob & Klein, 2000). Additionally, low-level (LCC), mid-level (MCC) and high-level (HCC) cloud cover fractions are respectively defined as the integration of all clouds from the surface to 800 hPa, 800 hPa to 450 hPa and from 450 hPa to the top of the atmosphere (TOA) (Forbes, 2017). In this study, the 2D single layer diagnostic cloud fractions are used for different analyses. Table I provides a summary of the different cloud variables used. Detailed documentation of the ERA5 data is provided at <https://confluence.ecmwf.int/display/CKB/ERA5+data+documentation>. Table 3.1 provides a summary of the cloud variables used.

Table 3.1: Summary of the different cloud cover variables of ERA5 and CERES data products used in this study. The definitions of cloud cover type are based on the pressure levels. TOA refers to “Top of the Atmosphere”.

Variable Name	Product Variable Definitions (by pressure levels)		Spatial Resolution	
	<i>CERES</i>	<i>ERA5</i>	<i>CERES</i>	<i>ERA5</i>
Low-level cloud cover (LCC)	surface to 700 hPa	surface to 800 hPa	$1^\circ \times 1^\circ$	extracted at $1^\circ \times 1^\circ$ (native horizontal resolution $\approx 0.3^\circ$)
Mid-level cloud cover (MCC)	low mid-level clouds (700 hPa to 500 hPa) high mid-level clouds (500 hPa to 300 hPa)	800 hPa to 450 hPa		
High-level cloud cover (HCC)	300 hPa to 50 hPa	450 hPa to TOA		
Total cloud cover (TCC)	Integration of all clouds from 50 hPa to surface	Integration of all clouds from TOA to surface		

Satellite observations

Passive satellite sensor observations of cloud cover are extracted over WA from the hourly CERES SYN1deg Ed4A (Minnis et al., 2016) product (hereinafter CERES). A combination of cloud properties measured by the MODIS sensor onboard the Terra and Aqua platforms and geostationary satellite (GEO) images (Minnis et al., 2011) are used to derive the CERES product. This product is intended for applications that require high temporally resolved (up to 1h) information on cloud cover and for regional diurnal process studies (ASDC, 2017).

The MODIS and GEO cloud information which are contained in the CERES product are spatially and instantaneously averaged into $1^\circ \times 1^\circ$ gridded regions at one-hourly intervals. Cloud cover information retrieved during the MODIS observation periods may be different from the surrounding GEO cloud cover information due to their retrieval differences.

The instantaneous gridded cloud cover fractions from the product are stratified by four pressure layers indicating the pressure at the cloud top height and thus leading to four cloud cover types; surface–700 hPa (low level clouds), 700 hPa–500 hPa (lower mid-level clouds), 500 hPa–300 hPa (higher mid-level clouds), and 300 hPa–50 hPa (high level clouds). We use these cloud cover variables in addition to the total cloud layer which is simply the 4-layer sum for a specific spatial and temporal resolution (Table 3.1).

The CERES sensors, like all passive sensors, have difficulty to identify multiple cloud layers and are usually unable to detect low clouds that occur below a higher cloud. Active sensors are less prone to these issues and may provide a solution. However, most of the presently available actively sensed cloud products such as the very useful CloudSat and CALIPSO (Stephens et al., 2018) do not provide a continuous high temporal resolution at a given location and may introduce some uncertainties when used for applications that require a continuous high-resolution data. The CERES product used in this study removes this issue by providing instantaneous hourly information on clouds for more than a decade. Comprehensive information on the CERES product including cloud retrieval algorithm, inputs, and potential issues has been already documented in ASDC (2017).

3.4.2 Methods

The datasets used in the study have the same temporal resolution. However, the native horizontal resolution of ERA5 is approximately 0.3° but has been extracted directly at a 1° resolution, equal to the resolution of CERES. CERES provides two mid-level cloud layers (mid-level high and mid-level low) whereas ERA5 provides just one. In order to compare them, a representative single mid-level layer is computed by summing the two mid-level layers of CERES. It must be noted that definitions of the different cloud cover layers provided by the two products are slightly different (Table 3.1).

In this study, we look at both seasonal and diurnal climatologies of the three cloud types. At the synoptic scale (the whole WA region), the mean cloud cover fraction is determined for each northern hemispheric season (i.e. winter: DJF, spring: MAM, summer: JJA, and fall: SON) by computing the mean of the instantaneous

hourly cloud cover fraction values. In addition, the seasonal mean diurnal variability of each cloud cover type is determined for five equal-sized bounded windows across the region as shown in Figure 3.1 and detailed in Table 3.2. The windows in Niger, Burkina Faso, and Senegal are located in the Sahelian climate region (Gbobaniyi et al., 2014) of WA. The other two windows are located in Benin and Cote d’Ivoire in the Sudanian and Guinean regions (Klein et al., 2015) of WA respectively. Both the Senegal and Cote d’Ivoire windows share proximity to the ocean (Atlantic Ocean to the west for Senegal and the Gulf of Guinea to the south for Cote d’Ivoire). Their proximity to the ocean diversifies cloud formation processes such as the contribution of sea-land breeze circulation to cloudiness (Parker & Diop-Kane, 2017), absent in the other Sahelian region where cloud systems primarily arise from Mesoscale Convective Systems (MCS) (Vizy & Cook, 2019) advected from east to west. North of latitude 15.5°N, the mean cloud coverage is very low (Hill et al., 2016), thus no window has been chosen in this part of WA.

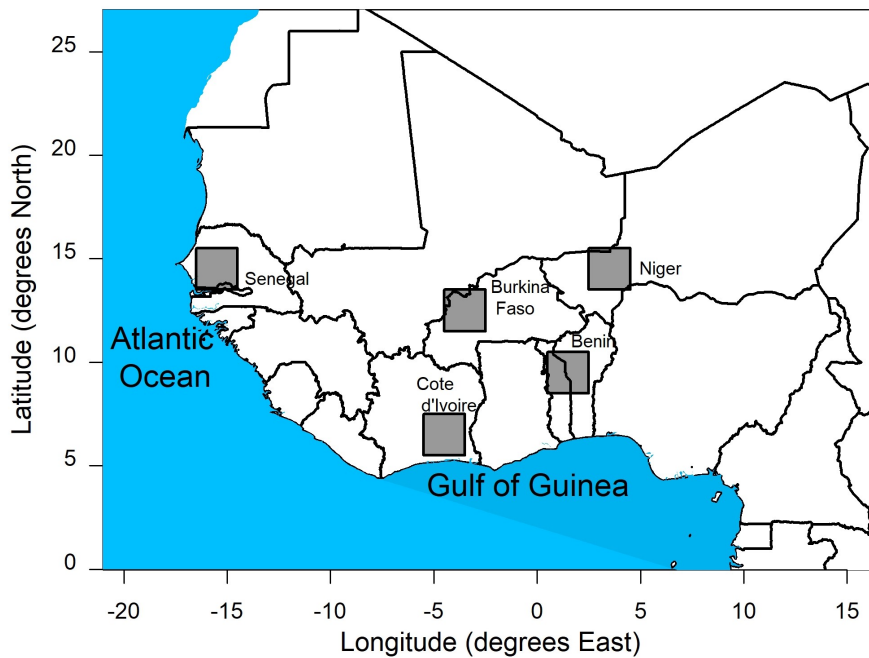


Figure 3.1: Map of WA showing the five $2^\circ \times 2^\circ$ bounded windows (grid boxes) selected for studying cloud variability at smaller space scale. The name assigned to each window is based on the country within which it lies. Niger, Burkina Faso and Senegal windows are located in the Sahelian climate region while Benin and Côte d’Ivoire are located in the Sudanian and Guinean climate regions respectively

Due to the dependence of surface solar radiation on clouds, the occurrence frequency (Cai et al., 2017) of cloud cover could be very useful to characterize, for example, fluctuations in incoming solar radiation received on solar panels in a given area. For the three cloud types being considered in the study, we computed

Table 3.2: Geographical coordinates of the five equal-sized windows selected for analysing cloud cover occurrences and variability across WA

Window name	Longitude bounds (°E)	Latitude bounds (°N)	Climate zone
Côte d’Ivoire	−5.5° to −3.5°	5.5° to 7.5°	Guinean
Benin	0.5° to 2.5°	8.5° to 10.5°	Sudanian
Burkina Faso	−4.5° to −2.5°	11.5° to 13.5°	Sahelian
Niger	2.5° to 4.5°	13.5° to 15.5°	Sahelian
Senegal	−16.5° to −14.5°	13.5° to 15.5°	Sahelian

(and compared) the occurrence frequency retrieved from the two datasets with only daytime hours (i.e., 0600 to 1700 UTC). Thus, the occurrence frequency is defined as the percentage of occurrences out of the total number of data records (i.e., 43824 daytime hours for ten years of records).

3.5 Cloud cover variability

In this section, we present a comparison of regional-scale, average daytime seasonal evolutions of cloud cover (i.e. total cloud cover and the three cloud types) determined from the satellite-derived CERES product and ERA5 reanalysis. We also present a comparison of the average diurnal evolutions of the cloud cover types for the two data products in some selected windows.

3.5.1 Seasonal evolution of cloud cover

Figure 3.2 and Figure 3.3 show the seasonal distributions of TCC, HCC, MCC, and LCC for CERES and ERA5 respectively. The evolution of TCC correlates well in the two products. In both products, higher coverage of clouds (greater than 40 %) is found over the oceanic and coastal regions of WA during DJF season while the inner land areas have lower fractions of cloud coverage. ERA5, however, shows relatively higher coverage of clouds extending from the north-western coast to some parts of the inner regions of Senegal, Mauritania, and Mali. From the southern coast, TCC increases and extends into the inner regions beginning from MAM. Maximum coverage occurs during JJA after which there is a decrease in cloud coverage in SON during which there is a shift of higher fractional coverages from the northern to the southern part of the region. Generally, the mean values of cloud coverage in ERA5 are slightly higher than in CERES.

The spatial and temporal occurrence of HCC and MCC are similar over the

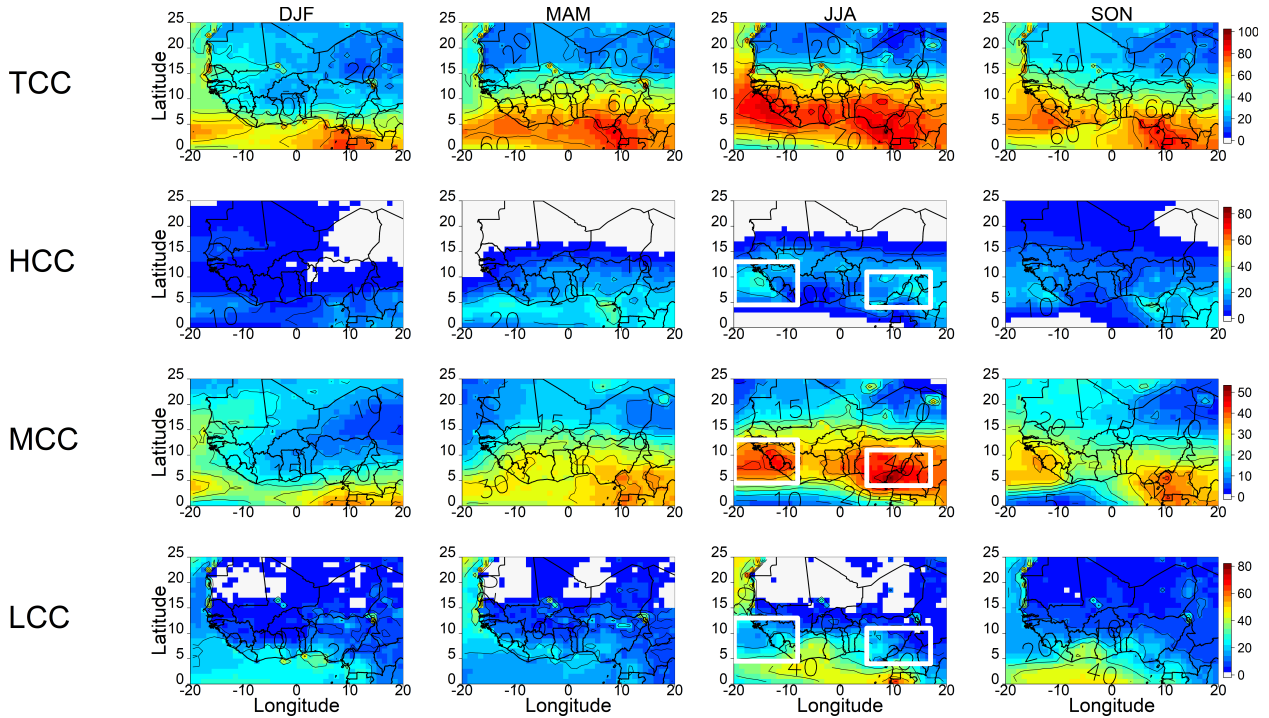


Figure 3.2: Seasonal average evolutions of TCC, HCC, MCC and LCC in percentage of coverage over WA of CERES satellite-based cloud products. The contours on the figure show the average fractional coverage of each cloud category. The average values of cloud fractions shown here are computed from the hourly daytime (0600 UTC to 1700 UTC) values for a 10-year period (2006–2015). The white rectangles in JJA for HCC, MCC and LCC show areas where high HCC and MCC obscure the satellite sensor from detecting lower lying clouds.

region in both products with both cloud types ubiquitous over the majority of the region throughout the year, while coverage strengthens during the monsoon season. However, the mean values of MCC are generally higher in CERES than in ERA5. Nevertheless, the mean values of HCC in CERES are much lower than the mean values in ERA5. This is perhaps explained by the difficulty to detect optically thin cirrus clouds by MODIS as revealed by previous studies (e.g., Hill et al. (2016), Lee et al. (2009), and Sun et al. (2011)), leading to the lower mean fractions of HCC. The slightly lower values of TCC shown by CERES than ERA5 could be attributed to this same reason but needs to be investigated further. In addition, water vapour channels on Terra-MODIS experienced some degradation around 2008, thus affecting cloud retrievals (ASDC, 2017).

LCC coverage is also characterized by high seasonal variability, generally present in higher fractions only around the coastal regions during the dry season (DJF), after which the density of coverage extends northwards reaching a maxi-

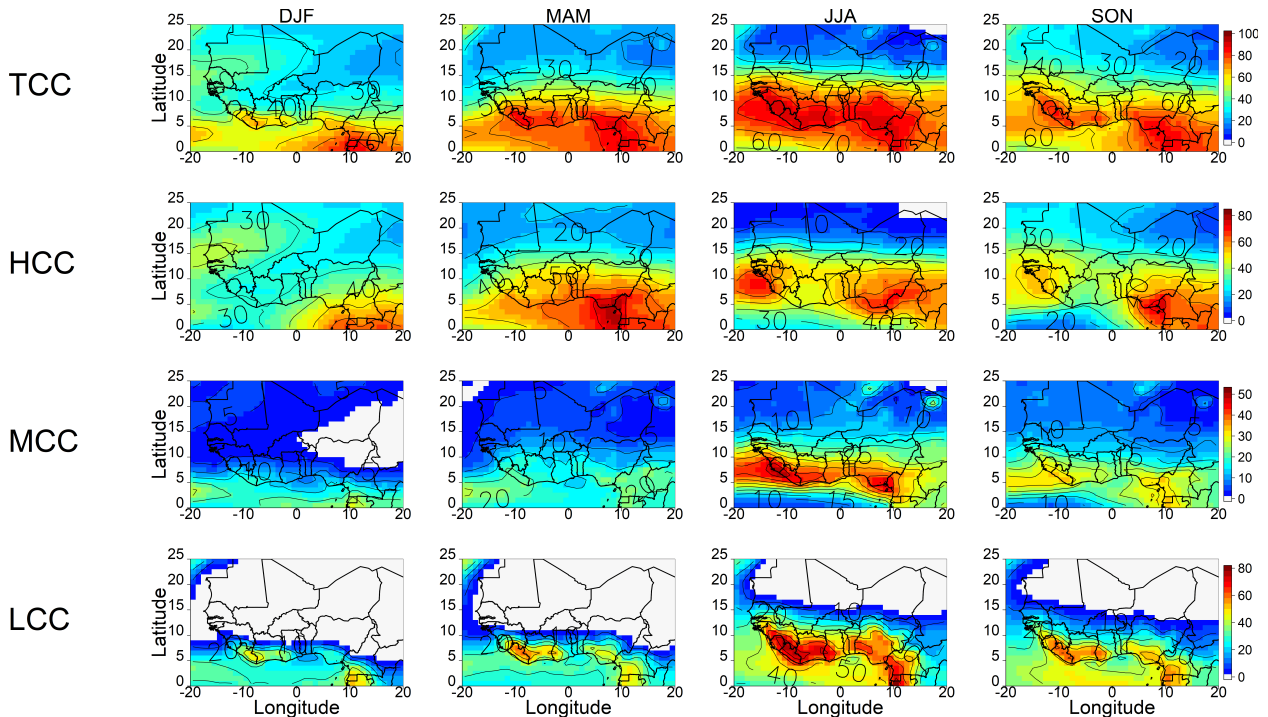


Figure 3.3: Seasonal average evolutions of TCC, HCC, MCC and LCC in percentage of coverage over WA of ERA5 cloud products. The contours on the figure show the average fractional coverage of each cloud category. The average values of cloud fractions shown here are computed from the hourly daytime (0600 UTC to 1700 UTC) values for a 10-year period (2006–2015).

mum during the monsoon season (JJA). In both products, there is a clear monsoon maxima of LCC coverage around the coastal regions of Cote d’Ivoire, Ghana, and parts of Nigeria in agreement with van der Linden et al. (2015). The signal is, however, relatively stronger in ERA5 than in CERES. Passive satellite sensors are not able to detect low clouds when there are over-lying clouds at higher altitudes (Karls-son & Johansson, 2013); this may explain the relatively low values of LCC fraction over the coastal areas (even during the monsoon season) for the CERES product. For instance, the highlighted areas in Figure 3.2 (white rectangles in JJA for HCC, MCC, and LCC) show regions with high mean HCC and MCC. In the same regions for LCC, mean cloud fractions are relatively lower than in the surrounding areas.

During the DJF and MAM, CERES does not show a well-marked spatial variability of LCC between the Guinean (south) and Sahel/Sahara (north) regions. Surprisingly, CERES shows LCC over the Sahel/Sahara areas (up to about 20%) during the entire year, considering that low clouds (example shallow convective systems) rarely occur over these areas except in the core of the monsoon season (Bouniol et al., 2012). A spatial gradient of low-level convection between the Sahelian and

Guinean regions is thus expected due to the proximity of the latter to the ocean, leading to an influx of moisture from oceanic breezes and thus enhancing convection over these regions. This is however not the case in the CERES LCC seasonal evolutions (especially in DJF, MAM and SON). Considering that previous versions of CERES had struggled to discriminate between clouds and dust (ASDC, 2017; Loeb et al., 2018), we suspect that dust particles over the Sahara could have been misinterpreted as LCC by the MODIS sensor and may have overestimated the presence of LCC over this region. Indeed, the local maxima of LCC found between Niger and Chad during DJF and SON seem to be an extension of the Bodélé depression (Koren et al., 2006; Middleton & Goudie, 2001), an important dust source in the Sahara Desert. Other LCC local maxima can be seen during the year in other parts of the Saharan region, seeming to follow some dust sources in the region (Crouvi et al., 2012; Knippertz & Todd, 2012).

While the spatial and temporal gradient of LCC is weaker in CERES, ERA5 shows stronger seasonal evolution and clearer spatial gradients of LCC between the southern and northern parts of WA. The seasonal evolution of LCC could be linked to the seasonal displacements of the Intertropical Convergence Zone (ITCZ), as also discussed by Bouniol et al. (2012). LCC is only present along the Guinea coast during the Sahelian dry season, strengthening and extending northwards during the monsoon season. During the monsoon season, ERA5 shows no LCC occurrence in large parts of the Sahara Desert (north of latitude 18°N). This behaviour may be linked to the failure of reanalysis products to efficiently represent (in this case underestimate) the northward shift of the WA Monsoon (WAM) as indicated by both Hill et al. (2016) and Thorncroft et al. (2011). Moreover, an underestimation of potential evapotranspiration in ERA5 over deserts as mentioned in the product documentation means that the model could be too dry to generate LCC in some cases. Nevertheless, ERA5 seems to give a better representation of the seasonal and spatial evolutions of LCC in the region than CERES.

3.5.2 Diurnal evolution of the cloud cover types

The mean seasonal diurnal cycles of HCC, MCC, and LCC are presented in Figure 3.4 for Côte d’Ivoire (Figure 3.4a) and Niger (Figure 3.4b). The grid boxes in Senegal and Burkina Faso presents similar cycles as that of Niger whiles the cycle in the Benin grid box is similar to Côte d’Ivoire. The cycles for these three grid cells have thus not been shown. The mean diurnal cycle (bold lines in Figure 3.4) is computed from hourly, day and night, data for the 10 years (2006-2015) and for both CERES and ERA5 datasets. The 10-year variability of the cloud fraction diurnal evolution within each season is characterized by the 10th and 90th inter-percentile

ranges (shaded regions) in Figure 3.4.

Generally, the diurnal variations of cloud fraction present an important spread around the mean values whatever the season, the cloud types or the regions. In both regions (Figure 3.4a,b), high-level clouds (HCC) present the largest intraseasonal variability in its diurnal cycle when compared to the ones associated with low and mid-level clouds across all seasons and for both products. For HCC, ERA5 presents a much uniform spread during the day while CERES has a much higher spread during the night hours than the daytime.

The HCC and MCC diurnal evolutions retrieved from the ERA5 dataset do not present any significantly marked diurnal cycle for average cloud fractions (thick solid lines) in both grid boxes. This absence of a well-marked diurnal cycle in ERA5 is unexpected considering the presence of distinctly marked diurnal cycles of HCC and MCC in previous studies (e.g., Bourgeois et al. (2018) and Hill et al. (2016)). CERES, however, shows some diurnal variation of HCC (but not for MCC) in both regions with higher cloud fractions in the night than during the day, more consistent with some previous studies in the region (e.g., Bouniol et al. (2012) and Hill et al. (2016)). The diurnal cycle of HCC in CERES could be linked to the development of convection during the daytime (Stein et al., 2011) and their consequent detrainment into anvil and cirrus clouds (Mace et al., 2006; Sassen et al., 2009) in the evening and nighttime. This is however missed by ERA5 and is likely due to the convective parameterization (Bechtold et al., 2014) used in the IFS.

The LCC diurnal cycles present different patterns. In the Côte d’Ivoire box, LCC retrieved from both datasets have a very strong diurnal evolution for all seasons. ERA5 presents an early morning peak (around 0600) for fractional coverage while the CERES dataset provides an afternoon peak (around midday). Considering the closer proximity of the Côte d’Ivoire box to the ocean, the diurnal evolution of the ERA5 product seems to be consistent with the diurnal cycle of the tropical lower level convection which generally reaches a maximum in the early morning in the oceanic and coastal areas (Yang & Slingo, 2001). The maximum fractions of HCC occur during the nighttime (until the early morning) and obscure the CERES sensors from properly detecting low-lying clouds in range. This may explain the gap between the peaking periods of LCC in the two datasets. In addition, it appears nighttime stratus decks in the region as revealed by van der Linden et al. (2015) are missed by the CERES product (very low or no LCC values at night in CERES relative to ERA5). This observation could also be attributed to the inability of CERES sensors to detect LCC at night when HCC is maximum and obscures the passive sensors. Additionally, lack of temperature contrast between warm surfaces

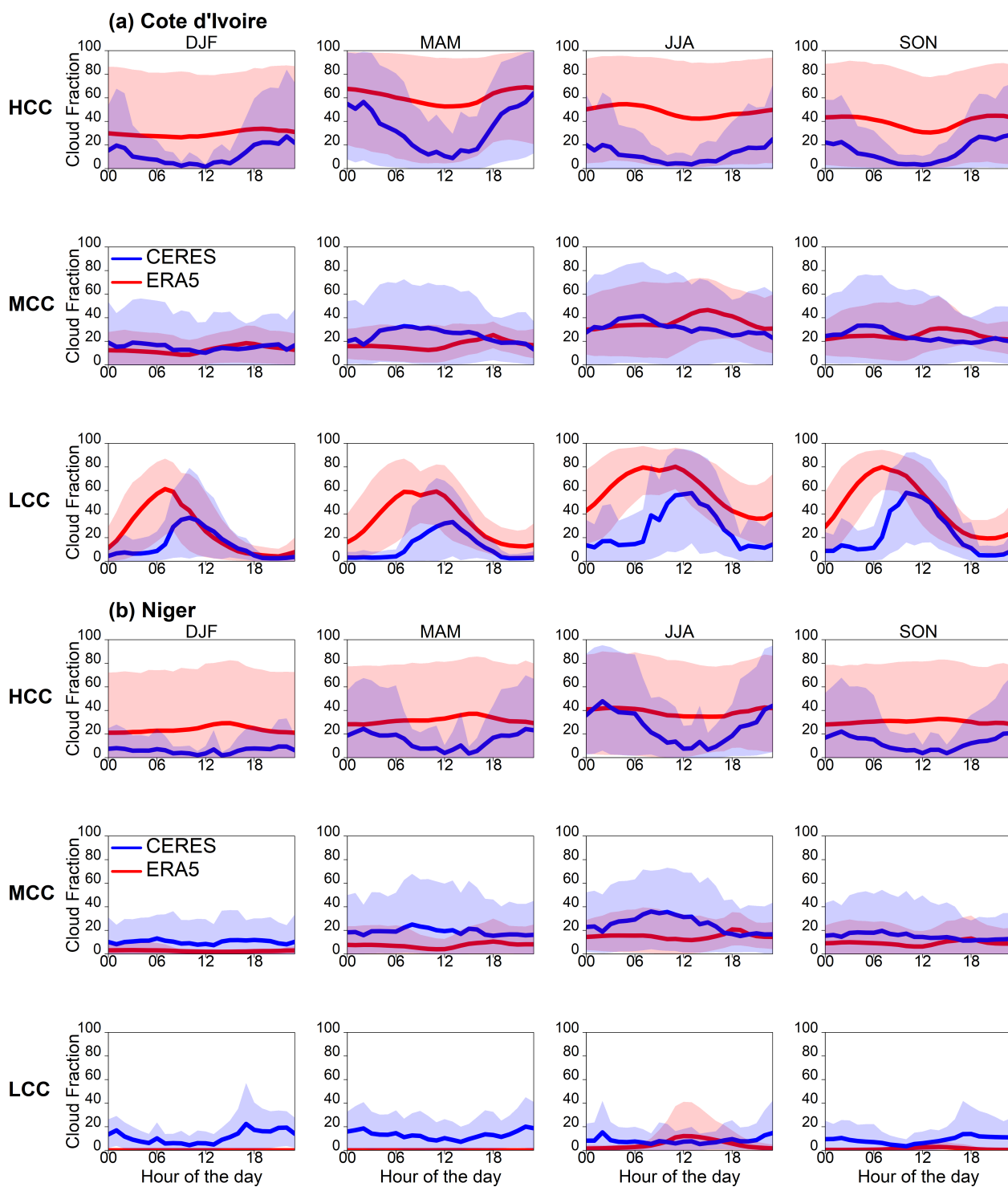


Figure 3.4: Seasonal average diurnal evolution of cloud fraction (in percentage of coverage) of high (HCC), mid- (MCC) and low (LCC) level clouds provided by CERES satellite-based and ERA5 reanalysis for two among five selected boxes in (a) Côte d'Ivoire and (b) Niger. The shaded regions bounding the mean cloud fraction curves (solid lines) represent the 10th and 90th inter-percentile range in the diurnal evolution of cloud cover fractions.

and low clouds at night makes it difficult for passive sensors (CERES in this case) to detect LCC during the night (Andersen & Cermak, 2018; Knippertz et al., 2011; van der Linden et al., 2015).

For the Niger box, important differences exist between the two products. Firstly, CERES shows fractions of LCC in all seasons with no clearly marked diurnal cycle while ERA5 reveals the occurrence of LCC only during JJA peaking around midday. The presence of LCC in all seasons for CERES can partly be linked to the presence of dust in the Sahel/Sahara areas which may be misinterpreted as clouds by the passive sensor as already discussed in subsection 3.5.1. The afternoon peak of LCC in ERA5 during the monsoon is consistent with the evolution of continental mesoscale convective systems (MCS) (Vizy & Cook, 2019). These MCSs, moving from east to west, are responsible for the majority of the clouds occurring in the Sahelian region during the monsoon season in WA. This also explains the difference in timing of the peak occurrence of LCC (for ERA5) in the two regions, i.e. 0600 UTC for Côte d’Ivoire, 1200 UTC for Niger. To a lesser extent, the differences in definitions of the cloud types for the two products could perhaps explain some of the differences between the two products.

3.6 Cloud occurrence frequency in West Africa

In this section, we present a 10-year climatology of clouds’ occurrence frequency under different perspectives. The cloud occurrence frequency is an important parameter to consider during the feasibility assessment for large-scale solar energy development. It could, for example, be used to characterize the fluctuations of surface solar radiation received on solar panels due to cloud cover. Here we look at the occurrence frequencies of clouds in WA from a general perspective and then for each cloud type. The occurrence frequency is principally expressed as a percentage of events of specific interest (n) relative to the total number of data observations (N). Where N is equal to 43824 hours i.e., the total number of the defined daytime hours (between 0600 and 1700 UTC) from 2006 to 2015.

3.6.1 General occurrence frequency

Figure 3.5 shows the frequencies of at least one cloud type occurrence, the simultaneous occurrence of all three cloud types and no cloud occurrence in the whole WA region for each season. These occurrence frequencies have been computed for both cloud products without taking into account the magnitude of cloud fraction.

The frequency of having at least one cloud type occurring (Figure 3.5a),

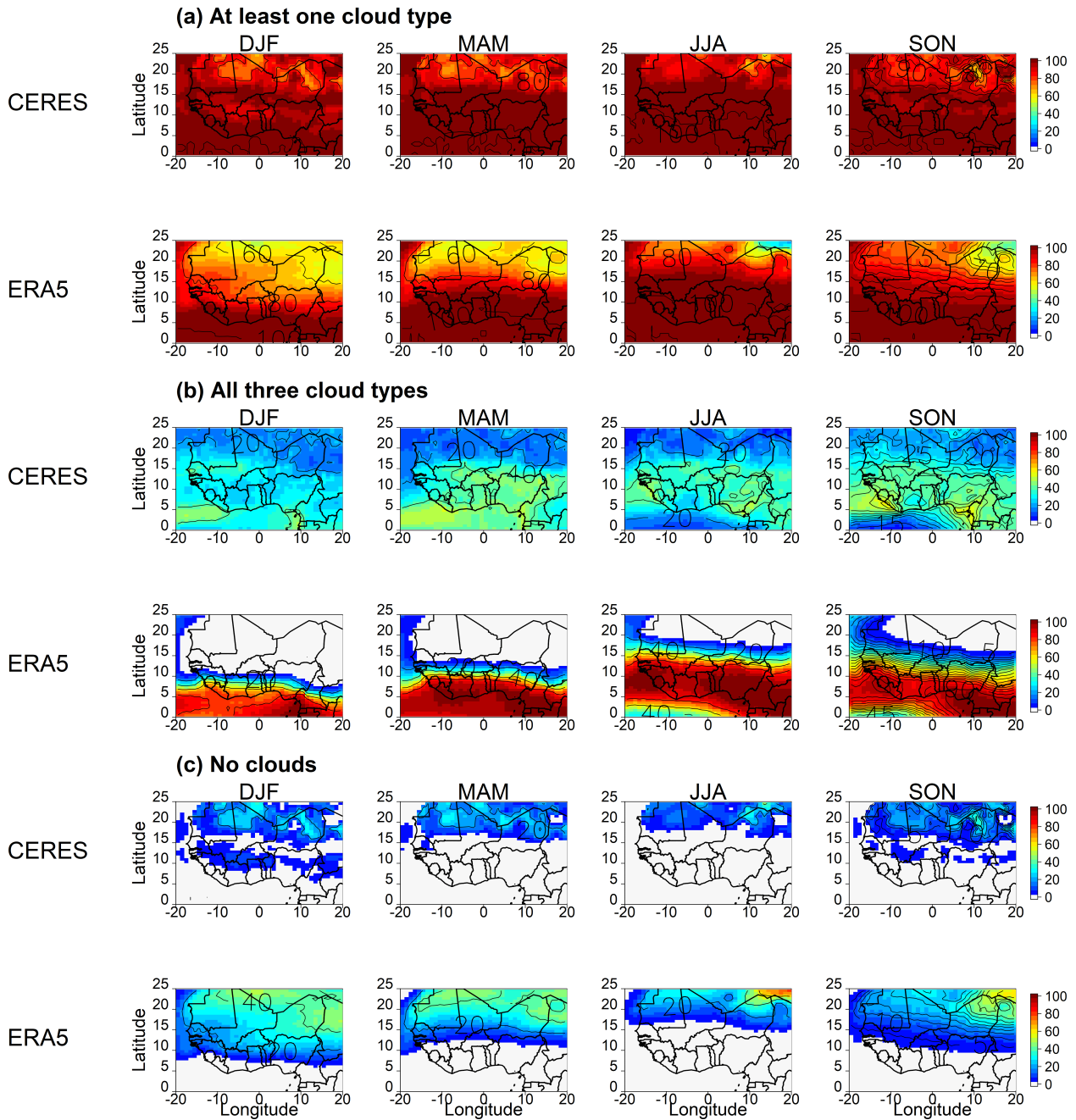


Figure 3.5: CERES and ERA5 climatologies of occurrence frequency (representing the percentage of occurrence out of total observations in each season) for (a) at least one cloud type presence, (b) all three cloud types simultaneously and (c) no cloud presence, over WA.

generally decreases from south to north in both products and for all seasons. Additionally, JJA has a higher frequency of at least one cloud type occurrence in a lot of areas in the region relative to other seasons. In JJA, both products reveal a 100 % frequency of at least one cloud type occurrence (i.e. a cloud is always present) in all areas south of latitude 15°N. Northwards of this latitude, frequencies are be-

low 100 % and decrease up to about 60 % for ERA5 and 80 % for CERES. In other seasons, the frequencies are rather lower in a lot of areas in the region. For example, during DJF in both products, only areas south of about 7°N (southern coastal region) experience 100 % frequency for at least a cloud to be always present while all areas northwards of this latitude have lower frequencies (up to 80 % for CERES and 60 % for ERA5). The relatively higher values of CERES than ERA5 north of latitude 15°N in all seasons could be explained by dust being misinterpreted by the CERES sensor as already discussed in subsection 3.5.1. In the ERA5 product, there is a northward progression of the latitude, south of which all areas experience a 100 % frequency of at least one cloud type occurrence from DJF, peaking in JJA and shifting southwards again in SON. This seasonal evolution could be linked to the evolution of the WAM. Since the magnitude of cloud fraction is not taken into account, the computed frequencies encompass cloudiness of all ranges including very small cloud fractions which might not be easily visible to humans or certain instruments.

Figure 3.5b also shows the frequency of all three cloud types occurring at the same time over the region (regardless of the cloud fraction) for each season. Both products agree on the spatial distribution of frequency of the simultaneous occurrence of all three cloud types but there are pronounced differences in terms of the magnitude of the frequencies. While there is a distinct northward progression of the frequency maxima from DJF to JJA and a slight southward shift in SON in the ERA5 product, the CERES product does not reveal a well-marked seasonal evolution of this frequency maxima shifts. Moreover, in all seasons, CERES shows that all three cloud types occur at the same time between 20 % and 30 % of the time in the Sahel/Sahara areas and up to about 50 % of the time in southern WA (south of 10°N). ERA5 however, reveals a 0 % occurrence frequency in areas north of 10°N in DJF and north of 15°N in MAM (all areas below these latitudes have frequencies ranging from 10 % to 90 %). In JJA and SON, only the northern parts of Mauritania, Niger, and Mali have a 0 % frequency of all three clouds occurring at the same time.

Figure 3.5c presents the frequency of no cloud occurrence in the WA region. While only a few coastal areas in southern WA have 0 % frequency of no cloud occurrence in DJF for both products, a large portion of WA (all areas south of latitude 15°N) in JJA has a 0 % no clouds occurrence frequency. This is due to the influx of moisture from the Gulf of Guinea during the active monsoon season, enhancing cloud formation over those areas. CERES shows relative lower frequencies of no cloud occurrence in northern WA across all seasons than ERA5. This could be attributed to dust particles that are misinterpreted as low clouds by the sensor

even in the absence of real clouds and thereby reducing the frequency of events of no cloud occurrence.

The probability density plots of cloud fraction in Côte d’Ivoire (Figure 3.6a) reveals that the CERES product has a much higher number of events of zero fractions (no cloud cover) for all three cloud types than ERA5. This subsequently reduces significantly, the number of possible events for simultaneous occurrence of all three cloud types leading to a much lower frequency of all three cloud types occurring simultaneously near the Guinean coast by the CERES product. On the other hand, in the Sahel (Figure 3.6b, Niger box), ERA5 presents more zero cloud fraction events than CERES for MCC and LCC (extremely high for low clouds). This explains the slightly higher frequencies of simultaneous occurrence of all three clouds, north of the Sahelian region by the CERES product.

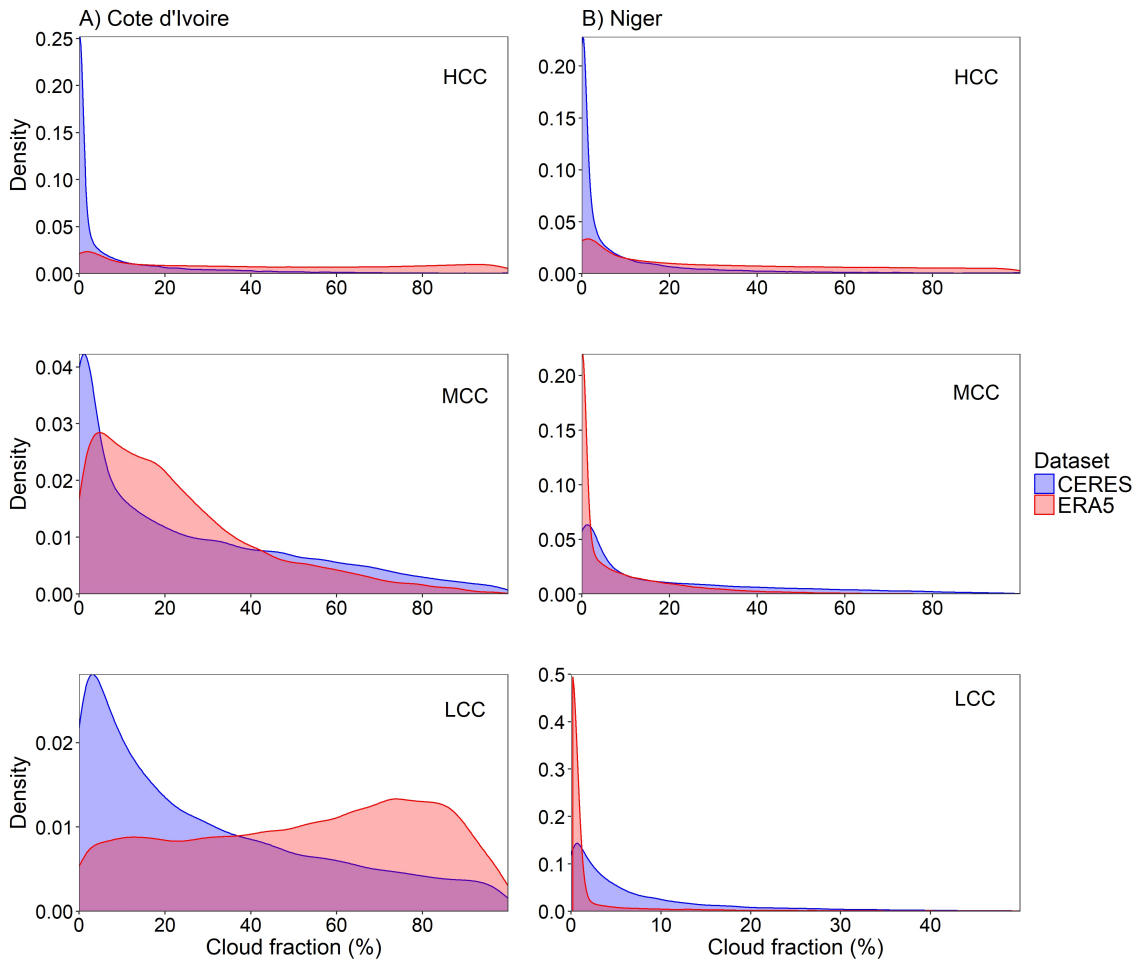


Figure 3.6: Probability density distributions of high-level (HCC), mid-level (MCC) and low-level (LCC) cloud fractions retrieved from the CERES and ERA5 datasets and for (a) the Côte d’Ivoire box and (b) the Nigerien box. This distribution is only generated from daytime hours between 0600 UTC and 1700 UTC.

3.6.2 Low-level cloud cover occurrence as a function of fractional coverage

LCC are known to have an important influence on the shortwave component of the radiation budget (Bouniol et al., 2012; Pyrina et al., 2013) depending on their thickness, fraction and water content (Liou, 2002). Thick low-level stratus and cumulus clouds block a large proportion of incoming solar radiation from reaching the earth's surface. In this section, we present the frequency of low-level clouds occurrences in WA as a function of their fractional coverage. We classified LCC occurrence events into three classes depending on the cloud fraction (CF) value. The three-class definitions are: low coverage $0 < CF < 40$, moderate coverage ($40 \leq CF < 80$) and high coverage/overcast ($CF \geq 80$). (Figure 3.7 presents the occurrence frequency for the three fractional coverage classifications of LCC (even when other cloud types are present) identified for all seasons in WA for the two products.

Over the entire region, the frequency of low coverage LCC is generally greater than moderate coverage LCC, which in turn is also greater than high coverage/overcast LCC. For low coverage of LCC (Figure 3.7a), CERES reveals a relatively less pronounced seasonal evolution of occurrence frequencies with values of at least 40% over the whole region. In all seasons, areas south of latitude 17°N have higher frequencies of low coverage LCC than areas northwards of this latitude. ERA5, however, reveals a more pronounced seasonal evolution of low coverage LCC with peak values progressing northwards from DJF to JJA (begins to shift southwards in SON). In DJF, almost the entire Sahel/Sahara regions have 0% frequency of low coverage LCC (as well as moderate and high coverage LCC). But in JJA and SON, only parts of northern Mauritania, Mali and Niger experience 0% occurrence of LCC.

Both products also reveal a reduction of low coverage LCC occurrence frequencies during JJA in southern WA (notably at areas closer to the coast). During the active monsoon season, the influx of moisture from the Atlantic Ocean enhances convection and thus LCC formation. The fractional coverage of LCC, therefore, increases, hence reducing the occurrence of low coverage LCC during this period. This is however not the case when moderate and high/overcast coverage LCC are considered (see JJA for Figure 3.7b,c) as the enhancement of convection development increases the fractions of LCC in the lower altitudes.

Moderate coverage of LCC (Figure 3.7b) is mostly confined to the coastal southern WA up to about 10% in CERES and 20% in ERA5 during DJF and MAM. In JJA and SON, moderate coverage LCC occurrence increases at the coastal areas

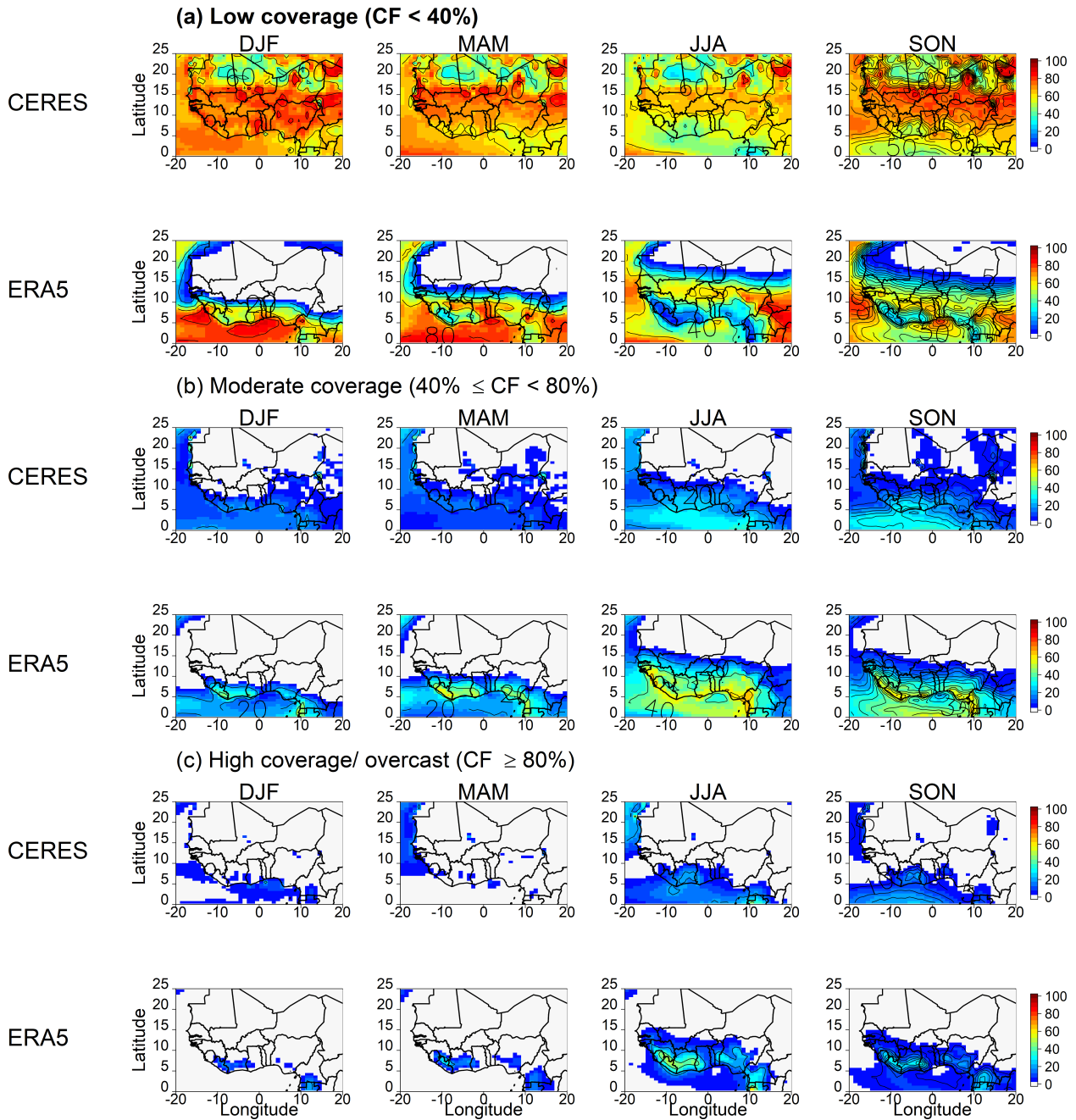


Figure 3.7: CERES and ERA5 climatologies of occurrence frequency of low-level cloud occurrence (percentage of occurrence out of total time in each season) as a function of fractional coverage: (a) low coverage, fractions less than 40 % (excluding 0 %), (b) moderate coverage, fractions between 40 % and 80 %, and (c) high coverage or overcast, fractions higher than 80 %.

of southern WA (up to about 60 % in ERA5 and up to about 40 % in CERES) and progresses to just south of the Sahelian region (south of latitude 15°N in ERA5 but also some other areas in the Sahara region in CERES). In the same way, it is more common to observe high fractional coverage or an overcast condition (Figure 3.7c)

of low-level clouds near the coastal regions of southern WA rather than in northern WA where such occurrences are very rare or non-existent in JJA and SON. In addition, the ERA5 product shows slightly higher frequencies than the CERES product over the coastal areas of southern WA when moderate and high coverage LCC are considered.

3.6.3 Solitary occurrence of cloud types

To determine the radiative effect of a particular cloud type (not done in the present work), it is necessary to consider only events of lone occurrence of that cloud type i.e. without the presence of other cloud types. For the two data products, we, therefore, computed the occurrence frequency of each cloud type when no other cloud types are present in all seasons. In these computations, we did not take into account the cloud fraction. The results are illustrated in Figure 3.8 and present important discrepancies between the two products especially for both LCC only and HCC only occurrences.

For LCC only (Figure 3.8a), CERES reveals occurrences with frequencies up to about 50% over the land areas of the region (except around some parts of southwestern Nigeria in JJA with 0%). ERA5, on the other hand, reveals that the occurrence of LCC only in the absence of other clouds is very rare over the land areas in WA except in some parts of southern WA closer to the coast in DJF. The higher values shown by CERES can be linked to the misrepresentation of dust as LCC as already discussed in subsection 3.5.1. Additionally, MODIS classifies very thin HCC over thicker LCC as low clouds (Hill et al., 2016) due to its inability to detect the former and may have increased LCC only frequency.

For the MCC only occurrence (Figure 3.8b), the two products are in a relatively better agreement with just slight differences unlike for LCC only and HCC only. Both show a regional maximum occurrence in the northern part of WA (north of 15°N except in DJF in ERA5).

For HCC only occurrence (Figure 3.8c), there are important differences between the two products. Generally, the CERES product has much lower frequencies than ERA5 and in addition, the number of areas with HCC only occurrence increases from DJF to SON in CERES while it decreases from DJF to JJA, increasing again in SON. For example, in DJF CERES reveals a 0% frequency of HCC only occurrence over almost the whole region while ERA5 shows frequencies up to about 60% (just a small area on the southern coast has 0% frequency). The 0% frequency shown over the entire WA by CERES could be partly due to the presence of LCC (dust misinterpreted as LCC) over the region but also the inability of the CERES

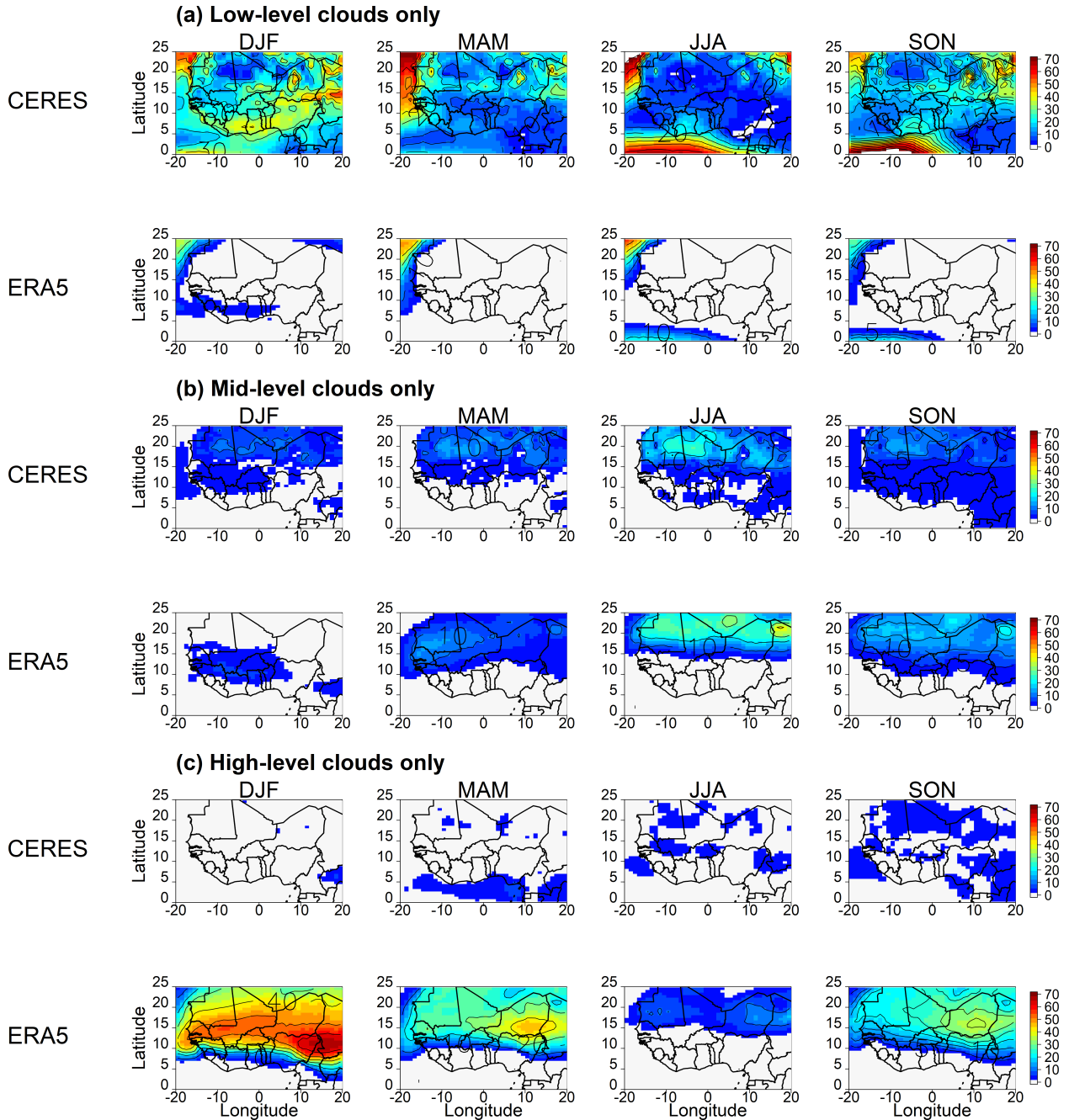


Figure 3.8: CERES and ERA5 climatology frequencies of cloud occurrence (percentage of occurrence out of total time in each season), for each cloud type: (a) LCC, (b) MCC, (c) HCC, when the other clouds are not present

sensor to detect very thin HCC in the atmosphere thereby missing many events of HCC only occurrence. In MAM, a similar occurrence is observed for both products but with reduced frequencies for ERA5 (with the area of 0% also shifting northwards) and also very low frequency values occurring at few areas over the Saharan region and Gulf of Guinea in the CERES product.

For ERA5 in JJA, all areas south of latitude 13°N have 0% frequency for HCC only occurrence and all areas north of this latitude have relatively lower frequencies than in other seasons. This could be linked to the relationship between HCC formation and daytime convection. The vertical development of LCC and consequent detrainment at higher altitudes leads to the formation of HCC. The presence of HCC only is likely to be less considering that at the time of HCC formation, lots of LCC could still exist in the lower altitudes of the atmosphere (especially since we have considered only daytime hours for this computation). Low frequencies can be seen in a few places over the region in the CERES product.

The large discrepancies observed between the two products for LCC only and HCC only occurrences needs to be investigated further for better understanding. The interpretation of Figure 3.8, however, needs to be made with caution. For example, it might not be surprising that CERES has a higher occurrence frequency of LCC only since they can only be detected by the satellite instruments if there are no optically thick higher-level clouds. Additionally, the possible misinterpretation of dust as LCC could increase their occurrences.

3.7 Summary and conclusions

In this study, we examined the variabilities and the occurrences of cloud cover in WA, which could be essential for any feasibility study of solar energy potential in this data-scarce region. We developed and compared a 10-year climatology of different cloud types in WA from two cloud products: the satellite-derived CERES SYN1deg and ERA5. Four main outputs of the two products including TCC, HCC, MCC, and LCC were used to document the regional-scale daytime seasonal evolutions and occurrence frequencies of cloud cover in WA. In addition, we presented the diurnal cycle of cloud cover fraction at grid-scale level for two selected equal-sized bounded windows across the Sahelian and Guinean climate zones of the WA region.

To an extent, both products agree on the spatial distribution of cloud cover over the region but with some differences in the magnitude of the fractional coverage. As expected, the southern part of WA is much cloudier in all seasons and receives lesser incoming solar radiation than the other parts of the region. TCC in the region intensifies during the monsoon season (JJA) and is very intense in southern WA where mean cloud fractions are up to 70% for the CERES product and up to 80% for ERA5. In the Sahelian and northern parts of the region, TCC fractions are much lower (less than 50%) during the core of the monsoon. The CERES product reveals much lower magnitudes of cloud fraction than ERA5 for the three cloud types even though the spatial distributions seem to be fairly correlated. This behaviour is

linked to the inability of the CERES sensors to detect optically thin HCC and MCC which occur in the region as well as the inability of passive sensors to detect low-lying clouds in multi-layered cloud cover events. In the ERA5 product, the seasonal evolution of LCC could be interpreted as being related to the seasonal movements of the ITCZ. This is, however, not readily noticeable in the CERES product, showing LCC over the entire region with a very little spatial gradient (except in the JJA and SON). This behaviour is attributed to the difficulty to discriminate between dust and clouds by CERES, hence misinterpreting dust as LCC over the Sahelian and Saharan areas.

The seasonal evolutions of the diurnal cycle for cloud fraction of the three cloud types have been investigated for five selected boxes: Cote d'Ivoire, Benin, Burkina Faso, Niger, and Senegal. For the sake of brevity, only the Ivorian and Nigerien contrasted regions are discussed in this paper. In the Ivorian and Nigerien regions, no clear diurnal variation is detected in the HCC and MCC evolutions provided by the ERA5 datasets. CERES, however, has a relatively marked diurnal variation for HCC (but not for MCC) with lower (higher) fractional coverage during the day (night), more consistent with previous studies (e.g., Bouniol et al. (2012) and Hill et al. (2016)). LCC have a much significantly marked diurnal variation for both products in the Ivorian region. In the Nigerien area, CERES does not reveal any clear cycle while the ERA5 product presents a clear diurnal cycle mainly in the monsoon season. With the ERA5 dataset, the evolution of the LCC fractions presents a peak in the morning (around 0600 UTC) in the Ivorian region and around midday in the Nigerien area. This pattern is not replicated when the CERES dataset is used since we observe a shift to midday for the peak in Cote d'Ivoire and no clear cycle in Niger. The pattern of the diurnal variation provided by ERA5 is consistent with WRF model simulations of Vizy and Cook (2019) and multi-satellite analysis of Yang and Slingo (2001) where early morning peak for tropical lower level convection at coastal/oceanic areas and a midday to evening peak of Mesoscale Convective Systems are explicitly pointed out.

We also investigated the daytime occurrence frequency of clouds in the region based on several criteria for each season. Generally, the middle and northern parts of the region (north of latitude 10°N) are associated with high frequencies of no cloud occurrence events (frequencies for no cloud occurrence are much higher in ERA5 – up to about 50% than in CERES – up to about 20% of the time). South of a given latitude (e.g. 15°N for both products in JJA) there is at least one cloud type occurring at all times (we do not consider the magnitude of cloud fraction in this assessment). Additionally, all three cloud types can occur at the same time at a given location. The frequency of simultaneous occurrence of all three cloud types

is much higher south of latitude 15°N but is considerably higher in ERA5 (up to 90 % in some coastal areas) than in CERES (up to 40 %) with reasons for such huge discrepancies already mentioned in the preceding paragraphs.

Considering the radiative effect of low clouds (i.e. thick stratocumulus and cumulus clouds) to incoming shortwave radiation and the dependence of the radiative effect on cloud cover extent, we expanded our investigations to occurrence frequency of LCC, taking the fractional coverage into account. The coastal areas of southern WA experience the highest occurrence frequencies of overcast conditions (coverage more than 80 %) of LCC i.e. up to 10 % in CERES and 20 % in ERA5. Along with the high frequencies of simultaneous occurrence of all three clouds, potential solar PV plants in this region are likely to produce a very low percentage of their nominal capacities for a significant number of times during the year (especially in the monsoon season due to the high reflectivity of the sky caused by clouds). Potential large-scale PV plants, therefore, require meticulous planning on plant sizing and/or distribution and number additional backup sources to cope with the potentially extreme fluctuations in power production.

The present study, therefore, provides comprehensive documentation of clouds occurrences and variability which could be extremely useful for planning largescale solar energy projects in such a data-scarce region. Comparisons between the two datasets used have also been used to identify discrepancies, agreements and possible drawbacks in each product. Individually, each of the two products has its strengths and uncertainties and can be used to complement each other for planning purposes. For instance, the diurnal cycle of HCC appears to be represented well by CERES product while the seasonal and diurnal cycles of LCC seems to be captured well in ERA5. The two datasets also agree on the seasonal variability of TCC and at least the spatial distribution of some occurrence frequencies.

Nevertheless, the study reveals some important differences between the two datasets used, starting with the cloud definition itself. The need for high quality and continuous database of cloud observations at high temporal resolution is thus imperative. Additionally, the study highlights the need to improve cloud retrieval algorithms in future CERES updates or planned satellite missions and to improve the microphysics schemes and parametrizations used in reanalysis products like ERA5. With a quality database of cloud observations in the region, this study lays out a blueprint for future assessment of solar energy development feasibility.

Future studies will be centered on identifying conditions for the occurrence of some cloud types (with datasets such as the state-of-the-art regional climate models for the region) and their associated shortwave radiative effect.

Chapter 4

Synoptic conditions related to clouds occurrence in West Africa

4.1 Chapter overview

Using a state-of-the-art global reanalysis, Chapter 4 delves deeper into low-level clouds, identifying the synoptic conditions in which they occur as well as their impacts on the earth's energy budget at the surface. Low-level clouds are chosen for further investigations because our analysis and other previous studies have shown that they have the largest impacts on the surface downwelling shortwave radiation. This is because low-level clouds are mainly composed of liquid water droplets unlike high-level clouds containing ice. The liquid water droplets are usually smaller in size than the ice particles, making them more compact and increasing their liquid water paths. Longer optical paths increase the optical depth clouds and thus increases their attenuation effects in the shortwave. Regardless of this, these clouds are not very well understood in WA.

This chapter presents the distribution of occurrence frequency for different classes of low clouds in WA. Atmospheric conditions that trigger the occurrence of these clouds are also discussed in detail. Finally, the effects of each class on surface heat fluxes and shortwave radiation are presented. The novelties in this chapter are as follows:

- Previous studies have usually focused on low clouds in the night. Here, only the daytime low clouds are considered.
- The study analyzes low clouds in both the dry and wet seasons, unlike previous studies that focus only on the wet seasons.

The contents of the following chapter are from an article published in the **Earth System Dynamics (ESD)** in 2020 (Danso et al., 2020a).

4.1.1 Contributions

Literature review and context formulation

Together with my advisors, the context of the study was formed based on gaps I identified in the available literature with regards to low clouds in the WA region. The idea was to first identify events of low clouds' occurrence in both the Guinean and Sahelian climate zones of WA. These two areas are marked by contrasting climate features. I proposed a simple low cloud classification based on the cloud fraction in the lowest 2 km of the atmosphere to analyze the synoptic drivers.

General methodology

Firstly, I delineated a spatial window each in the Guinean and Sahelian regions of WA. Within each window, I identified events of low cloud occurrence. From the identified events, I performed a composite analysis of various atmospheric processes including circulation, moisture transport, and temperature advection. The composite analysis was based on two seasons: DJF and JAS. Instead of JJA (as used in Chapter 3), JAS was chosen because it is usually considered to be the core of the monsoon season in the Sahel region. I also made composites of the vertical profile of the cloud hydrometeors in both the Guinean and Sahelian and compared this with the known vertical structure of convection in WA.

Data retrieval, processing and evaluation

The ERA5 dataset was used for this analysis. I retrieved the 3D distribution of the data from the ECMWF repository. I used the same preprocessing tools as in Chapter 3 to prepare the data for my computations and analysis. Before the analysis, I performed an extensive evaluation of the low clouds provided by ERA5 (see Chapter 2). For the evaluation, I used the combined CloudSat and CALIPSO cloud fraction product (known as the 2B-GEOPROF-LIDAR). In the 2B-GEOPROF-LIDAR product, cloud fraction is provided on several layers in the atmosphere with a vertical resolution of 250 m. The ERA5 low clouds variable is defined as an integration of all clouds from the surface to about 2 km in the atmosphere. Therefore, I computed the low cloud fraction in the 2B-GEOPROF-LIDAR product from all the layers in the lowest 2 km using the maximum-random overlap rule.

I also evaluated the surface shortwave radiation of ERA5 with surface obser-

vations from the AMMA-CATCH Database and a few other data products described in Chapter 2.

Visualizations and analysis

I performed all post-processing of the data and subsequent plotting of figures in the *R* programming environment. The figures were then interpreted and analyzed by all co-authors of the article.

Drafting and editing

I drafted the first version of the manuscript and edited it after integrating comments from my advisors and all co-authors. The manuscript was then submitted to ESD and reviewed by three anonymous reviewers. I revised the manuscript after two rounds of reviews after which it was accepted and published in the journal.

Presentations

So far, the results of in this chapter have only been presented internally in my two affiliated laboratories.

4.2 Article: Daytime low-level clouds in West Africa – occurrence, associated drivers and short-wave radiation attenuation

Abstract: This study focuses on daytime low-level clouds (LLC) that occur within the first 2 km of the atmosphere over West Africa (WA). These daytime LLCs play a major role in the earth’s radiative balance, yet, their understanding is still relatively low in WA. We use the state-of-the-art ERA5 dataset to understand their occurrence and associated drivers as well as their impact on the incoming surface solar radiation in the two contrasting Guinean and Sahelian regions of WA. The diurnal cycle of the daytime occurrence of three LLC classes namely No LCC, LLC Class-1 (LLCs with lower fraction), and LLC Class-2 (LLCs with higher fraction) are first studied. The monthly evolutions of hourly and long-lasting LLC (for at least 6 consecutive hours) events are then analyzed as well as the synoptic-scale moisture flux associated with the long-lasting LLC events. Finally, the impact of LLC on the surface heat fluxes and the incoming solar irradiance is investigated. During the summer months in the Guinean region, LLC Class-1 occurrence is low while LLC Class-2 is frequent (occurrence frequency around 75 % in August). In the Sahel, LLC Class-1 is dominant in the summer months (occurrence frequency more than 80 % from June to October), however the peak occurrence frequency of Class-2 is also in the summer. In both regions, events with No LLC do not present any specific correlation with the time of the day. However, a diurnal evolution that appears to be strongly different from one region to the other is noted for the occurrence of LLC Class-2. LLC occurrence in both regions is associated with high moisture flux driven by strong southwesterly winds from the Gulf of Guinea and significant background moisture levels. LLC Class-2 in particular leads to a significant reduction in the upward transfer of energy and a net downward energy transfer caused by the release of large amounts of energy in the atmosphere during the cloud formation. In JAS, most of the LLC Class-2 events may likely be the low-level stratiform clouds that occur frequently over the Guinean region while they may be deep convective clouds in the Sahel. Additionally, LLC Class-2 causes high attenuation of the incoming solar radiation, especially during JAS where about 49 % and 44 % of the downwelling surface shortwave radiation is lost on average in Guinea and Sahel respectively.

Authors: Derrick Kwadwo Danso, Sandrine Anquetin, Arona Diedhiou, Kouakou Kouadio, Arsène Koba

4.3 Introduction

In West Africa (WA), the prediction of key features of the climate such as the West African Monsoon (WAM) is known to have large uncertainties (Christensen et al., 2013). Most of the uncertainties are essentially linked to the inability of climate models to efficiently represent convection and cloudiness, in particular low-level clouds (LLCs) (Hannak et al., 2017). Climate models struggle to properly reproduce the planetary boundary layer above the ocean and the continental surface as well as the land-ocean flux gradients that drive the triggering and the variability of LLC systems. These clouds and their temporal variation strongly influence the reflectivity of the atmosphere. As a result, large uncertainties exist in the prediction of surface solar radiation in the region (Knippertz et al., 2011). In the light of the recent increased interest in solar energy projects in WA (WorldBank, 2019) after the Paris Agreement in 2015, predictability of surface solar radiation (Armstrong & Hurley, 2010; Kosmopoulos et al., 2015) thus, remains a key issue for any feasibility study concerning solar energy during either dry or wet seasons in the region.

WA is characterized by a frequent occurrence of different cloud types. Near the Gulf of Guinea in the southern part of WA, LLCs are prevalent all year round (Adler et al., 2017; Danso et al., 2019; Schrage & Fink, 2012; van der Linden et al., 2015). Farther north in the Sahelian region, these clouds are frequently observed during the WAM season from July to September (Bouniol et al., 2012). These LLCs consist of stratified clouds, most of which are nocturnal low stratus clouds covering wide areas and persisting into the early afternoon (Babić et al., 2019a; Schuster et al., 2013) as well as shallow convective clouds. LLCs composed of liquid water are well known to have a large impact on radiative transfer (Hill et al., 2018; Liou, 2002; Turner et al., 2007). As a result, they drive the diurnal cycle of convection and the planetary boundary layer (Gounou et al., 2012; Grabowski et al., 2006). During the daytime, these clouds block a large portion of the incoming shortwave radiation reducing the irradiance at the earth’s surface (Kniffka et al., 2019).

Several studies have been carried out in WA to understand LLCs, their variability, and the processes that aid in their formation, maintenance, and dissipation (e.g., Dione et al. (2019), Kalthoff et al. (2018), Lohou et al. (2020), Pedruzo-Bagazgoitia et al. (2020), Schrage and Fink (2012), and Schuster et al. (2013)). The majority of those studies were carried out within the framework of two major field campaigns; the African Monsoon Multidisciplinary Analysis (AMMA) (Redelsperger et al., 2006) in 2006 and the Dynamics–Aerosol–Chemistry–Cloud Interactions in West Africa (DACCWA) (Knippertz et al., 2015) in 2016. Both of these field campaigns provided an unprecedented database of surface-based observations of different

cloud properties. Other studies on LLCs in the region have also been performed with satellite observations and model data (Adler et al., 2017; Hannak et al., 2017; van der Linden et al., 2015). These studies suggest that LLCs formation is linked to a number of processes including but not limited to cooling caused by horizontal cold air advection and the occurrence and strengthening of the nocturnal low-level jet (Adler et al., 2017; Babic et al., 2019b; Schrage & Fink, 2012).

Most of these studies, however, focused on night-time LLCs in the southern part of WA (e.g., Adler et al. (2017), Babic et al. (2019b), Schrage and Fink (2012), and Schuster et al. (2013)). In the night, the nocturnal LLCs have no influence on the surface solar radiation due to the absence of sunlight. However, they persist long into the morning and early afternoon, thus, directly influencing the amount of incoming solar irradiance and having a considerable impact on the energy balance of the earth surface as shown by Lohou et al. (2020). The conditions associated with these low clouds during the daytime in the region are less documented. As a result, our understanding of the impacts of these clouds on surface solar irradiance during the daytime is relatively limited. Moreover, most of the previous studies have been limited to the WAM season (e.g., Dione et al. (2019), Knippertz et al. (2011), Schuster et al. (2013), and van der Linden et al. (2015)). This is understandable as WA is cloudiest during the WAM season. However, it was shown that daytime LLCs exist in all seasons especially over southern WA (Danso et al., 2019). It is therefore important to understand the nature of such daytime LLCs over the whole region and not only during the WAM season. This is particularly challenging due to the lack of a long-term surface-based observational dataset in WA, thus, limiting our understanding of these cloud systems. Few studies which were done with simulations, reanalysis, and satellite data in the region (e.g., Adler et al. (2017), Knippertz et al. (2011), Schuster et al. (2013), and van der Linden et al. (2015)) have nevertheless shown results similar to those of ground observational studies (e.g., Adler et al. (2019) and Babic et al. (2019b)) to some extent.

In this general context, the main contribution of this study is to enhance our understanding of daytime LLCs in WA by focusing on daytime LLCs in both the dry and wet seasons with a state-of-the-art reanalysis dataset. Firstly, we will present the seasonal and diurnal distributions of the occurrence frequency of the daytime LLCs in two areas of WA with contrasting climate regimes (the Sahelian and the Guinean regions). We will then identify synoptic-scale conditions (specifically the moisture flux) associated with the presence of the daytime LLCs. Additionally, we will investigate the impact of LLC on surface heat fluxes and estimate the percentage of incoming surface shortwave (SW) radiation that is attenuated when these clouds are present.

This paper is organized as follows: section 4.4 and section 4.5 describe the study area, datasets and the methodology. section 4.6 presents the diurnal and monthly distribution of occurrence of daytime LLCs while the synoptic and local conditions associated with the occurrence of long-lasting LLCs are discussed in section 4.7. section 4.8 presents the estimated attenuation of incoming shortwave radiation during the occurrence of LLCs. Finally, conclusions are drawn in section 4.9.

4.4 Data

In this study, we analyze the 5th generation of the European Centre for Medium-range Weather Forecasts (ECMWF) Re-analysis – ERA5¹ (Hersbach et al., 2020) to understand the occurrence of LLCs and their associated synoptic conditions and land surface fluxes and to discuss their impacts on incoming shortwave radiation in WA (Figure 4.1). The reanalysis is available at a temporal resolution of an hour and has a native horizontal resolution of 0.25°. However, due to more emphasis on large-scale conditions in this study, the data was directly extracted on a regular 1° × 1° grid from ECMWF. A period of 10 years from 2006 to 2015 was analyzed for the study. For this period a total of 43800 data points consisting of only daytime hours from 0600 to 1700, were thus considered.

ERA5 provides different variables of cloud cover properties. These cloud variables are produced in *CY41R2* of the ECMWF’s Integrated Forecasting System (IFS) and documented in Part IV of the IFS Documentation². The cloud cover variables consist of cloud fraction (*CF*) and cloud hydrometeors (liquid or ice water) and are available as 3D or 2D distributions. Here, we use the 3D distribution of cloud liquid and ice water content to show the atmospheric vertical profiles of clouds in selected areas over WA. The occurrence frequency of clouds may be defined by the hydrometeor content or the *CF* value. In this study, we determine the occurrence frequency based on the value of the 2D single-level *CF*, although, the liquid and ice water paths mostly determine the attenuation of incoming solar radiation in the atmosphere. The ERA5 *CF* depends on the subgrid-scale cloud scheme in the ECMWF IFS and can be non-zero when the cloud water content is zero (see Appendix B). The atmospheric conditions and radiative impacts are analyzed based on this occurrence. In this study, we focus on low clouds defined by ECMWF in the ERA5 product as all clouds integrated from the surface to 2km altitude in the atmosphere (≈ 800 hPa). This includes all clouds with bases below 2 km.

¹Detailed documentation at <https://confluence.ecmwf.int/display/CKB/ERA5+data+documentation>

²Available at <https://www.ecmwf.int/en/elibrary/16648-part-iv-physical-processes>

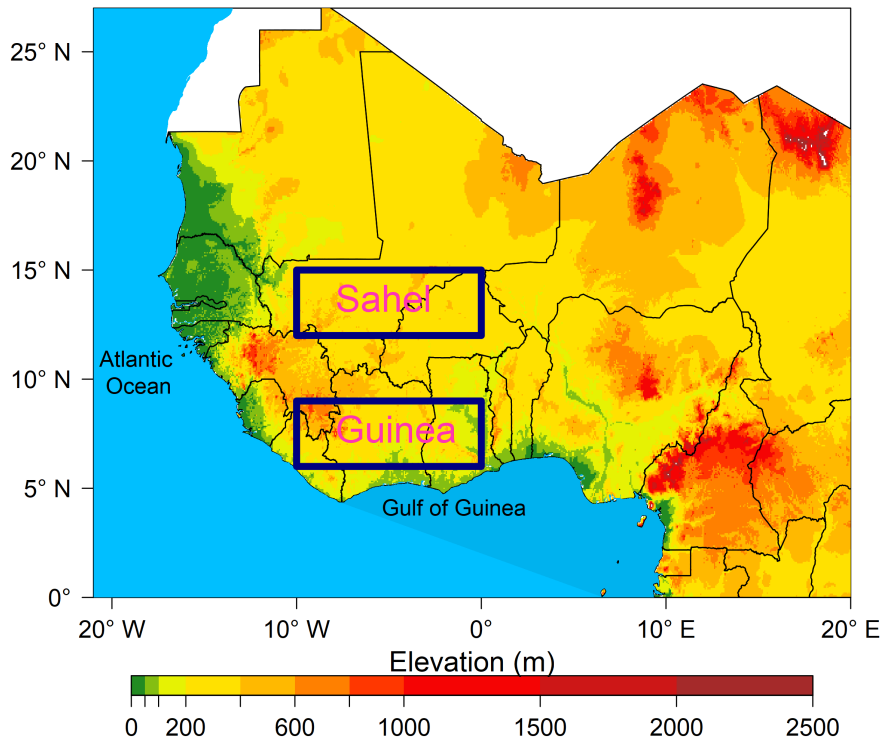


Figure 4.1: Map of West Africa showing the two selected windows (dark blue rectangles) used for identification of LLC events. The name denoted for each window is based on the climate zone of the window in the region.

Other ERA5 variables are analyzed to show some of the atmospheric and surface conditions during the occurrence of LLCs in order to understand the possible interactions between the surface and the lower atmosphere. These include specific humidity, zonal and meridional wind components, and the surface sensible and latent heat fluxes. Furthermore, we use the incoming downwelling shortwave radiation variable in ERA5 to estimate the percentage of incoming solar radiation that is attenuated in the presence of LLCs. We first performed a detailed evaluation of the ERA5 cloud fraction and radiation data with surface and satellite-based observations for some locations in WA. This evaluation revealed a reasonably good performance by ERA5 in reproducing the observations (see Chapter 2).

4.5 Methods

4.5.1 Identification of low-level clouds occurrence

Our analysis is based on the occurrence of LLCs in two sub-regional windows over WA (rectangular boxes in Figure 4.1) denoted here as Guinea (10°W to 0°E and

6°N to 9°N) and Sahel (10°W to 0°E and 12°N to 15°N). These areas are chosen primarily due to their contrasting climate regimes (Gbobaniyi et al., 2014). The Guinea region which includes countries like Ghana and Cote d’Ivoire is currently undergoing significant economic and infrastructural developments and thus the need for clean energy keeps increasing. Consequently, there are many ongoing solar energy projects in this region such as the 155 MW Nzema solar PV power project in Ghana (Kuwonu, 2016), which when completed will be the largest solar farm on the African continent. Côte d’Ivoire has planned to increase its share of variable renewable energy up to 11 % by the end of 2020 and up to 16 % by 2030. Thus, a 25 MW solar power plant is under construction in the Northern part of the country in Korhogo while two solar power plants projects with a capacity of 30 MW each have been approved and will be built in the localities of Tuoba and Laboa in the northwestern part of the country (MPEER, 2014). Additionally, there are several planned and existing solar energy projects in the Sahel window, especially in Burkina Faso with the 33 MW-capacity Zagtouli solar power plant (Moner-Girona et al., 2017) which is currently the largest solar energy project in the Sahelian part of WA.

Occurrence or no-occurrence of LLC are first identified from the extracted data points based on the quantitative value of the CF in the two selected windows. This is used to show the diurnal and monthly distribution of the LLC occurrence. All timestamps with zero CF in the lower atmospheric level (up to 2 km) are designated as No LLC. Thus, hourly events of LLC occurrence are all timestamps with non-zero CF values including those with very small CF values. LLC events with very low CF values may show no or weak signals of the conditions that exist during their occurrence. Moreover, cloud radiative forcing is strongly dependent on the fractional coverage of clouds (Liu et al., 2011). Each LLC occurrence event is therefore classified as one of two classes depending on the CF value for that event. The definitions of the classes are provided in Table 4.1.

Table 4.1: Definitions of the three classes of LLC occurrence based on cloud fraction.

Class of LLC occurrence	Description
No LLC	$CF = 0$
Class-1	$0 < CF \leq 0.5$
Class-2	$CF > 0.5$

Though the focus of this study is on LLC occurrence and the definition of the different classes is based on the CF in the lower atmosphere only, the convoluted cloud climatology in WA with frequent multilayer clouds (Stein et al., 2011) may

also mean that other clouds at higher altitudes may exist in addition to LLCs. Figure 4.2 illustrates this multilayer nature of clouds in WA in connection with LLC occurrence, by showing the mean (of all hourly events) vertical profile of cloud water content of each class in the two selected regions. For LLC Class-1 and Class-2 in both windows, the trimodal vertical distribution of tropical convection (Johnson et al., 1999) indicates the presence of higher altitude clouds in addition to the LLCs. In the case of No LLC, high- and mid-level clouds could exist but with very low water content. This suggests and agrees with the satellite-based climatology of Stein et al. (2011) that LLCs frequently exist together with upper-level clouds in WA.

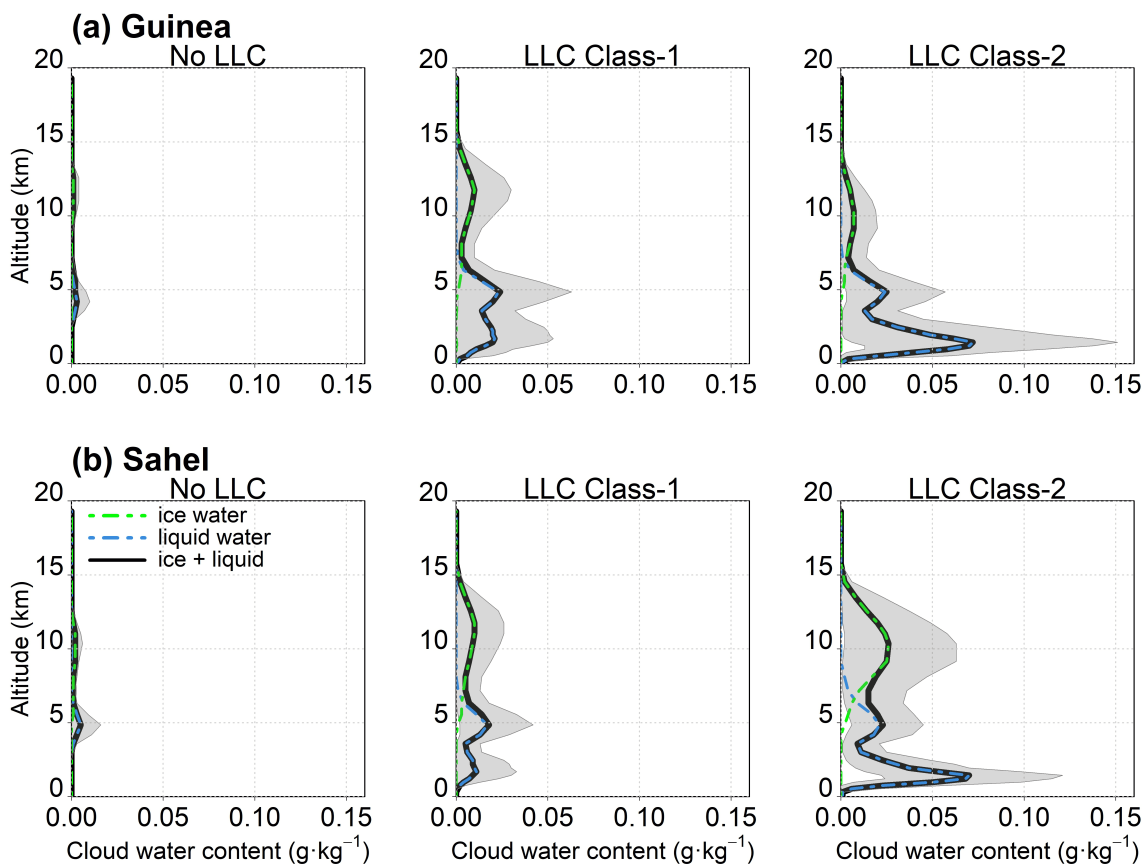


Figure 4.2: Mean vertical profiles of cloud water content (ice water (dotted green line), liquid water (dotted blue line), and total water content (black line)) during the occurrence of each LLC class in Guinea (top) and Sahel (below). Shaded areas refer to the 90th and 10th inter-percentile range.

4.5.2 Identification of synoptic conditions during LLC occurrence

Recent studies (e.g., Adler et al. (2019) and Babic et al. (2019b)) have identified some physical processes relevant to the formation and maintenance of LLC in WA.

They include but are not limited to the strengthening of the nocturnal low-level jet, horizontal cold air advection and background moisture level. Babic et al. (2019b) suggested the latter could play an important role in the formation of LLCs but this has not received as much attention as the other processes. Based on the different classes defined in Table 4.1, the regional atmospheric circulation and moisture flux were analyzed for the 10-year period of this study. For that, a composite approach was used to produce robust results based on a large number of events. We only take into account the occurrence of the different LLC classes that last for a sufficiently long time for their associated mean atmospheric and surface conditions to be significant at the regional scale. Therefore, an event here refers to the occurrence of a given LLC class that lasts for at least six consecutive hours during the daytime. Composite analysis of the moisture flux (Q_{flux}) and wind at 950 hPa was performed. Here, Q_{flux} is defined as:

$$Q_{flux} = \frac{1}{N} \sum_{i=1}^N q_i v_i \quad (4.1)$$

where q is the specific humidity (in g kg^{-1}), v is the meridional wind component (in ms^{-1}) and N is the total number of events in a given LLC occurrence class. Since q is always positive, Q_{flux} can either be negative or positive depending on the wind direction, with positive or negative values indicating northward and southward air movements respectively. Over the sea, positive values of Q_{flux} from the ocean toward the continent thus suggest that moisture is likely transported onto the land along with the wind.

Lohou et al. (2020) have shown that LLC occurrence also has a considerable impact on the surface heat fluxes in WA. Here, we examine the local surface sensible and latent heat fluxes in the selected windows to understand the daytime interaction of the land surface with the boundary layer and LLC occurrence. Due to the definition of LLCs used, the present study does not consider the impact of the atmospheric boundary layer (ABL) that may considerably modify the altitude of the low cloud. Indeed, ABL clouds have their bases higher than 2 km especially in the Sahel region during the dry season. In addition, some studies (Lohou et al., 2020; Pedruzo-Bagazgoitia et al., 2020; Zouzoua et al., 2020) have shown that some LLCs can be decoupled from the surface and are therefore not influenced by the surface heat fluxes. Therefore, having a higher cloud base threshold for LLCs may alter the analysis of the surface heat fluxes. The analysis was performed for two seasons representing two contrasting climate regimes associated with the southernmost position of the Inter-Tropical Convergence Zone (ITCZ) over Guinea (in December,

January, February (DJF)) and the northernmost position of the ITCZ over Sahel (in July, August, September (JAS)).

4.5.3 Determination of cloud shortwave attenuation effects

To investigate the quantity of incoming downwelling shortwave radiation attenuated in the presence of LLCs (in W m^{-1}) at a given time t , the cloud shortwave radiative effect ($CRE_{SW\downarrow}$) was estimated by finding the difference between the downwelling shortwave radiation in all-sky conditions (SW^\downarrow) and the corresponding downwelling shortwave radiation in clear-sky conditions (SW_{CS}^\downarrow). The SW_{CS}^\downarrow which is directly available in ERA5, is a theoretical value computed at a given time based on the same atmospheric conditions (temperature, humidity, aerosols, etc.) as the SW^\downarrow but assuming there are no clouds. To eliminate the influence of the wide range of daytime hours on its mean value, we expressed $CRE_{SW\downarrow}$ as a percentage of the attenuated SW_{CS}^\downarrow . Since SW^\downarrow is usually lower than SW_{CS}^\downarrow , the mean $CRE_{SW\downarrow}$ over all events in a given LLC class will be negative. To avoid presenting a negative mean $CRE_{SW\downarrow}$, the absolute of this value is used. Thus, the mean $CRE_{SW\downarrow}$ of all events for a given LLC class is given by:

$$CRE_{SW\downarrow} = \left| \frac{1}{N} \sum_{i=1}^N \frac{SW^\downarrow(i) - SW_{CS}^\downarrow(i)}{SW_{CS}^\downarrow(i)} \times 100 \right| \quad (4.2)$$

4.6 Temporal distribution of occurrence of daytime low-level clouds

The monthly distribution of the occurrence frequency (hourly) of the three LLC classes is presented in Figure 4.3 for the two selected regions (occurrences that last for at least six consecutive hours are shown as black bars). In Guinea, events of No LLC are very rare (less than 200 in the 10 years data) and occur only in the DJF. On the other hand, LLCs occur in all months in this area. The occurrence of LLC events with lower fractional coverage (LLC Class-1) shows a clear seasonal cycle with the highest number of events in the dry and transitional seasons and the lowest number of events during JJAS which corresponds to the core of the monsoon season (Sultan et al., 2003). Coincidentally, LLC events with higher fractional coverage (LLC Class-2) occur most during the monsoon season. This period is associated with increased moisture influx from the Gulf of Guinea (Sultan & Janicot, 2003; Thorncroft et al., 2011) and cold air advection which enhances low clouds formation over the region during this period as shown by Adler et al. (2019) and Babic et al.

(2019b). Interestingly, the peak of LLC Class-2 events occurs in August, the so-called “little dry season” in southern WA (Adejuwon & Odekunle, 2006; Chineke et al., 2010; Froidurot & Diedhiou, 2017). Whether this peak of LLC Class-2 events in August which coincides with reduced rainfall in southern WA is due to an increased occurrence of non-rain-bearing low clouds (and a decrease in rain-bearing ones) or not is beyond the scope of this paper but needs to be investigated in future.

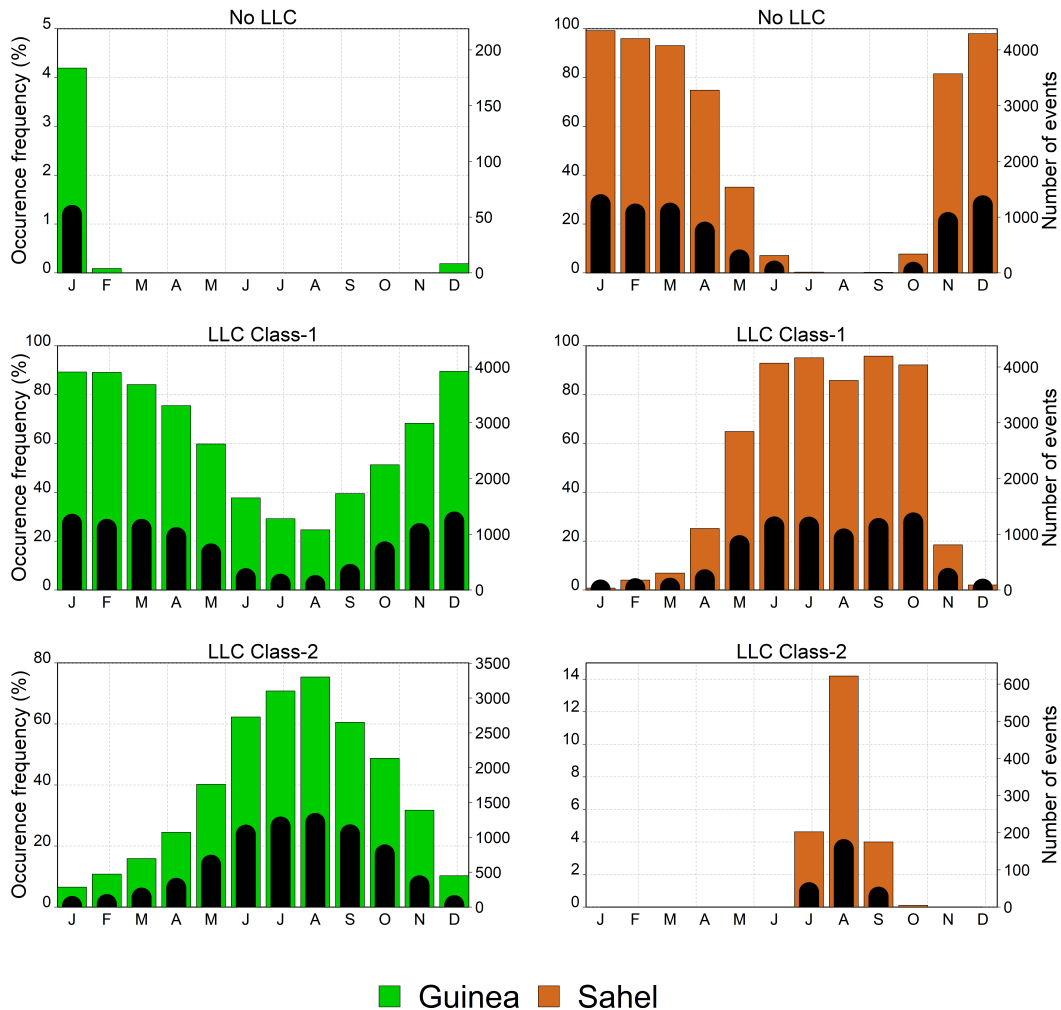


Figure 4.3: Monthly distribution of the occurrence frequency of hourly events for the three daytime LLC classes during the daytime in the Guinea (green bar) and Sahel (orange bar) regions defined in Figure 4.1. The shorter black bars are the distribution of occurrences that last for at least six consecutive hours (the actual value has been multiplied by a factor of 4 to improve the legibility of the distribution).

In Sahel, events of No LLC are rather frequent (unlike Guinea) and occurs in every month except in August when the monsoon is fully developed over the Sahelian region of WA (Sultan & Janicot, 2003; Thorncroft et al., 2011). Similarly, LLC

Class-1 events are frequent throughout the year but with the highest occurrences from July to October (with a slight decrease in August) and lowest occurrences during the dry season. LLC Class-2 events are marked with a strong seasonal signature, occurring only from July to October with a distinct peak occurrence in August when the Inter-Tropical Convergence Zone (ITCZ) is at its northernmost latitude over WA (Nicholson, 2009; 2018; Sultan & Janicot, 2000). This period also coincides with the maximum rainfall over the Sahelian region (Nicholson, 2013) and suggests a strong link between the occurrence of LLC Class-2 events and the Sahelian rainfall. This is an indication that LLC Class-2 in the Sahel are likely related to rainfall events in the region. Again, Mathon et al. (2002b) showed that cloud cover associated with a sub-population of Mesoscale Convective Systems (MCS) in the Sahel is modulated at the synoptic-scale during the African easterly wave activity, with an increase of the cloud cover in and ahead of the trough and maximum rainfall behind of the wave trough.

The daytime distribution of occurrence frequency of the three LLC classes is presented in Figure 4.4 for the two selected areas. The distribution presents the total occurrence frequency of all seasons combined. In Guinea, the occurrence frequency of No LLC events does not present a very well-marked diurnal cycle with a slightly higher number of events occurring at 1700 UTC, though these events are extremely rare (less than 25 for the 10 years). In contrast, both LCC Class-1 and Class-2 occurrences present well-defined diurnal cycles. The occurrence of LLC Class-1 events is low during the early morning (lowest at 0700 UTC) and increases progressively throughout the day to late in the afternoon. On the contrary, LLC Class-2 events are high early in the morning (highest at 0700 UTC) but decrease continuously over the course of the day to the late afternoon (1700 UTC). The early morning peak in the LLC Class-2 events could be as a result of the contribution of residuals from nocturnal low-level stratus clouds which persist long into the day (Kalthoff et al., 2018). These clouds usually have large fractional coverage during their occurrence in the night (van der Linden et al., 2015) but start to dissipate during the daytime (Kalthoff et al., 2018). The continuous decreasing and increasing in the event number of LLC Class-2 and LLC Class-1 respectively, from morning to late afternoon could, therefore, be linked to the gradual dissipation of those nocturnal low-level stratus clouds during the day. Additionally, the early morning peak in the events of LLC Class-2 could also be partly linked to contributions from tropical oceanic low-level convection which is maximum during the early morning (Yang & Slingo, 2001). The proximity of the Guinean region to the ocean means that cold air over the Gulf of Guinea could be advected inland which will, in turn, enhance LLC formation.

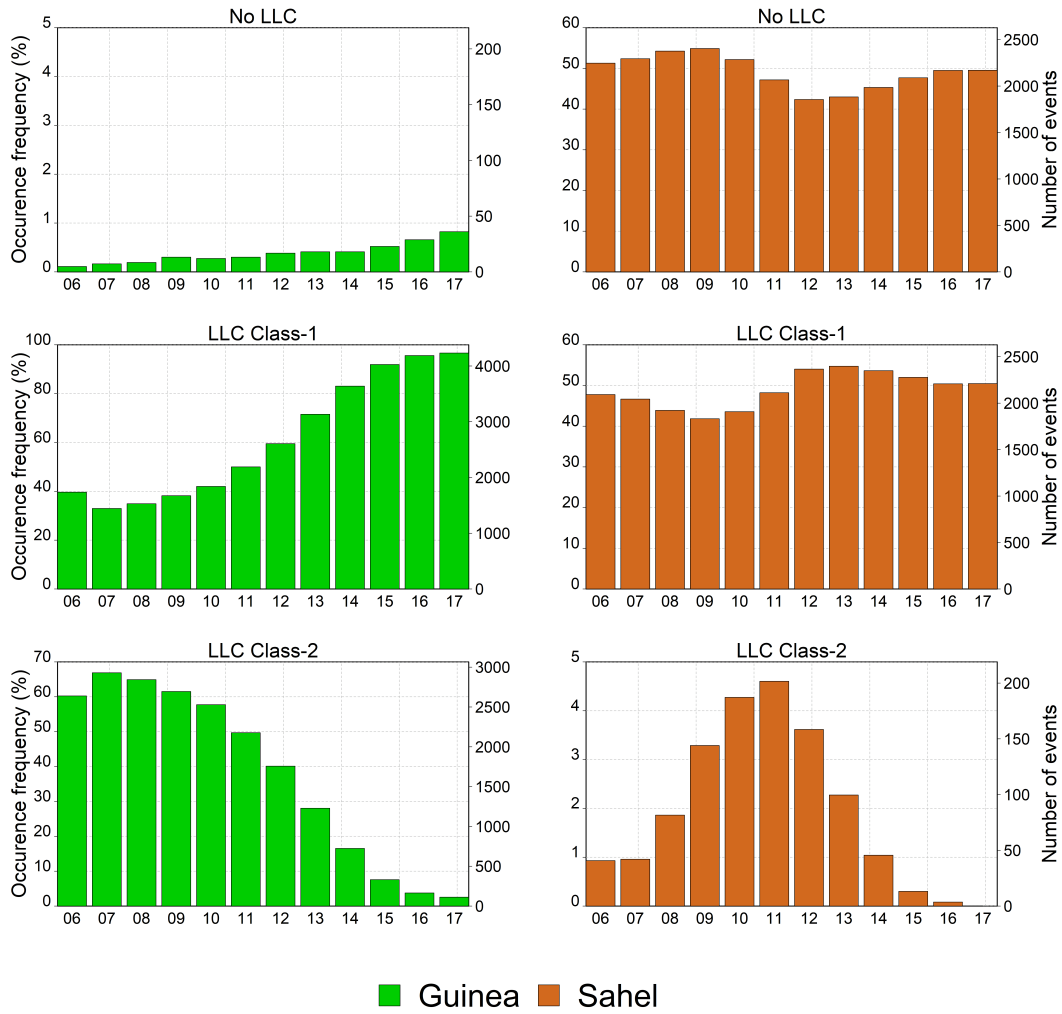


Figure 4.4: Diurnal distribution of occurrence frequency of the three daytime LLC classes during the daytime in the Guinea and Sahel regions as defined in Figure 4.1. All seasons are included in the distribution shown.

In the Sahel region, events of No LLC occur without a well-marked diurnal cycle but are slightly lower around midday. Similarly, LLC Class-1 events do not present a very distinct diurnal cycle. On the other hand, events of LLC Class-2 show a clear and well-marked diurnal cycle with a higher occurrence frequency in the late morning to midday (highest at 1100 UTC) and lower values during early mornings and late afternoon. This tendency seems to be strongly controlled by surface processes such as continental daytime solar heating (Mallet et al., 2009). Moreover, it could further be related to the occurrence of deep MCSs whose convective parts will be considered as low clouds if found within the lowest 2 km of the atmosphere. These MCSs present a fairly similar evolution (both seasonally (Figure 4.3) and diurnally) as the LLC Class-2 in this region of WA (Vizy & Cook, 2019). Therefore, there is a higher likelihood of an MCS in the LLC Class-2 events than Class-1 and

it is reasonable to assume that most of the LLC Class-2 events in the Sahel are the well documented deep MCSs (Figure B.1 in Appendix B) that are responsible for around 90 % of total rainfall in the region (Goyens et al., 2012; Mathon et al., 2002a; Vizy & Cook, 2019).

4.7 Synoptic conditions related to the occurrence of daytime low-level clouds

The synoptic conditions associated with the occurrence of the different LLC classes are mainly presented for the JAS and DJF seasons. The total number of daytime hours in JAS and DJF during the 10 years are 11040 and 10800 respectively. Only occurrences that last for at least six consecutive hours are considered to analyze these conditions (i.e., here, an event refers to an occurrence that persists for at least six consecutive hours). Table 4.2 presents the number of the ‘six-consecutive hours’ events extracted for each class and for both seasons over the 10 years. During the JAS season, no occurrence of No LLC events was detected in both Guinea and Sahel window (i.e., daytime LLCs are always present in both regions during the JAS). LLC Class-1 events dominated the Sahel region during JAS (with 793 events) but on the contrary, LLC Class-2 events dominated the Guinea region (with 852 events). In DJF, No LLC events dominated the Sahel (with 877 events) and no LLC Class-2 occurrence has been identified in this area during this season. In Guinea, on the other hand, LLC Class-1 occurrences dominated the area during DJF (with 878 events). Composites of the different variables are thus analyzed and then discussed only based on the extracted events for each class and each season, as presented in Table 4.2.

Table 4.2: Number of events found for the occurrence of the three LLC classes in JAS and DJF. Composite analysis is performed based on these events for each class and season. For the study period, the total number of daytime hours are 11040 and 10800 in JAS and DJF respectively.

	JAS		DJF	
	<i>Guinea</i>	<i>Sahel</i>	<i>Guinea</i>	<i>Sahel</i>
Number of No LLC events	0	0	13	877
Number of LLC Class-1 events	122	793	878	16
Number of LLC Class-2 events	852	56	22	0
Total number of hours in season	11040		10800	

4.7.1 Atmospheric circulation and moisture flux

The occurrence of daytime LLC events in the selected windows is related to large-scale dynamics of the atmosphere over the WA region. Figure 4.5 and Figure 4.6 present the composites of Q_{flux} and the atmospheric circulation at 950 hPa for JAS and DJF respectively, and for the two studied regions. During JAS in both regions (Figure 4.5), the occurrence of LLC Class-1 and Class-2 events is related to high moisture flux dominated by strong southwesterly winds (positive Q_{flux}) from the Guinean Gulf. The moisture flux is stronger during the occurrence of LLC Class-2 events than LLC Class-1 events. This is true for LLC occurrence in both regions; however, the moisture flux is more intense for LLC occurrence in Sahel in terms of its inland penetration. There are no events of No LLC in both Sahel and Guinea during JAS. During DJF in both regions (Figure 4.6), events with No LLC are characterized by dry northeasterly winds that inhibit LLC formation. The occurrence of LLC Class-1 events in Guinea and Sahel is characterized by southerly winds just at the southern coast but do not penetrate the area of the two windows. Nevertheless, both LLC Class-1 and Class-2 events are associated with significant specific humidity (true for both seasons) unlike No LLC events with very low specific humidity (see Figure B.2 in Appendix B). This is in agreement with Babic et al. (2019b) who found that the most distinct difference between LLC and No LLC events is in the specific humidity, suggesting that the background moisture may play a crucial role in the formation and maintenance of low clouds in WA. Additionally, the LLC Class-1 events during DJF (in Sahel) are related to positive anomalies of specific humidity that seem to have been transported onto the continent from the North Atlantic (not shown). LLC Class-2 events in Guinea are associated with a much stronger moisture flux in the region (Figure 4.6) as well as a positive anomaly of specific humidity within and around the window (not shown).

The moisture fluxes presented so far are those present when LLC events are identified. However, it is also interesting to investigate the moisture flux before and after the LLCs occurrence in order to analyse their contribution to the maintenance or triggering of these systems. To do this, we analyze the composite moisture flux (at 950 hPa) of the first hour just before the LLC event ($1h_{Before}LLC$) and the first hour just after the LLC disappears ($1h_{After}LLC$), and the difference between the two periods. This is illustrated for LLC Class-2 during the JAS season in both Guinea and Sahel (Figure 4.7). In both regions, the moisture flux during $1h_{Before}LLC$ is larger than $1h_{After}LLC$ and there is a significant difference between the two periods as shown in Figure 4.7. This is also true for the composites of specific humidity only (not shown). During $1h_{Before}LLC$, the water vapour associated with the moisture flux is likely cooled by some cold air advection into the region which

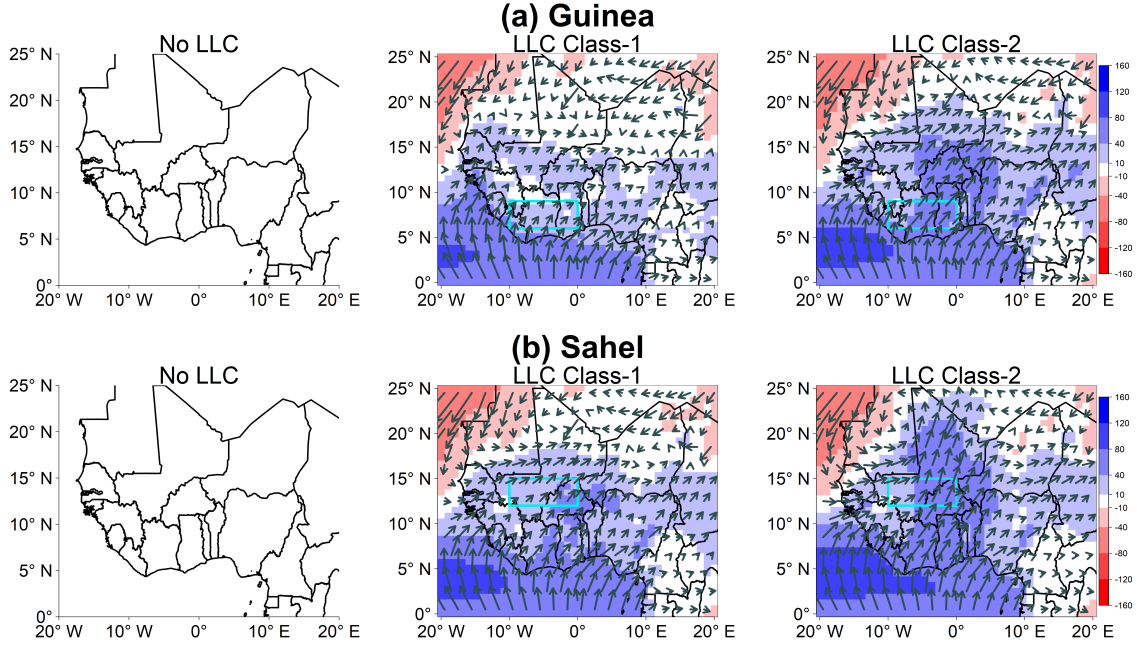


Figure 4.5: Composites of 950 hPa moisture flux (colours, $\text{g kg}^{-1} \text{m s}^{-1}$) and wind (vectors, m s^{-1}) over WA for the three LLC occurrence classes in the Guinea (top) and Sahel (below) windows during JAS from 2006 to 2015. Only occurrences that last for at least six consecutive hours are considered. Wind vectors are averaged over 2 grid points in both the x and y directions. No event of the No LLC class has been extracted in the Guinea and Sahel regions during JAS, hence the empty plots.

leads to saturation and consequently, LLC formation. Indeed, the vertical profile of the potential temperature in the lower atmosphere during the two periods shows a strong temperature decrease just before the LLC occurrence and an increase after its disappearance (Figure B.3 in Appendix B). This result, which is in agreement with the finding of Babic et al. (2019b), may be an indication of the cooling caused by the cold air advection. Over the Guinea region, studies have shown that cooling by the horizontal advection of cold air from the Gulf of Guinea contributes significantly to the formation of LLC (e.g., Adler et al. (2019) and Babic et al. (2019b)). In the Sahel region, moist air advection may be crucial for LLC formation as suggested by Parker et al. (2005) and Monerie et al. (2020). However, before LLC formation in the Sahel region, there may also be some cooling due to meridional advection (Marsham et al., 2013) as well as cold air advection from the North Atlantic, which could explain the strong temperature reduction during $1h_{\text{Before LLC}}$ (Figure B2).

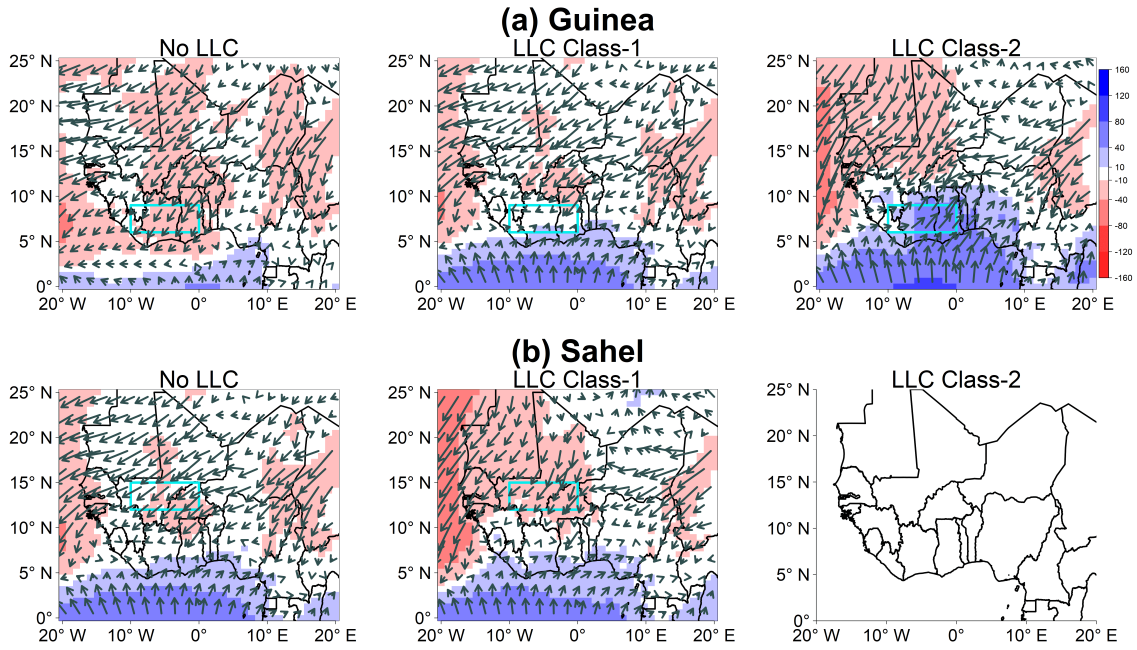


Figure 4.6: Same as Figure 4.5 but for DJF. No event of LLC Class-2 has been extracted in the Sahel area during DJF, hence the empty plot.

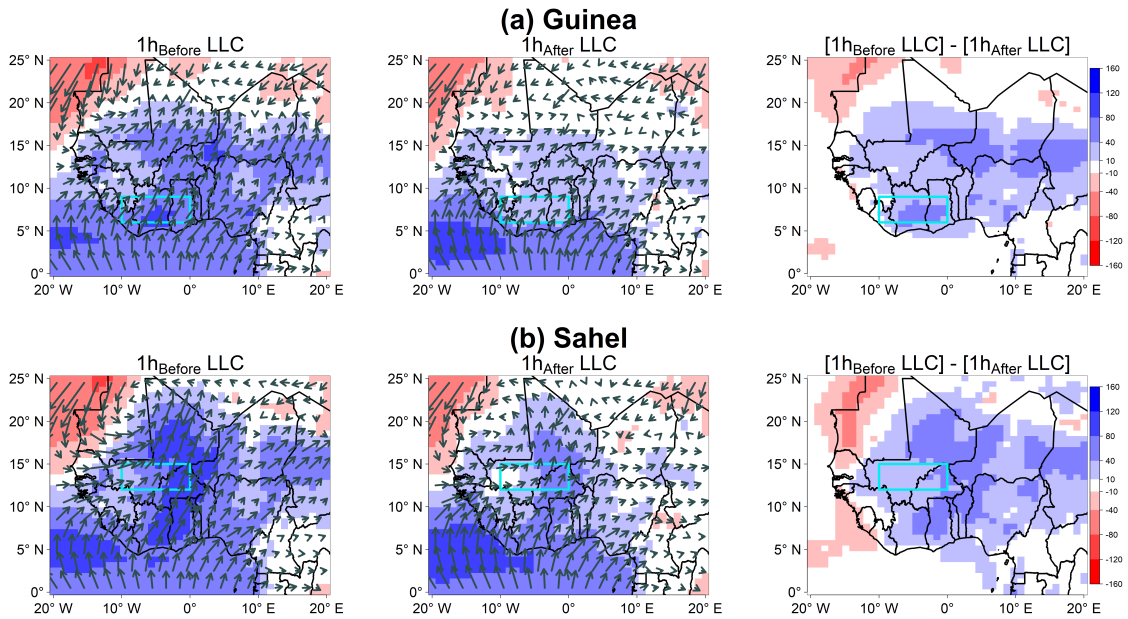


Figure 4.7: Composites of 950 hPa moisture flux (colours, $\text{g kg}^{-1} \text{m s}^{-1}$) and wind (vectors, m s^{-1}) over WA for the hour preceding LLC Class-2 occurrence ($1h_{\text{Before LLC}}$) and after it disappears ($1h_{\text{After LLC}}$) and the difference between the two periods during JAS from 2006 to 2015. Wind vectors are averaged over 2 grid points in both the x and y directions.

4.7.2 Surface heat fluxes

Figure 4.8 and Figure 4.9 respectively present the monthly mean and anomalies of the surface heat fluxes, computed over the two selected regions for the three LLC occurrence classes. For a particular hour i , on a given day and month during the 10 years, the heat flux anomaly is the difference between the actual heat flux value and the 10-year mean. For example, the heat flux anomaly at 12 UTC on 1st January 2006 was determined by taking the difference between the actual heat flux at 12 UTC on 1st January 2006 (HF_i) and the 10-year mean of all heat flux values at 12 UTC on 1st January (\overline{HF}) i.e.,

$$HF_{anom_i} = HF_i - \overline{HF} \quad (4.3)$$

where, HF_{anom_i} is the heat flux anomaly. The mean monthly anomaly is then computed by finding the mean of hourly anomalies in the month. The ECMWF convention for vertical fluxes including the sensible and latent heat fluxes, is positive downwards and negative upwards.

No LLC events occur almost throughout the entire year in the Sahel (except JAS) and only during January in the Guinean region. In both areas, the occurrence of these events leads to high negative sensible heating (Figure 4.8) indicating an upward transfer of sensible heat. Indeed, during No LLC events, much of the incoming radiation heats the surface, making it warmer than the air directly above it, leading to an upward sensible heat flux. Both regions are characterized by negative anomalies of sensible heat (Figure 4.9) suggesting a much stronger than usual upward transfer of sensible heat. The mean latent heat fluxes during No LLC events are also negative but significantly lower than the sensible heat (Figure 4.8). Thus, most of the energy from the surface is used to heat the atmosphere rather than evaporating moisture. This could be as a result of a low moisture gradient between the soil and the air during those events especially in the dry season when both soil and air moisture are extremely low in the region. The lack of moisture in the region inhibits the formation of LLC during these events. In the Sahel region, there are positive anomalies of latent heat (from April to June), indicating reduced upward transfer of latent heat likely due to a lack of moisture during those events.

During LLC occurrence, a portion of the incoming SW radiation is blocked. Therefore, the warming of the surface is reduced during LLC occurrence in both regions. However, due to the higher cloud fraction during LLC Class-2 events, a larger quantity of the downwelling shortwave radiation is blocked. Consequently, the associated surface warming is much lower during LLC Class-2 than the Class-1 events (lower negative sensible heat fluxes than Class-1 events in Figure 4.8a).

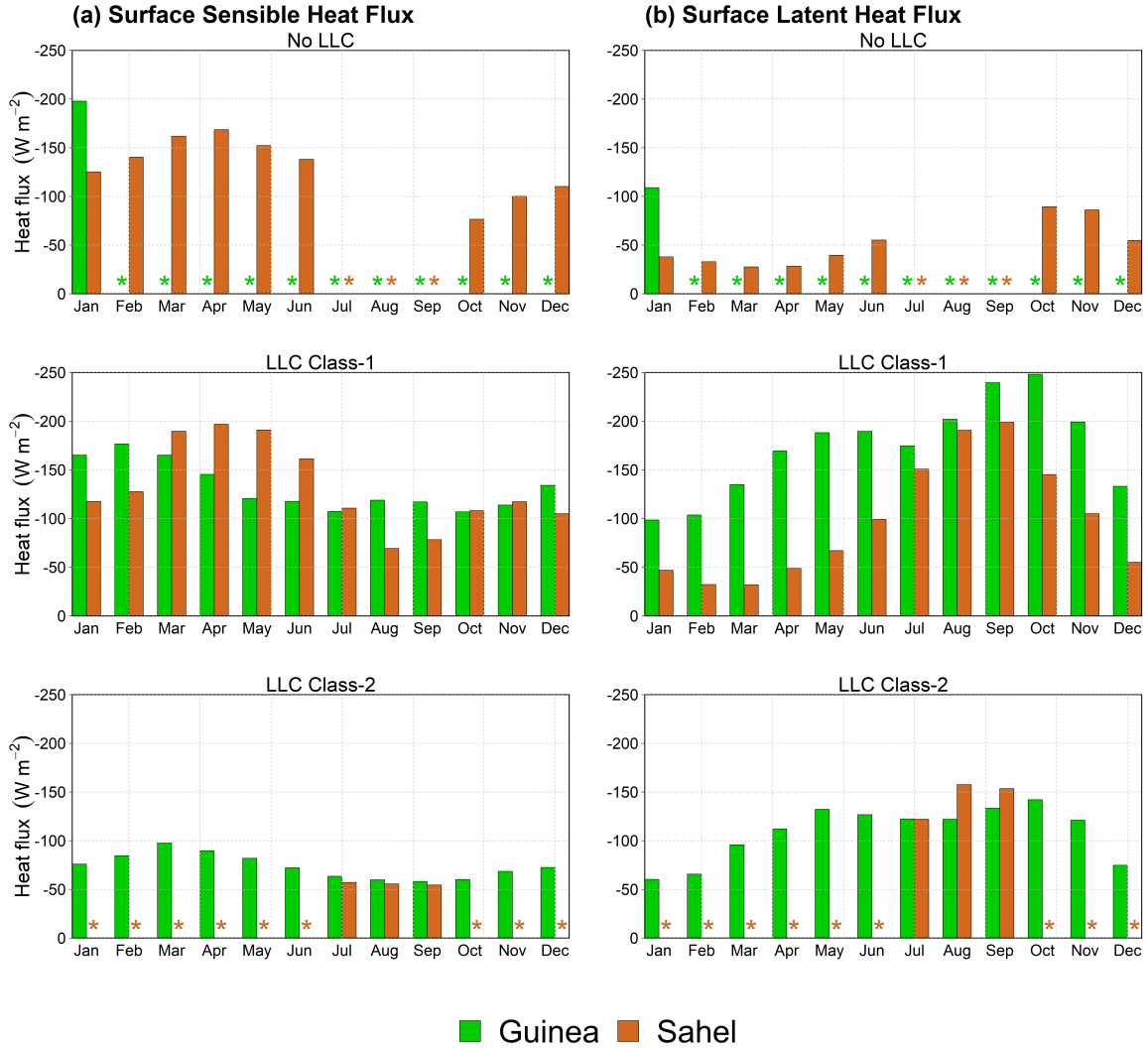


Figure 4.8: Monthly mean (a) surface sensible heat and (b) surface latent heat fluxes computed in the Guinea and Sahel regions during the occurrence of the three LLC classes from 2006 to 2015. The orange and green stars mean that there was no occurrence of the particular LLC class events in the region during that month, hence the composites were not computed. Only occurrences that last for at least six consecutive hours are considered.

This result suggests that the LLC Class-2 events are most likely the low stratiform clouds which are known to cover large portions of the sky or the deep convective clouds which extends to the upper levels of the atmosphere, generating anvils in the process. With regards to the former, Lohou et al. (2020) have shown that these low stratiform clouds have significant impacts on the energy balance of the earth's surface during the daytime in the Guinea region. The latter has also been shown to have large impacts on the incoming shortwave radiation, especially in the Sahel region during the monsoon season (Bouniol et al., 2012).

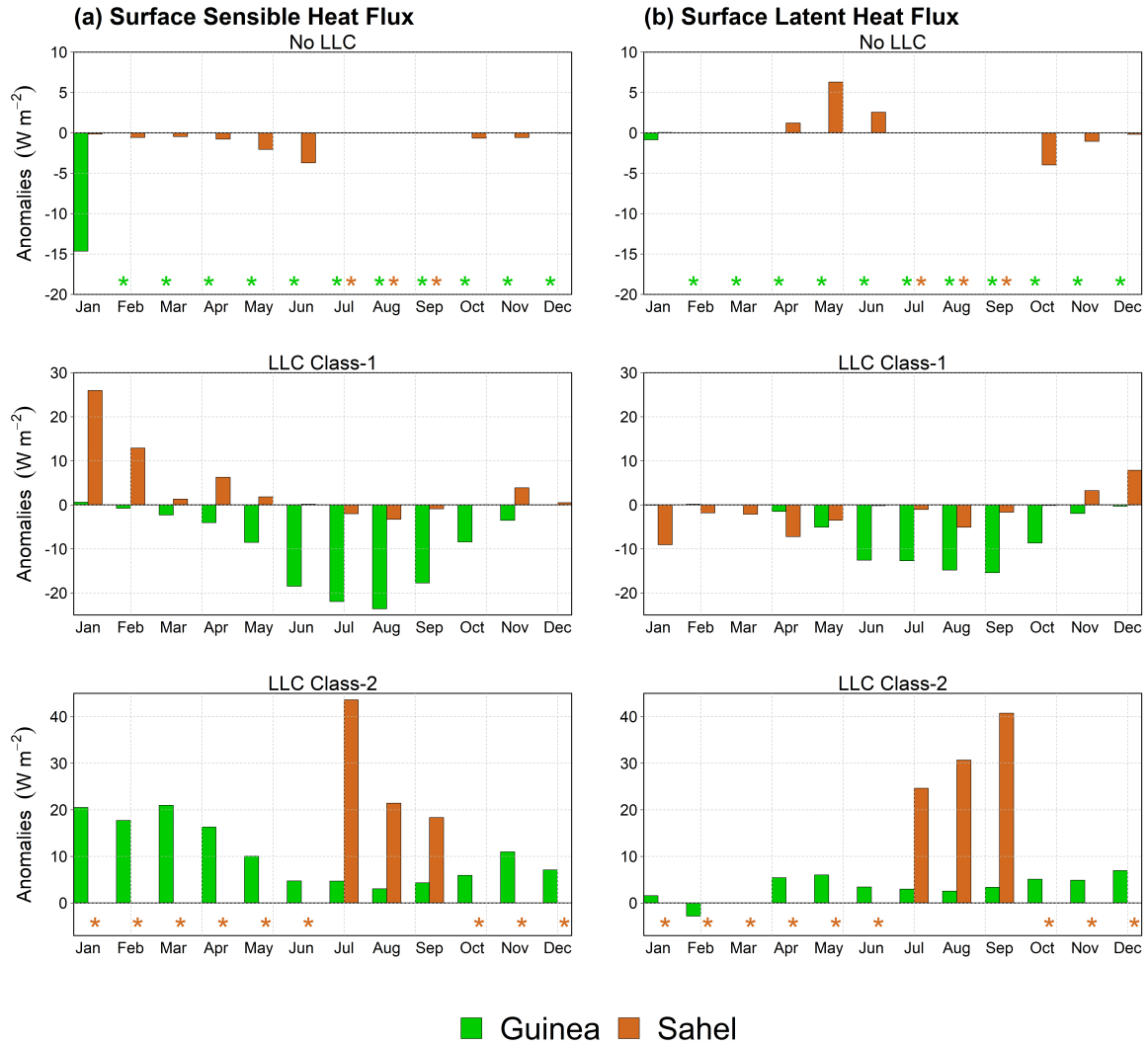


Figure 4.9: Monthly mean anomalies of (a) surface sensible heat and (b) surface latent heat fluxes computed in the Guinea and Sahel regions for the occurrence of the three LLC classes from 2006 to 2015. The orange and green stars mean that there was no occurrence of the particular LLC class events in the region during that month, hence the composites were not computed. Only occurrences that last for at least six consecutive hours are considered.

In terms of anomalies, the LLC Class-2 events present positive values (Figure 4.9a) over both regions suggesting reduced upward sensible heat transfer. This could be explained by two main reasons. Firstly, a larger portion of the sky is blocked during these events leading to lower sensible heating at the surface. Additionally, large amounts of energy are released in the lower atmosphere during the formation of these clouds, which in turn leads to a higher sensible heat flux in the atmosphere than when there are no LLCs or when the cloud fraction is low. On the other hand, LLC Class-1 in the Guinean region presents negative anomalies of

sensible heat that suggest a net upward transfer of sensible heat during these events. As these LLCs do not cover a large portion of the sky, a large amount of shortwave radiation still warms the surface. Moreover, the energy released in the atmosphere is not as much as for LLC Class-2 events. Thus, during these events, the atmosphere has a relatively lower sensible heat flux. It is rather surprising that the Sahel region presents positive anomalies (except in JAS) for sensible heat. As suggested by Bouniol et al. (2012), such a result should not be interpreted exclusively in terms of the radiative effects of clouds but rather the coupled interactions between fluctuations in temperature, water vapor, and clouds in this region. However, this is beyond the scope of the present study.

During LLC occurrence, the large mean negative latent heat values indicate more evaporation from the surface (Figure 4.8b). Interestingly, the transfer of latent heat upwards is higher in Class 1 than in Class 2. Since only a small portion of the sky is covered during LLC Class-1 events, the surface still receives a significant amount of downwelling shortwave radiation. Therefore, the surface continues to be warmed better by the sun’s radiation during LLC Class-1 events than Class-2 events. As a result, the evaporation of moisture at the surface is much higher during the occurrence of the former. There are negative anomalies of the surface latent heat (Figure 4.9b) in both regions during LLC Class-1 events in all months (except in November and December in the Sahel). This signifies a more intense upward transfer of latent energy due to higher evaporation during these events. On the other hand, LLC Class-2 events are associated with positive anomalies of latent heat. This is likely due to the reduced incoming downwelling shortwave radiation which in turn decreases the evaporation at the surface.

4.8 Attenuation of incoming shortwave radiation during LLC occurrence

In Figure 4.10 and Figure 4.11, the regional distribution of cloud radiative effect on incoming downwelling shortwave radiation during JAS and DJF is presented respectively as the percentage of incoming shortwave radiation attenuated during the occurrence of LLCs in the two regions as computed with Equation 4.2 ($CRE_{SW\downarrow}$). In this section, we will focus more on the mean $CRE_{SW\downarrow}$ in each of the regions. Firstly, there is a strong seasonal variability of $CRE_{SW\downarrow}$ over the entire WA region. It is obvious that shortwave attenuation is much higher during JAS than during DJF over the entire region as a result of increased cloud coverage during the monsoon season (Bouniol et al., 2012; Danso et al., 2019). This is true whether LLCs are

present or not. During the occurrence of LLCs, the values of $CRE_{SW\downarrow}$ are much lower for LLC Class-1 than LLC Class-2 events, whatever the region and the season. This clearly shows the strong dependence of $CRE_{SW\downarrow}$ on the fractional coverage of clouds as previously discussed by Liu et al. (2011).

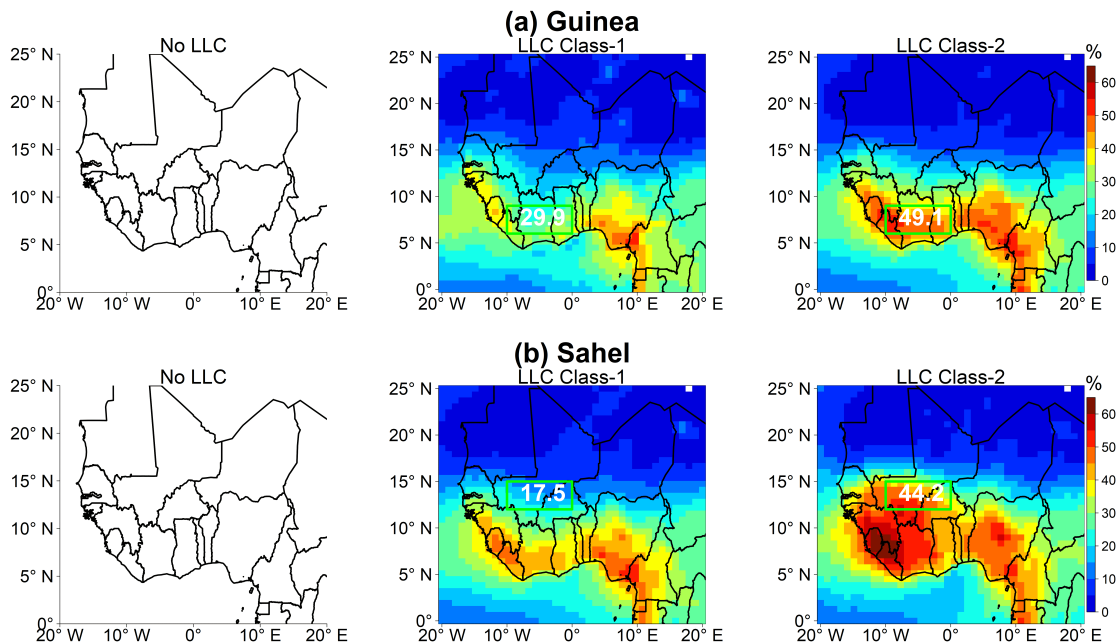


Figure 4.10: Mean attenuation of incoming downwelling shortwave radiation (%) during JAS from 2006 to 2015 over WA for occurrence of the three LLC classes in the Guinea (top) and Sahel (below) regions. Only occurrences that last for at least six consecutive hours are considered. Numbers in the box refer to the mean percentage attenuation of incoming shortwave radiation in that specific area. No event of the No LLC class has been extracted in the Guinea and Sahel regions during JAS, hence the empty plots.

In JAS, the strong impacts of LLCs on incoming shortwave radiation is seen from the high $CRE_{SW\downarrow}$ values during LLC occurrence. During the occurrence of LLC Class-1 events, the mean percentage attenuation of incoming shortwave radiation becomes 29.9% and 17.5% respectively in the Guinean and Sahelian regions. In the same way, 49.1% and 44.2% of incoming shortwave radiation are attenuated on average in Guinea and Sahel, respectively during events of LLC Class-2. Though these values are attenuated in the two regions under consideration, higher losses can be experienced in different areas over the region during those events. For instance, during LLC Class-2 events in the Sahel, the areas around the southern coast and the Guinea highlands experience much higher $CRE_{SW\downarrow}$ values (up to 65%). This could be due to the presence of more clouds in those areas which extend into the Sahel region

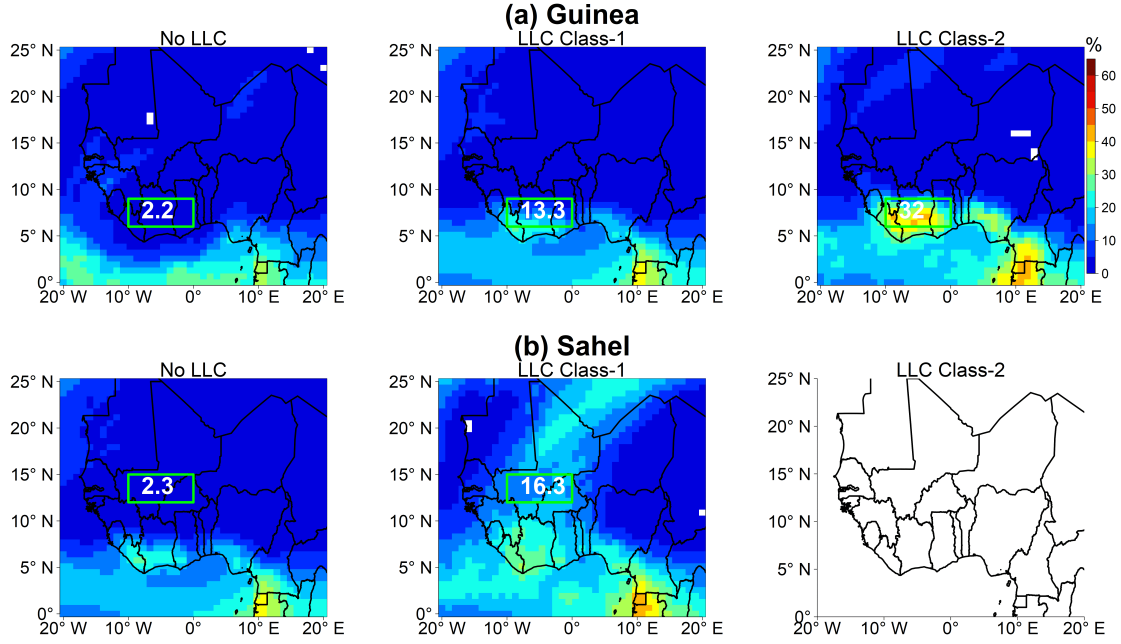


Figure 4.11: Same as Figure 4.10 but for DJF. No event of LLC Class-2 has been extracted in the Sahel region during DJF, hence the empty plot.

During DJF, during events of No LLC in Guinea and Sahel, about 2.2% and 2.3% (Figure 4.11) of the incoming shortwave radiation is lost on average respectively. Even though there is no LLC occurrence during these events, this attenuation value is due to the possible presence of other cloud types at the upper levels. However, similar to the JAS season, the occurrence of LLCs leads to higher $CRE_{SW\downarrow}$ in both regions. In Guinea, 13.3% of incoming shortwave radiation is lost on average during the occurrence of LLC Class-1 events while 32% is lost during LLC Class-2 events. In Sahel, the mean attenuation during the occurrence of LLC Class-1 events is 16.3%.

The large attenuation of incoming shortwave radiation during LLC occurrence (especially LLC Class-2) could be detrimental to planned solar energy application projects if not properly planned. For instance, during the JAS season in the Guinea region (and southern part of WA in general), the dominance of LLC Class-2 events (Table 4.2 and Figure 4.3) means that surface solar radiation will be significantly reduced for a large number of periods. Although there are equally high losses of incoming solar radiation in the Sahel during LLC Class-2 events in JAS, these events are rarer than in the Guinea region. Besides, the Sahel region has several persistent periods with no LLCs compared to the Guinea region in the other months of the year, especially during DJF. However, other issues that are not discussed in this paper such as dust (e.g., Bonkaney et al. (2017)) could severely

hinder solar energy projects in the Sahel region. In all cases, the implementation of large-scale solar energy projects in both regions requires meticulous planning to ensure that the intense cloudiness over the region and the high variability of these clouds as shown by Danso et al. (2019) do not compromise the long-term aims of those developments.

4.9 Conclusions

In this paper, we made use of the state-of-the-art hourly reanalysis dataset from ECMWF – ERA5 from 2006 to 2015 to analyze the occurrence of daytime LLCs in WA. The analysis was performed for both the wet (JAS) and dry (DJF) seasons and focused on two climatically contrasting areas in the region (i.e., Guinea and Sahel). We have first identified events of LLC occurrence in both regions. We then analyzed some regional- and local-scale environmental conditions which occur during those events of LLC occurrence. This analysis mainly focused on the moisture flux before, during and after the LLC occurrence. We also analyzed the impacts of the LLC occurrence on the surface heat fluxes. Finally, the attenuation of incoming shortwave radiation during the occurrence of LLC in the region was estimated. To account for the influence of fractional coverage of LLC on the attenuation of incoming shortwave radiation, we classified the events of LLC occurrence into two groups: events with low fractional coverage (LLC Class-1) and events with high fractional coverage (LLC Class-2). The main findings of the study are summarized below:

- The occurrence frequency of daytime LLCs is characterized by significant diurnal and seasonal variations: (i) Over Guinea, the occurrence of LLC Class-1 events is rarer during the core of the monsoon season (JJAS) while LLC Class-2 events are much higher during this period. During the day, LLC Class-2 events occur frequently during the early morning while LLC Class-1 is rather frequent during the late afternoon. (ii) Over Sahel, the occurrence of both LLC Class-1 and LLC Class-2 events is higher during the core of the monsoon season. Occurrence frequency of LLC Class-2 events is higher around midday while for LLC Class-1 events, it does not show a strong diurnal variation.
- During JAS, the occurrence of LLCs (both Class-1 and Class-2) in both Guinea and Sahel is associated with high moisture flux dominated by significant background moisture and strong southwesterly winds from the Gulf of Guinea. We also found that just before the occurrence of LLC, the temperature in the lower atmosphere is significantly reduced (Appendix B). This is due to cold air advection which leads to saturation as shown in previous studies (e.g., Adler

et al. (2019) and Babić et al. (2019a)).

- In the dry season, the moisture flux is not as intense as in JAS but the background moisture content is significant during occurrence of LLCs. The region is dominated by dry northeasterly winds during this period. Other processes such as the atmospheric waves and jets in the region (African Easterly wave, African Easterly Jet, etc.) may also contribute to the occurrence of LLCs but these are not analyzed in this study. These processes are, however, only relevant in the wet season.
- The occurrence of LLCs has significant impacts on surface heat fluxes. LLC Class-2 events lead to a significant reduction in the transfer of energy (both sensible and latent) upward and significant release of energy in the atmosphere which causes a net downward transfer of energy.
- Attenuation of incoming shortwave radiation is higher during JAS than DJF and depends on the fractional coverage of LLCs. In JAS, the occurrence of LLC Class-1 leads to mean attenuations of 29.9 % and 17.5 % respectively in Guinea and Sahel. LLC Class-2 leads to mean attenuations of 49.1 % and 44.2 % in Guinea and Sahel respectively. In DJF, mean attenuations of 13.3 % and 32 % are experienced in Guinea for LLC Class-1 and Class-2 events respectively. In Sahel, the occurrence of LLC Class-1 events leads to a 16.3 % attenuation of incoming shortwave radiation. It should however be noted that ERA5 slightly overestimates cloud fraction in the lower atmosphere over WA (see Chapter 2).

By using the ERA5 cloud cover dataset in this study, we have provided important information on daytime LLCs in WA – a region notably known for its lack of surface observations. Previous studies have mostly focused on nighttime LLCs in the southern part of WA and only during the WAM season. Here, we expanded to the Sahel region and investigated the occurrence of LLCs during the dry season as well. The study helps to identify some conditions such as the background moisture level which is known to contribute to LLC formation in the region. Again, this study also helps to provide an idea on the impacts of these clouds on the surface energy budget especially on the attenuation of incoming shortwave radiation during LLC occurrence. The results on the seasonal and diurnal distributions of LLCs as well as on that on the attenuation of incoming shortwave radiation during LLC occurrence could be useful when making feasibility studies for large-scale solar energy projects.

Chapter 5

Impacts of clouds on the availability and variability of the solar resource in West Africa

5.1 Chapter overview

After presenting the cloud occurrence properties and associated conditions in Chapters 3 and 4, this chapter provides a discussion of the impacts of cloud occurrence on the incoming shortwave radiation for solar power production. Here, we quantify the effects of clouds on the value and variability of the incoming radiation. Also, this chapter presents an analysis of the persistence of cloudy and cloudless conditions in the region. Finally, a classification of the received surface radiation independent of cloud occurrence is made. The persistence of the different classes of radiation in each season are then presented. This analysis directly provides an idea of how often solar power production will be above or below a certain threshold and how long it will last.

The contributions of this chapter include the novel analysis of the persistence of cloudy and cloudless conditions and the different classes of the received radiation in the region. Moreover, the quantification of radiation losses and variability due to clouds is a significant feasibility analysis for solar energy development in the region.

The goal of this work is to provide a climate service for stakeholders involved in the planning of solar energy integration in WA. As such, the results obtained have been published in the Special Issue “*Towards Inclusive and Operational Weather and Climate Services to Strengthen Resilience to Climate Change*” of **Atmosphere** (Danso et al., 2020b).

5.1.1 Contributions

Formulation of study idea and context

The idea to provide a climate service came about during one of my frequent exchanges with my advisors. From the earlier results in Chapters 3 and 4, it was imperative to know the quantitative effects of cloud occurrence on the incoming radiation in the study region. To quantify the effects, the cloud radiation attenuation for shortwave radiation, and the coefficient of variation were estimated. I then proposed the analysis of multi-hour persistence of different sky conditions and ranges of the incoming radiation.

Numerical computations and general methodology

I wrote the scripts to calculate the cloud radiation attenuation and the coefficient of variation of the incoming radiation in selected areas over WA. The selected areas are the same spatial windows chosen in Chapter 3. I also wrote an algorithm in the *R* environment to estimate the occurrence frequency of cloudy events lasting for at least one hour to more than six hours. I then proposed a classification of the surface radiation based on its value and independent of the presence of clouds. I then applied the algorithm for estimating persistence on the three classes of surface radiation. I computed the persistence for each of the four northern hemispheric seasons.

Visualizations and analysis

All figures were done in the *R* programming environment. The figures were then interpreted and analyzed in collaboration with my advisors.

Drafting and editing

The chapter is the third article from this PhD thesis; it is published in *Atmosphere*. I drafted the first version of the manuscript and edited it after integrating comments from my advisors. After submission, we received reviews from 4 anonymous referees. I revised the manuscript and was accepted for publication after the first round of review.

Presentations

Part of the results in this chapter were presented at AGU 2019 Fall Meeting in San Francisco, USA and SPSAS summer school 2019 in Sao Paulo, Brazil. I have also presented internally at IGE and LAPA-MF.

5.2 Article: Cloudiness information services for solar energy management in West Africa

Abstract: In West Africa (WA), interest in solar energy development has risen in recent years with many planned and ongoing projects currently in the region. However, a major drawback to this development in the region is the intense cloud cover which reduces the incoming solar radiation when present and causes fluctuations in solar power production. Understanding the occurrence of clouds and their link to the surface solar radiation in the region is, therefore, important in making plans to manage future solar energy production. In this study, we use the state-of-the-art ERA5 dataset to examine the occurrence and persistence of cloudy and clear-sky conditions in the region. We then investigate the effects of cloud cover on the quantity and variability of the incoming solar radiation. The cloud shortwave radiation attenuation (CRA_{SW}^{\downarrow}) is used to quantify the amount of incoming solar radiation that is lost due to clouds. The results showed that the attenuation of incoming solar radiation is stronger in all months over the southern part of WA near the Guinea Coast. Across the whole region, the maximum attenuation occurs in August with a mean CRA_{SW}^{\downarrow} of about 55 % over southern WA and between 20 % and 35 % in the Sahelian region. Southern WA is characterized by a higher occurrence of persistent cloudy conditions while the Sahel and northern WA are associated with frequent clear-sky conditions. Nonetheless, continuous periods with extremely low surface solar radiation were found to be few over the whole region. The analysis also showed that the surface solar radiation received from November to April only varies marginally from one year to the other. There is, however, a higher uncertainty during the core of the monsoon season (June to October) with regards to the quantity of incoming solar radiation. The results obtained show the need for robust management plans to ensure the long-term success of solar energy projects in the region.

Authors: Derrick Kwadwo Danso, Sandrine Anquetin, Arona Diedhiou, Rabani Adamou

5.3 Introduction

According to the fifth assessment report of the Intergovernmental Panel on Climate Change (IPCC), concentrations of greenhouse gases (GHGs) have risen in recent times with a 40 % increase in CO₂ concentration since pre-industrial times (Stocker et al., 2014). This has led to the observed warming of the earth’s surface and atmosphere. In 2017, anthropogenic warming due to GHG emissions reached about 1°C above pre-industrial levels (Allen et al., 2018). Nearly two-thirds of all GHG emissions emanate from the energy sector (IEA, 2019b), primarily due to the combustion of fossil fuels such as coal and petroleum. With growing demands for energy due to economic growth around the world, continued GHG emissions will lead to further warming of the earth’s atmosphere. The Paris Agreement, however, was made in 2015 to ensure that the rise in global average temperature is kept below 2°C above the pre-industrial levels within this century. As a result, one of the major global responses has been to develop and/or increase consumption of renewable energies such as solar energy, while reducing fossil energy use (Rogelj et al., 2018).

In West Africa (WA), projects dealing with solar energy development and implementation have attracted lots of interest from many governments and industries since the Paris Agreement due to the high potential for solar power generation in the region (Hermann et al., 2014; Yushchenko et al., 2018). Countries like Ghana and Cote d’Ivoire are currently undergoing significant economic and infrastructural developments and thus the need for clean energy keeps increasing. In Cote d’Ivoire for instance, the national renewable energy policy is focused on increasing the contribution of variable renewables to total electricity generation up to 16 % by 2030. Consequently, a 25 MW solar photovoltaic (PV) power plant is currently under construction in northern Cote d’Ivoire while two other 30 MW capacity plants have been approved for construction in the northwestern part of the country (MPEER, 2014). In Ghana, a 155 MW capacity solar PV power plant is currently under construction in the southwestern part of the country and will be the largest solar farm in the WA region when completed (Kuwonu, 2016). Also, there are many planned and existing solar energy projects in the Sahelian region of WA. These include the 33 MW capacity Zagtoui solar PV power plant in Burkina Faso (Moner-Girona et al., 2017), currently the largest operational PV plant in the Sahelian region of WA.

Despite the high solar resource availability in the region (Hermann et al., 2014; Yushchenko et al., 2018), large-scale development of solar energy such as in a 100 % off-grid solar PV system, could seriously be hindered by drawbacks associated with crustal dust and cloud cover. When present, dust and cloud cover strongly decrease the surface solar radiation available for solar power generation (Bouniol

et al., 2012; Dajuma et al., 2016; Pyrina et al., 2013). In West Africa, some studies (e.g., Dajuma et al. (2016) and Stanelle et al. (2010)) have investigated the impacts of dust on the efficiency of PV modules and solar power production but very little has been done on clouds in a similar context. Clouds largely drive the albedo of the atmosphere that determines the amount of solar radiation reaching the earth's surface during the daytime (Liou, 2002). Additionally, the temporal evolution of clouds controls the variability of the incoming solar radiation (Engeland et al., 2017; Wang et al., 2012). Thus, understanding the impacts of clouds on the availability and evolution of surface solar radiation in WA is essential for the successful integration of solar energy in the regional power pool. This could help to anticipate potential risks associated with largescale solar energy development in the region. This study, therefore, focuses on the effects of clouds on solar radiation in the framework of managing solar energy production in the region.

The climate of WA which is controlled by the West African Monsoon, is typically characterized by an intense coverage of different cloud types (Hill et al., 2016; van der Linden et al., 2015) associated with a high spatial-temporal variability (Danso et al., 2019). However, the impacts of these clouds on the incoming solar radiation needed for power generation are not very well studied in the region. Due to the lack of surface observations, only a few studies (e.g., Bonkaney et al. (2017) and Bouniol et al. (2012)) have tried to address this important issue, essential for any feasibility analysis concerning solar energy development in the region. These studies are however limited to only a few locations where surface observations are available. As a result, a regional overview of the effects of clouds on the incoming solar radiation is lacking, leaving many open key questions concerning the long-term feasibility of regional-scale solar energy projects. Addressing some of these questions could help to develop effective plans that would be crucial to managing the risks of integrating large shares of solar energy in the region. This could further help to alleviate fears of massively investing in the development of the solar energy potential in the region. Thus, the goal of this study is to contribute to the answers to the following key questions:

- How does the sub-daily surface solar radiation vary from one year to the other in WA?
- What percentage of incoming solar radiation is attenuated by clouds in WA?
- How persistent are cloudy and cloudless conditions in the region?

The ambition is to provide relevant and usable information for stakeholders involved in the planning of solar energy projects in the region. For instance, the persistence

of cloudiness at a location is important in the siting and sizing of solar PV farms. Although WA is known to be cloudy, the persistence of cloudiness is still relatively unknown in many areas within the region, thus, casting uncertainties in the feasibility of integrating large shares of solar PV power into the power systems. This important issue is addressed in this study in the context of solar energy production. Again, the estimation of the attenuation effect of clouds and the variability of solar radiation at several locations over WA (in different climatic zones) will provide an added value to previous studies (e.g., Bouniol et al. (2012) and Hill et al. (2018)) that focused on single locations. This approach could help to develop specific plans tailored for managing solar energy production in different areas within the WA region. It is worth noting that dust has important effects on the incoming solar radiation but we focus only on clouds in this study.

The article is organized as follows: section 5.4 presents the dataset, study area and methodology. section 5.5 presents and discusses the findings of the study. In section 5.6, we conclude and provide insights for the future.

5.4 Materials and methods

5.4.1 Data

In this study, cloud cover and incoming surface solar radiation flux data are analyzed and the attenuation of the solar radiation by clouds is determined. The cloud cover and radiation data are extracted from the fifth generation of the state-of-the-art European Centre for Medium-range Weather Forecasts (ECMWF) Re-Analysis also known as ERA5 (C3S, 2017). In Sterl et al. (2018), the ERA5 dataset was evaluated and used to analyze the synergies between renewable energy sources including solar energy in WA. The dataset is available at an hourly resolution with a horizontal resolution of $0.25^\circ \times 0.25^\circ$ on a regular grid. For this study, we analyzed only daytime hours for a 10-year period spanning from 2006 to 2015.

ERA5 provides 2D (and 3D) distributions of different cloud properties integrated for all levels within some predefined layers in the atmosphere. Here, we analyze the cloud fraction which includes the total cloudiness (TC), low-level cloudiness (LLC), mid-level cloudiness (MLC), and high-level cloudiness (HLC). In the ERA5 dataset, TC, LLC, MLC, and HLC are clouds integrated from the surface to the top of the atmosphere (TOA), the surface to 800 hPa, 800 hPa to 450 hPa and 450 hPa to TOA respectively (Forbes, 2017). In addition to the cloud fraction, ERA5 provides the surface downwelling shortwave radiation fluxes in all-sky and clear-sky conditions. Table 5.1 provides a summary of all input data used for this

study:

Table 5.1: Summary of input data extracted from ERA5 and used for this study.

Input data	Symbol	Details
Surface downwelling shortwave radiation, all-sky	SW^\downarrow	Input for cloud radiative attenuation of all clouds and of different cloud types
Surface downwelling shortwave radiation, clear-sky	SW_{CS}^\downarrow	
Total cloudiness	TC	Input for cloud radiative attenuation of all clouds
High-level cloudiness	HLC	Input for cloud radiative attenuation of high-level clouds
Mid-level cloudiness	MLC	Input for cloud radiative attenuation of mid-level clouds
Low-level cloudiness	LLC	Input for cloud radiative attenuation of low-level clouds

Data evaluation

A necessary condition for using the ERA5 dataset for such a study is to first evaluate its ability to reproduce the actual observations in the region of interest. In a recent study by Danso et al. (2019) in WA, the ERA5 cloud fraction was compared with some synoptic in situ observations (and satellite data) from the region obtained from the Integrated Surface Database (Lott et al., 2001). The comparison showed a satisfactory agreement between the reanalysis and in situ dataset (see Appendix S1 in Danso et al. (2019)). Here, we evaluate the surface downwelling shortwave radiation flux with in situ observations in WA. For this, we use surface measurements from two sites of the AMMA-CATCH observatory (African Monsoon Multidisciplinary Analysis - Couplage de l'Atmosphère Tropicale et du Cycle eco-Hydrologique (Galle et al., 2018)). The two sites (red triangles in Figure 5.1) are located at Wankama South (2.6334°E and 13.6476°N) in Niger and Nalohou (1.6049°E and 9.7448°N) in Benin and provide complete surface solar radiation flux measurements for the period of study. Solar radiation data from the closest grid points to the two sites in the ERA5 dataset are thus used for the evaluation complemented by the satellite-based Surface Radiation Data Set – Heliosat (SARAH) hourly solar irradiance time series (Pfeifroth et al., 2019), extracted from EUMETSAT Satellite Application Facility on Climate Monitoring (CM-SAF).

Figure 5.2 presents two Taylor diagrams showing the performance of ERA5

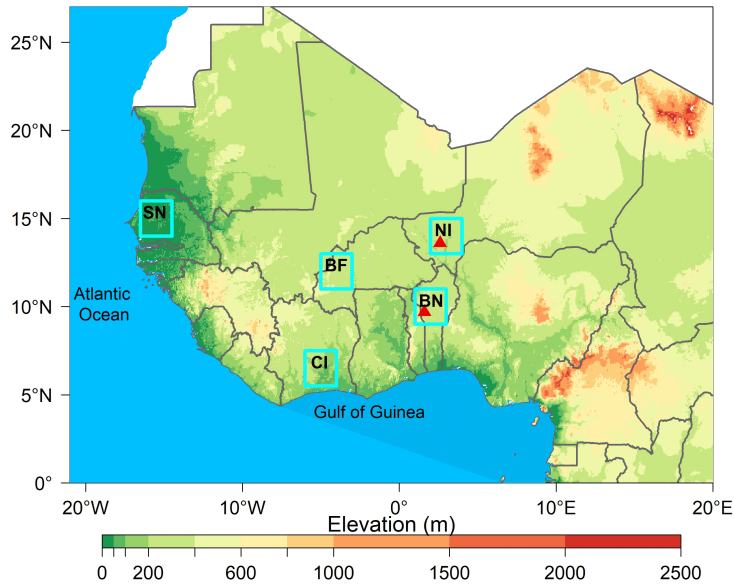


Figure 5.1: Elevation map of West Africa showing five $2^\circ \times 2^\circ$ boxes across the region in Senegal (SN), Burkina Faso (BF), Niger (NI), Benin (BN, (and part of Togo)), and Cote d'Ivoire (CI). The map also shows the locations of the two AMMA-CATCH observatories in Benin and Niger (red triangles).

and SARAH in the evaluation with the surface observations in Benin and Niger respectively. In Benin, ERA5 shows a good agreement with the surface observations with a correlation coefficient of about 0.92 and a root mean square error (RMSE) of 123 W m^{-2} . Likewise, in Niger, ERA5 shows a reasonable agreement with the surface observation with a correlation coefficient of about 0.84 and root mean square error of 182 W m^{-2} . Also, in both stations, the ERA5 data exhibits similar scatter around the mean (standard deviation) as the observation. It should be noted that, these values take into account the seasonal signals in the data. Removing the seasonality changes the values (see Figure 2.8), and thus, the evaluation presented here must be interpreted with caution.

5.4.2 Methodology

The study domain is the whole of West Africa (Figure 5.1) but investigations are mainly performed over the five $2^\circ \times 2^\circ$ bounded windows (light blue in Figure 5.1) across the WA region. These windows are located in different climatic and vegetation zones and their selection help to provide a regional overview of cloud cover effects on the incoming solar radiation. Three of the windows are located in Senegal, Burkina Faso, and Niger, all in the Sahelian climate zone of WA (Gbobaniyi et al., 2014). The two other windows are located in Cote d'Ivoire and Benin in the Guinean and Sudanian climate zones of WA respectively (Klein et al., 2015). Additionally,

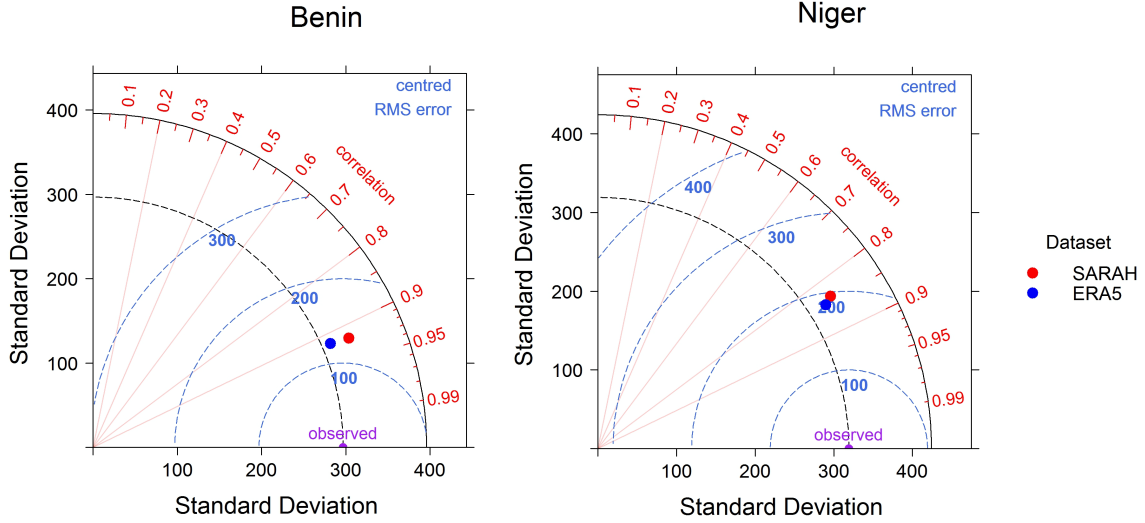


Figure 5.2: Taylor’s diagrams showing the evaluation of ERA5 (and SARAH) with surface observations from the AMMA-CATCH observatories.

all of these five windows are located in countries with plans for utility-scale solar energy development. The selection of the Niger and Benin windows is also motivated by the availability of complete surface observations used for the evaluation of the ERA5 data (Figure 5.2). Though the Senegal window is located in the Sahel region of WA, its proximity to the ocean (like the Cote d’Ivoire window) could lead to increased cloudiness compared to the other two Sahelian windows (Parker & Diop-Kane, 2017). No window is located north of latitude 16°N because this area is usually characterized by very low cloud coverage throughout the year (Danso et al., 2019; Hill et al., 2016).

To capture how the sub-daily surface solar radiation varies from one year to the other, the interannual variability of the hourly surface downwelling shortwave radiation flux, SW^{\downarrow} , is investigated with the coefficient of variation (CV) (Brown, 1998) over the five $2^{\circ} \times 2^{\circ}$ windows in the WA region. The CV is unitless and is defined as the ratio of the standard deviation to the mean. In each window, the CV shows how the SW^{\downarrow} measured for a given day and time varies across all years for the same day and time. Unlike the standard deviation, the interpretation of the CV is independent of the mean value or unit of measurement. It is therefore very suitable to compare the variability of the SW^{\downarrow} from one window to the other and also within a particular window, the variability from one period (e.g., months and seasons) to the other.

We then analyze the occurrence and persistence of cloudy and cloudless sky conditions across the WA region. However, the impacts of the clouds on the incoming solar radiation have been determined over the five windows. To quantify the

attenuation of incoming solar radiation by clouds at any given time t , we define the cloud shortwave radiation attenuation (CRA_{SW}^\downarrow). CRA_{SW}^\downarrow refers to the quantity of incoming solar radiation that is lost through absorption or reflection (back to space) by clouds at any time. It is estimated by finding the difference between the SW^\downarrow in W m^{-2} , and the clear-sky surface downwelling shortwave radiation flux, SW_{CS}^\downarrow in W m^{-2} (Bouniol et al., 2012; Ramanathan et al., 1989). SW_{CS}^\downarrow is computed for the same atmospheric conditions of temperature, humidity, ozone, trace gases and aerosols as the corresponding SW^\downarrow (with clouds), but assuming that there are no clouds. Therefore, CRA_{SW}^\downarrow only accounts for the effects of clouds on the incoming solar radiation but not aerosols. To eliminate the influence of the time of the day and thus the solar elevation angle on the mean CRA_{SW}^\downarrow value, we express the CRA_{SW}^\downarrow at a given time as a percentage of the SW_{CS}^\downarrow at that time. Thus,

$$CRA_{SW}^\downarrow = \left| \frac{1}{N} \sum_{i=1}^N \frac{SW^\downarrow(i) - SW_{CS}^\downarrow(i)}{SW_{CS}^\downarrow(i)} \times 100 \right| \quad (5.1)$$

For each window, CRA_{SW}^\downarrow is computed for all daytime hours from 06 UTC to 17 UTC at each grid point when clouds are present (i.e., when $TC > 0$) and the mean is determined. For each window, we assume that nearby areas will have similar characteristics in terms of the mean solar radiation received at the surface as well as its variability.

The computation of CRA_{SW}^\downarrow considers the total cloudiness and does not differentiate the impacts of each cloud type (i.e., LLC , MLC , and HLC) on the incoming solar radiation. The impact of a particular cloud type can be determined following the same procedure and assumptions as Equation 5.1 but assuming only that cloud type is present while the other cloud types are absent in the atmosphere. Thus, for each cloud type, we computed the associated CRA_{SW}^\downarrow for periods during which only that cloud type was present i.e.,

$$CRA_{SW_{cloudtype}}^\downarrow = \begin{cases} CRA_{SW_{HLC}}^\downarrow, & \text{if } HLC > 0, MLC = 0, LLC = 0 \\ CRA_{SW_{MLC}}^\downarrow, & \text{if } MLC > 0, HLC = 0, LLC = 0 \\ CRA_{SW_{LLC}}^\downarrow, & \text{if } LLC > 0, HLC = 0, MLC = 0 \end{cases} \quad (5.2)$$

From this, it is possible to determine the relationship between the coverage area (i.e., the cloud fraction) occupied a given cloud type and its associated CRA_{SW}^\downarrow .

5.5 Results and discussion

5.5.1 Variability of received surface solar radiation

An important challenge for solar energy development is the intermittent nature of solar radiation mainly due to the high temporal variations in cloudiness leading to important fluctuations in solar power generation. This unfavorable situation is largely unavoidable at individual solar power plants but robust planning can help to reduce the overall impact on the power grid. Knowledge of the short-term (e.g., one minute) variations of surface solar radiation at a given location is very important for the day-to-day management of the power grid. Estimating the variability of incoming solar radiation in WA at such short timescales may prove challenging given the lack of surface observations. Additionally, the hourly resolution of the ERA5 data makes it impossible to capture the intra-hour variability of surface solar radiation associated with cloud motion. Nevertheless, knowledge of a longer-term variability (e.g., month-to-month, season-to-season, year-to-year) is important for the successful integration of large shares of solar energy into the regional power systems. For this, it is necessary to understand how the solar radiation received at a specific place and time (hour, day, or month) varies from one year to the other. This could help to characterize the uncertainty associated with the surface solar radiation received during different periods in a year.

Figure 5.3 shows the annual cycle of the CV computed from the interannual hourly surface solar radiation data over the 10 years for all the five selected windows. The cycle of the variability is similar in all the windows with a higher CV during the summer months in the core of the monsoon season and lower CV during the driest months (ranging from November to May depending on the region). This implies that the surface solar radiation received in the dry season does not change much from one year to the other while there is a higher uncertainty during the summer months. This result is in agreement with results from other tropical regions where the most humid months are found to be associated with the largest variability of surface solar radiation (e.g., Luiz et al. (2018) in Brazil). Generally, the variability appears to be higher in the southern part of WA where humidity is highest. For instance, during the core of the monsoon season, the variability is slightly higher in the Cote d'Ivoire and Benin windows compared to others. Moreover, in the dry months, the variability is highest in the windows that are close to the ocean (Cote d'Ivoire and Senegal). This result suggests that siting solar farms at humid locations in WA will present greater challenges and uncertainties mostly associated with fluctuations in power production. Thus, rigorous solutions such as the spatial diversification of PV farm sites (Shivashankar et al., 2016) are required to alleviate the overall impacts

of such challenges on the power grid.

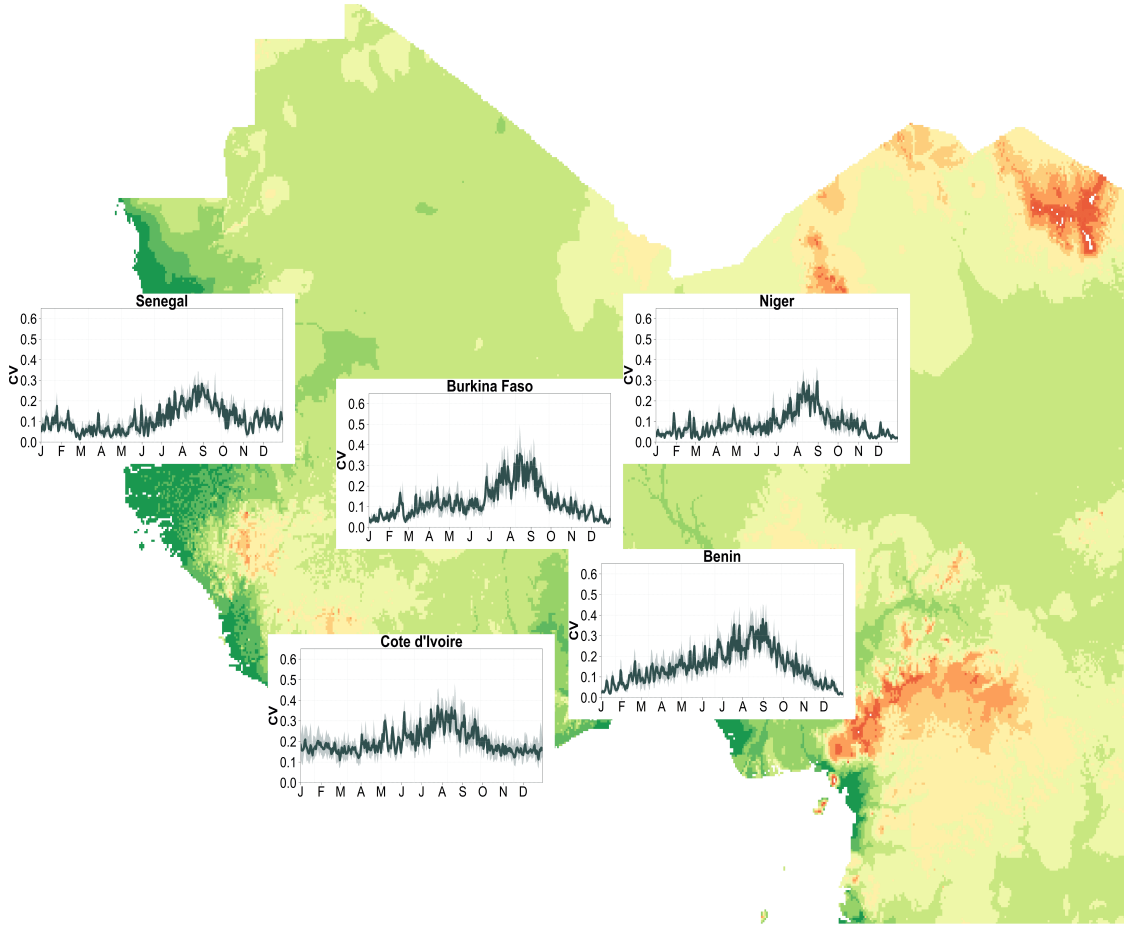


Figure 5.3: Annual cycle of coefficient of variation for the interannual hourly surface solar radiation received in West Africa.

5.5.2 Attenuation of incoming solar radiation by clouds

The mean annual evolution of the CRA_{SW}^{\downarrow} (for total cloud cover) is shown in Figure 5.4. In all windows, the mean attenuation of incoming solar radiation by clouds (solid red curve) is highest in the summer from July to October which corresponds to the core of the monsoon season in the region (Sultan & Janicot, 2003). During this period, WA is characterized by moisture influx from the Guinean Gulf which increases cloud cover over the region, thus, intensifying the attenuation of incoming solar radiation which in turn will lead to a decrease in solar power generation. The maximum attenuation occurs in August when the Inter-Tropical Convergence Zone (ITCZ) is at its northernmost position in WA (Nicholson, 2009; 2018; Sultan & Janicot, 2000). On the other hand, very low attenuations are observed from December to February when most of the WA region is characterized by dry weather conditions.

This cycle of CRA_{SW}^{\downarrow} follows the annual evolution of clouds in the region as shown in available cloud climatologies (e.g., Danso et al. (2019)).

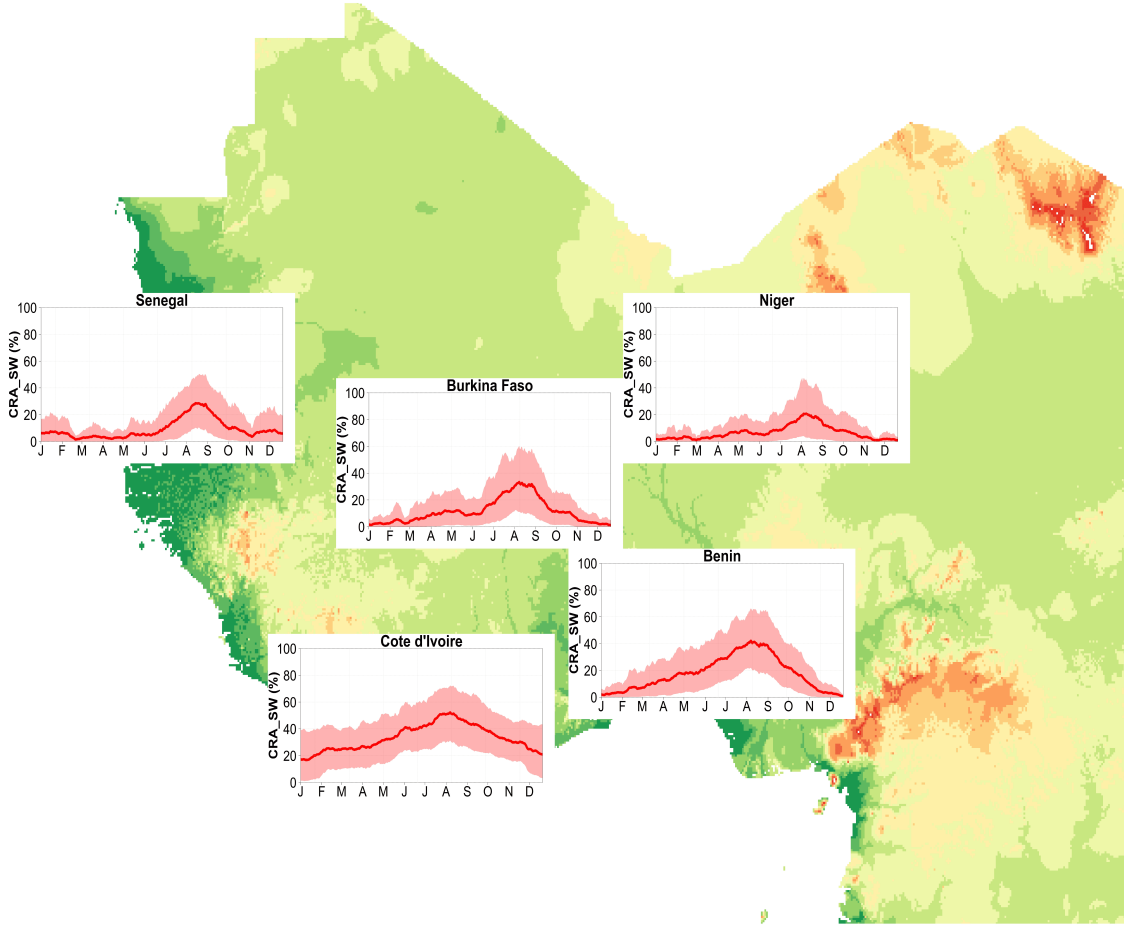


Figure 5.4: Mean annual cycle (solid curve) of cloud shortwave radiation attenuation in West Africa. Shaded regions are the 10th and 90th inter-percentile range.

Although all the windows display similar annual cycles of CRA_{SW}^{\downarrow} , the attenuation of incoming solar radiation is highest in the southern part of WA. In all months, the mean CRA_{SW}^{\downarrow} is higher in the Cote d'Ivoire and Benin windows compared to the other windows. In August, around 55 % and 40 % of incoming solar radiation are lost on average due to clouds in Cote d'Ivoire and Benin respectively compared to about 20 %, 30 %, and 35 % in Niger, Senegal and Burkina Faso. On the other hand, the mean attenuation is around 5 % or less in all windows during January except in Cote d'Ivoire where about 20 % of the incoming solar radiation is lost. If we assume a CRA_{SW}^{\downarrow} threshold of 30 % as reasonable for exploiting the solar resource potential in WA, many areas could be considered suitable for siting solar power plants as the mean CRA_{SW}^{\downarrow} does not exceed this threshold in several months. In the Sahelian region, the mean CRA_{SW}^{\downarrow} is rarely 30 % or more except in August in Burkina Faso and Senegal. In the southern part of WA, the mean attenuation

exceeds this arbitrary threshold value for longer periods i.e., from July to September in Benin and May to November in Cote d’Ivoire.

Furthermore, CRA_{SW}^{\downarrow} in the summer months is associated with a large variability in all windows (shaded region representing the 10th and 90th inter-percentile range). This could be due to a high degree of variation in the optical properties (such as cloud optical thickness) of the different cloud systems that occur over the region but this needs to be investigated further. Places like Cote d’Ivoire and Benin with high mean CRA_{SW}^{\downarrow} values exceeding the assumed threshold (especially in the summer) could thus have many other periods with lower attenuations. It is worth noting that in Cote d’Ivoire, the range of variability does not change throughout the year. In the other windows, however, the variability is mostly higher from June to September (April to June for Benin). Additionally, it is important to highlight that the mean and variability of CRA_{SW}^{\downarrow} in the Senegal window is not very different from the other Sahelian windows, regardless of its proximity to the Atlantic Ocean.

Figure 5.5 shows the mean seasonal evolution (from 2006 to 2015) of daily average surface downwelling shortwave radiation in clear-sky and cloudy conditions computed with ERA5. In the Northern Hemisphere, daylengths are longer (shorter) during the summer (winter) and thus the radiation arriving at the top of the atmosphere is highest (lowest) during this period (Hayward & Oguntoyinbo, 1987). In a hypothetical scenario with no clouds in the atmosphere, the incoming solar radiation over WA will thus be highest in the summer months from March to May (MAM) followed by June to August (JJA) and lowest from December to February (DJF) followed by September to November (SON) as shown in Figure 5.5a. In the southern part of WA however, the frequent occurrence of thick multi-layered clouds (Stein et al., 2011) responsible for the high CRA_{SW}^{\downarrow} values, severely reduces the incoming solar radiation during the summer months (JJA in Figure 5.5b). On the other hand, although the attenuation of incoming solar radiation in the Sahel and north of WA (north of latitude 10°N) is larger during the summer months, maximum solar radiation is received during this period. This is due to the relatively lower coverage of clouds in the Sahel as shown by Hill et al. (2016) and Danso et al. (2019). Again, most clouds occurring in the Sahelian region are thin (Bourgeois et al., 2018) (mid-and high-level clouds), thus, their total impact on the incoming shortwave radiation is relatively low. Moreover, daylengths are longer at higher latitudes during the summer and thus, the Sahel receives more solar radiation. During DJF, the amount of solar radiation received over the Sahel region with or without clouds in the atmosphere is similar. The reason for this is that cloud coverage in DJF is extremely low over this area.

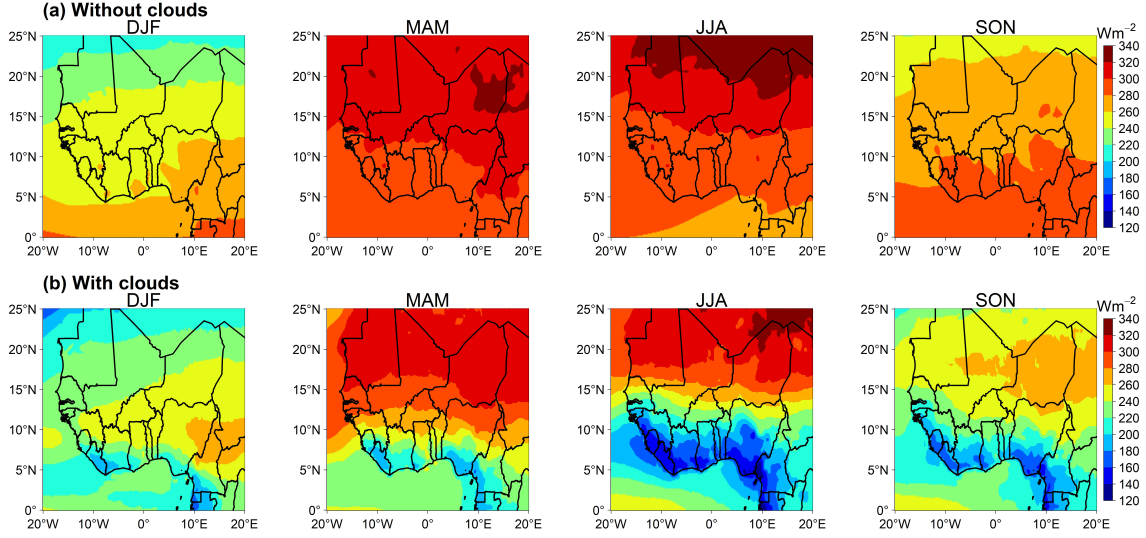


Figure 5.5: Mean seasonal evolution (2006 to 2015) of daily average surface downwelling shortwave radiation in (a) clear-sky and (b) cloudy conditions computed with ERA5. DJF refers to the December-January-February period, MAM to March-April-May, JJA to June-July-August and SON to September-October-November.

In terms of cloudiness, the most challenging period to manage a power grid integrated with solar energy in WA is the summer period due to high CRA_{SW}^{\downarrow} values and the associated variance (Figure 5.4). With a similar variance of CRA_{SW}^{\downarrow} across all windows (20% as shown in Figure 5.4) during the summer months, the difficulty in the management will be the same over the whole region, even though the Sahel and north of WA receives more solar radiation than the south (Figure 5.5). On the other hand, the variance in the other months is rather low in all windows except in Cote d'Ivoire which has high variance throughout the entire year. The high mean values and variance of CRA_{SW}^{\downarrow} in Cote d'Ivoire is likely due to the all-year-long presence of LLCs in this area of WA as shown by Danso et al. (2020a). Theoretically, this will make the management of solar energy production and power grid even more difficult in Cote d'Ivoire and its environs (southern WA). PV farms in this region will thus have to be oversized to reduce the impacts of the uncertainty in power production due to the high variability of CRA_{SW}^{\downarrow} throughout the year. Nevertheless, even though the variance in other months is low in the other windows (especially in the Sahel windows), higher temperatures during those months (Gbobaniyi et al., 2014) could also reduce the conversion efficiency of the PV cells. In a nutshell, cloudiness should not be a blocking factor for investing in solar energy in southern WA but there is a need to consider all of this information in the operational daily management and seasonal planning of solar power generation over the entire WA region.

5.5.3 Dependence of cloud radiation attenuation of cloud fraction

So far, we have only shown the impact of total cloud coverage on the attenuation of incoming solar radiation. However, differences in microphysical properties mean that CRA_{SW}^{\downarrow} differs across cloud types (Liou, 2002). Macrophysical properties such as cloud fraction could have a significant influence on the radiative effect of the different clouds. The influence may however differ from one cloud type to another. Here, we will investigate the relationship between the fractional coverage of each cloud type and its associated CRA_{SW}^{\downarrow} using the correlation coefficient (R). The R between cloud fraction and CRA_{SW}^{\downarrow} for each cloud type is presented in Table 5.2. In all the five selected windows, CRA_{SW}^{\downarrow} shows a strong dependence on the cloud fractional coverage for LLCs and MLCs. Thus, a larger (smaller) fraction of LLC or MLC results in a higher (lower) attenuation of the incoming solar radiation. As shown by Danso et al. (2019), during JJA the fractional coverage of LLC and MLC intensifies over southern WA, especially near the coastal areas. This leads to the high mean CRA_{SW}^{\downarrow} in the summer (Figure 5.4) and explains the low values of surface solar radiation around this area in JJA (Figure 5.5b). On the contrary, the dependence of CRA_{SW}^{\downarrow} on cloud fractional coverage is relatively weaker for HLCs. This is likely due to the optically thin nature of HLCs, which allows a large proportion of incoming solar radiation to pass through with very low attenuation. Liou (2002) showed that given representative environmental conditions for the same liquid water path and ice water path, clouds containing only liquid particles have larger optical depths and thus higher solar albedo effects. It was revealed in the same study that clouds that are composed entirely of water particles have a higher solar albedo effect due to the large liquid water paths. HLCs consist mostly of ice particles, unlike MLCs and LLCs which are largely composed of liquid water particles which explains why the CRA_{SW}^{\downarrow} of HLCs does not show a strong relationship with the fractional coverage.

Table 5.2: Relationship between cloud fraction and cloud shortwave radiation attenuation for the different cloud types in the five selected windows.

Region	R (CRA_{SW}^{\downarrow} vs. cloud fraction)		
	<i>HLC</i>	<i>MLC</i>	<i>LLC</i>
Senegal	0.59	0.94	0.93
Burkina Faso	0.53	0.93	0.99
Niger	0.5	0.92	0.91
Benin	0.45	0.93	0.96
Cote d'Ivoire	0.72	0.97	0.92

5.5.4 Multi-timescale persistence of sky conditions

Given the strong positive relationship between cloud fraction and CRA_{SW}^{\downarrow} for LLCs and MLCs, we analyze their occurrence and persistence within a given temporal window to qualitatively infer the reliability of solar power generation from solar plants in the region. As shown by Bouniol et al. (2012), these LLCs and MLCs are associated with high attenuation effects on incoming solar radiation in WA. Taking this into account together with the dependence of the attenuation on the fractional coverage of these cloud types, we can assume that a significant amount of the incoming solar radiation will be lost when a large fraction of the sky is covered by LLCs and/or MLCs. Figure 5.6 shows the annual mean occurrence frequency of LLCs, MLCs, and cloudless sky conditions that persist for a few to several hours during the daytime. Only LLCs and MLCs with high coverage in the sky (at least 50 %) are considered here.

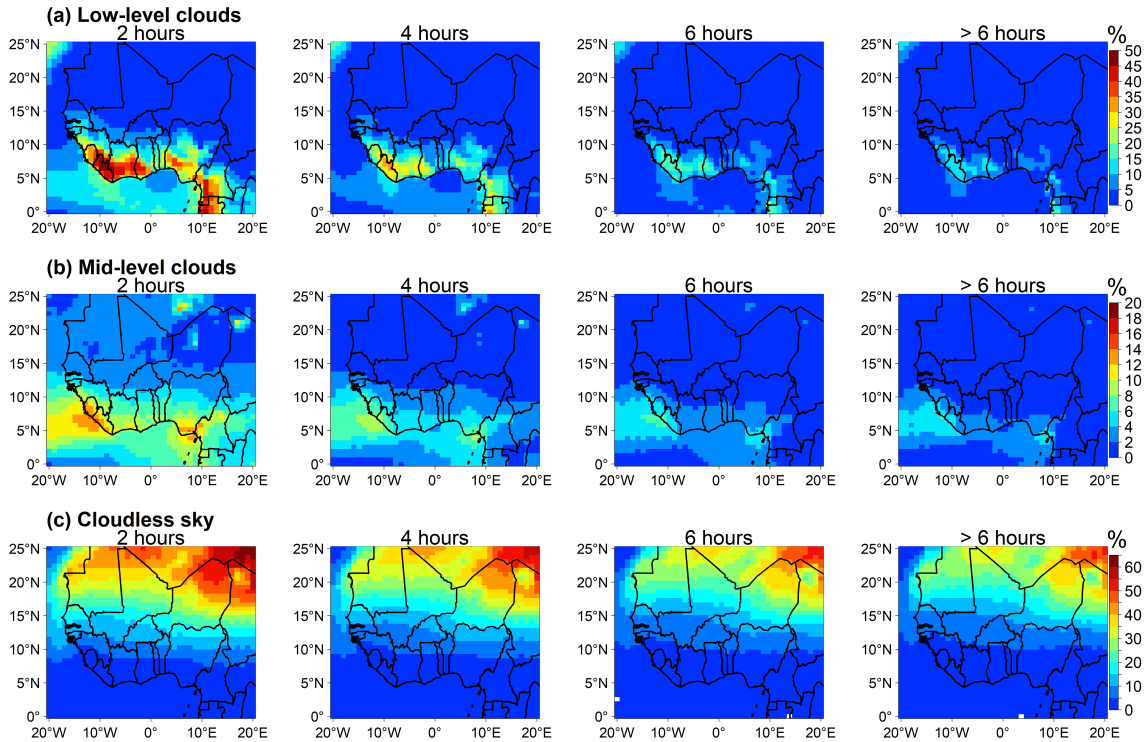


Figure 5.6: Spatial distribution of the occurrence frequency of (a) low-level cloudiness (LLC), (b) mid-level cloudiness (MLC) and (c) cloudless sky conditions that persist for multiple hours in West Africa. Only LLC and MLC occurrences with at least 50 % coverage are considered.

In general, there is a high occurrence frequency for LLCs (Figure 5.6a) and MLCs (Figure 5.6b) that persist for at least two consecutive hours in the southern part of WA (south of latitude 10°N) especially around the coastal areas. LLCs persist

for exactly two consecutive hours from 30 % to 50 % of the time in an average year. Over these same regions, LLCs occurrence can persist for several consecutive hours (more than 2 hours) during a significant number of times in a year. This includes about 5 % to 15 % extreme cases during which LLCs can persist for more than six consecutive hours. This means that for about 18 to 55 days in an average year, the received surface solar radiation will likely be well below the expected average for at least more than half of the time during each day. In the same way, MLCs can persist for exactly two consecutive hours during about 8 % to 16 % of the time in an average year. MLCs can also persist for several consecutive hours (more than 2) for a lot of days in a given year. For example, in Liberia and Sierra Leone as well as the southern parts of Cote d'Ivoire, Ghana, and Nigeria, MLCs can persist for more than six consecutive hours during 2 % to 6 % of the year (about 7 to 22 days). Thus, solar power generation could be severely disrupted during those periods over southern WA.

The Sahelian and northern parts of WA (north of latitude 10°N) are characterized by a high occurrence frequency of cloudless sky conditions (Figure 5.6c). Without clouds in the atmosphere, only a small fraction of the incoming solar radiation will be attenuated due to other atmospheric constituents (water vapour, trace gases, ozone etc.). This is an ideal case for solar PV farm managers as the solar PV panels receive maximum solar radiation to produce energy. Over the northern parts of Niger, Mali, and Mauritania for instance, cloudless sky conditions can persist for more than six consecutive hours during about 30 % of the time in an average year. These areas are however characterized by a high concentration of dust particles (Crouvi et al., 2012; Knippertz & Todd, 2012) which could severely reduce the incoming solar radiation. This issue of dust influence on incoming solar radiation is however not addressed in this study.

For solar energy management, it is also relevant to show the distribution of these persistent conditions in seasons or months. Figure 5.7 shows the mean occurrence frequency of persistent LLCs, MLCs, and cloudless sky conditions in the five selected windows for each season. Due to the steep spatial gradient of the occurrence frequency of cloudy and cloudless condition between the north and south of WA, the range of the y-axis differs across the chosen region; up to 20 % for the three Sahelian windows, 30 % for Benin and 60 % for Cote d'Ivoire. In general, the persistence of cloudiness in all seasons, seems to decrease with latitude except for the Senegal window which is situated at a higher latitude than the Niger window, yet has a relatively higher frequency of persistent LLCs and MLCs. This is likely due to the proximity of Senegal to the Atlantic Ocean which leads to an intrusion of cold moist westerly winds enhancing cloud formation and occurrence in this area.

This enhanced cloud formation could explain the relatively higher CRA_{SW}^{\downarrow} during the rainy season in Senegal than Niger.

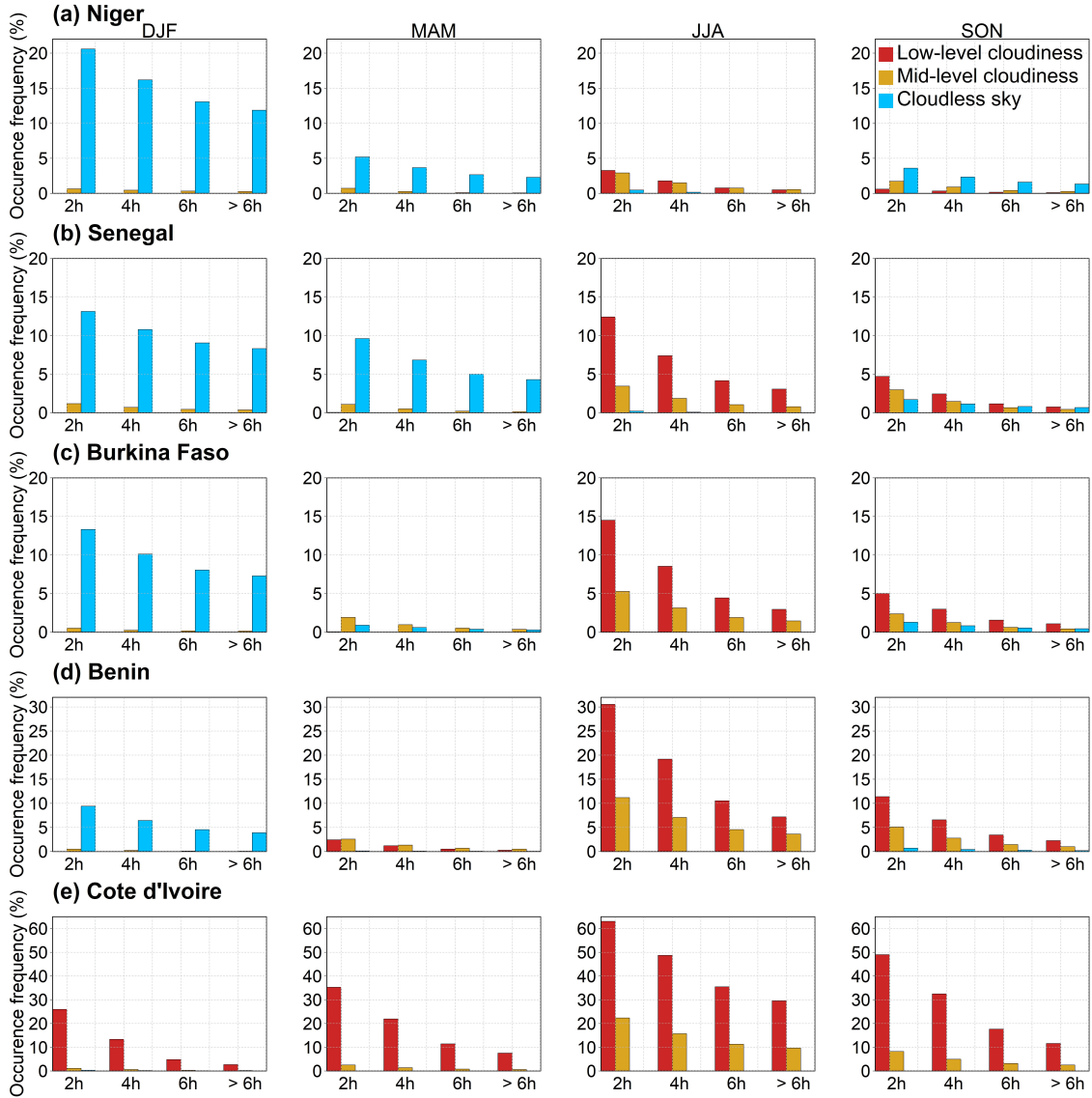


Figure 5.7: Seasonal mean occurrence frequency of low-level cloudiness (LLC), mid-level cloudiness (MLC), and cloudless sky conditions that persist for multiple hours in the selected windows across WA. Only LLC and MLC occurrences with at least 50 % coverage are considered. Note the differences in the range of the y-axis for the different regions.

In the three Sahel windows, occurrence of persistent LLCs and MLCs are usually limited to JJA and SON (not in Niger). They are most frequent in JJA, with a mean occurrence frequency for LLCs (MLCs) that occur for exactly two hours, around 12.5 % (4 %), 14.5 % (5.5 %), and 3.5 % (3 %) in Senegal, Burkina Faso, and Niger respectively. The occurrence frequency of LLCs that persist for more than six hours is about 3 % in JJA in both Senegal and Burkina Faso. Persistent cloudless

sky conditions, on the other hand, are spread across all seasons except in JJA. Their occurrence is high in DJF and MAM (not in Burkina Faso). In Cote d'Ivoire on the other hand, persistent LLCs are spread across all seasons (highest in JJA) while persistent MLCs occur mostly in JJA and SON. In Benin, the persistent LLCs and MLCs mostly occur in JJA and SON (and few occurrences in MAM). The occurrence of persistent cloudless sky conditions is rare in Cote d'Ivoire during all seasons while they occur only during DJF in Benin. The implication for the all-year-long spread of persistent LLCs and MLCs (in JJA and SON) in Cote d'Ivoire is that reduction in solar power generation can happen anytime during the year and can persist for longer durations. Emergency backup power sources are thus needed at all times. In the other windows, reduction in solar power generation are likely to occur for relatively short periods (i.e., mostly in JJA).

During overcast conditions, when the entire view of the sky is covered by one cloud type or a mix of cloud types, significant amounts of incoming solar radiation could be lost. The occurrence of persistent overcast conditions is very low over parts of the Sahel region and high over southern WA (not shown). Nevertheless, several hours of overcast weather does not necessarily imply significant losses of the incoming solar radiation. For instance, overcast conditions of only HLCs will not lead to significant losses of the incoming solar radiation due to the optically thin nature of such clouds and the associated low attenuation effects as shown by Bouniol et al. (2012). Overcast conditions of LLCs and/or MLCs however, could reduce a large portion of the incoming solar radiation available for solar power generation. The occurrence frequency of such overcast conditions is thus to be interpreted with caution.

For the overall management of the PV plant, it is also necessary to characterize the received surface solar radiation (as usable or non-usable) and the persistence associated with each category. Here, we divide the received surface solar radiation into three classes, namely: Low ($SW^\downarrow < 100W m^{-2}$), Moderate ($100W m^{-2} \leq SW^\downarrow \leq 500W m^{-2}$), and High ($SW^\downarrow > 500W m^{-2}$). It should be noted that the thresholds associated with the three categories are arbitrarily chosen. With a single PV panel, the category of *Low* SW^\downarrow will lead to a very low power production which may be considered non-usable while the other categories will lead to relatively higher productions. However, in a large solar farm with several hundreds of PV panels, the collective power output when the solar radiation class is *Low* can still be significant (provided SW^\downarrow is not zero). Figure 5.8 shows the seasonal occurrence frequency of persistent of *Low*, 'Moderate', and 'High' available surface solar radiation for the Niger, Benin and Cote d'Ivoire windows in the Sahel, Savannah and Guinean vegetation zones of WA respectively. The results for the Senegal and Burkina Faso

windows are not shown because they are similar to those obtained for Niger.

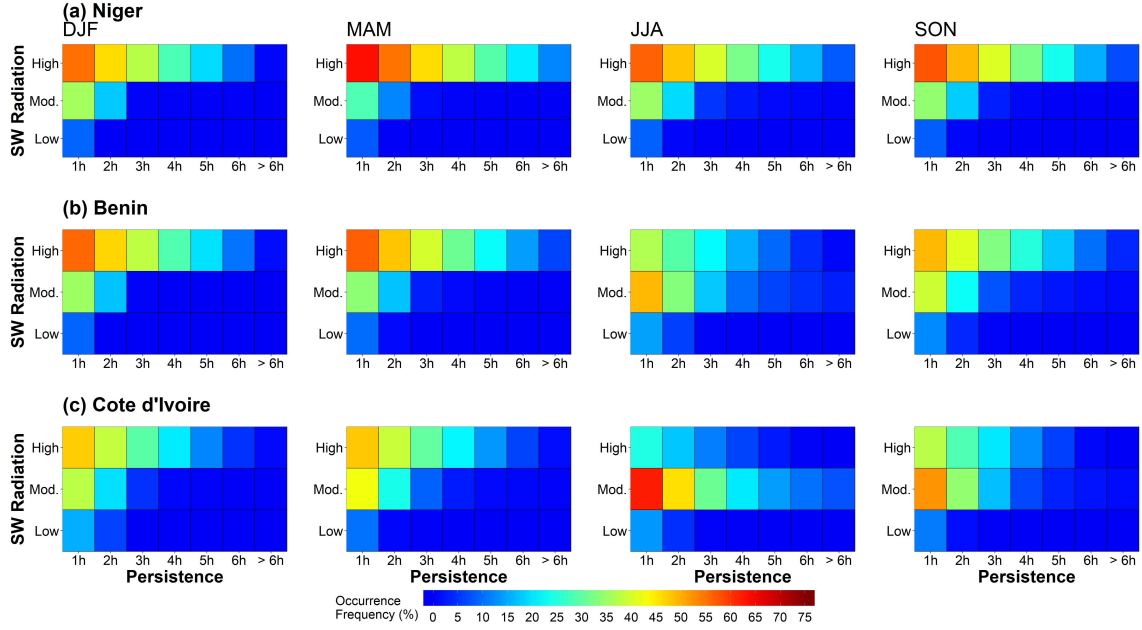


Figure 5.8: Seasonal mean occurrence frequency of Low ($SW^\downarrow < 100W m^{-2}$), Moderate ($100W m^{-2} \leq SW^\downarrow \leq 500W m^{-2}$), and High ($SW^\downarrow > 500W m^{-2}$), received surface irradiance that persist for multiple hours in the (a) Niger, (b) Benin and (c) Cote d'Ivoire windows for all seasons.

In all the windows, there are very few occurrences of persistent events of *Low* SW^\downarrow in all seasons. On the other hand, persistent *Moderate* and *High* SW^\downarrow events are more frequent in all seasons. Persistent *High* SW^\downarrow dominates in Niger and Benin in all seasons. For example, during JJA in Niger, the *High* SW^\downarrow can persist up to three consecutive hours for about 45 % of the time. Similarly, during DJF and MAM in Cote d'Ivoire, persistent *High* SW^\downarrow are more frequent. However, persistent *Moderate* SW^\downarrow events dominate during JJA in Cote d'Ivoire, which is likely a result of the intensification of cloud coverage over the area during this period. Therefore, solar power production during JJA in Cote d'Ivoire is expected to be moderate for prolonged periods. Power plants in this area will thus need to be oversized to compensate for the reduced productions. It is interesting to see that the frequency of persistent *Low* SW^\downarrow events in Cote d'Ivoire is very low in all seasons, regardless of the intense cloud coverage in the southern part of WA. Consequently, extremely low solar power production will not linger for long periods. This is also true for all the other areas considered in the study as shown in Figure 5.8.

Generally, the high frequency of persistent *High* SW^\downarrow events found in all windows (except JJA in Cote d'Ivoire) could be considered as favourable for solar energy development in the region. For solar power production, this result can be

interpreted in different ways depending on the type and size (capacity) of the PV plant. For small-scale off-grid PV power systems without battery storage, certain tasks that may require up to a given number of hours (e.g., 3 hours) of power supply (like water pumping in a household or office building) can be performed frequently during the season. Some of these tasks (e.g., water pumping) are not performed every day, and so it is necessary to schedule periods when they will be performed. This scheduling activity may require to also understand the spread of such persistent events of *High SW[↓]* during the season. This is however beyond the scope of this study but needs to be investigated. On the other hand, for large-scale PV power plants (off-grid or grid-connected), persistent *High SW[↓]* events may lead to excess power production, especially during off-peak hours. This excess electricity will be lost unless there is a storage facility (e.g., battery) to temporarily store the excess energy produced and released when needed.

5.6 Summary and Conclusions

In this paper, we used the state-of-the-art ERA5 reanalysis dataset to show the occurrence of cloud cover in WA and assess its impacts on surface solar radiation in the context of planned large-scale solar energy generation in the region. The goal was to contribute to answering some key relevant questions to provide useful information for stakeholders involved in the planning of large-scale solar energy projects in the region.

The results showed that the attenuation of incoming solar radiation by cloud cover is strongest in the summer months during the core of the monsoon season in all parts of WA. Analysis of the year-to-year variability of the surface solar radiation also revealed a higher uncertainty in the received solar radiation during the summer (wetter) months as compared to the drier months. The southern part of WA is characterized by a much stronger attenuation of incoming solar radiation due to intense cloudiness as well as a relatively higher uncertainty in the summertime surface solar radiation. This does not necessarily imply that southern WA is not suitable for siting solar power plants, however, as there is still enough solar radiation received over this region as shown in Figure 5.4b and in previous studies (e.g., Yushchenko et al. (2018)). It is however necessary to develop robust plans to successfully integrate solar energy in the power grid of countries across the region, such as identifying synergies with other renewable sources and developing reliable backup sources to increase the flexibility of power systems. Indeed, many countries across the world receive lower solar radiation but still have successfully running solar power plants (e.g., in Europe (Pfeifroth et al., 2018)).

We also showed that cloudy conditions can persist for several hours over southern WA, thus reducing the incoming solar radiation for a significant period. In contrast, cloudless weather conditions occur frequently in the northern part of WA. This result is to be interpreted with caution, however. Firstly, the 1-hour resolution of the ERA5 data could lead to uncertainty in the analysis of cloud persistence as clouds can vary at much shorter timescales (e.g., a few minutes). Again, even though there is a high occurrence frequency of persistent cloudless conditions in northern WA, this region is however associated with high amounts of dust particles which also have important attenuation effects on the incoming solar radiation. Also, high temperatures in northern WA may reduce the conversion efficiency of PV cells.

Due to the lack of surface observations in the region, reanalysis and satellite-derived products provide a viable alternative to assess solar energy feasibility in the future. It is important to note, however, that the reanalysis data used in this study has some biases over the study region as shown in Chapter 2 and in subsection 5.4.1, although it also presents satisfactory agreement with surface observations. Satellite products are also associated with some uncertainties. For example, as shown by Hill et al. (2016), large differences exist between different satellite products over the WA region. Again, passive geostationary satellites, which usually have a high temporal resolution, have difficulty in detecting low-lying clouds when there are overlying upper-level clouds, which in turn affects shortwave radiation estimates. Most active satellite sensors that are less prone to this issue also lack continuity which may lead to large uncertainties. Hence, an integrated assessment with different data products may help to mitigate such uncertainties in future studies.

This study provides important climate information with a regional overview for stakeholders involved in the planning of large-scale and long-term renewable energy projects in WA. It also provides a blueprint for carrying out future analysis, ideally with a higher resolution dataset, needed to address the feasibility of solar energy development in the region. An important extension of this work would be to consider the decadal fluctuations of solar irradiance which was not considered in this study since only ten years of data were used. This may be important to assess the long-term feasibility of solar energy projects in the region and needs to be investigated. Again, it could be useful to assess the combined effect of both clouds and dust on the incoming solar radiation as well as to distinguish between the spatiotemporal radiative effects of both parameters.

Chapter 6

The future of solar energy in West Africa: Impacts of climate change

6.1 Chapter overview

This chapter extends the study into the future period. Chapters 3, 4, and 5 have analyzed cloud occurrence and variability and related these to the solar resource and energy management in WA. These analyses have all been based on the historical period. However, global warming and the changing climate are likely to affect atmospheric parameters that influence the solar energy potential in the region. For instance, climate change may affect the occurrence of clouds and surface solar radiation. Also, rising temperatures could impact the efficiency of solar photovoltaic cells in converting solar irradiance to electricity. Other factors such as aerosols, which also influence surface radiation might also change in the future.

Thus, this chapter uses a suite of CMIP6 GCM ensembles to investigate the future evolution of potential solar power generation in the region. Additionally, this chapter will also investigate the changes in the atmospheric factors that drive the surface solar irradiance. The main novelty of this work deals with the use of the CMIP6 model projections, which have not been used before to study the impacts of climate change on the available solar resource in WA. Another novelty related to the work in this chapter is the investigation of the drivers of solar power in general as well as the surface irradiance in the region. Also, only a few studies in WA have tried to assess the impacts of climate change on the solar energy potential. Thus, this study is a very important addition to the regional portfolio.

The contents of this chapter will be submitted for publication.

6.1.1 Contributions

The study idea was formulated by myself and my supervisors: Sandrine Anquetin and Arona Diedhiou. I then extracted all the CMIP6 data used for the work. Afterward, I processed the downloaded data and used it for the next steps. I evaluated the model data with satellite observations, after which my supervisors and I had several discussions about the suitability of the model output for the work. We also received some vital inputs from Christophe Lavaysse and Benoit Hingray during this stage. After this, I carried out all the remaining software/numerical work, including the computations and visualization. I also drafted and edited the manuscript with the help of all co-authors. I presented part of this work to the HMCIS team at IGE.

6.2 Article: Potential climate change impacts on solar photovoltaic energy and its atmospheric drivers in West Africa

ABSTRACT: Many solar photovoltaic energy projects are currently being planned and/or developed in West Africa to help bridge the increasing gap between electricity demand and supply in the region sustainably. However, climate change is likely to affect solar power generation and the atmospheric factors that control it. In this study, four CMIP6 models were used to investigate the potential future evolution of solar power generation and the main atmospheric parameters that influence it in West Africa. The results showed a decrease in the solar power generation over the entire West Africa region, with most models projecting about -20% reduction around the southern part of the region in the second part of the 21st century. We found that the surface irradiance and air temperature will decrease and increase respectively, leading to the projected changes in solar power. However, the decrease of the surface irradiance was found to be the main reason for the reduction of solar power generation. Temperature-induced changes in solar power generation will be small. Further investigations revealed that cloud liquid water path and aerosol optical depth will generally increase in the future to reduce the surface irradiance and hence the solar power generation. Although there are uncertainties due to differences in the magnitude of change in individual models, the projected decrease in solar power generation could prove critical in the future if robust long-term management strategies are not present.

Authors: Derrick Kwadwo Danso, Sandrine Anquetin, Arona Diedhiou, Christophe Lavaysse, Benoit Hingray, Damien Raynaud, Arsène Koba

6.3 Introduction

In West Africa (WA), the conversion of solar irradiance into electricity with solar photovoltaic (PV) panels is gradually increasing in many countries. To help reduce the energy deficit due to increasing populations and electricity demand in the region (Eshun & Amoako-Tuffour, 2016; Ouedraogo, 2017), solar electricity generation is further projected to increase significantly in the coming years (DeGhetto et al., 2016). The interest in solar electricity generation became apparent after the signing of the Paris Agreement during which many WA countries committed to develop and utilize solar energy in the region to minimize greenhouse gas emissions. Although expected to increase, the present contribution of solar PV power (PVP) to total electricity generation is less than 1% in all of sub-Saharan Africa (IEA, 2019a). Nevertheless, there are plans to construct large solar farms in many countries across the region (Kuwonu, 2016; Moner-Girona et al., 2017).

Understanding relevant climate factors is important for making optimal decisions in the development of large solar farms. While the solar resource is abundant in WA (Hermann et al., 2014), climate factors may reduce it or affect its conversion to energy (Dajuma et al., 2016; Danso et al., 2020a). Factors such as intense cloudiness, higher temperatures, and dust which negatively affect solar PVP generation are all abundant in WA (Danso et al., 2019; Gbobaniyi et al., 2014; Knippertz & Todd, 2012). Some recent studies have investigated the current potential (e.g., Yushchenko et al. (2018)) of solar PVP as well as the direct impacts of atmospheric conditions on the solar resource over historical periods in the region (e.g., Bonkaney et al. (2017), Bouniol et al. (2012), Danso et al. (2020b), and Hill et al. (2018)). However, climate change is likely to affect the atmospheric conditions that influence solar PVP. It is then also necessary to investigate the long-term evolution and changes in potential solar PVP and the climate factors that influence it.

Presently in WA and even across the entire African continent, only a few studies have attempted to address the issue of climate change impacts on solar energy potential (Bichet et al., 2019; Sawadogo et al., 2020; Soares et al., 2019). These studies estimated a decrease in the future solar PVP potential in WA. These past studies are all based on climate model projections obtained for some Representative Concentration Pathway (RCP) scenarios. However, climate model projections are evolving with the inclusion of updated and more inclusive future emission and land use scenarios (Meinshausen et al., 2020; Riahi et al., 2017). Therefore, it is important to assess the future evolution of solar PVP and the factors that affect it using some of the updated climate projections. In the Coupled Model Intercomparison Project Phase 6 (CMIP6) (Eyring et al., 2016), future projections by the Scenario Model

Intercomparison Project (ScenarioMIP) (O'Neill et al., 2016) are based on human and societal development possibilities incorporated into the RCPs. The new set of human and societal development possibilities known as the Shared Socioeconomic Pathways (SSPs) (O'Neill et al., 2014) are based on updated data on recent emission trends. Together with updated versions of climate models, the SSPs make up the major difference between the CMIP6 and previous versions of climate models used to study the future evolution of solar energy in WA.

In addition, most of the previous studies only focused on estimating the expected changes in the solar PVP potential. For example, solar PVP potential in WA is projected to decrease by about 4% in an extreme warming scenario (Sawadogo et al., 2020). Bichet et al. (2019) estimated a similar amount of reduction in the solar PVP potential over the region. However, the origins of the projected changes are not investigated. Moreover, most of the future assessments in WA were based on single 30-year future periods. It is necessary to assess the evolution of future solar PVP generation based on a continuous and relatively longer period so that policymakers can make plans to facilitate the short-term integration and the long-term sustainability of solar PVP generation in the region.

In the context presented above, the goal of this study is to assess the changes in potential solar PVP in WA based on an updated and more inclusive scenario of the CMIP6 global climate models (GCMs). The assessment will be carried out for the very near-future period as well as for a much distant future period. Also, this study will investigate changes in some of the main climate factors (irradiance, temperature, cloud cover etc.) that may influence the projected changes in PVP over WA.

A description of the study area, data, and methodology is presented in section 6.4. Section 3 will present the different GCM projections of solar PVP changes in WA. Section 4 will present the climate conditions responsible for the solar PVP changes. A discussion and conclusions of the results will be given in Section 5.

6.4 Data and methodology

6.4.1 Study area

This study will be performed over the whole of WA; however, we will emphasize some results over specific areas in the region (rectangular windows in Figure 4.1). These areas are located in the Guinea (also called Guinea Coast) and Sahel climate zones of WA; two areas with distinct climate conditions in the WA region (Gbobaniyi

et al., 2014). Besides, the two windows are chosen because they contain numerous solar PV energy projects in WA. These include the largest operational solar power plant currently in the region (Moner-Girona et al., 2017) as well as an uncompleted 155 MW capacity plant that will be the largest solar PV plant on the whole of the African continent when completed (Kuwonu, 2016).

The WA region which is currently developing at an unprecedented pace is also experiencing an increase in the demand for electricity due to economic and population growth. Many countries in the region have planned to develop large solar farms to help reduce the energy gaps. While the current contribution of solar PVP to total electricity generation is significantly lower than 1%, many working scenarios, including the African Agenda 2063 (DeGhetto et al., 2016) project a significant increase in its share by the middle of the 21st century (IEA, 2019a). Nevertheless, the overall capacity of fossil-based electricity generation is also projected to significantly increase to satisfy the expected huge growth in electricity demand.

6.4.2 Data

In this study, we will use some CMIP6 GCM ensembles to assess the impact of climate change on potential solar PVP generation and the climate conditions that influence it in WA. To do this, we will compare the historical solar PVP potential with the projected future potential for the new SSP5-8.5 scenario. This scenario is an update of the RCP8.5 in CMIP5, which have been used in many climate impacts studies over WA Africa in the last decade (e.g., Ajayi and Ilori (2020), Akinsanola and Zhou (2019), Guan et al. (2017), Klutse et al. (2018), and Sarr (2017)). It envisions significant societal development with high radiative forcing.

Four CMIP6 GCM ensembles are selected for this work (Table 6.1). These models are chosen primarily due to the availability of the used parameters for both the historical and SSP5-8.5 experiments and at the same spatial and temporal resolutions. All the selected GCMs have a nominal resolution of 100 km and at a 3-hourly temporal resolution. The main variables considered in this study are the global horizontal irradiance (GHI), also known as the surface downwelling short-wave radiation (in W m^{-2}), and the near-surface air temperature (in $^{\circ}\text{C}$). We will, however, analyze some cloud and aerosol properties as well.

Table 6.1: Ensemble sizes for all models for the historical and SSP5-8.5 experiments

Model	Ensemble Size	
	<i>Historical</i>	<i>SSP5-8.5</i>
AWI-CM-1-1-MR	5	1
EC-Earth3	8	8
MPI-ESM1-2-HR	10	2
MRI-ESM2-0	5	1

6.4.3 Estimation of changes in potential solar PVP generation

Since the focus of the study is on changes in solar PVP we based our computations on only periods when solar radiation is available. As a result, we eliminated all nighttime hours from the GCM ensemble datasets and made all computations based on only the daytime hours. In addition to the historical estimations, two future periods are defined; the near-future from 2015 to 2049 and the far-future from 2050 to 2084.

There are many models for estimating solar PVP generation, ranging from simple models that take a few climate parameters as inputs (e.g., Perpiñan et al. (2007)) to more complex models that take more than a few parameters (e.g., Jerez et al. (2015) and Mertens (2018)). In this study, we implemented a model that estimates the solar PVP generation using the effective surface irradiance received by solar panels at an optimal tilt angle I_s (W m^{-2}) and near-surface air temperature T_a ($^{\circ}\text{C}$) (Danso et al., 2021; François et al., 2016). We have computed I_s using the CMIP6 models' GHI and following the method described by McPherson et al. (2017). At a given time t in a grid box i , solar PVP is given as:

$$PPV(i, t) = BI_s(i, t) (1 - \mu(T_a(i, t) - T_{c,STC}) - \mu CI_s(i, t)) \quad (6.1)$$

where B is an efficiency coefficient defined as the product of the surface area (m^2) of the solar PV array and the efficiencies of the solar PV generator and inverter. μ and C are the temperature and radiation dependent efficiency reduction factors respectively. These two are specific to a given PV technology and ensure that PV cell efficiency changes due to temperature and irradiance are accounted for. $T_{c,STC}$ ($^{\circ}\text{C}$) is the PV cell temperature corresponding to standard test conditions.

The estimated solar PVP time series is then normalized so that the mean is equal to 1. Relative to the historical period, the change in potential future solar

PVP generation ΔPVP is estimated as:

$$\Delta PPV = \frac{PVP_{fut} - PVP_{hist}}{PVP_{hist}} \times 100\% \quad (6.2)$$

where, PPV_{hist} and PPV_{fut} are the historical and future solar PVP generations respectively.

The individual contributions of I_s and T_a to the future changes in PVP are also estimated. This is achieved simply by computing the future PVP generation again but by keeping either of I_s and T_a fixed to the historical period (i.e., using its historical time series) while the future time series of the other variable is used:

$$\Delta PPV_{\Delta I_s} = \frac{PVP_{\Delta I_s} - PVP_{hist}}{PVP_{hist}} \times 100\% \quad (6.3)$$

$$\Delta PPV_{\Delta T_a} = \frac{PVP_{\Delta T_a} - PVP_{hist}}{PVP_{hist}} \times 100\% \quad (6.4)$$

where $\Delta PPV_{\Delta I_s}$ and $\Delta PPV_{\Delta T_a}$ are the first order future changes in PVP generation due to changes in irradiance and air temperature respectively and are estimated as:

$$PPV_{\Delta I_s}(i, t) = BI_{s,FUT}(i, t) (1 - \mu(T_{a,HIST}(i, t) - T_{c,STC}) - \mu CI_{s,FUT}(i, t)) \quad (6.5)$$

$$PPV_{\Delta T_a}(i, t) = BI_{s,HIST}(i, t) (1 - \mu(T_{a,FUT}(i, t) - T_{c,STC}) - \mu CI_{s,HIST}(i, t)) \quad (6.6)$$

where $I_{s,HIST}$ and $I_{s,FUT}$ are the historical and future irradiance time series respectively and $T_{a,HIST}$ and $T_{a,FUT}$ are the historical and future air temperature time series respectively.

6.5 Changes in future solar PVP generation

Over the 21st century, solar PVP generation will decrease over the entire WA in the SSP5-8.5 scenario. Figure 6.1 presents the annual mean difference (%) in solar PVP generation averaged for the two future periods relative to the historical period for all four models. In the near-future (Figure 6.1a), all models agree on the spatial distribution of the expected change in solar PVP over WA. Solar PVP will decrease

up to -7% in the region, with southern WA experiencing a larger decrease than the northern part. This is true for all models; however, the MRI-ESM2-0 (hereafter MRI-ESM) presents a slightly smaller decrease in solar PVP for the near future period.

Similarly, all the four models generally agree on the spatial distribution of solar PVP change in the second half of the 21st century (Figure 6.1b). All models (except MRI-ESM) show a clear south-north gradient, with southern WA experiencing a larger decrease of solar PVP in the far-future. Over the land area in WA, solar PVP can decrease to around -20% in some places around the Guinea Coast. The magnitude of change presented by MRI-ESM is, however, significantly smaller than the other models. For example, the largest decrease over the entire WA land area is around -7% near the Guinea Coast. Possible reasons for this large difference in the magnitude of the change between MRI-ESM and the other models will be discussed in section 6.6. Also, MRI-ESM shows a slight increase (1% to 3%) in solar PVP generation around Central Africa (lower right edge of plot area). This feature, although outside of the study area, is absent in all the other models. Overall, the decreasing future solar PVP generation is in agreement with the previous RCP-based studies in Africa (Bichet et al., 2019; Sawadogo et al., 2020; Soares et al., 2019); however, our results present larger future decreases which could be explained by the updated scenarios used in the CMIP6.

A closer look at the changes in annual PVP evolution in the Guinea and Sahel windows reveals a distinct seasonal change pattern. Figure 6.2 presents the mean annual evolution of the future solar PVP change (solid curves) and the 90% confidence interval (denoted by the 95th and 5th percentile range, shaded region) for the GCM ensembles in the Guinea and Sahel windows. In the near-future (Figure 6.2a), all models appear to agree on the seasonal evolution of the solar PVP change in both regions (except for a slight deviation in the curve for the MRI-ESM from June to August). In both regions, the largest mean solar PVP change occurs during the summer months in the core of the monsoon season (June to October). During this period, the mean change in solar PVP can reach around -16% for all models in Guinea (except MRI-ESM) and -19% for EC-Earth3 (hereafter EC-Earth) and AWI-CM-1-1-MR (hereafter AWI-CM) in the Sahel region. It is important to note that the annual cycle of future PVP change does not always have negative values. In Guinea, for instance, the AWI-CM and MPI-ESM1-2-HR (hereafter MPI-ESM) projects a slight increase in solar PVP in April and May (up to 8% for AWI-CM). The 90% confidence interval for all models suggests some interannual variability which is larger in the Guinea region especially during the summer months. Although the confidence interval is also predominantly negative values, some positive

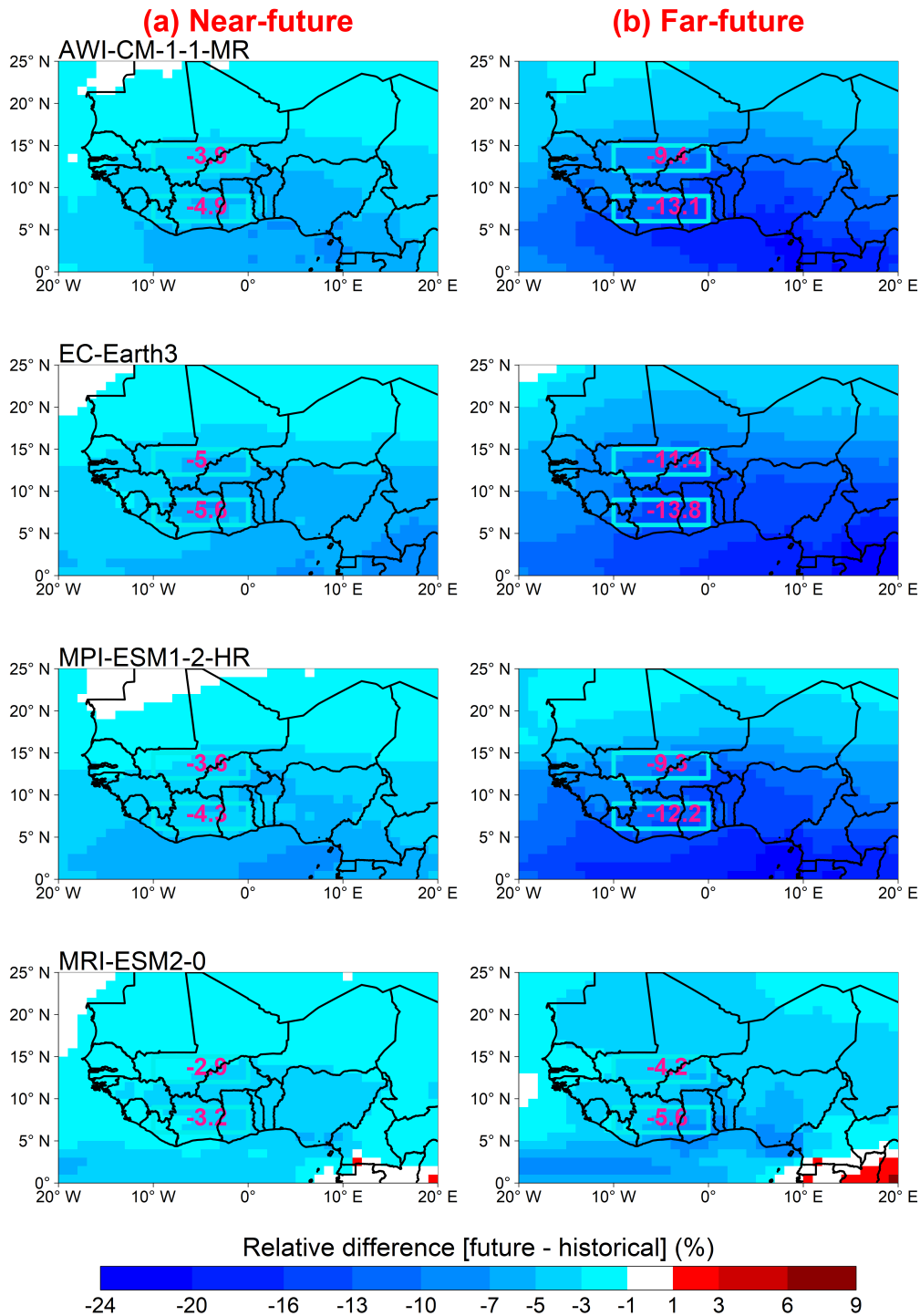


Figure 6.1: Annual mean change (%) of potential solar photovoltaic power generation for the (a) near-future (2015 – 2049) and (b) far-future (2050 – 2084) relative to the historical period (1980 – 2014) for four CMIP6 models under the SSP5-8.5. The ensemble mean of each model is used for the computation. The values written in pink colour are the mean changes for the Guinea and Sahel windows.

values suggest an increase in PVP at some points in the annual cycle for some years.

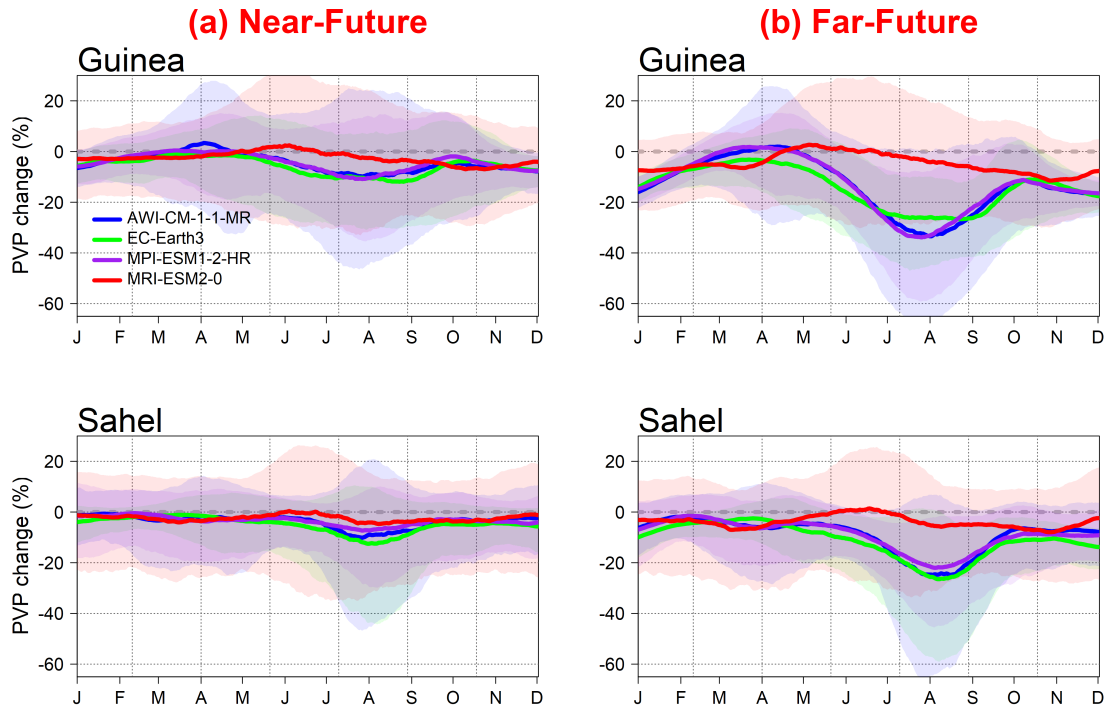


Figure 6.2: Relative changes in the mean annual cycle of solar photovoltaic power generation (solid curves) in the Guinea and Sahel regions of West Africa. The shaded areas represent the interannual 95th and 5th percentile range.

The near-future solar PVP change is further amplified in the second part of the 21st century (Figure 6.2b). During the far-future period, the mean annual cycle of solar PVP generation change is predominantly negative throughout the year, with higher decreases during the summer months in both regions. In Guinea, the summertime decrease of mean solar PVP reaches about -40% for AWI-CM and MPI-ESM and -30% for EC-Earth. The MRI-ESM, however, shows significantly smaller decreases in the future solar PVP (between -10% and 0%) and slight increases in some cases. This is also true for the Sahel region where the three other models agree on both the sign and magnitude of solar PVP change throughout the year. It is important to note that the 90% confidence interval during the summertime is almost entirely negative values for all models (and can reach about -60%) except MRI-ESM.

Regardless of the large difference between the MRI-ESM and the other models especially during the summer months of the far-future period, all the four GCMs project significant downward trends in the solar PVP generation in both the guinea and Sahel regions (Figure 6.3). This suggests that all models project solar PVP generation to decrease in the future. AWI-CM, EC-Earth, and MPI-ESM, however,

presents relatively steeper decreasing trends than MRI-ESM. In addition, the downward trend in the Guinea window is slightly steeper than in the Sahel region for all models.

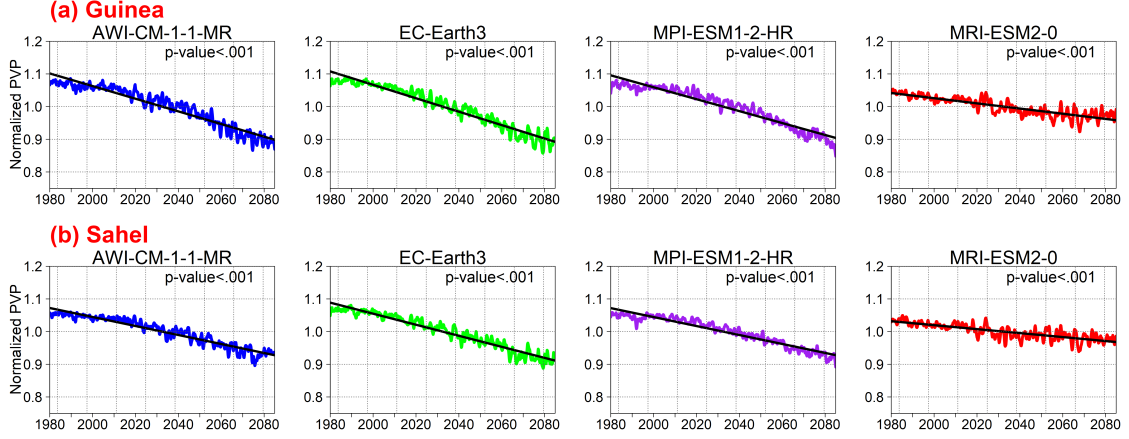


Figure 6.3: Time evolution (historical and future) and trend lines (black lines) of mean annual solar photovoltaic power generation potential in the Guinea and Sahel regions of West Africa.

6.6 Drivers of projected changes in solar PVP

The projected change in future solar PVP is driven by changes in the underlying physical parameters that determine the generation. Here, we first explore the direct impacts of the changes in incoming solar irradiance and air temperature on potential future solar PVP generation under the SSP5-8.5. Changes in other atmospheric parameters such as wind speed and humidity may also affect solar PVP but their impacts in WA are very small as shown by Bichet et al. (2019) and Sawadogo et al. (2020) hence, only the surface irradiance and temperature are considered in this study. We then explore the impact of changes in cloudiness and aerosols on changes in PVP.

6.6.1 Surface irradiance and near-surface air temperature

Figure 6.4 shows the direct changes in future solar PVP induced by changes in the surface irradiance and air temperature over the entire WA for the near-future period. In all four climate models, projected changes in the surface irradiance will induce a higher change in future solar PVP generation (Figure 6.4a). The mean annual change of solar PVP induced by the surface irradiance ranges from about -6% in southern WA to -1% in parts of northern WA. On the contrary, the change in solar PVP induced by changes in the air temperature is small (Figure 6.4b). The future

solar PVP change is just about -0.2% around the Guinea Coast and about -0.7% in the northern part of WA across all models.

Similarly, the far-future change in the solar PVP generation is more due to changes in the surface irradiance rather than the air temperature (Figure 6.5). Irradiance-induced solar PVP change reaches about -18% around the Guinea Coast for AWI-CM, EC-Earth, and MPI-ESM, while it is smaller for MRI-ESM (Figure 6.5a). This difference in the magnitude of change is consistent with the overall future solar PVP change (Figure 6.1 and Figure 6.2). On the other hand, the largest temperature-induced solar PVP change is about -2% and occurs in the north of WA for all models (Figure 6.5b). In all cases, the magnitude of the change induced is greater in the far-future than in the near-future.

While the temperature-induced future change in solar PVP is small, it does not necessarily imply that the future temperature change will not be significant, especially for the far-future. Indeed, all four models project the near-surface air temperature to increase over the entire WA in both future periods (see Figure C.1 in Appendix C). In both cases, the northern part of the region will experience a higher increase than the south. In the far-future, the air temperature is expected to increase upwards of 4°C in large parts of WA under the SSP5-8.5. However, the increase in air temperature will not induce a very pronounced change in the solar PVP generation. Rather, reductions in the future surface solar irradiance (see Figure C.2 in Appendix C) will be the predominant cause of the projected changes in future solar PVP generation. The decrease in the future surface irradiance for all the models is coherent with the estimated change in solar PVP generation (Figure 6.1 and Figure 6.2), with a much lesser decrease for the MRI-ESM than the other models (Figure C.2 in Appendix C).

6.6.2 Cloudiness and aerosols

As already discussed, the projected future change of solar PVP across WA will be largely due to changes in the surface solar irradiance. The irradiance received on the surface depends on the variability of atmospheric reflectivity and/or absorptivity due to cloud cover (Bouniol et al., 2012; Danso et al., 2020b; Hill et al., 2018) and suspended aerosol particles (Papadimas et al., 2012; Qian et al., 2007) in the atmosphere. Changes in the cloud and aerosol properties will thus modify the surface irradiance in the future. Therefore, to explain the large decreases in the future solar PVP due to the decrease in surface irradiance, it is important to understand the future evolution of some cloud and aerosol properties. It could also help to explain the large differences of the projected future changes in solar irradiance and PVP

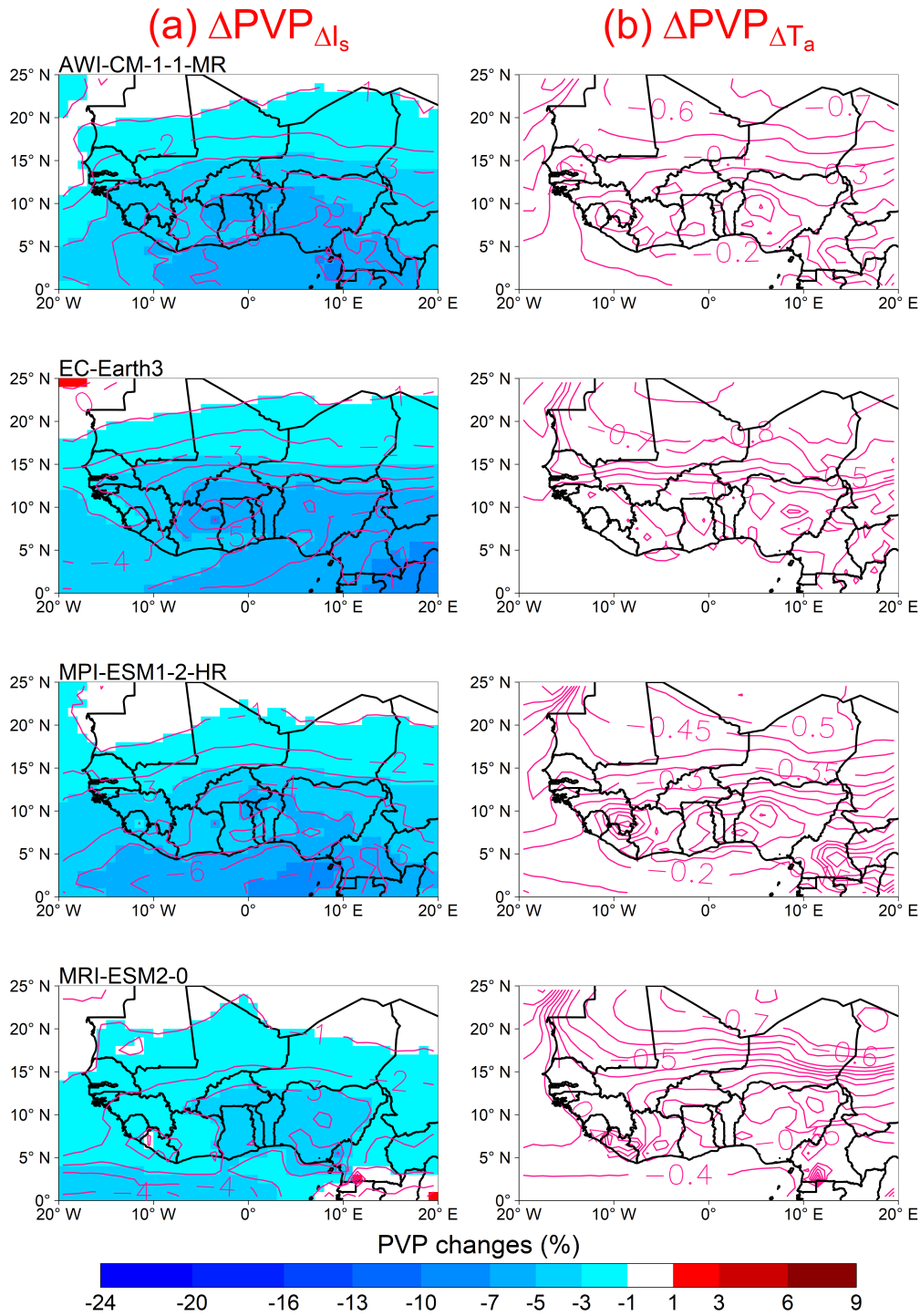


Figure 6.4: The annual mean change (%) of potential solar photovoltaic power generation induced by projected changes in the (a) surface irradiance and (b) near-surface air temperature for the near-future period (2015 – 2049) relative to the historical period (1980 – 2014) for four CMIP6 models under the SSP5-8.5. Contours are also mean annual change values. The ensemble mean of each model is used for the computation.

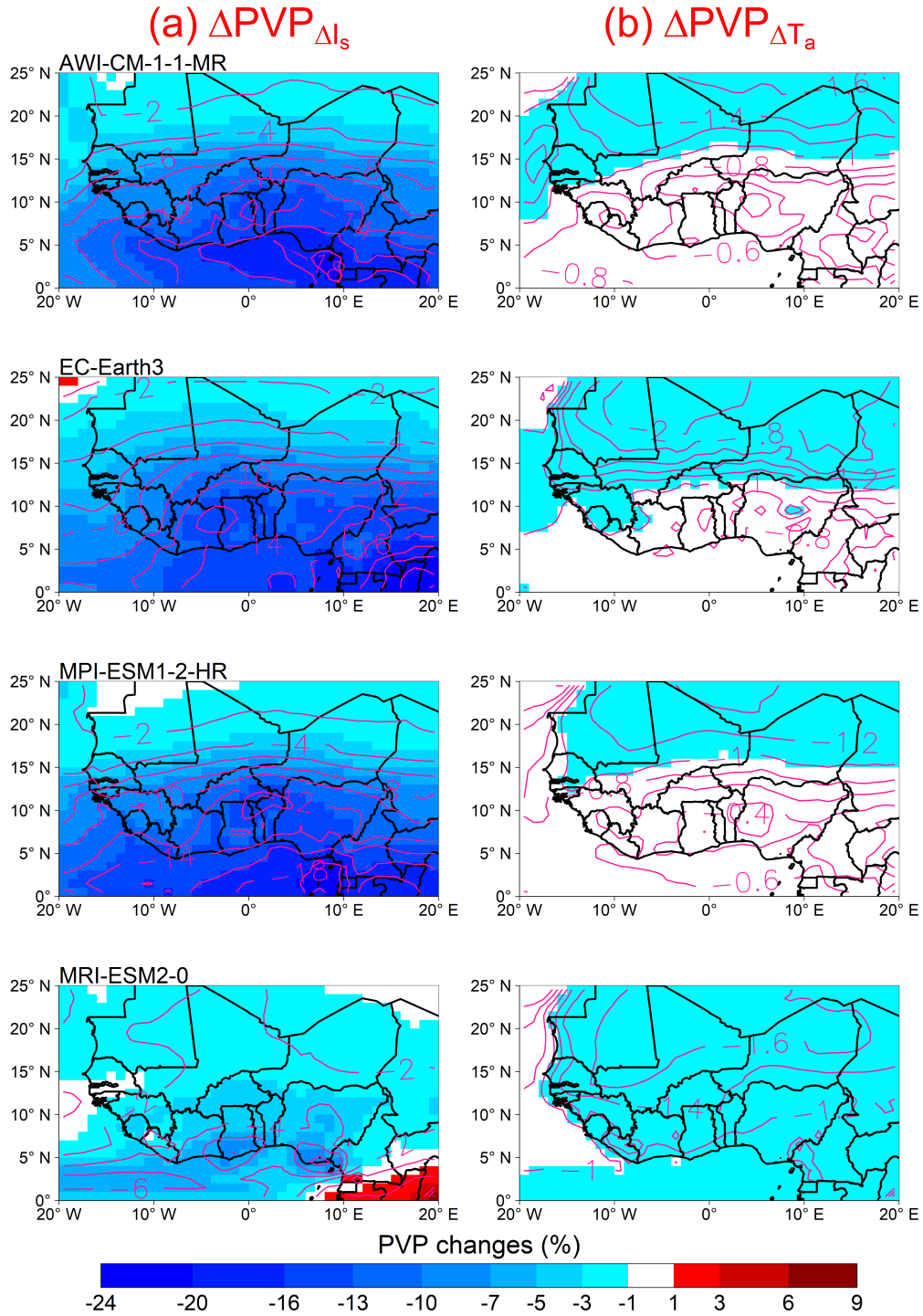


Figure 6.5: Same as Figure 6.4 but for the far-future period (2050 – 2084).

between the MRI-ESM and the other models.

The cloud liquid water path (simply the cloud water path [CWP]) is directly related to the optical depth of clouds that determines the amount of sunlight reflected by clouds (Liou, 2002). Thus, a larger CWP will lead to more reflection of incoming shortwave radiation (Sengupta et al., 2003) and lower PVP. Similarly, the

aerosol load in the atmosphere influences the incident surface shortwave radiation. In general, aerosols directly absorb and/or scatter part of the incoming radiation (Kosmopoulos et al., 2017; Nair et al., 2017; Yamasoe et al., 2017; Zhang et al., 2018). Furthermore, aerosols can impact the cloud microphysics to influence the radiative properties of the clouds in the region through the Twomey effect (Jose et al., 2020; Ramachandran, 2018) (i.e., the aerosol indirect effect).

Figure 6.6 presents the projected annual mean difference of the CWP between the two future periods and the historical period. For all models (except MRI-ESM), CWP increases over large portions of WA. As already discussed above, this is expected to increase the cloud albedo in the region, and thus, can partly explain the decrease of surface irradiance. However, this is not the case for the MRI-ESM in the far-future. In this model, both the CWP and irradiance (Figure C.2) decrease over large areas of WA. Nevertheless, the CWP decrease cannot explain the reduction of surface irradiance and PVP. This is because a decrease in CWP should rather reduce the optical depth (and albedo) of clouds, assuming all other factors remain constant (Sengupta et al., 2003). This inconsistency suggests that changes in other physical properties such as the water vapour content or the aerosol load are likely responsible for the decrease of irradiance in the MRI-ESM. For example, all the four models project an increase in the water vapour path in the near- and far-future periods (Figure C.3 in Appendix C). Water vapour can absorb part of the incoming shortwave radiation (Di Biagio et al., 2012; Kampouris et al., 2017; Obregón et al., 2015; Radel et al., 2015).

A look at the aerosol optical depth (AOD) at 550 nm presents an interesting insight on a possible reason for the reduction of PVP potential in MRI-ESM as well as the huge difference in the magnitude of reduction relative to the other models (Figure 6.7). Here we compare the future changes in AOD for MPI-ESM and MRI-ESM only (this parameter was not found for AWI-CM and EC-Earth at the time of data extraction). It should be noted that only the MRI-ESM has a dynamically interactive aerosol model coupled to its other components (Tanaka et al., 2003; Yukimoto et al., 2019). The aerosol forcings of the other models are based on some existing climatology (Giorgetta et al., 2013; Kinne et al., 2013; Tegen et al., 1997). Moreover, MPI-ESM and AWI-CM are basically the same model but with different oceanic and sea-ice components (Semmler et al., 2020). Thus, the aerosol load in MPI-ESM can be assumed to be similar to the other models (at least for AWI-CM), and a comparison between MPI-ESM and MRI-ESM is assumed to be reasonably representative.

In the near-future, the difference in AOD for MPI-ESM is mostly positive

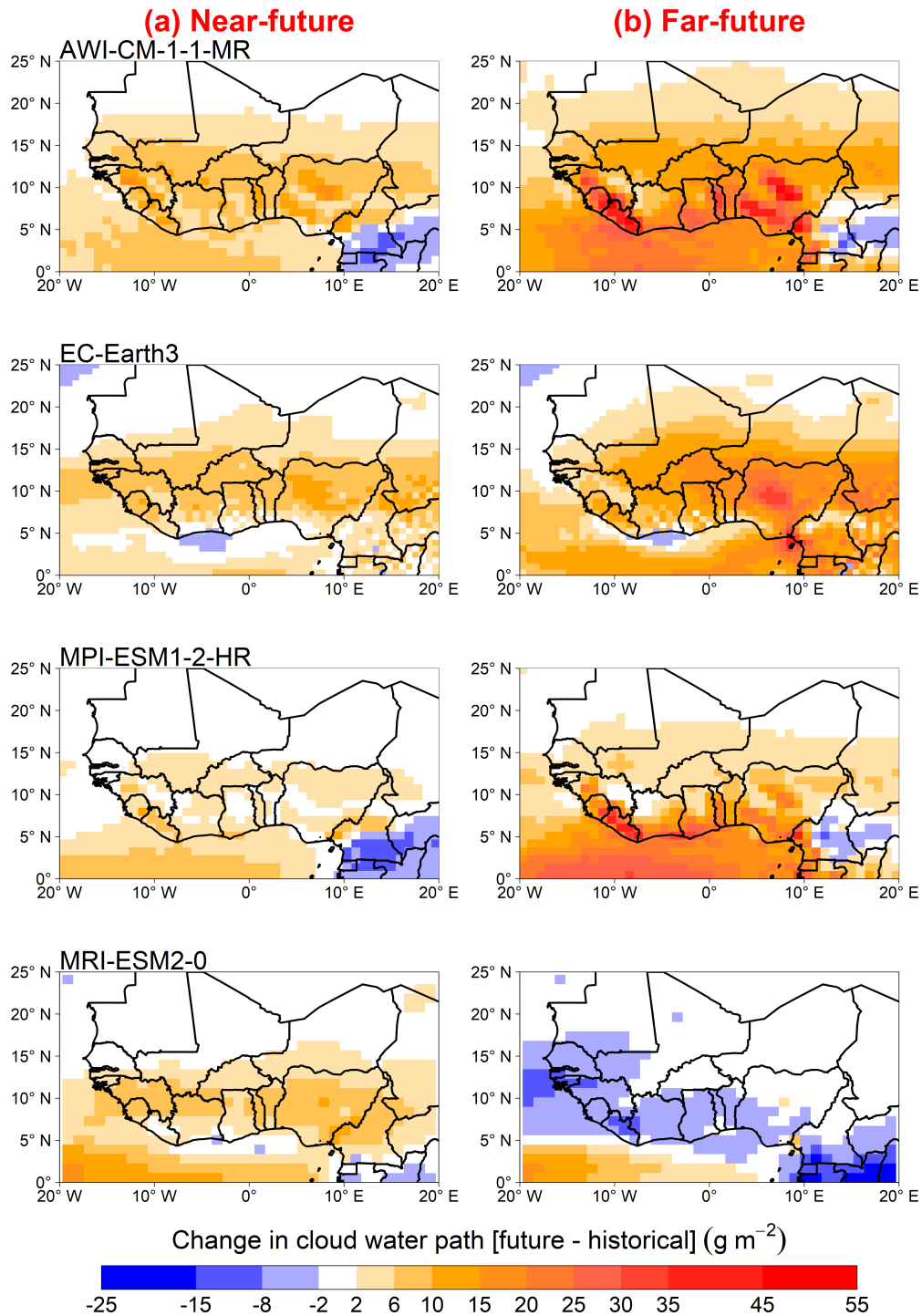


Figure 6.6: Annual mean difference (future minus historical) of cloud liquid water path for the (a) near-future (2015 – 2049) and (b) far-future (2050 – 2084) for four CMIP6 models under the SSP5-8.5.

over the region. On the other hand, MRI-ESM presents only slightly positive values around some parts of the Gulf of Guinea and negative values at the north-eastern part of WA. Likewise, in the far-future, AOD difference is positive over most of WA

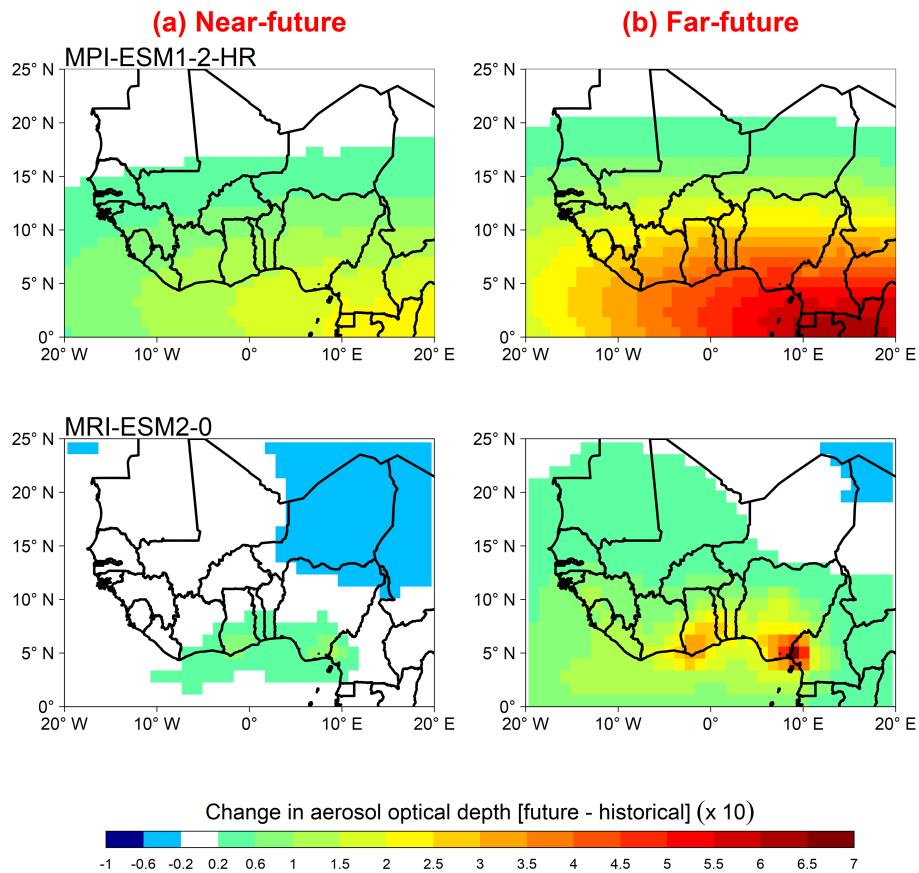


Figure 6.7: Annual mean difference (future minus historical) of aerosol optical depth at 550 nm for the (a) near-future (2015 – 2049) and (b) far-future (2050 – 2084) for the MPI-ESM (climatological aerosol forcing) and MRI-ESM (dynamic aerosol forcing) under the SSP5-8.5.

for both models. The increase in the AOD also partly explains the reduction of surface irradiance and PVP in the models' projections. Interestingly, the increase in AOD for both future periods is lower in the MRI-ESM than MPI-ESM suggesting a future with a much higher aerosol load in the latter. Thus, both the direct and indirect effects of aerosols will be greater in MPI-ESM (and the other models) than in the MRI-ESM. The higher aerosol load in the MPI-ESM will not only increase the absorption of incoming radiation but also the formation of smaller cloud water droplets that have a higher albedo than clouds formed in a much cleaner atmosphere like in the MRI-ESM. Both of these effects lead to a reduction surface irradiance and solar PVP. Thus, the higher future aerosol load in the MPI-ESM than in MRI-ESM could explain why the decrease in surface irradiance and solar PVP is smaller in the latter.

With the increase in AOD seemingly stronger from the Central Africa region (southwestern edge of the map) and gradually decreasing toward the west for the

MPI-ESM, one can assume that this is a result of increasing biomass burning aerosols in the future. Indeed, Fiedler et al. (2019) found steep increases in the AOD in most of Africa’s biomass burning regions, especially in Central Africa, across most of the CMIP6 future scenarios. In addition, these remote biomass burning aerosols have in the past dominated parts of southern WA as shown by the Dynamics–Aerosol–Chemistry–Cloud Interactions in West Africa (DACCIWA) field campaign in 2016 (Haslett et al., 2019). These biomass and fossil fuel burning aerosols have also been shown in previous studies to be more effective at reducing the incoming shortwave radiation than other aerosols such as dust particles (e.g., Gu et al. (2006) and Ramachandran (2018)). Over the Sahara and parts of the Sahel regions, the difference in AOD does not appear to be very significant for both models suggesting small changes between the historical and future Saharan dust emissions. Moreover, Evan et al. (2016) used CMIP5 multimodel mean projections under the RCP 8.5 to show that dust emissions from the Sahara across the region and over the North Atlantic will only decrease slightly in the 21st century.

The reasons for the large difference in AOD increase between the models is not clear at this moment. Nevertheless, one can assume that this difference could be related to the inclusion of a dynamically interactive aerosol model in the MRI-ESM and the climatology-based aerosol forcing in the other models. Some previous studies (e.g., Palacios-Peña et al. (2020), Rotstayn et al. (2010), and Zhang et al. (2012)) have suggested the inclusion of a dynamically interactive aerosol model in climate simulations improves the overall ability of models to reproduce aerosol-cloud-radiation interactions. Nevertheless, considering the large uncertainties in aerosol emissions and their associated radiative effects by current climate models (e.g., Brown et al. (2021), Bukowski and Heever (2020), Liu et al. (2007), and Pantillon et al. (2016)), this issue remains an open discussion. However, this is beyond the scope of the present study and should be considered in future research work.

6.7 Discussion and conclusion

Under the SSP5-8.5 scenario, this study finds that the potential of future solar PVP generation in WA will decrease across all four CMIP6 GCM ensembles in the 21st century. This result is in agreement with previous (Bichet et al., 2019; Sawadogo et al., 2020) however, our study reveals that the decrease in the future solar PVP generation will be much greater than in the previous studies. This is true even for the MRI-ESM model, which projects a much lesser decrease in mean solar PVP generation than the other models used in this study. In AWI-CM, EC-Earth,

and MPI-ESM, the mean annual change in solar PVP generation is expected to reach about -20% in some parts of southern WA during the second part of the 21st century while it will reach around -7% in the MRI-ESM. It should be noted that the previous studies in the region are based on regional climate models (RCMs). Bichet et al (2019) found that RCM uncertainty accounted for the highest contribution to total uncertainty of projections in the region. This could partly explain the large difference between our results based on the CMIP6 GCMs and the previous results. Thus, a similar analysis with RCMs based on the new CMIP6 forcings and scenarios is needed to improve the understanding of future PVP projections.

A further look at the Guinea and Sahel areas of WA revealed a significant downward trend for solar PVP generation across all four models. The results then showed that the decrease in solar PVP generation will be extreme during the summer period in both the Guinea and Sahel areas. We also showed that the reduction of solar PVP generation will be small in the near-future. Therefore, high capacities of solar energy can be easily integrated into the power system with the help of current infrastructure in the region, such as hydropower reservoirs (Danso et al., 2021; Jurasz et al., 2020). However, the results revealed significant decreases in solar PVP in the distant future. This result calls for developing robust management plans to ensure that the future electricity demand in the region can be satisfied sustainably.

Our analysis revealed that even though the near-surface air temperature will rise in the future (by more than 4°C in the far-future), its effect on solar PVP generation will be small. On the other hand, changes in the surface irradiance will induce a strong reduction in the future solar PVP generation across all four model ensembles. The incoming shortwave radiation is expected to decrease significantly in the future. We linked the projected reduction to some factors.

Firstly, the water content of clouds is expected to increase over WA in the future. The increasing water content in clouds will, in turn, increase the albedo of clouds leading to a greater reduction of the surface irradiance. Although all four models projected CWP to increase in the near-future period, the MRI-ESM projected a decrease in the far-future in contrast to the others. Secondly, the AOD is projected to increase in the future but the increase is higher in MPI-ESM than in MRI-ESM. Since a higher AOD causes more reduction in the surface irradiance, this could explain why the MRI-ESM projects a lesser decrease than the other models.

For the MPI-ESM, the increase in aerosol load appears to be linked to an increase in biomass burning aerosols from Central Africa that extends into the WA region. Studies have found that biomass burning aerosols in climate models are too absorbing and could also explain why the decrease in surface irradiance is so high in

MPI-ESM (and also AWI-ESM, and EC-Earth) than in MRI-ESM. However, it is not the case for the MRI-ESM, which has a dynamic aerosol model unlike the other three models, although its AOD increase could also be due to biomass burning aerosols that have their source in WA. These uncertainties in the future aerosol emission projections remain an open discussion for future studies. In future studies, it could be necessary to consider a comprehensive evaluation of the aerosol load of different climate models (including some dynamic aerosol models) over the region.

In general, given the projected decrease of future solar PVP generation, this study calls for stakeholders to develop robust management plans to be able to successfully and sustainably integrate solar energy in the power systems of WA. The plans need to consider both the near and distant future evolution of potential solar PVP. Furthermore, the study focuses on only changes in the mean solar PVP production. However, changes in the sub-daily fluctuations in the solar PVP could also be critical for solar energy integration if more high-frequency variations occur in the near- or far-future. It is therefore important to investigate how the sub-daily fluctuations will also change in the future. Moreover, this study shows the need to also improve current climate models to reduce uncertainties in long-term future projections as well as very short-term predictions.

Chapter 7

Conclusion

7.1 Summary and implications of main outcomes of thesis

Due to the abundance of solar radiation in WA, solar power is a viable and sustainable alternative for future electricity generation. However, the intense cloud cover in the region and its spatiotemporal evolution, as well as other climate factors, challenges a massive development. Additionally, the relative lack of understanding of clouds in WA further complicates this prospect. As a result, many open questions regarding the feasibility of massive solar energy development exist. Despite the numerous projects that have been discussed, the lack of understanding of climate factors that affect solar energy, such as cloudiness, is likely to be one of the main reasons for the currently limited implementation of solar energy in the region (less than 1 % of total electricity generation). This study mainly sought to understand the regional evolution of cloudiness directly in the context of solar energy development and management in WA.

This thesis attempted to provide important meteorological information that could be essential in any feasibility studies involving the development of the solar resource in WA for electricity production. It started with developing a climatology of occurrence and space-time variability of different cloud types in the region based on long-term historical data. It was also necessary to understand the drivers and processes associated with the cloud occurrence in the region. Finally, the impact of the clouds on the incoming solar radiation was quantified in both time and space. This was to ascertain how much, where, and when the incoming radiation is lost. Such quantified information could help in both the siting and sizing of solar farms in the region. It was imperative to extend the analysis into the future to understand

how climate change could impact the solar resources and potential energy generation in WA. This was achieved by using a suite of 20th and 21st-century state-of-the-art climate model projections. Although the study is carried out over the entire WA, some results were mainly focused on the Guinean and Sahelian vegetation zones of the region.

The main findings and conclusions of this thesis are summarized below:

7.1.1 The frequency and evolution of clouds in West Africa

A climatology of the variability of different cloud types was created and documented using the ERA5 and CERES SYN1deg datasets. The climatology showed that cloud cover varies greatly in time and across the entire region. In general, cloud cover in WA is characterized by a south-north gradient, with the southern areas near the Guinea Coast cloudiest at all times. High elevation points like the highlands of Guinea and Nigeria also have intense cloudiness at all times than the other areas. The study showed that the total cloudiness is most intense during JJA, the core of the monsoon season. During this period, the mean total cloudiness is between 70 % and 80 % around the Guinea Coast and less than 50 % in the Sahel and north of WA. In the other seasons, the mean total cloudiness is lesser.

We also analyzed the season and evolution of different cloud types based on the level of the cloud base in the atmosphere.

- Low clouds have the most distinctive seasonal and spatial variability. During the dry season (DJF), these clouds are mainly found around the Guinea Coast but their fractional coverage intensifies and extend northwards into the Sahelian region during the wet season. The seasonal evolution of the low clouds appears to follow the seasonal shifts of the ITCZ. These low clouds also have a distinct diurnal cycle in all seasons in the southern part of WA. In the Sahel region, they usually occur in JJA with a marked diurnal cycle.
- High and middle clouds are present across the entire region in all seasons but their coverage intensifies during the JJA season, especially around the Guinea Coast. The diurnal variations of both of these cloud types are relatively lower.
- Passive satellite observations sometimes misrepresent dust from the Sahara Desert as low clouds. The passive satellite sensors are also not able to detect optically thin high clouds and some low clouds when there are overlying clouds. This leads to an underestimation of their actual values.

The daytime occurrence frequency of clouds in the region was also investigated

using the two datasets. South of latitude 15°N , at least one cloud type exists at all times. Additionally, the occurrence frequency of simultaneous presence of all three cloud types is higher in these areas. Low clouds are also frequent over these areas, especially around the coastal regions of southern WA. The occurrence frequency of overcast cloudy conditions in the lower atmosphere, which leads to significant loss of incoming radiation, is between 10 % and 20 % around the Guinea Coast in JJA. On the other hand, all areas north of latitude 10° are characterized by high frequencies cloudless events. These results are true for all the datasets.

These results have direct implications for the siting of solar farms in the region. For instance, considering the high radiative effects of low clouds on the incoming shortwave radiation (Bouniol et al., 2012), solar farm developers may decide to site large solar farms further away from the Guinea Coast, given the constant presence of these clouds over the region. Moreover, along with the high frequencies of simultaneous occurrence of all three cloud types, potential solar PV plants located in Guinea are likely to produce a very low percentage of their nominal capacities for significant periods. This is especially true in the monsoon season due to the intensification of clouds and the increase in the frequency of simultaneous occurrence of all three cloud types. The Sahel region and northern parts of WA may appear to be favorable for siting large solar farms due to the relatively lower coverage and occurrence frequency of cloudiness. However, these areas also have issues of dust particles from the Sahara Desert, which can block radiation and settle on solar panels to reduce power generation. However, dust was not analyzed in this study. Thus, there should be robust plans dealing with plant sizing, distribution, and the capacity of additional backup sources, before the development of any large-scale solar farms in the region.

This study uses both reanalysis and satellite datasets that distinguish between different cloud types based on the heights of the clouds' bases in the atmosphere. As a result, different kinds of clouds may be classified as one (e.g., cumulus and stratocumulus clouds will all be in the category of low clouds). This is one of the limitations of the study. Nevertheless, the study provides an important climatology of cloud cover based on a long-term database that could be essential for assessing the feasibility of planned solar energy projects in the region.

7.1.2 Synoptic drivers of cloud occurrence in West Africa

After presenting the climatology of clouds in the region, we investigated the synoptic processes that exist in the presence of or trigger the clouds. We only focused on daytime low clouds due to their significant impact on the incoming solar radiation

relative to the other cloud types. With the ERA5 dataset, three categories of low clouds based on the fractional coverage were defined and analyzed: No LLC, LLC Class-1, and LLC Class-2. LLC Class-1 and Class-2 are events with low (up to 50 %) and high (more than 50 %) coverage of low clouds in the sky, respectively, while No LLC is when there are no low clouds at all. The results showed that the occurrence of the different low clouds classes in both the Guinea and Sahel regions of WA is marked with significant diurnal and seasonal variations:

- From June to September, LLC Class-1 occurrence is low while the Class-2 is high in the Guinea region. During the day, the LLC Class-2 events are more frequent in the early morning, while the Class-1 events are frequent during the late afternoon. This diurnal cycle is linked to the occurrence of nighttime low clouds over the region, which persists into the day and gradually dissipates (Babić et al., 2019a).
- Over the Sahel, both the LLC Class-1 and Class-2 events peak during the core of the monsoon season. The Class-2 events are higher during the midday, while Class-1 events do not show any marked diurnal variation.

During the wet season, both LLC Class-1 and Class-2 events are characterized by high moisture flux dominated by a significant amount of background moisture and strong southwesterly winds blowing from the Gulf of Guinea. The moisture flux intensifies just before the clouds are formed and weakens right after they dissipate. There is also a strong cooling just before these clouds occur. This is indicated by a reduction of the temperature in the period preceding the cloud occurrence. The cooling, which leads to saturation and subsequent cloud formation, is due to cold air advection, as shown recently by Babic et al. (2019b).

In the dry season, the moisture flux during the clouds' occurrence is not as strong as the wet season. However, the background moisture plays a significant role in cloud occurrence. By showing these processes for both the wet and dry seasons, this study has extended on previous studies in WA that focused on only the monsoon season.

We also investigated the impacts of low clouds' occurrence on the surface energy budget. The presence of low clouds leads to a net downward transfer of energy in the region. These clouds also lead to strong attenuation of the incoming solar radiation (up to about 50 % reductions in some cases).

7.1.3 Effects of clouds on the incoming shortwave radiation

Moving forward, it became imperative to consider how the technical information on cloud occurrence and evolution can be directly applied to the management of solar farms. As a form of climate service for stakeholders in the region, we quantitatively determined the effects of clouds on the incoming solar radiation.

In the southern part of WA, clouds lead to around a 55% decrease of the incoming solar radiation on average in August. The value is between 20% and 35% in the Sahel region during the same period. These values were estimated for the total cloud cover. The amount of the incoming radiation that is lost due to low and middle clouds depends strongly on the clouds' fractional coverage in the sky. However, this is not the case for high clouds.

The study also showed that cloudy events that persist for several hours are frequent over southern WA but not in the Sahel and north of WA. In the Sahel, cloudless sky conditions persist for several hours. Despite this, periods with extremely low surface radiation do not linger for long all of WA. In Guinea, for instance, persistent periods with very high surface radiation are the most common in all seasons except JJA. During JJA, persistent periods with moderate surface radiation dominate. In the Sahel, persistent high solar radiation periods dominate in all seasons.

From analyzing the year-to-year variability, we found that the coefficient of variation of the incoming radiation is highest during the summer months (June to October) and lowest in the dry season (November to April) across the whole region. Furthermore, the variability is higher in the southern part of WA.

The results of this study contribute directly to the ongoing feasibility studies and have direct implications for the siting of solar farms in the region. The high frequency of persistent cloudy conditions and large attenuation of the incoming radiation in southern WA may suggest poor suitability for siting solar farms. One may argue that the Sahel and north of WA present better conditions for developing solar farms. However, these areas are associated with intense dusty conditions throughout the year, which reduces the incoming solar radiation and decreases solar power generation. Also, temperatures in these areas are extremely high and may reduce the efficiency of PV cells. Furthermore, despite the high attenuation of incoming radiation in southern WA, the region receives higher solar radiation than many areas with successfully implemented solar energy generation systems in the world (e.g., Pfeifroth et al. (2018)). Therefore, solar plants can be developed and integrated successfully into the power systems in the region when efficient management strategies are put in place. These can include but not limited to oversizing

of plants (McTigue et al., 2020), having a flexible storage-release operation (Danso et al., 2021) and diversification (Sterl et al., 2018).

The results also showed that the radiation received during the summertime is associated with higher uncertainty. This calls for efficient forecasting techniques to improve the prediction of solar power generation in advance. It will ensure that backup systems can be made available in advance to avoid mismatches between demand and supply.

7.1.4 Impacts of climate change on solar energy and its drivers

This part of the thesis extended our investigations into the future period using CMIP6 climate model projections for the historical period and the SSP5-8.5. The historical outputs of the models were first evaluated using the CERES satellite observations. A quantile mapping bias correction was applied to reduce the biases in the climate models. Potential solar power generation over WA in both the historical and future periods was estimated using the bias-corrected model outputs. The solar power generation time series was estimated with a simple model that uses the surface irradiance and temperature as inputs.

The computation of solar power generation for the historical period and future periods based on the SSP5-8.5 scenario allowed us to determine the possible impacts of climate change on future solar energy projects in the region. All four models project a decrease of the annual mean future solar power potential relative to the historical period, with significant downward trends in the entire region. The magnitude of the reduction is rather smaller in one of the models (i.e., MRI-ESM). For most of the models, the annual mean solar power decrease could reach about -20% in parts of southern WA during the second half of the 21st-century. The reduction of the solar power potential will be most extreme during the summer months. In general, the projected reduction in solar energy generation is huge and could lead to critical implications for the long-term sustainability of the proposed projects if they are not strategically developed considering the possible climate change effects.

While the near-surface air temperature will increase significantly in the future, it will not induce a significant change in the solar power potential over the whole region. The surface irradiance, which is projected to decrease, however, will be the predominant cause of the future changes in solar power potential over the whole region. The projected decrease of the surface irradiance is primarily due to the following reasons:

- Generally, all models project an increase in the cloud liquid water path. This will, in turn, increase the albedo of clouds in the region, leading to a decrease in the incoming solar radiation.
- Aerosol load is also projected to increase in the future, thus, enhancing both the direct and indirect aerosol effects. This appears to have a significant influence on the incoming solar radiation in the region.

These results are novel in many ways. Firstly, the use of CMIP6 for assessing the impacts of climate change on solar power potential is unprecedented in the region. The results obtained show larger magnitudes of decreasing solar power potential relative to the previous studies, which were based on CMIP5. Also, this is the first study in the region that has attempted to assess changes in some of the factors (i.e., aerosols, cloud water) that influence the drivers of solar power generation.

7.2 Future research directions

7.2.1 Improving cloud climatology

Data

The cloud climatology developed in this study is based on the ERA5 and CERES datasets. Although both products reproduced cloud occurrence well, they also have uncertainties. A direct improvement of this study will be to use surface observations. At the moment, this will be difficult to achieve due to the lack of a long-term continuous collection of surface observations of clouds and cloud properties in the region. Some short-term observational records exist in the region. However, these are usually a few weeks of measurements obtained from field campaigns such as the AMMA and recent DACCIWA projects. In terms of developing a climatology for assessing the feasibility of solar energy in WA, these few weeks of measurements may not be suitable. However, these valuable measurements can be used to study and understand the underlying processes of cloud formation and evolution in the region (e.g., Babic et al. (2019b), Dione et al. (2019), and Lohou et al. (2020)). Some of these field campaign measurements could also be incorporated into forecasting systems (van der Linden et al., 2020) to improve predictions. They could also be used to evaluate satellite-based observations or outputs of climate model simulations.

ERA5 provides both 3D and 2D distributions of cloud fractions. We used the 2D cloud distribution dataset to create the climatology of clouds. The definitions of the ERA5 2D cloud types are slightly different from those in CERES and could partly explain the differences between the two products. A fairer comparison between the

two products could be accomplished by using the 3D distribution of clouds in ERA5. One can recalculate the ERA5 2D cloud fractions using the 3D distribution and the pressure thresholds of the corresponding atmospheric layer and cloud type as defined in the CERES product. The computation could be done easily by applying some cloud overlap assumptions, although it may be extremely time-consuming to retrieve the ERA5 3D distribution for a long period, such as in this study.

Climatology of specific cloud systems

Cloud types in the ERA5 (and CERES) dataset are categorized using stratified layers. This means that all clouds that occur within one stratified layer (e.g., low-level) are classified as one cloud type. While this is a common approach for most model and satellite products, it can lead to a mix of different cloud systems to be considered as one type. For example, stratocumulus and cumulus clouds are all classified as low clouds because both are found in the lower atmosphere. Similarly, cirrus clouds and anvils of deep convective clouds will be classified as high clouds. These individual cloud systems have different drivers, processes, and radiative properties and thus, could lead to some uncertainties when classified as one and used for radiative transfer computations.

Given the cloud optical thickness and cloud top pressure, it could be possible to isolate the individual cloud systems following the International Satellite Cloud Climatology Project (ISCCP) classification technique (Hahn et al., 2001). One can then develop cloud climatology and estimate the radiative effects of individual cloud systems. Also, this study investigated only the drivers of low clouds' occurrence. An extension for future studies would be to determine the drivers and processes associated with the other cloud types.

Extension to other climate zones

Some results of the study were provided for areas in the Guinean and Sahelian climate zones. The chosen areas only covered part of the two zones. The study can, therefore, be extended by using the entire demarcations of the zones. Moreover, other climate zones (such as the Sudano and Savannah zones) in the region should also be considered in future studies.

7.2.2 Extension to aerosols

This work provided important information on clouds' occurrence and how they affect surface radiation. However, aerosols also have critical impacts on the incoming radiation and the efficiency of solar panels. Suspended aerosols in the atmosphere

absorb and scatter part of the incoming solar radiation. They also settle on solar panels, which may reduce the efficiency of the panels over time. The Sahara Desert is an important source of mineral dust in WA. Over the north of WA, these particles are suspended in the atmosphere throughout the year. The strong dry winds of the harmattan transport some of the mineral dust particles to the south of WA during the dry season. Also, biomass-burning aerosols are present in the region, especially between June and September. Recent studies have also shown that some biomass burning plumes from Central Africa are advected into WA (Haslett et al., 2019). These aerosol particles influence the incoming solar radiation; thus, it is necessary to characterize the long-term evolution and the impacts.

A possible improvement of the study will be to:

- determine the combined radiative effects of clouds and aerosols on the incoming solar radiation. This would represent a relatively complete overall representation of the impacts of the atmosphere on the surface irradiance. The combined radiative effects would be more relevant in the selection of sites for constructing solar farms.
- develop the climatology and determine the radiative effects of individual aerosol types in the region.

7.2.3 CMIP6 models' uncertainties

The uncertainties presented by climate models mean that future projections have to be interpreted carefully. Overall, the quantification of all sources of variability can help make better decisions now and in the future. For example, with four climate model ensembles, our work revealed that the surface irradiance will decrease in the 21st-century. However, the magnitude of the reduction is different among the climate models (the reduction in one model was significantly lower than the others). This creates uncertainty in future projections and complicates the interpretation of the results. An estimation of the future changes in the variables with the multi-model ensemble mean may be more relevant and straightforward in future studies, although this will not eliminate the uncertainties. In this case, the uncertainty that arises due to the individual models' projections should be quantified. Also, the uncertainty due to the internal variability of climate models should be quantified.

Another significant extension of this work will be to quantify the scenario uncertainty for future projections. The future projection in this work is based solely on the SSP5-8.5 scenario. However, there is a catalog of other future scenarios that can be considered. For example, future studies could compare projections

based on the two optimistic development pathways; thus, helping to characterize future regimes under a far-end emission scenario with a fossil-based economy or an increasing shift toward sustainable practices.

The results of our study revealed some significant differences in the AOD of the MPI-ESM and MRI-ESM. The former uses a climatology-based aerosol forcing, while the latter has a dynamic aerosol model coupled to the other model components. Although both models projected an increase in AOD, the results of this study also showed two differences between the two models. Firstly, the AOD increase in the 21st-century is higher in the MPI-ESM. This discrepancy partly explains the projected higher decrease of surface irradiance in the MPI-ESM than the MRI-ESM. Secondly, the sources of increase of the AOD appear to be different for the models. In the MPI-ESM, AOD increase seems to be biomass burning aerosols that emanate from Central Africa. On the other hand, the AOD increase in the MRI-ESM appears to be an increase in emission from sources already located in WA. These discrepancies present an opportunity to have further discussions in the future regarding climate models' ability to simulate aerosol emission.

7.2.4 Developing and managing solar energy

Diversification/complementarity with other resources

While this study provides information on the attenuation effects of clouds on the solar resource, it does not assess ways to efficiently manage the solar power generation when integrated into the regional power systems. One approach will be to explore the complementarity between the solar resource and other renewable energy sources. For instance, this study shows that the solar resource will be strongly reduced during the monsoon season in southern WA. Hence, other renewable energy sources such as wind, which intensifies during the same period, may be used to complement solar energy generation. Presently, only one study in the whole of WA has investigated this possibility of synergizing solar and wind energy (Sterl et al., 2018). Further studies are needed to see how other resources may be used to complement solar energy or vice versa. Also, regional complementarity presents an opportunity for developing a massive regional solar power pool. One may envision assessing the potential of using spatial diversification to minimize the fluctuation of solar power generation. Although this has been shown to work effectively in other regions, we do not yet know if it will be possible in WA and should be investigated.

Using storage as flexibility

Integrating large shares of solar power into the national grid requires flexibility in the power system. Apart from diversification, as already discussed above, flexibility can be provided by energy storage. Due to the existence of several large hydropower reservoirs, there is a huge potential in WA to use storage as a means of flexibility to integrate large shares of solar energy. Water in the reservoir is stored during periods with high solar power generation (assuming it can supply all the demand). It will then be released when the solar power generation is low with a supply-demand deficit. If there is an excess solar generation, it can be used to pump water from downstream rivers into the upstream reservoir and released later. Recently, Danso et al. (2021) has shown that large shares of solar energy can be integrated into the power system of Ghana with the help of one of the largest hydropower reservoirs in Africa. However, it was demonstrated for just one country of WA. Thus, the results might be different from other areas in the region. Further investigations are therefore needed to understand the full potential of this flexibility in the region. Future studies can also incorporate the impacts of the changing climate on the hydro resource availability in WA.

Oversizing

Flexibility can also come from the sizing of solar plants. Oversizing solar farms mean that during periods with intense cloudiness and reduced surface irradiance, power plants may still produce enough energy to supply the demand. During periods with no clouds, excess power generation may be stored or traded to neighbouring regions.

Improving predictions

Integration of solar energy can be efficient with improved predictions. Present model forecasts have errors that mainly come from forcing datasets that are often other model outputs themselves. The errors are due to the inability of climate models to correctly represent convection and cloudiness in WA (Hannak et al., 2017). To get better and accurate radiation forecasts, it is imperative to improve the underlying physical representations in these climate models. Therefore, future studies are needed to explore efficient ways representing the physical atmospheric processes in climate models to improve the accuracy of the forecasts in WA.

Appendix A

Additional information on CMIP6 models

A.1 Model configurations

Table A.1 presents some of the model set-up characteristics of the four CMIP6 GCMs used in this study. The AWI-CM and MPI-ESM are basically similar in all aspects except in the ocean and sea-ice component.

Table A.1: Model configurations of the CMIP6 GCMs used in this study.

	AWI-CM-1-1-MR	EC-Earth3	MPI-ESM-2-HR	MRI-ESM-2.0
Name of the atmospheric model	ECHAM6.3 (Stevens et al., 2013)	IFS cy36r4 (ECMWF, 2010)	ECHAM6.3 (Stevens et al., 2013)	MRI-AGCM3.5 (Yukimoto et al., 2019)
Number of vertical levels	95	91	95	80
Horizontal resolution	100 km	80 km	100 km	120 km
Altitude of model top	0.01 hPa	0.01 hPa	0.01 hPa	0.01 hPa

Cumulus convection parameterization	Tiedtke-Nordeng-Tiedtke (Nordeng, 1994; Tiedtke, 1989)	Tiedtke scheme (Tiedtke, 1989)	Tiedtke-Nordeng-Tiedtke (Nordeng, 1994; Tiedtke, 1989)	Yoshimura scheme (Yoshimura et al., 2015)
Stratiform parameterization	Sundqvist scheme (Sundqvist et al., 1989)	Tiedtke scheme (Tiedtke, 1989)	Sundqvist scheme (Sundqvist et al., 1989)	Kawai scheme (Kawai & Inoue, 2006)
Microphysics	Lohmann-Roeckner scheme (Lohmann & Roeckner, 1996)	Sundqvist and Kessler schemes (Kessler, 1969; Sundqvist, 1978)	Lohmann-Roeckner scheme (Lohmann & Roeckner, 1996)	Lohmann scheme (Lohmann et al., 2007)
Land surface model	JSBACH (Reick et al., 2013)	TESSEL scheme (van den Hurk et al., 2000)	JSBACH (Reick et al., 2013)	MRI-AGCM3.5 (Yukimoto et al., 2019)
Aerosol model	climatology	climatology	climatology	MASINGAR mk-2r4c (Tanaka et al., 2003)
Ocean and sea-ice model	FESOM (Wang et al., 2014)	NEMO 3.6 and LIM3 (Madec et al., 2017; Rousset et al., 2015)	MPIOM 1.6.2 (Jungclaus et al., 2013)	MRI.COMv4 (Tsujino et al., 2017)
Ocean model resolution	Unstructured	1°	0.4°	1° × 0.5° (0.3° between 10°S and 10°N)

A.2 Seasonal evaluation of models

A seasonal evaluation of the CMIP6 model ensembles was performed for both the raw and bias-corrected data. Figure A.1 and Figure A.2 present the evaluation of cloud fraction for Guinea and Sahel respectively. In Guinea, all models (uncorrected) underestimate the cloud fraction except EC-Earth in JJA (colored bars in Figure A.1). The largest biases occur in the DJF season. Applying the quantile mapping method generally reduces the biases (shaded bars in Figure A.1). However, there are a few exceptions where the bias-corrected output does not improve the raw GCM output. For example, applying quantile mapping to both the AWI-CM and MPI-ESM in SON actually increases the biases. It is important to note that both models share similar atmospheric components but different oceanic and sea-ice components (Semmler et al., 2020). For both the raw and corrected data of each GCM the biases across the individual ensemble members do not differ a lot (as indicated by the standard deviation bars).

In the Sahel region, the biases do not follow a similar pattern like in Guinea (Figure A.2). Instead, the sign of the biases depends on the season and the model. This is true for both the raw and corrected GCM ensembles. Application of the quantile mapping technique is also not very straightforward in the Sahel region. In some cases, it reduces the biases in the model outputs, and increases it in other cases.

We also evaluated the GCMs' surface downwelling shortwave radiation output. In the Guinea region, all the raw GCM ensembles overestimated the surface radiation in all seasons (Figure A.3). This is coherent with the underestimation of cloud fraction (Figure A.1) with the exception of the EC-Earth model which overestimated both the cloud fraction and surface radiation in JJA. An investigation into the microphysical properties of the EC-Earth model could explain this inconsistency. The largest biases for the GCMs occur in DJF and MAM. Nonetheless, applying the quantile mapping technique reduces the biases significantly across all models in all seasons.

The biases of the raw GCM outputs in the Sahel region are relatively low (Figure A.4). For the raw GCM's the lowest biases occur in the DJF and SON seasons. Application of the quantile mapping technique reduces the biases in MAM and JJA but not in DJF.

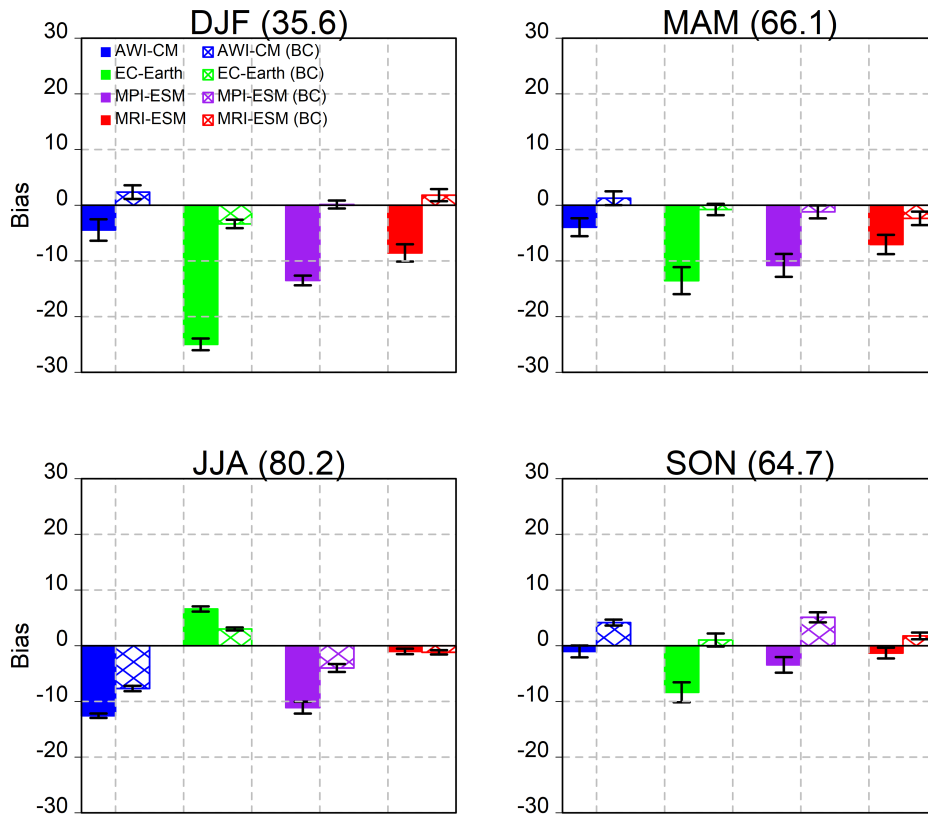


Figure A.1: Mean GCM seasonal biases in Guinea for cloud fraction. Coloured bars are biases for raw GCM ensemble means. Shaded bars are biases for bias-corrected ensemble means. Error bars represent the standard deviation of biases across individual ensemble members. Numbers in brackets are the seasonal mean cloud fraction (%) of the reference observations.

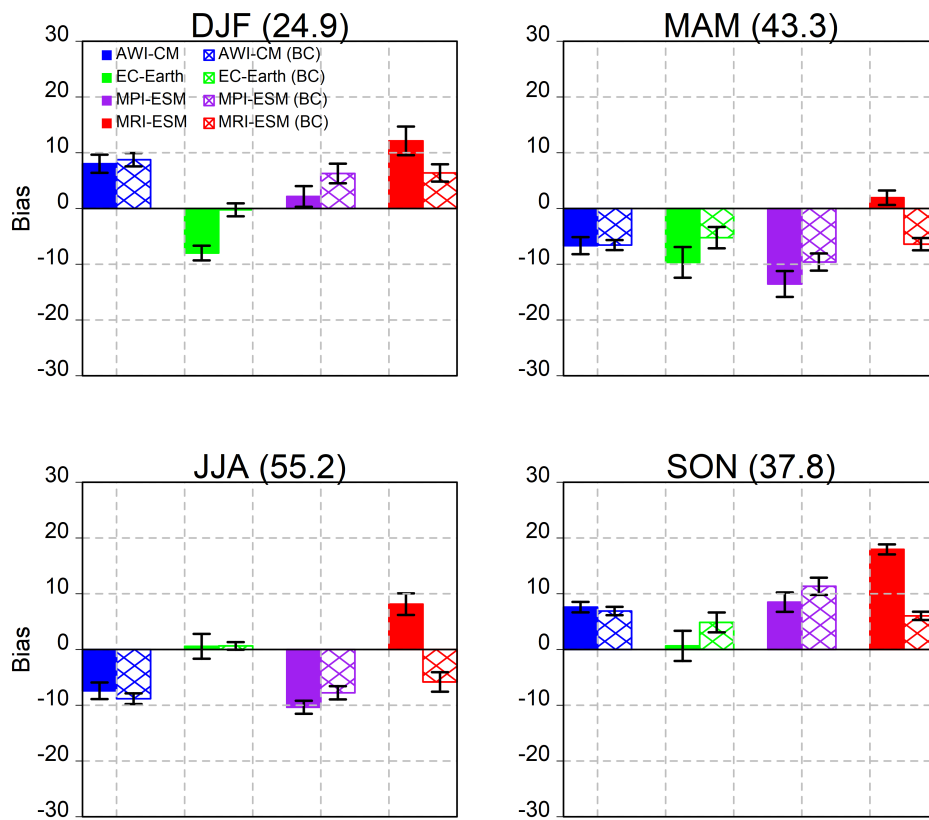


Figure A.2: Same as Figure A.1 but for Sahel.

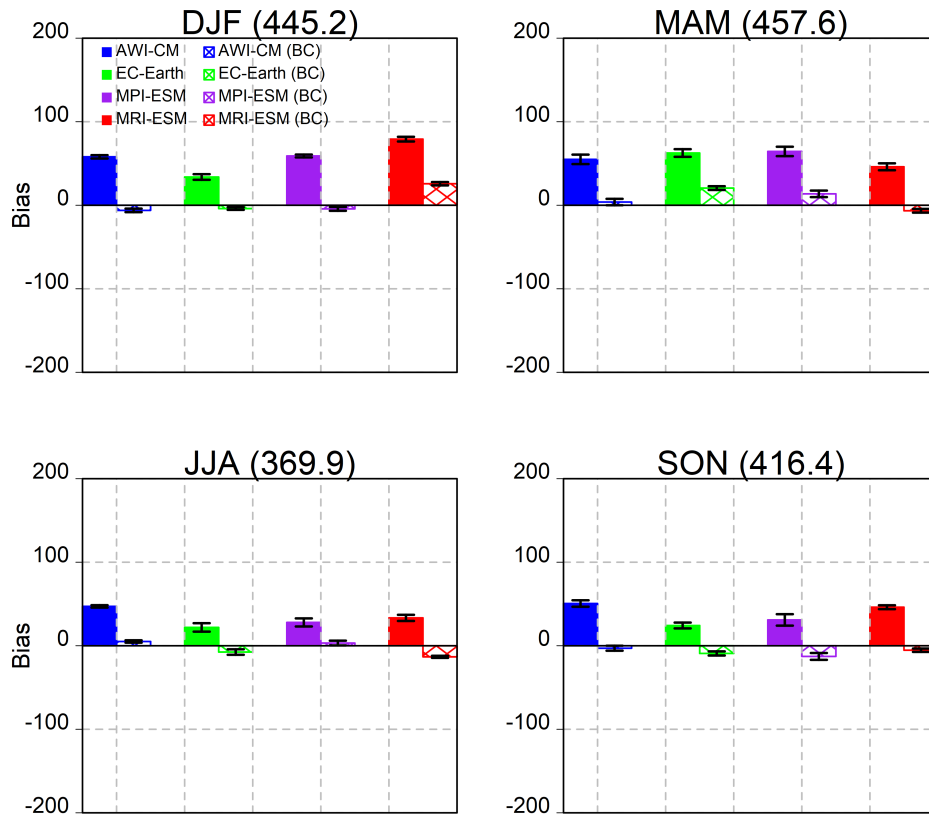


Figure A.3: Mean GCM seasonal biases in Guinea for surface irradiance. Coloured bars are biases for raw GCM ensemble means. Shaded bars are biases for bias-corrected ensemble means. Error bars represent the standard deviation of biases across individual ensemble members. Numbers in brackets are the seasonal mean surface irradiance (W m^{-2}) of the reference observations.

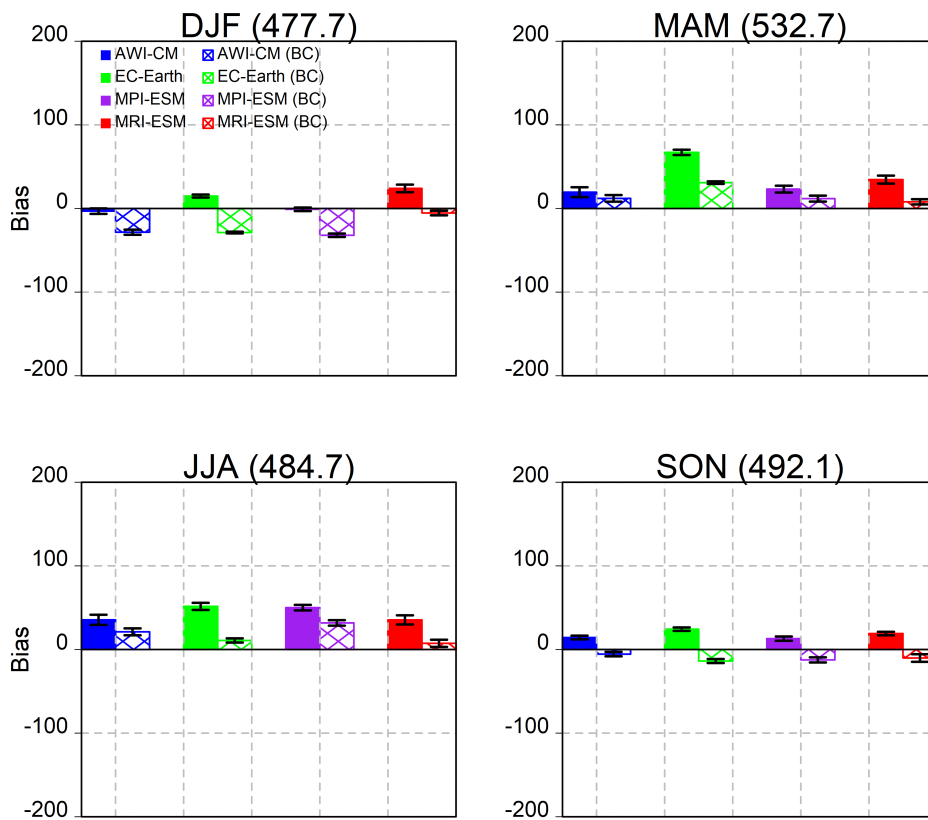


Figure A.4: Same as Figure A.3 but for Sahel.

Appendix B

Supplementary information for article 2

B.1 Vertical profiles of cloud hydrometeor content during LLC occurrence

The occurrence frequency of clouds may be defined based on the value of the cloud water content (liquid and ice) or the cloud fraction (CF). In this study, we defined the occurrence frequency of low-level clouds (LLC) based on the value of CF. LLC occurrence was first classified as Class-1 ($0 < CF \leq 0.5$) or Class-2 ($CF > 0.5$). In ERA5, CF can be larger than zero for zero liquid or ice water content. This is because ERA5 employs a subgrid-scale cloud scheme. Typically, subgrid-scale cloud cover schemes depend only on the relative humidity (RH) (Quaas, 2012). Using the ERA-Interim forecast in West Africa, Hannak et al. (2017) showed that low clouds can exist for $RH < 100\%$. In other words, in the subgrid-scale cloud scheme employed in the ERA-Interim product, which is also the same in ERA5, low clouds can occur when cloud water (which occurs when $RH > 100\%$) has not yet been formed.

This is illustrated in Figure B.1 which shows the vertical profiles of cloud water content during the occurrence of random LLC Class-1 and Class-2 events. It can be seen in some of the profiles (for Class-1) that the liquid and ice water content in the lowest 2 km is null (but these events have $CF > 0$ in the lowest 2 km in the profile). Figure B.1 is also used to suggest the kind of cloud types that may be dominant in each class. In this case, we say that, in the Sahel region, there is a higher probability of getting a Mesoscale Convective System (MCS) in the LLC Class-2 than Class-1. Figure B.1 is the vertical profile of 12 random events of LLC

Class-1 and Class-2 in the Sahel region. Based on the work of Storer and Van den Heever (2013), we designate an event as a ‘MCS event’ when there is a column containing at least 0.01 g kg^{-1} cloud water (black dashed vertical line in Figure B.1) through a continuous depth of 8 km. From the twelve random profiles in Figure B.1, there are at least seven LLC Class-2 events (and just one for LLC Class-1) that satisfy this MCS definition. The number LLC Class-2 events are extremely low compared to LLC Class-1 (see Figure 4.3), therefore, the likelihood that an event will be an MCS is relatively higher in the LLC Class-2 events.

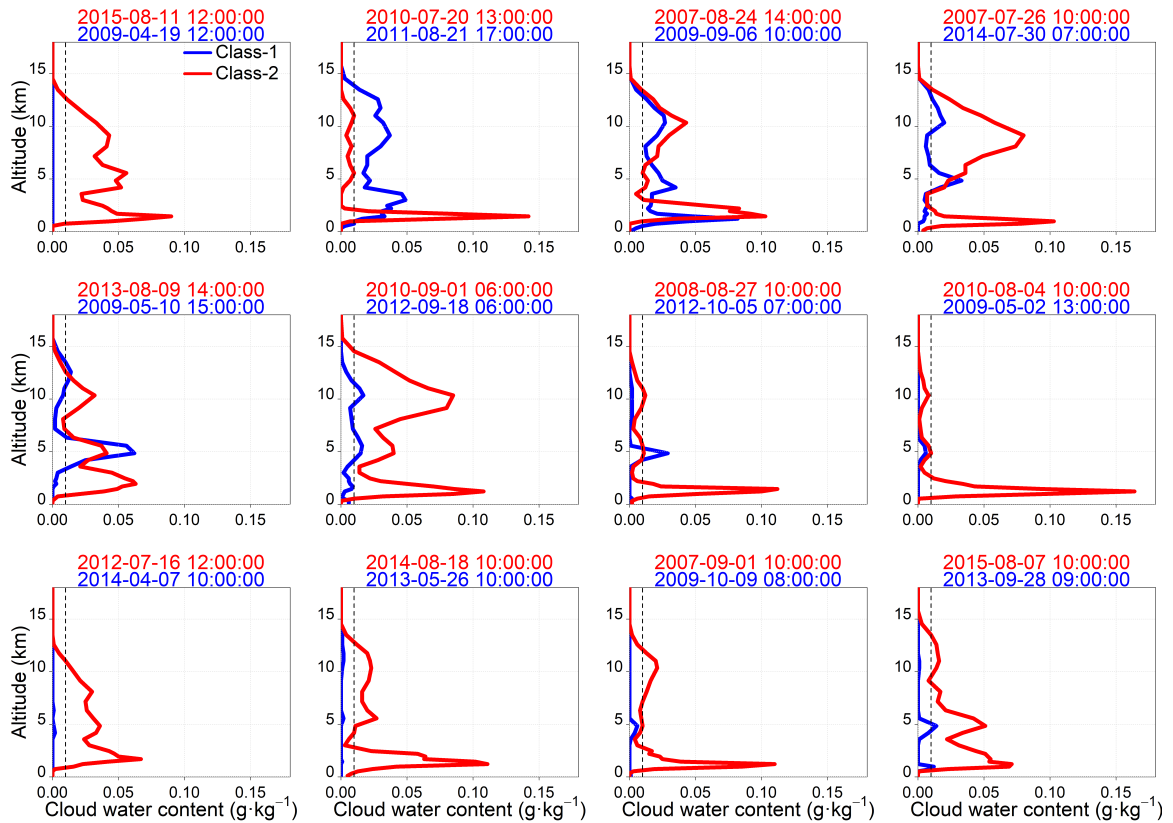


Figure B.1: Vertical profiles of cloud hydrometeor content (liquid and ice water) during the occurrence of LLC Class-1 and Class-2 events in the Sahel region. These events are randomly chosen. The timestamps at the top of each plot are the times for those LLC events. The black dashed vertical line shows the threshold for deep convective clouds as defined by Storer and Van den Heever (2013)

B.2 Specific humidity associated with LLC occurrence and potential temperature before and after low-level cloud formation

Figure B.2 shows the composites of specific humidity (colours) and winds (vectors) during the occurrence of the different LLC occurrence classes in both Guinea and Sahel for the DJF season. During No LLC events, the moisture content in the region of the two windows is very low or zero. However, during LLC occurrence, the moisture content in the region is significant. This indicates that the background moisture plays an important role in the occurrence of these clouds. This result is confirmed in the recent study of Babic et al. (2019b) who found that in southern WA, the most distinct difference between LLC and No LLC events is in the specific humidity.

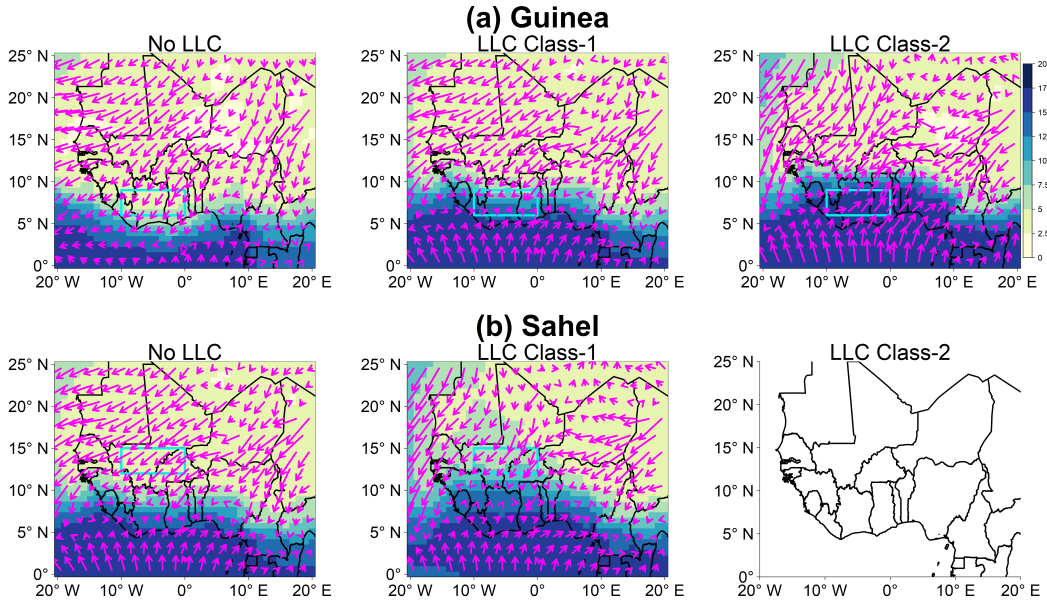


Figure B.2: Composites of 950 hPa specific humidity (colours, g kg^{-1}) and wind (vectors, m s^{-1}) over WA for the three LLC occurrence classes in the Guinea (top) and Sahel (below) windows during DJF from 2006 to 2015. Only occurrences that last for at least six consecutive hours are considered. Wind vectors are averaged over 2 grid points in both the x and y directions. No event of LLC Class-2 has been extracted in the Sahel area during DJF, hence the empty plot.

Figure B.3 presents the composite vertical profile of the potential temperature for the hour before ($1h_{\text{Before LLC}}$) and after ($1h_{\text{After LLC}}$) the occurrence of LLC Class-2 in both regions for DJF and JAS. The profile is shown for the lowest 2 km of the atmosphere. There is no LLC Class-2 event in the Sahel during DJF,

hence the empty plot. The profiles presented here suggest that before the LLC occurrence, there is a significant temperature decrease in the lower atmosphere. In the Guinea region, this is likely due to the well documented horizontal cold air advection from the Gulf of Guinea (Adler et al., 2019; Babic et al., 2019b) which leads to saturation of water vapour and consequent formation of LLCs. There could also be some cold air advection in the Sahel region, as suggested by Marsham et al. (2013). The temperature sharply increases after the disappearance of the LLC and this could be due to enhanced surface warming from incoming shortwave radiation (since attenuation of the incoming radiation is less in cloudless conditions).

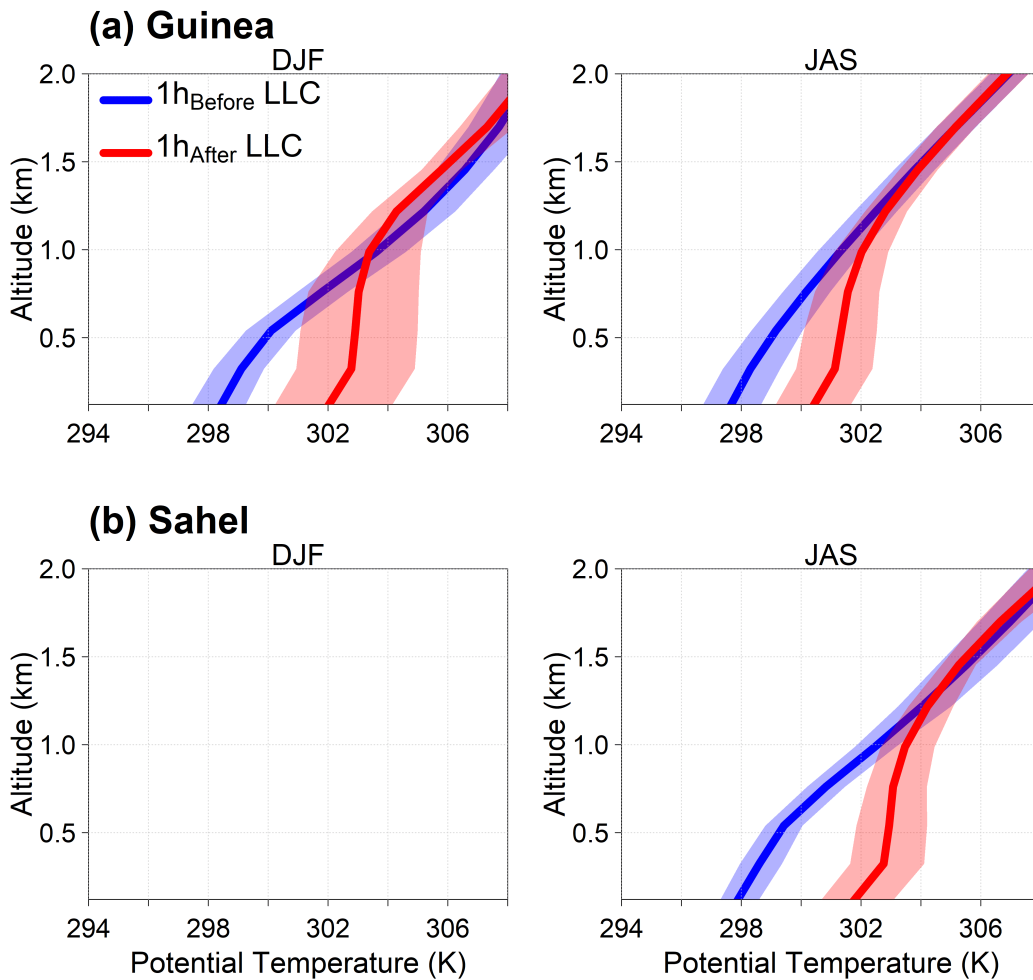


Figure B.3: Vertical profile of the mean potential temperature (solid line) for the lowest 2 km of the atmosphere, computed in Guinea and Sahel for all the ‘one-hours’ preceding LLC Class-2 occurrence and all the ‘one-hours’ after its disappearance. The shaded regions represent the 10th and 90th interpercentile range. No event of LLC Class-2 has been extracted in the Sahel area during DJF, hence the empty plot.

Appendix C

Supplementary information for article 4

C.1 Projected changes in air temperature and surface solar irradiance in West Africa

Under the SSP5-8.5 scenario, the near-surface air temperature in WA is mostly projected to increase in the future across all models (Figure C.1). In both the near- and far-future periods, the projected air temperature increase is higher over the northern part of WA. For instance, the air temperature is projected to increase between 1 °C and 2 °C in parts of northern WA for all models in the near-future (Figure C.1a). This will further exacerbate in the far-future (Figure C.1b) with the air temperature rising by more than 3.5 °C in northern WA across all models (some models project up to 5 °C rise). In all cases, the temperature rise in southern WA is lower than in the north. This result is consistent with the temperature-induced changes in future solar PVP generation (Figure 6.4b and Figure 6.5b).

The future changes in the potential of solar PVP generation is predominantly due to the projected decrease in the surface irradiance. Figure C.2 shows the differences between the future and historical annual mean surface irradiance over WA. For both the near- and far-future periods, the surface irradiance is projected to decrease across all models. However, the surface irradiance will decrease more in the far-future period. The magnitude of the decrease of surface irradiance is significantly lower in the MRI-ESM compared to the other models in both future periods. This is consistent with the relatively small reduction of the future solar PVP potential in the MRI-ESM (Figure 6.1 and Figure 6.2). The discrepancy between the MRI-ESM and the other models is linked to differences in CWP and AOD as discussed

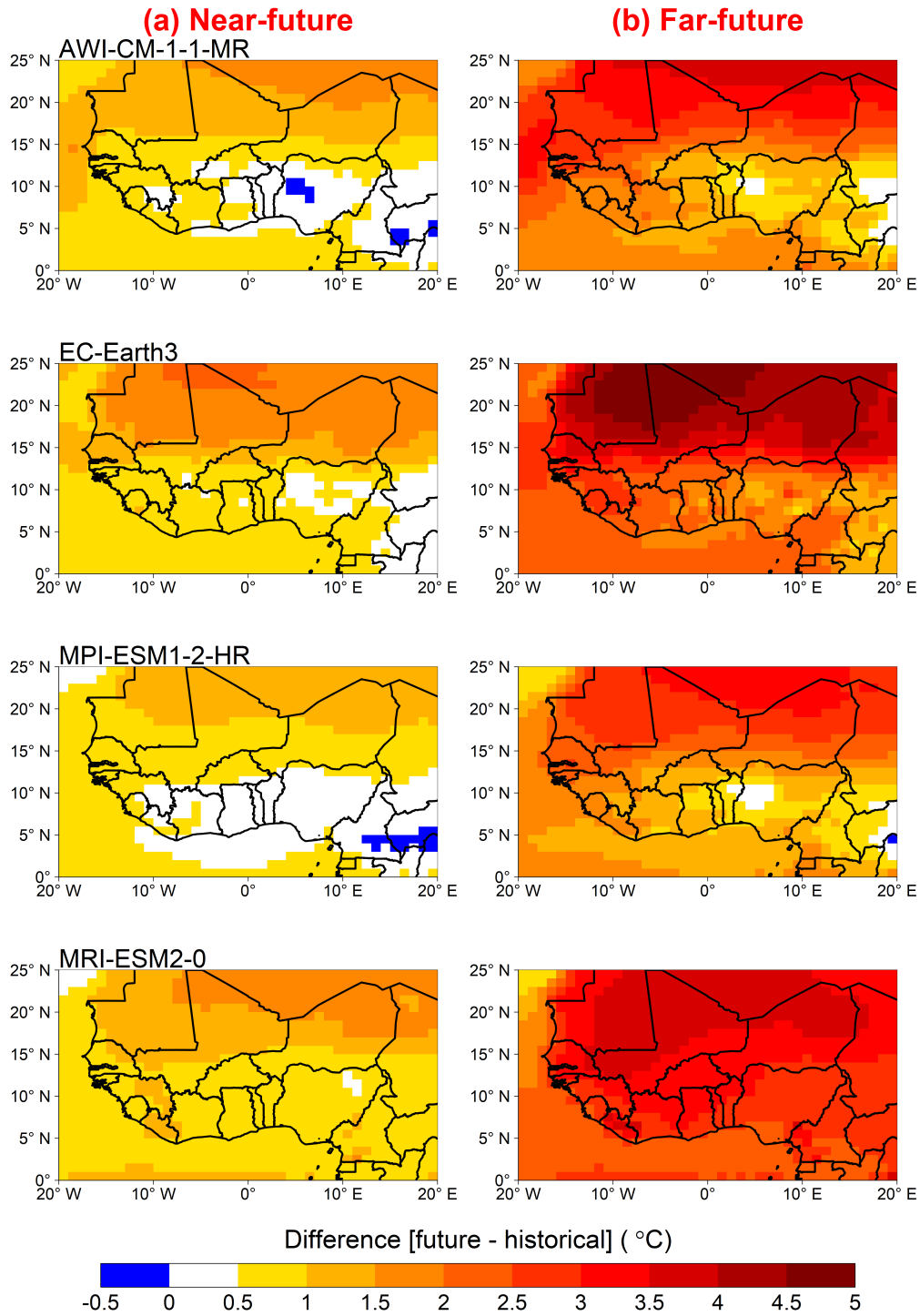


Figure C.1: The annual mean difference (future minus historical) of near-surface air temperature for the (a) near-future (2015 – 2049) and (b) far-future (2050 – 2084) relative to the historical period (1980 – 2014) for four CMIP6 models under the SSP5-8.5. The ensemble mean of each model is used for the computation.

in section 6.6.

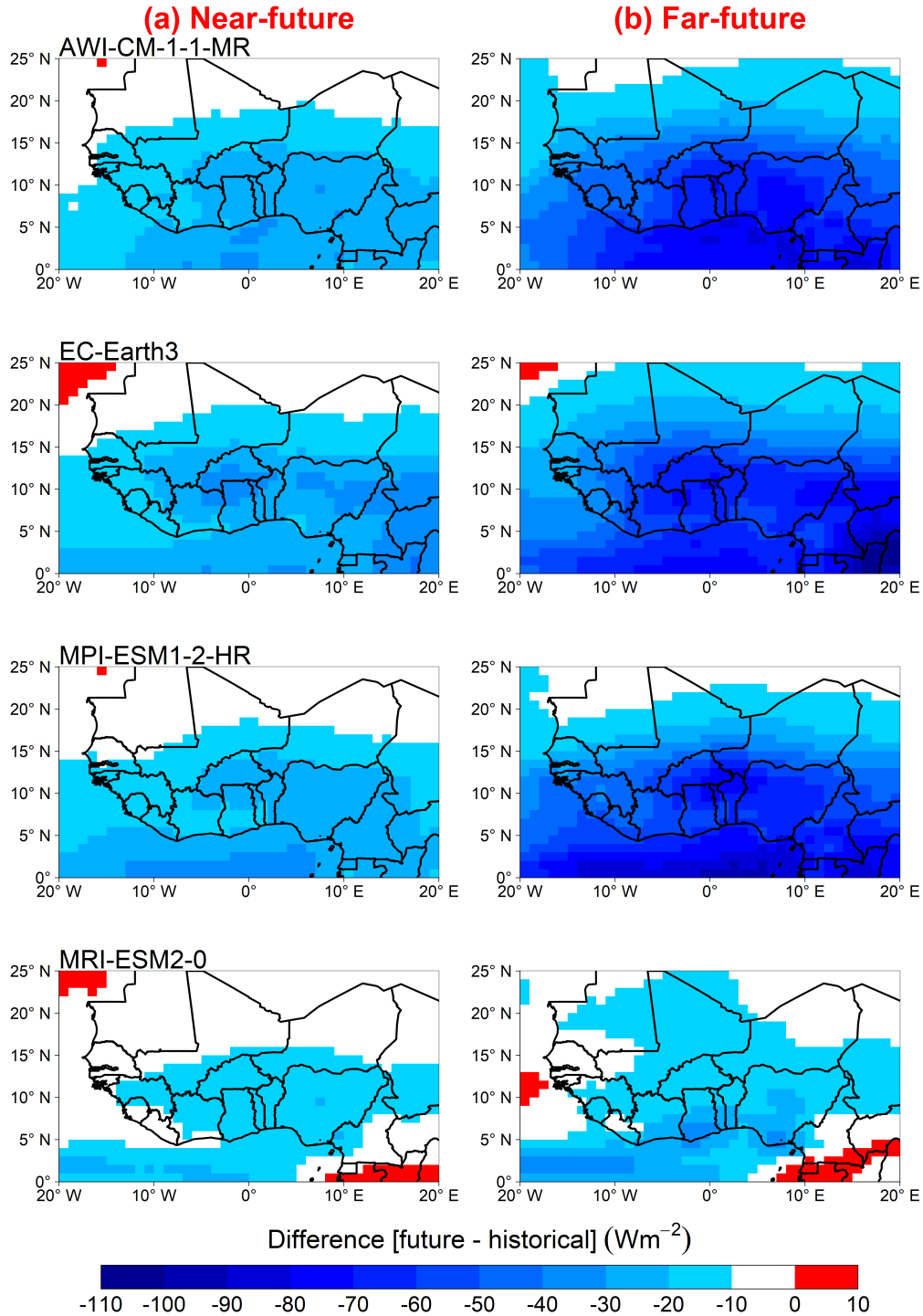


Figure C.2: The annual mean difference (future minus historical) of surface solar irradiance for the (a) near-future (2015 – 2049) and (b) far-future (2050 – 2084) relative to the historical period (1980 – 2014) for four CMIP6 models under the SSP5-8.5. The ensemble mean of each model is used for the computation.

The projected changes in the potential of future solar PVP generation could also be linked to the water vapour content in the atmosphere. As shown by Di Biagio et al. (2012) and Radel et al. (2015), water vapour in the atmosphere can absorb a part of the incoming shortwave radiation. Thus, an increase in the atmospheric water vapour content in future could lead to a reduction in the surface irradiance and thus the solar PVP generation. Figure C.3 presents the difference between the future and historical water vapour path in WA. For all models, the water vapour path is projected to increase in the future. The increase is however, higher in the far-future than the near-future. Southern WA (especially around the Gulf of Guinea) is projected to have a higher water vapour in both future periods. Furthermore, the increase of water vapour is also lower in the AWI-CM and MPI-ESM than EC-Earth and MRI-ESM.

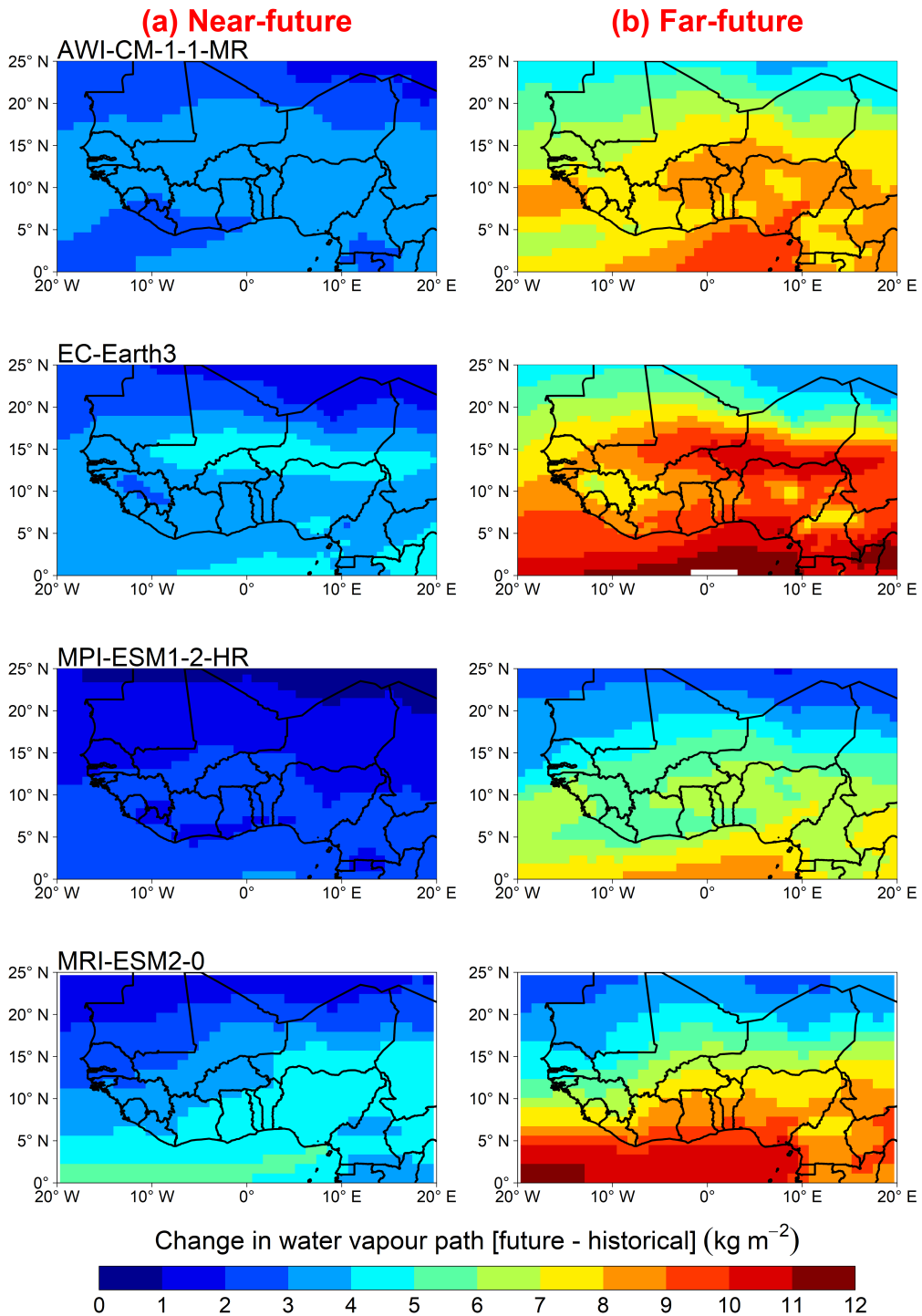


Figure C.3: The annual mean difference (future minus historical) of water vapour path for the (a) near-future (2015 – 2049) and (b) far-future (2050 – 2084) relative to the historical period (1980 – 2014) for four CMIP6 models under the SSP5-8.5.

Bibliography

- Abiodun, B. J., Adeyewa, Z. D., Oguntunde, P. G., Salami, A. T., & Ajayi, V. O. (2012). Modeling the impacts of reforestation on future climate in West Africa. *Theoretical and Applied Climatology*, 110(1-2), 77–96.
- Adejuwon, J. O., & Odekunle, T. O. (2006). Variability and the severity of the little dry season in southwestern Nigeria. *Journal of climate*, 19(3), 483–493.
- Adler, B., Babić, K., Kalthoff, N., Lohou, F., Lothon, M., Dione, C., Pedruzo-Bagazgoitia, X., & Andersen, H. (2019). Nocturnal low-level clouds in the atmospheric boundary layer over southern West Africa: An observation-based analysis of conditions and processes. *Atmospheric Chemistry & Physics*, 19(1).
- Adler, B., Kalthoff, N., & Gantner, L. (2011). Initiation of deep convection caused by land-surface inhomogeneities in West Africa: A modelled case study. *Meteorology and Atmospheric Physics*, 112(1-2), 15–27.
- Adler, B., Kalthoff, N., & Gantner, L. (2017). Nocturnal low-level clouds over southern West Africa analysed using high-resolution simulations. *Atmospheric Chemistry & Physics*, 17(2).
- Ajayi, V. O., & Ilori, O. W. (2020). Projected drought events over West Africa using RCA4 regional climate model. *Earth Systems and Environment*, 4(2), 329–348.
- Akinsanola, A., & Zhou, W. (2019). Projection of West African summer monsoon rainfall in dynamically downscaled CMIP5 models. *Climate dynamics*, 53(1-2), 81–95.
- Aliyu, A. K., Modu, B., & Tan, C. W. (2018). A review of renewable energy development in africa: A focus in South Africa, Egypt and Nigeria. *Renewable and Sustainable Energy Reviews*, 81, 2502–2518.
- Allen, M., Dube, O., Solecki, W., Aragon-Durand, F., Cramer, W., Humphreys, S., & Zickfeld, K. (2018). "Framing and Context" in Global Warming of 1.5 C: An IPCC Special Report on the impacts of global warming of 1.5 C above pre-industrial levels and related global greenhouse gas emission pathways, in the context of strengthening the global response to the threat of climate change, sustainable development, and efforts to eradicate poverty.

- Amjad, M., Yilmaz, M. T., Yucel, I., & Yilmaz, K. K. (2020). Performance evaluation of satellite-and model-based precipitation products over varying climate and complex topography. *Journal of Hydrology*, *584*, 124707.
- Andersen, H., & Cermak, J. (2018). First fully diurnal fog and low cloud satellite detection reveals life cycle in the Namib. *Atmospheric Measurement Techniques*, *11*(10).
- Armstrong, S., & Hurley, W. (2010). A new methodology to optimise solar energy extraction under cloudy conditions. *Renewable energy*, *35*(4), 780–787.
- Arto, I., & Dietzenbacher, E. (2014). Drivers of the growth in global greenhouse gas emissions. *Environmental science & technology*, *48*(10), 5388–5394.
- ASDC. (2017). *CERES SYN1deg Ed4A data quality summary*. Atmospheric Science Data Center. Retrieved December 12, 2018, from <https://ceres.larc.nasa.gov/dqs.php#level3table>
- Asenso Barnieh, B. A., Jia, L., Menenti, M., Zhou, J., & Zeng, Y. (2020). Mapping land use land cover transitions at different spatiotemporal scales in West Africa. *Sustainability*, *12*(20), 8565.
- AU. (2015). *Agenda 2063* (tech. rep.). The African Union Commission.
- Babic, K., Kalthoff, N., Adler, B., Quinting, J. F., Lohou, F., Dione, C., & Lothon, M. (2019b). What controls the formation of nocturnal low-level stratus clouds over southern West Africa during the monsoon season? *Atmos. Chem. Phys*, *19*, 13489–13506.
- Babić, K., Adler, B., Kalthoff, N., Andersen, H., Dione, C., Lohou, F., Lothon, M., & Pedruzo-Bagazgoitia, X. (2019a). The observed diurnal cycle of low-level stratus clouds over southern West Africa: A case study. *Atmospheric Chemistry and Physics*, *19*(2), 1281–1299.
- Barker, H. W. (1996). A parameterization for computing grid-averaged solar fluxes for inhomogeneous marine boundary layer clouds. part i: Methodology and homogeneous biases. *Journal of the atmospheric sciences*, *53*(16), 2289–2303.
- Barker, H. W. (2008). Representing cloud overlap with an effective decorrelation length: An assessment using CloudSat and CALIPSO data. *Journal of Geophysical Research: Atmospheres*, *113*(D24).
- Bartlett, J. S., Ciotti, Á. M., Davis, R. F., & Cullen, J. J. (1998). The spectral effects of clouds on solar irradiance. *Journal of Geophysical Research: Oceans*, *103*(C13), 31017–31031.
- Baurzhan, S., & Jenkins, G. P. (2016). Off-grid solar PV: Is it an affordable or appropriate solution for rural electrification in Sub-Saharan African countries? *Renewable and Sustainable Energy Reviews*, *60*, 1405–1418.

- Bechtold, P., Semane, N., Lopez, P., Chaboureau, J.-P., Beljaars, A., & Bormann, N. (2014). Representing equilibrium and nonequilibrium convection in large-scale models. *Journal of the Atmospheric Sciences*, *71*(2), 734–753.
- Bedi, J., & Toshniwal, D. (2019). Deep learning framework to forecast electricity demand. *Applied energy*, *238*, 1312–1326.
- Bichet, A., Hingray, B., Evin, G., Diedhiou, A., Kebe, C. M. F., & Anquetin, S. (2019). Potential impact of climate change on solar resource in Africa for photovoltaic energy: Analyses from CORDEX-AFRICA climate experiments. *Environmental Research Letters*, *14*(12), 124039.
- Bindoff, N. L., Stott, P. A., AchutaRao, K. M., Allen, M. R., Gillett, N., Gutzler, D., Hansingo, K., Hegerl, G., Hu, Y., Jain, S., et al. (2013). *Detection and attribution of climate change: From global to regional*. Cambridge, United Kingdom, New York, NY, USA, Cambridge University Press.
- Bivand, R., Keitt, T., Rowlingson, B., & Pebesma, E. (2016). Rgdal: Bindings for the geospatial data abstraction library. *R package version*, *1*(10).
- Bodansky, D. (1993). The United Nations framework convention on climate change: a commentary. *Yale J. Int'l l.*, *18*, 451.
- Böhringer, C. (2003). The Kyoto protocol: a review and perspectives. *Oxford Review of Economic Policy*, *19*(3), 451–466.
- Bonkaney, A., Madougou, S., & Adamou, R. (2017). Impacts of cloud cover and dust on the performance of photovoltaic module in Niamey. *Journal of Renewable Energy*, *2017*.
- Bouniol, D., Couvreur, F., Kamsu-Tamo, P.-H., Leplay, M., Guichard, F., Favot, F., & O'Connor, E. J. (2012). Diurnal and seasonal cycles of cloud occurrences, types, and radiative impact over West Africa. *Journal of applied meteorology and climatology*, *51*(3), 534–553.
- Bourgeois, E., Bouniol, D., Couvreur, F., Guichard, F., Marsham, J. H., Garcia-Carreras, L., Birch, C. E., & Parker, D. J. (2018). Characteristics of mid-level clouds over West Africa. *Quarterly Journal of the Royal Meteorological Society*, *144*(711), 426–442.
- Brisson, E., Van Weverberg, K., Demuzere, M., Devis, A., Saeed, S., Stengel, M., & van Lipzig, N. P. (2016). How well can a convection-permitting climate model reproduce decadal statistics of precipitation, temperature and cloud characteristics? *Climate Dynamics*, *47*(9), 3043–3061.
- Brooks, N., & Legrand, M. (2000). Dust variability over northern Africa and rainfall in the Sahel. *Linking climate change to land surface change* (pp. 1–25). Springer.
- Brown, C. (1998). Coefficient of variation. *Applied multivariate statistics in geohydrology and related sciences*. (pp. 155–157). Springer-Verlag.

- Brown, H., Liu, X., Pokhrel, R., Murphy, S., Lu, Z., Saleh, R., Mielonen, T., Kokkola, H., Bergman, T., Myhre, G., et al. (2021). Biomass burning aerosols in most climate models are too absorbing. *Nature communications*, *12*(1), 1–15.
- Bruckner, T., Bashmakov, I. A., Mulugetta, Y., Chum, H., de la Vega Navarro, A., Edmonds, J., Faaij, A., Fungtammasan, B., Garg, A., Hertwich, E., Honnery, D., Infield, D., Kainuma, M., Khennas, S., Kim, S., Nimir, H. B., Riahi, K., Strachan, N., Wisner, R., & X., Z. (2014). *Energy Systems. In: Climate Change 2014: Mitigation of Climate Change. Contribution of Working Group III to the Fifth Assessment Report of the Intergovernmental Panel on Climate Change*. Cambridge, United Kingdom, New York, NY, USA, Cambridge University Press.
- Bukowski, J., & Heever, S. C. (2020). Convective distribution of dust over the Arabian Peninsula: the impact of model resolution. *Atmospheric Chemistry and Physics*, *20*(5), 2967–2986.
- C3S. (2017). ERA5: Fifth generation of ECMWF atmospheric reanalyses of the global climate. *Copernicus Climate Change Service Climate Data Store (CDS)*.
- Cai, H., Feng, X., Chen, Q., Sun, Y., Wu, Z., & Tie, X. (2017). Spatial and temporal features of the frequency of cloud occurrence over China based on CALIOP. *Advances in Meteorology*, 2017.
- Chineke, T. C., Jagtap, S. S., & Nwofor, O. (2010). West African monsoon: Is the August break breaking in the eastern humid zone of southern Nigeria? *Climatic change*, *103*(3-4), 555–570.
- Christensen, J. H., Kanikicharla, K. K., Aldrian, E., An, S. I., Cavalcanti, I. F. A., de Castro, M., Dong, W., Goswami, P., Hall, A., Kanyanga, J. K., et al. (2013). Climate phenomena and their relevance for future regional climate change. *Climate change 2013 the physical science basis: Working group i contribution to the fifth assessment report of the intergovernmental panel on climate change* (pp. 1217–1308). Cambridge University Press.
- CILSS. (2016). *Landscapes of West Africa – a window on a changing world*. Comit Permanent Inter- tats de Lutte contre la S cheresse dans le Sahel. 47914 252nd St, Garretson, SD 57030, United States, U.S. Geological Survey EROS.
- Crouvi, O., Schepanski, K., Amit, R., Gillespie, A. R., & Enzel, Y. (2012). Multiple dust sources in the Sahara Desert: The importance of sand dunes. *Geophysical Research Letters*, *39*(13).
- Dajuma, A., Ogunjobi, K. O., Vogel, H., Knippertz, P., Silué, S., N’Datchoh, E. T., Yoboué, V., & Vogel, B. (2020). Downward cloud venting of the central african biomass burning plume during the West Africa summer monsoon. *Atmospheric Chemistry and Physics*, *20*(9), 5373–5390.

- Dajuma, A., Yahaya, S., Touré, S., Diedhiou, A., Adamou, R., Konaré, A., Sido, M., & Golba, M. (2016). Sensitivity of solar photovoltaic panel efficiency to weather and dust over West Africa: Comparative experimental study between Niamey (Niger) and Abidjan (Côte d'Ivoire). *Computational Water, Energy, and Environmental Engineering*, *5*(4), 123–147.
- Danso, D. K., Anquetin, S., Diedhiou, A., Kouadio, K., & Kobea, A. T. (2020a). Daytime low-level clouds in West Africa – occurrence, associated drivers and shortwave radiation attenuation. *Earth System Dynamics*, *11*(4), 1133–1152.
- Danso, D. K., Anquetin, S., Diedhiou, A., & Adamou, R. (2020b). Cloudiness information services for solar energy management in West Africa. *Atmosphere*, *11*(8), 857.
- Danso, D. K., Anquetin, S., Diedhiou, A., Lavaysse, C., Kobea, A., & Touré, N. E. (2019). Spatio-temporal variability of cloud cover types in West Africa with satellite-based and reanalysis data. *Quarterly Journal of the Royal Meteorological Society*, *145*(725), 3715–3731.
- Danso, D. K., François, B., Hingray, B., & Diedhiou, A. (2021). Assessing hydropower flexibility for integrating solar and wind energy in West Africa using dynamic programming and sensitivity analysis. Illustration with the Akosombo reservoir, Ghana. *Journal of Cleaner Production*, *287*, 125559.
- DeGhetto, K., Gray, J. R., & Kiggundu, M. N. (2016). The African Union's agenda 2063: aspirations, challenges, and opportunities for management research. *Africa Journal of Management*, *2*(1), 93–116.
- Denjean, C., Bourriane, T., Burnet, F., Mallet, M., Maury, N., Colomb, A., Dominutti, P., Brito, J., Dupuy, R., Sellegri, K., et al. (2020). Overview of aerosol optical properties over southern West Africa from DACCIWA aircraft measurements. *Atmospheric Chemistry and Physics*, *20*(8), 4735–4756.
- Déqué, M. (2007). Frequency of precipitation and temperature extremes over France in an anthropogenic scenario: Model results and statistical correction according to observed values. *Global and Planetary Change*, *57*(1-2), 16–26.
- Di Biagio, C., di Sarra, A., Eriksen, P., Ascanius, S. E., Muscari, G., & Holben, B. (2012). Effect of surface albedo, water vapour, and atmospheric aerosols on the cloud-free shortwave radiative budget in the Arctic. *Climate Dynamics*, *39*(3-4), 953–969.
- Dione, C., Lohou, F., Lothon, M., Adler, B., Babić, K., Kalthoff, N., Pedruzco-Bagazgoitia, X., Bezombes, Y., & Gabella, O. (2019). Low-level stratiform clouds and dynamical features observed within the southern West African monsoon. *Atmospheric Chemistry and Physics*, *19*(13), 8979–8997.
- Doelling, D. R., Loeb, N. G., Keyes, D. F., Nordeen, M. L., Morstad, D., Nguyen, C., Wielicki, B. A., Young, D. F., & Sun, M. (2013). Geostationary enhanced

- temporal interpolation for CERES flux products. *Journal of Atmospheric and Oceanic Technology*, 30(6), 1072–1090.
- Dolinar, E. K., Dong, X., Xi, B., Jiang, J. H., & Su, H. (2015). Evaluation of CMIP5 simulated clouds and TOA radiation budgets using NASA satellite observations. *Climate Dynamics*, 44(7-8), 2229–2247.
- Dubey, S., Sarvaiya, J. N., & Seshadri, B. (2013). Temperature dependent photovoltaic (PV) efficiency and its effect on PV production in the world—a review. *Energy Procedia*, 33, 311–321.
- ECMWF. (2010). IFS Documentation CY36R1 - Part IV: Physical Processes [Operational implementation 26 January 2010]. *Iifs documentation cy36r1*. ECMWF. <https://doi.org/10.21957/2loi3bxcz>
- Elum, Z., & Momodu, A. (2017). Climate change mitigation and renewable energy for sustainable development in Nigeria: A discourse approach. *Renewable and Sustainable Energy Reviews*, 76, 72–80.
- Engeland, K., Borga, M., Creutin, J.-D., François, B., Ramos, M.-H., & Vidal, J.-P. (2017). Space-time variability of climate variables and intermittent renewable electricity production—a review. *Renewable and Sustainable Energy Reviews*, 79, 600–617.
- Enongene, K., Abanda, F., Otene, I., Obi, S., & Okafor, C. (2019). The potential of solar photovoltaic systems for residential homes in lagos city of Nigeria. *Journal of environmental management*, 244, 247–256.
- Eshun, M. E., & Amoako-Tuffour, J. (2016). A review of the trends in Ghana s power sector. *Energy, Sustainability and Society*, 6(1), 1–9.
- ESMAP. (2020). *Global photovoltaic power potential by country*. Energy Sector Management Assistance Program. Washington DC, USA, The World Bank Group.
- Evan, A. T., Flamant, C., Gaetani, M., & Guichard, F. (2016). The past, present and future of African dust. *Nature*, 531(7595), 493–495.
- Eyring, V., Bony, S., Meehl, G. A., Senior, C. A., Stevens, B., Stouffer, R. J., & Taylor, K. E. (2016). Overview of the Coupled Model Intercomparison Project Phase 6 (CMIP6) experimental design and organization. *Geoscientific Model Development*, 9(5), 1937–1958.
- Fahad, M. G. R., Saiful Islam, A., Nazari, R., Alfi Hasan, M., Tarekul Islam, G., & Bala, S. K. (2018). Regional changes of precipitation and temperature over Bangladesh using bias-corrected multi-model ensemble projections considering high-emission pathways. *International Journal of Climatology*, 38(4), 1634–1648.
- Ferguson, W. (1985). Integrating crops and livestock in West Africa. *FAO Animal Production and Health Paper*, 41.

- Fiedler, S., Stevens, B., Gidden, M., Smith, S. J., Riahi, K., & Vuuren, D. v. (2019). First forcing estimates from the future CMIP6 scenarios of anthropogenic aerosol optical properties and an associated Twomey effect. *Geoscientific Model Development*, *12*(3), 989–1007.
- Fink, A. H., Christophe, M., Born, K., Br cher, T., Piecha, K., Pohle, S., Schulz, O., & V, E. (2010a). Climate. *Impacts of global change on the hydrological cycle in west and northwest Africa* (pp. 54–58). Springer.
- Fink, A. H., Engel, T., Ermert, V., van der Linden, R., Schneidewind, M., Redl, R., Afiesimama, E., Thiaw, W. M., Yorke, C., Evans, M., et al. (2017). Mean climate and seasonal cycle. *Meteorology of tropical West Africa: The forecasters handbook* (pp. 1–39). Wiley Online Library.
- Fink, A. H., Paeth, H., Ermert, V., Pohle, S., & Diederich, M. (2010b). I-5.1 meteorological processes influencing the weather and climate of Benin.
- Flamant, C., Knippertz, P., Fink, A. H., Akpo, A., Brooks, B., Chiu, C. J., Coe, H., Danuor, S., Evans, M., Jegede, O., et al. (2018). The dynamics–aerosol–chemistry–cloud interactions in West Africa field campaign: Overview and research highlights. *Bulletin of the American Meteorological Society*, *99*(1), 83–104.
- Forbes, R. (2017). *Clouds and precipitation: From models to forecasting. use and interpretation of ECMWF products*. Retrieved January 15, 2019, from <https://confluence.ecmwf.int/display/FUG/Clouds>
- François, B., Hingray, B., Raynaud, D., Borga, M., & Creutin, J. (2016). Increasing climate-related-energy penetration by integrating run-of-the river hydropower to wind/solar mix. *Renewable Energy*, *87*, 686–696.
- Frappart, F., Hiernaux, P., Guichard, F., Mougin, E., Kergoat, L., Arjounin, M., Lavenu, F., Koité, M., Paturel, J.-E., & Lebel, T. (2009). Rainfall regime across the Sahel band in the Gourma region, Mali. *Journal of Hydrology*, *375*(1-2), 128–142.
- Froidurot, S., & Diedhiou, A. (2017). Characteristics of wet and dry spells in the West African monsoon system. *Atmospheric Science Letters*, *18*(3), 125–131.
- Furkan, D., & Mehmet Emin, M. (2010). Critical factors that affecting efficiency of solar cells. *smart grid and renewable energy, 2010*.
- Galle, S., Grippa, M., Peugeot, C., Moussa, I. B., Cappelaere, B., Demarty, J., Mougin, E., Panthou, G., Adjomayi, P., Agbossou, E., et al. (2018). Amma-catch, a critical zone observatory in West Africa monitoring a region in transition. *Vadose Zone Journal*, *17*(1), 1–24.
- Gbobaniyi, E., Sarr, A., Sylla, M. B., Diallo, I., Lennard, C., Dosio, A., Diedhiou, A., Kamga, A., Klutse, N. A. B., Hewitson, B., et al. (2014). Climatology, annual cycle and interannual variability of precipitation and temperature in

- CORDEX simulations over West Africa. *International Journal of Climatology*, 34(7), 2241–2257.
- Gelaro, R., McCarty, W., Suárez, M. J., Todling, R., Molod, A., Takacs, L., Randles, C. A., Darmenov, A., Bosilovich, M. G., Reichle, R., et al. (2017). The modern-era retrospective analysis for research and applications, version 2 (MERRA-2). *Journal of Climate*, 30(14), 5419–5454.
- Geleyn, J., & Hollingsworth, A. (1979). An economical analytical method for the computation of the interaction between scattering and line absorption of radiation. *Beitr. Phys. Atmos.*, 52, 1–16.
- Ghazi, S., & Ip, K. (2014). The effect of weather conditions on the efficiency of PV panels in the southeast of UK. *Renewable energy*, 69, 50–59.
- Giorgetta, M. A., Jungclaus, J., Reick, C. H., Legutke, S., Bader, J., Böttinger, M., Brovkin, V., Crueger, T., Esch, M., Fieg, K., et al. (2013). Climate and carbon cycle changes from 1850 to 2100 in MPI-ESM simulations for the Coupled Model Intercomparison Project phase 5. *Journal of Advances in Modeling Earth Systems*, 5(3), 572–597.
- Gounou, A., Guichard, F., & Couvreux, F. (2012). Observations of diurnal cycles over a West African meridional transect: Pre-monsoon and full-monsoon seasons. *Boundary-layer meteorology*, 144(3), 329–357.
- Goyens, C., Lauwaet, D., Schröder, M., Demuzere, M., & Van Lipzig, N. P. (2012). Tracking mesoscale convective systems in the Sahel: Relation between cloud parameters and precipitation. *International Journal of Climatology*, 32(12), 1921–1934.
- Grabowski, W., Bechtold, P., Cheng, A., Forbes, R., Halliwell, C., Khairoutdinov, M., Lang, S., Nasuno, T., Petch, J., Tao, W.-K., et al. (2006). Daytime convective development over land: A model intercomparison based on LBA observations. *Quarterly Journal of the Royal Meteorological Society: A journal of the atmospheric sciences, applied meteorology and physical oceanography*, 132(615), 317–344.
- Gu, G., & Adler, R. F. (2004). Seasonal evolution and variability associated with the West African monsoon system. *Journal of climate*, 17(17), 3364–3377.
- Gu, Y., Liou, K.-N., Xue, Y., Mechoso, C., Li, W., & Luo, Y. (2006). Climatic effects of different aerosol types in China simulated by the UCLA general circulation model. *Journal of Geophysical Research: Atmospheres*, 111(D15).
- Guan, K., Sultan, B., Biasutti, M., Baron, C., & Lobell, D. B. (2017). Assessing climate adaptation options and uncertainties for cereal systems in West Africa. *Agricultural and Forest Meteorology*, 232, 291–305.

- Hahn, C. J., Rossow, W. B., & Warren, S. G. (2001). ISCCP cloud properties associated with standard cloud types identified in individual surface observations. *Journal of Climate*, *14*(1), 11–28.
- Hannak, L., Knippertz, P., Fink, A. H., Kniffka, A., & Pante, G. (2017). Why do global climate models struggle to represent low-level clouds in the West African summer monsoon? *Journal of Climate*, *30*(5), 1665–1687.
- Hartmann, D. L. (1993). Radiative effects of clouds on earth’s climate. *Aerosol cloud climate interactions* (pp. 151–173). Elsevier.
- Haslett, S. L., Taylor, J. W., Evans, M., Morris, E., Vogel, B., Dajuma, A., Brito, J., Batenburg, A. M., Borrmann, S., Schneider, J., et al. (2019). Remote biomass burning dominates southern West African air pollution during the monsoon. *Atmospheric Chemistry and Physics*, *19*(24), 15217–15234.
- Hayward, D. F., & Oguntoyinbo, J. S. (1987). *Climatology of West Africa*. Rowman & Littlefield.
- Hermann, S., Miketa, A., & Fichaux, N. (2014). *Estimating the renewable energy potential in Africa: a GIS-based approach*. International Renewable Energy Agency. Abu Dhabi, UAE. <https://www.iea.org/reports/global-energy-co2-status-report-2019>
- Hersbach, H., Bell, B., Berrisford, P., Hirahara, S., Horányi, A., Muñoz-Sabater, J., Nicolas, J., Peubey, C., Radu, R., Schepers, D., et al. (2020). The ERA5 global reanalysis. *Quarterly Journal of the Royal Meteorological Society*, *146*(730), 1999–2049.
- Highwood, E. J., & Ryder, C. L. (2014). Radiative effects of dust. *Mineral dust* (pp. 267–286). Springer.
- Hijmans, R. J., & van Etten, J. (2016). Raster: Geographic data analysis and modeling. *R package version*, *2*(8).
- Hill, P. G., Allan, R. P., Chiu, J. C., Bodas-Salcedo, A., & Knippertz, P. (2018). Quantifying the contribution of different cloud types to the radiation budget in southern West Africa. *Journal of Climate*, *31*(13), 5273–5291.
- Hill, P. G., Allan, R. P., Chiu, J. C., & Stein, T. H. (2016). A multisatellite climatology of clouds, radiation, and precipitation in southern West Africa and comparison to climate models. *Journal of Geophysical Research: Atmospheres*, *121*(18), 10–857.
- Iacono, M. J., Delamere, J. S., Mlawer, E. J., Shephard, M. W., Clough, S. A., & Collins, W. D. (2008). Radiative forcing by long-lived greenhouse gases: Calculations with the AER radiative transfer models. *Journal of Geophysical Research: Atmospheres*, *113*(D13).
- IEA. (2019a). *Africa energy outlook 2019*. International Energy Agency (IEA). Paris, France, International Energy Agency.

- IEA. (2019b). *Global Energy and CO2 Status Report 2019*. International Energy Agency (IEA). Paris, France. <https://www.iea.org/reports/global-energy-co2-status-report-2019>
- Ikejamba, E. C., Mpuan, P. B., Schuur, P. C., & Van Hillegersberg, J. (2017). The empirical reality & sustainable management failures of renewable energy projects in Sub-Saharan Africa (part 1 of 2). *Renewable energy*, *102*, 234–240.
- IPCC. (2014). *Climate Change 2014: Mitigation of Climate Change. Contribution of Working Group III to the Fifth Assessment Report of the Intergovernmental Panel on Climate Change*. Intergovernmental Panel on Climate Change. Cambridge, United Kingdom, New York, NY, USA, Cambridge University Press.
- Jakob, C., & Klein, S. A. (2000). A parametrization of the effects of cloud and precipitation overlap for use in general-circulation models. *Quarterly Journal of the Royal Meteorological Society*, *126*(568), 2525–2544.
- Jerez, S., Tobin, I., Vautard, R., Montávez, J. P., López-Romero, J. M., Thais, F., Bartok, B., Christensen, O. B., Colette, A., Déqué, M., et al. (2015). The impact of climate change on photovoltaic power generation in Europe. *Nature communications*, *6*(1), 1–8.
- Johnson, R. H., Rickenbach, T. M., Rutledge, S. A., Ciesielski, P. E., & Schubert, W. H. (1999). Trimodal characteristics of tropical convection. *Journal of climate*, *12*(8), 2397–2418.
- Jose, S., Nair, V. S., & Babu, S. S. (2020). Anthropogenic emissions from South Asia reverses the aerosol indirect effect over the northern Indian Ocean. *Scientific reports*, *10*(1), 1–8.
- Jungclaus, J., Fischer, N., Haak, H., Lohmann, K., Marotzke, J., Matei, D., Mikolajewicz, U., Notz, D., & Von Storch, J. (2013). Characteristics of the ocean simulations in the Max Planck Institute Ocean Model (MPIOM) the ocean component of the MPI-Earth system model. *Journal of Advances in Modeling Earth Systems*, *5*(2), 422–446.
- Jurasz, J., Kies, A., & Zajac, P. (2020). Synergetic operation of photovoltaic and hydro power stations on a day-ahead energy market. *Energy*, *212*, 118686.
- Kalthoff, N., Lohou, F., Brooks, B., Jegede, G., Adler, B., Dione, C., Ajao, A., Amekudzi, L. K., et al. (2018). An overview of the diurnal cycle of the atmospheric boundary layer during the West African monsoon season: Results from the 2016 observational campaign.
- Kampouris, E., Salamalikis, V., & Kazantzidis, A. (2017). The atmospheric water vapor effect on direct normal irradiance under clear skies. *Perspectives on atmospheric sciences* (pp. 1163–1168). Springer.

- Kanteh Sakiliba, S., Sani Hassan, A., Wu, J., Saja Sanneh, E., & Ademi, S. (2015). Assessment of stand-alone residential solar photovoltaic application in Sub-Saharan Africa: a case study of Gambia. *Journal of Renewable Energy*, 2015.
- Karlsson, K.-G., & Johansson, E. (2013). On the optimal method for evaluating cloud products from passive satellite imagery using CALIPSO-CALIOP data: Example investigating the CM-SAF CLARA-A1 dataset. *Atmospheric Measurement Techniques Discussions*, 6(1).
- Kasten, F., & Czeplak, G. (1980). Solar and terrestrial radiation dependent on the amount and type of cloud. *Solar energy*, 24(2), 177–189.
- Kato, S., Rose, F. G., & Charlock, T. P. (2005). Computation of domain-averaged irradiance using satellite-derived cloud properties. *Journal of Atmospheric and Oceanic Technology*, 22(2), 146–164.
- Kawai, H., & Inoue, T. (2006). A simple parameterization scheme for subtropical marine stratocumulus. *SOLA*, 2, 17–20.
- Kessler, E. (1969). On the distribution and continuity of water substance in atmospheric circulations. *On the distribution and continuity of water substance in atmospheric circulations* (pp. 1–84). Springer.
- Kinne, S., O'Donnell, D., Stier, P., Kloster, S., Zhang, K., Schmidt, H., Rast, S., Giorgetta, M., Eck, T. F., & Stevens, B. (2013). MAC-v1: A new global aerosol climatology for climate studies. *Journal of Advances in Modeling Earth Systems*, 5(4), 704–740.
- Klein, C., Heinzeller, D., Bliefernicht, J., & Kunstmann, H. (2015). Variability of West African monsoon patterns generated by a WRF multi-physics ensemble. *Climate Dynamics*, 45(9-10), 2733–2755.
- Klein, C., Nkrumah, F., Taylor, C. M., & Adefisan, E. A. (2020). Seasonality and trends of drivers of mesoscale convective systems in southern West Africa. *Journal of Climate*, 34(1), 71–87.
- Klutse, N. A. B., Ajayi, V. O., Gbobaniyi, E. O., Egbebiyi, T. S., Kouadio, K., Nkrumah, F., Quagraine, K. A., Olusegun, C., Diasso, U., Abiodun, B. J., et al. (2018). Potential impact of 1.5 C and 2 C global warming on consecutive dry and wet days over West Africa. *Environmental Research Letters*, 13(5), 055013.
- Kniffka, A., Knippertz, P., & Fink, A. H. (2019). The role of low-level clouds in the West African monsoon system. *Atmospheric Chemistry & Physics*, 19(3).
- Knippertz, P., Coe, H., Chiu, J. C., Evans, M. J., Fink, A. H., Kalthoff, N., Liousse, C., Mari, C., Allan, R. P., Brooks, B., et al. (2015). The DACCIIWA project: Dynamics–aerosol–chemistry–cloud interactions in West Africa. *Bulletin of the American Meteorological Society*, 96(9), 1451–1460.

- Knippertz, P., Fink, A. H., Schuster, R., Trentmann, J., Schrage, J. M., & Yorke, C. (2011). Ultra-low clouds over the southern West African monsoon region. *Geophysical research letters*, *38*(21).
- Knippertz, P., & Todd, M. C. (2012). Mineral dust aerosols over the sahara: Meteorological controls on emission and transport and implications for modeling. *Reviews of Geophysics*, *50*(1).
- Koren, I., Kaufman, Y. J., Washington, R., Todd, M. C., Rudich, Y., Martins, J. V., & Rosenfeld, D. (2006). The Bodélé depression: a single spot in the Sahara that provides most of the mineral dust to the Amazon forest. *Environmental Research Letters*, *1*(1), 014005.
- Kosmopoulos, P. G., Kazadzis, S., Lagouvardos, K., Kotroni, V., & Bais, A. (2015). Solar energy prediction and verification using operational model forecasts and ground-based solar measurements. *Energy*, *93*, 1918–1930.
- Kosmopoulos, P. G., Kazadzis, S., Taylor, M., Athanasopoulou, E., Speyer, O., Raptis, P. I., Marinou, E., Proestakis, E., Solomos, S., Gerasopoulos, E., et al. (2017). Dust impact on surface solar irradiance assessed with model simulations, satellite observations and ground-based measurements. *Atmospheric Measurement Techniques*, *10*(7), 2435–2453.
- Kucharski, F., Zeng, N., & Kalnay, E. (2013). A further assessment of vegetation feedback on decadal Sahel rainfall variability. *Climate dynamics*, *40*(5-6), 1453–1466.
- Kuwonu, F. (2016). *Harvesting the sun. scaling up solar power to meet Africa s energy needs*. Retrieved May 15, 2020, from <https://www.un.org/africarenewal/magazine/april-2016/harvesting-sun>
- Lampert, B. L. (2008). Comparison of gridded multisatellite rainfall estimates with gridded gauge rainfall over West Africa. *Journal of Applied Meteorology and Climatology*, *47*(1), 185–205.
- Lavaysse, C., Flamant, C., & Janicot, S. (2010). Regional-scale convection patterns during strong and weak phases of the Saharan heat low. *Atmospheric Science Letters*, *11*(4), 255–264.
- Lavaysse, C., Vrac, M., Drobinski, P., Lengaigne, M., & Vischel, T. (2012). Statistical downscaling of the French Mediterranean climate: Assessment for present and projection in an anthropogenic scenario. *Natural Hazards and Earth System Sciences*, *12*(3), 651–670.
- Lebel, T., Parker, D. J., Flamant, C., Boulès, B., Marticorena, B., Mougou, E., Peugeot, C., Diedhiou, A., Haywood, J., Ngamini, J.-B., et al. (2010). The AMMA field campaigns: Multiscale and multidisciplinary observations in the West African region. *Quarterly Journal of the Royal Meteorological Society*, *136*(S1), 8–33.

- Lee, J. T., & Callaway, D. S. (2018). The cost of reliability in decentralized solar power systems in sub-Saharan Africa. *Nature Energy*, *3*(11), 960–968.
- Lee, J., Yang, P., Dessler, A. E., Gao, B.-C., & Platnick, S. (2009). Distribution and radiative forcing of tropical thin cirrus clouds. *Journal of the atmospheric sciences*, *66*(12), 3721–3731.
- Lee, M.-H., Im, E.-S., & Bae, D.-H. (2019). Impact of the spatial variability of daily precipitation on hydrological projections: a comparison of GCM-and RCM-driven cases in the Han River basin, Korea. *Hydrological Processes*, *33*(16), 2240–2257.
- Liou, K.-N. (2002). *An introduction to atmospheric radiation*. Elsevier.
- Liu, X., Penner, J. E., Das, B., Bergmann, D., Rodriguez, J. M., Strahan, S., Wang, M., & Feng, Y. (2007). Uncertainties in global aerosol simulations: Assessment using three meteorological data sets. *Journal of Geophysical Research: Atmospheres*, *112*(D11).
- Liu, Y., Wu, W., Jensen, M., & Toto, T. (2011). Relationship between cloud radiative forcing, cloud fraction and cloud albedo, and new surface-based approach for determining cloud albedo. *Atmospheric Chemistry and Physics*, *11*(14), 7155.
- Loeb, N. G., Doelling, D. R., Wang, H., Su, W., Nguyen, C., Corbett, J. G., Liang, L., Mitrescu, C., Rose, F. G., & Kato, S. (2018). Clouds and the earth's radiant energy system (CERES) energy balanced and filled (EBAF) top-of-atmosphere (TOA) edition-4.0 data product. *Journal of Climate*, *31*(2), 895–918.
- Lohmann, U., & Roeckner, E. (1996). Design and performance of a new cloud microphysics scheme developed for the ECHAM general circulation model. *Climate Dynamics*, *12*(8), 557–572.
- Lohmann, U., Stier, P., Hoose, C., Ferrachat, S., Kloster, S., Roeckner, E., & Zhang, J. (2007). Cloud microphysics and aerosol indirect effects in the global climate model ECHAM5-HAM. *Atmospheric Chemistry and Physics*, *7*(13), 3425–3446.
- Lohou, F., Kalthoff, N., Adler, B., Babić, K., Dione, C., Lothon, M., Pedruzo-Bagazgoitia, X., & Zouzoua, M. (2020). Conceptual model of diurnal cycle of low-level stratiform clouds over southern West Africa. *Atmospheric Chemistry and Physics*, *20*(4), 2263–2275.
- Lott, N., Baldwin, R., & Jones, P. (2001). The FCC integrated surface hourly database, a new resource of global climate data National Climatic Data Center Technical Report No. 2001-01.
- Luiz, E. W., Martins, F. R., Gonçalves, A. R., & Pereira, E. B. (2018). Analysis of intra-day solar irradiance variability in different Brazilian climate zones. *Solar Energy*, *167*, 210–219.

- Mace, G. G., Deng, M., Soden, B., & Zipser, E. (2006). Association of tropical cirrus in the 10–15-km layer with deep convective sources: An observational study combining millimeter radar data and satellite-derived trajectories. *Journal of the atmospheric sciences*, *63*(2), 480–503.
- Mace, G. G., Vane, D., Stephens, G., & Reinke, D. (2007). Level 2 radar-lidar GEO-PROF product version 1.0 process description and interface control document. *JPL, Pasadena, USA*, 1–20.
- Mace, G. G., Zhang, Q., Vaughan, M., Marchand, R., Stephens, G., Treppe, C., & Winker, D. (2009). A description of hydrometeor layer occurrence statistics derived from the first year of merged Cloudsat and CALIPSO data. *Journal of Geophysical Research: Atmospheres*, *114*(D8).
- Madec, G., Bourdallé-Badie, R., Bouttier, P.-A., Bricaud, C., Bruciaferri, D., Calvert, D., Chanut, J., Clementi, E., Coward, A., Delrosso, D., et al. (2017). NEMO ocean engine. *Institut Pierre-Simon Laplace (IPSL), France*.
- Mallet, M., Tulet, P., Serça, D., Solmon, F., Dubovik, O., Pelon, J., Pont, V., & Thouron, O. (2009). Impact of dust aerosols on the radiative budget, surface heat fluxes, heating rate profiles and convective activity over West Africa during march 2006.
- Maranan, M., Fink, A. H., & Knippertz, P. (2018). Rainfall types over southern West Africa: Objective identification, climatology and synoptic environment. *Quarterly Journal of the Royal Meteorological Society*, *144*(714), 1628–1648.
- Marsham, J. H., Dixon, N. S., Garcia-Carreras, L., Lister, G. M., Parker, D. J., Knippertz, P., & Birch, C. E. (2013). The role of moist convection in the West African monsoon system: Insights from continental-scale convection-permitting simulations. *Geophysical Research Letters*, *40*(9), 1843–1849.
- Mas’ud, A. A., Wirba, A. V., Muhammad-Sukki, F., Albarracín, R., Abu-Bakar, S. H., Munir, A. B., & Bani, N. A. (2016). A review on the recent progress made on solar photovoltaic in selected countries of sub-Saharan Africa. *Renewable and sustainable energy reviews*, *62*, 441–452.
- Mathon, V., Diedhiou, A., & Laurent, H. (2002b). Relationship between easterly waves and mesoscale convective systems over the Sahel. *Geophysical research letters*, *29*(8), 57–1.
- Mathon, V., Laurent, H., & Lebel, T. (2002a). Mesoscale convective system rainfall in the Sahel. *Journal of applied meteorology*, *41*(11), 1081–1092.
- McPherson, M., Sotiropoulos-Michalakakos, T., Harvey, L., & Karney, B. (2017). An open-access web-based tool to access global, hourly wind and solar PV generation time-series derived from the MERRA reanalysis dataset. *Energies*, *10*(7), 1007.

- McTigue, J. D., Wendt, D., Kitz, K., Gunderson, J., Kincaid, N., & Zhu, G. (2020). Assessing geothermal/solar hybridization—integrating a solar thermal topping cycle into a geothermal bottoming cycle with energy storage. *Applied Thermal Engineering*, *171*, 115121.
- Meinshausen, M., Nicholls, Z. R., Lewis, J., Gidden, M. J., Vogel, E., Freund, M., Beyerle, U., Gessner, C., Nauels, A., Bauer, N., et al. (2020). The shared socio-economic pathway (SSP) greenhouse gas concentrations and their extensions to 2500. *Geoscientific Model Development*, *13*(8), 3571–3605.
- Mertens, K. (2018). *Photovoltaics: Fundamentals, technology, and practice*. John Wiley & Sons.
- Middleton, N., & Goudie, A. (2001). Saharan dust: Sources and trajectories. *Transactions of the Institute of British Geographers*, *26*(2), 165–181.
- Miller, M. A., & Slingo, A. (2007). The ARM Mobile Facility and its first international deployment: Measuring radiative flux divergence in West Africa. *Bulletin of the American Meteorological Society*, *88*(8), 1229–1244.
- Minnis, P., Hong, G., Sun-Mack, S., Smith Jr, W. L., Chen, Y., & Miller, S. D. (2016). Estimating nocturnal opaque ice cloud optical depth from MODIS multispectral infrared radiances using a neural network method. *Journal of Geophysical Research: Atmospheres*, *121*(9), 4907–4932.
- Minnis, P., Sun-Mack, S., Young, D. F., Heck, P. W., Garber, D. P., Chen, Y., Spangenberg, D. A., Arduini, R. F., Trepte, Q. Z., Smith, W. L., et al. (2011). CERES Edition-2 cloud property retrievals using TRMM VIRS and Terra and Aqua MODIS data part i: Algorithms. *IEEE Transactions on Geoscience and Remote Sensing*, *49*(11), 4374–4400.
- Moner-Girona, M., Bódis, K., Korgo, B., Huld, T., Kougiyas, I., Pinedo-Pascua, I., Monforti-Ferrario, F., & Szabó, S. (2017). Mapping the least-cost option for rural electrification in Burkina Faso. *European Commission Joint Research Centre*.
- Moner-Girona, M., Solano-Peralta, M., Lazopoulou, M., Ackom, E., Vallve, X., & Szabó, S. (2018). Electrification of Sub-Saharan Africa through PV/hybrid mini-grids: Reducing the gap between current business models and on-site experience. *Renewable and Sustainable Energy Reviews*, *91*, 1148–1161.
- Monerie, P.-A., Sanchez-Gomez, E., Gaetani, M., Mohino, E., & Dong, B. (2020). Future evolution of the Sahel precipitation zonal contrast in CESM1. *Climate Dynamics*, *55*(9), 2801–2821.
- Morcrette, J., Barker, H. W., Cole, J., Iacono, M. J., & Pincus, R. (2008). Impact of a new radiation package, McRad, in the ECMWF Integrated Forecasting System. *Monthly weather review*, *136*(12), 4773–4798.

- MPEER. (2014). *Rapport d'activités MPEER 2018*. Ministre du Pétrole, de l'Énergie et des E. R. Abidjan, Côte d'Ivoire. http://www.mpeder.ci/uploads/documents/rapports/RAPPORT_D_ACTIVITES_MPEER_2018.pdf
- Mueller, R., Pfeifroth, U., & Traeger-Chatterjee, C. (2015). Towards optimal aerosol information for the retrieval of solar surface radiation using Heliosat. *Atmosphere*, *6*(7), 863–878.
- Müller, W. A., Jungclaus, J. H., Mauritsen, T., Baehr, J., Bittner, M., Budich, R., Bunzel, F., Esch, M., Ghosh, R., Haak, H., et al. (2018). A Higher-resolution Version of the Max Planck Institute Earth System Model (MPI-ESM1.2-HR). *Journal of Advances in Modeling Earth Systems*, *10*(7), 1383–1413.
- Nair, V. S., Babu, S. S., Manoj, M., Moorthy, K. K., & Chin, M. (2017). Direct radiative effects of aerosols over South Asia from observations and modeling. *Climate Dynamics*, *49*(4), 1411–1428.
- Navarro-Racines, C., Tarapues, J., Thornton, P., Jarvis, A., & Ramirez-Villegas, J. (2020). High-resolution and bias-corrected CMIP5 projections for climate change impact assessments. *Scientific data*, *7*(1), 1–14.
- Nicholson, S. E. (2009). A revised picture of the structure of the monsoon and land ITCZ over West Africa. *Climate Dynamics*, *32*(7-8), 1155–1171.
- Nicholson, S. E. (2013). The West African Sahel: A review of recent studies on the rainfall regime and its interannual variability. *International Scholarly Research Notices*, *2013*.
- Nicholson, S. E. (2018). The ITCZ and the seasonal cycle over equatorial Africa. *Bulletin of the American Meteorological Society*, *99*(2), 337–348.
- Nordeng, T.-E. (1994). Extended versions of the convective parametrization scheme at ECMWF and their impact on the mean and transient activity of the model in the tropics. (206), 41. <https://doi.org/10.21957/e34xwhysw>
- Obi, M., & Bass, R. (2016). Trends and challenges of grid-connected photovoltaic systems—a review. *Renewable and Sustainable Energy Reviews*, *58*, 1082–1094.
- Obregón, M., Costa, M. J., Serrano, A., & Silva, A. M. (2015). Effect of water vapor in the SW and LW downward irradiance at the surface during a day with low aerosol load. *IOP Conference Series: Earth and Environmental Science*, *28*(1), 012009.
- Odou, O. D. T., Bhandari, R., & Adamou, R. (2020). Hybrid off-grid renewable power system for sustainable rural electrification in Benin. *Renewable Energy*, *145*, 1266–1279.
- Ohunakin, O. S., Adaramola, M. S., Oyewola, O. M., Matthew, O. J., & Fagbenle, R. O. (2015). The effect of climate change on solar radiation in Nigeria. *Solar Energy*, *116*, 272–286.

- Omubo-Pepple, V., Israel-Cookey, C., & Alaminokuma, G. (2009). Effects of temperature, solar flux and relative humidity on the efficient conversion of solar energy to electricity. *European Journal of Scientific Research*, *35*(2), 173–180.
- O’Neill, B. C., Tebaldi, C., Vuuren, D. P. v., Eyring, V., Friedlingstein, P., Hurtt, G., Knutti, R., Kriegler, E., Lamarque, J.-F., Lowe, J., et al. (2016). The scenario model intercomparison project (ScenarioMIP) for CMIP6. *Geoscientific Model Development*, *9*(9), 3461–3482.
- Oreopoulos, L., & Barker, H. W. (1999). Accounting for subgrid-scale cloud variability in a multi-layer 1D solar radiative transfer algorithm. *Quarterly Journal of the Royal Meteorological Society*, *125*(553), 301–330.
- Ouedraogo, N. S. (2017). Modeling sustainable long-term electricity supply-demand in Africa. *Applied Energy*, *190*, 1047–1067.
- O Neill, B. C., Kriegler, E., Riahi, K., Ebi, K. L., Hallegatte, S., Carter, T. R., Mathur, R., & van Vuuren, D. P. (2014). A new scenario framework for climate change research: The concept of shared socioeconomic pathways. *Climatic change*, *122*(3), 387–400.
- Palacios-Peña, L., Montávez, J. P., López-Romero, J. M., Jerez, S., Gómez-Navarro, J. J., Lorente-Plazas, R., Ruiz, J., & Jiménez-Guerrero, P. (2020). Added value of aerosol-cloud interactions for representing aerosol optical depth in an online coupled climate-chemistry model over Europe. *Atmosphere*, *11*(4), 360.
- Pantillon, F., Knippertz, P., Marsham, J. H., Panitz, H.-J., & Bischoff-Gauss, I. (2016). Modeling haboob dust storms in large-scale weather and climate models. *Journal of Geophysical Research: Atmospheres*, *121*(5), 2090–2109.
- Papadimas, C., Hatzianastassiou, N., Matsoukas, C., Kanakidou, M., Mihalopoulos, N., & Vardavas, I. (2012). The direct effect of aerosols on solar radiation over the broader Mediterranean basin. *Atmospheric Chemistry and Physics*, *12*(15), 7165–7185.
- Parker, D., Burton, R., Diongue-Niang, A., Ellis, R., Felton, M., Taylor, C., Thorncroft, C., Bessemoulin, P., & Tompkins, A. (2005). The diurnal cycle of the West African monsoon circulation. *Quarterly Journal of the Royal Meteorological Society: A journal of the atmospheric sciences, applied meteorology and physical oceanography*, *131*(611), 2839–2860.
- Parker, D. J., & Diop-Kane, M. (2017). *Meteorology of tropical West Africa: The forecasters’ handbook*. John Wiley & Sons.
- Pedruzo-Bagazgoitia, X., De Roode, S. R., Adler, B., Babić, K., Dione, C., Kalthoff, N., Lohou, F., Lothon, M., & Vilà-Guerau de Arellano, J. (2020). The diur-

- nal stratocumulus-to-cumulus transition over land in southern West Africa. *Atmospheric Chemistry and Physics*, 20(5), 2735–2754.
- Perpiñan, O., Lorenzo, E., & Castro, M. (2007). On the calculation of energy produced by a PV grid-connected system. *Progress in Photovoltaics: research and applications*, 15(3), 265–274.
- Pfeifroth, U., Kothe, S., Müller, R., Trentmann, J., Hollmann, R., Fuchs, P., & Werscheck, M. (2019). Surface Radiation Data Set–Heliosat (SARAH)–Edition 2, Satellite Application Facility on Climate Monitoring.
- Pfeifroth, U., Sanchez-Lorenzo, A., Manara, V., Trentmann, J., & Hollmann, R. (2018). Trends and variability of surface solar radiation in Europe based on surface-and satellite-based data records. *Journal of Geophysical Research: Atmospheres*, 123(3), 1735–1754.
- Piani, C., Haerter, J., & Coppola, E. (2010). Statistical bias correction for daily precipitation in regional climate models over Europe. *Theoretical and Applied Climatology*, 99(1), 187–192.
- Pierce, D. (2012). ncd4: Interface to Unidata netCDF (version 4 or earlier) format data files. *R package*, URL <http://CRAN.R-project.org/package=ncdf4>.
- Pincus, R., Barker, H. W., & Morcrette, J.-J. (2003). A fast, flexible, approximate technique for computing radiative transfer in inhomogeneous cloud fields. *Journal of Geophysical Research: Atmospheres*, 108(D13).
- Pyrina, M., Hatzianastassiou, N., Matsoukas, C., Fotiadi, A., Papadimas, C., Pavlakis, K., & Vardavas, I. (2013). Cloud effects on the solar and thermal radiation budgets of the Mediterranean basin. *Atmospheric Research*, 152, 14–28.
- Qian, Y., Wang, W., Leung, L. R., & Kaiser, D. P. (2007). Variability of solar radiation under cloud-free skies in China: The role of aerosols. *Geophysical Research Letters*, 34(12).
- Quaas, J. (2012). Evaluating the critical relative humidity as a measure of subgrid-scale variability of humidity in general circulation model cloud cover parameterizations using satellite data. *Journal of Geophysical Research: Atmospheres*, 117(D9).
- Radel, G., Shine, K. P., & Ptashnik, I. V. (2015). Global radiative and climate effect of the water vapour continuum at visible and near-infrared wavelengths. *Quarterly Journal of the Royal Meteorological Society*, 141(688), 727–738.
- Rahman, M., Hasanuzzaman, M., & Rahim, N. A. (2015). Effects of various parameters on PV-module power and efficiency. *Energy Conversion and Management*, 103, 348–358.
- Ramachandran, S. (2018). *Atmospheric aerosols: Characteristics and radiative effects*. CRC Press.

- Ramanathan, V., Cess, R., Harrison, E., Minnis, P., Barkstrom, B., Ahmad, E., & Hartmann, D. (1989). Cloud-radiative forcing and climate: Results from the Earth Radiation Budget Experiment. *Science*, *243*(4887), 57–63.
- Redelsperger, J.-L., Thorncroft, C. D., Diedhiou, A., Lebel, T., Parker, D. J., & Polcher, J. (2006). African Monsoon Multidisciplinary Analysis: An international research project and field campaign. *Bulletin of the American Meteorological Society*, *87*(12), 1739–1746.
- Reichler, T., & Kim, J. (2008). Uncertainties in the climate mean state of global observations, reanalyses, and the GFDL climate model. *Journal of Geophysical Research: Atmospheres*, *113*(D5).
- Reick, C., Raddatz, T., Brovkin, V., & Gayler, V. (2013). Representation of natural and anthropogenic land cover change in MPI-ESM. *Journal of Advances in Modeling Earth Systems*, *5*(3), 459–482.
- Riahi, K., Van Vuuren, D. P., Kriegler, E., Edmonds, J., O'Neill, B. C., Fujimori, S., Bauer, N., Calvin, K., Dellink, R., Fricko, O., et al. (2017). The shared socioeconomic pathways and their energy, land use, and greenhouse gas emissions implications: An overview. *Global Environmental Change*, *42*, 153–168.
- Ritchie, H. (2020). *Sector by sector: Where do global greenhouse gas emissions come from?* Retrieved December 2, 2020, from <https://ourworldindata.org/ghg-emissions-by-sector>
- Ritchie, H., & Roser, M. (2017). CO2 and greenhouse gas emissions. *Our world in data*.
- Rogelj, J., Den Elzen, M., Höhne, N., Fransen, T., Fekete, H., Winkler, H., Schaeffer, R., Sha, F., Riahi, K., & Meinshausen, M. (2016). Paris Agreement climate proposals need a boost to keep warming well below 2 C. *Nature*, *534*(7609), 631–639.
- Rogelj, J., Shindell, D., Jiang, K., Fifita, S., Forster, P., Ginzburg, V., Handa, C., Kheshgi, H., Kobayashi, S., Kriegler, E., et al. (2018). Mitigation pathways compatible with 1.5 C in the context of sustainable development.
- Rotstayn, L. D., Collier, M. A., Dix, M. R., Feng, Y., Gordon, H. B., O'Farrell, S. P., Smith, I. N., & Syktus, J. (2010). Improved simulation of Australian climate and ENSO-related rainfall variability in a global climate model with an interactive aerosol treatment. *International Journal of Climatology: A Journal of the Royal Meteorological Society*, *30*(7), 1067–1088.
- Rousset, C., Vancoppenolle, M., Madec, G., Fichefet, T., Flavoni, S., Barthélemy, A., Benschila, R., Chanut, J., Lévy, C., Masson, S., et al. (2015). The Louvain-La-Neuve sea ice model LIM3. 6: global and regional capabilities. *Geoscientific Model Development*, *8*(10), 2991–3005.

- Rutan, D. A., Kato, S., Doelling, D. R., Rose, F. G., Nguyen, L. T., Caldwell, T. E., & Loeb, N. G. (2015). CERES synoptic product: Methodology and validation of surface radiant flux. *Journal of Atmospheric and Oceanic Technology*, *32*(6), 1121–1143.
- Sarr, A. (2017). Multi-scale characteristics of precipitation and temperature over West Africa using SMHI-RCA driven by GCMs under RCP8.5. *American Journal of Climate Change*, *6*(3), 455–486.
- Sassen, K., Wang, Z., & Liu, D. (2009). Cirrus clouds and deep convection in the tropics: Insights from CALIPSO and CloudSat. *Journal of Geophysical Research: Atmospheres*, *114*(D4).
- Sawadogo, W., Abiodun, B. J., & Okogbue, E. C. (2020). Impacts of global warming on photovoltaic power generation over West Africa. *Renewable Energy*, *151*, 263–277.
- Schrage, J. M., & Fink, A. H. (2012). Nocturnal continental low-level stratus over tropical West Africa: Observations and possible mechanisms controlling its onset. *Monthly weather review*, *140*(6), 1794–1809.
- Schulzweida, U., Kornblueh, L., & Quast, R. (2006). CDO user's guide. *Climate data operators, Version*, *1*(6), 205–209.
- Schumacher, C., & Houze Jr, R. A. (2006). Stratiform precipitation production over sub-Saharan Africa and the tropical East Atlantic as observed by TRMM. *Quarterly Journal of the Royal Meteorological Society: A journal of the atmospheric sciences, applied meteorology and physical oceanography*, *132*(620), 2235–2255.
- Schuster, R., Fink, A. H., & Knippertz, P. (2013). Formation and maintenance of nocturnal low-level stratus over the southern West African monsoon region during AMMA 2006. *Journal of the atmospheric sciences*, *70*(8), 2337–2355.
- Semmler, T., Danilov, S., Gierz, P., Goessling, H. F., Hegewald, J., Hinrichs, C., Koldunov, N., Khosravi, N., Mu, L., Rackow, T., et al. (2020). Simulations for CMIP6 with the AWI climate model AWI-CM-1-1. *Journal of Advances in Modeling Earth Systems*, *12*(9), e2019MS002009.
- Sengupta, M., Clothiaux, E. E., Ackerman, T. P., Kato, S., & Min, Q. (2003). Importance of accurate liquid water path for estimation of solar radiation in warm boundary layer clouds: An observational study. *Journal of climate*, *16*(18), 2997–3009.
- Shea, Y. L., Wielicki, B. A., Sun-Mack, S., & Minnis, P. (2017). Quantifying the dependence of satellite cloud retrievals on instrument uncertainty. *Journal of climate*, *30*(17), 6959–6976.

- Shivashankar, S., Mekhilef, S., Mokhlis, H., & Karimi, M. (2016). Mitigating methods of power fluctuation of photovoltaic (PV) sources—a review. *Renewable and Sustainable Energy Reviews*, *59*, 1170–1184.
- Soares, P. M., Brito, M. C., & Careto, J. A. (2019). Persistence of the high solar potential in Africa in a changing climate. *Environmental Research Letters*, *14*(12), 124036.
- Soden, B. J., & Held, I. M. (2006). An assessment of climate feedbacks in coupled ocean–atmosphere models. *Journal of climate*, *19*(14), 3354–3360.
- Söhne, N., Chaboureau, J.-P., & Guichard, F. (2008). Verification of cloud cover forecast with satellite observation over West Africa. *Monthly Weather Review*, *136*(11), 4421–4434.
- Solmon, F., Elguindi, N., & Mallet, M. (2012). Radiative and climatic effects of dust over West Africa, as simulated by a regional climate model. *Climate Research*, *52*, 97–113.
- Stanelle, T., Vogel, B., Vogel, H., Bäumer, D., & Kottmeier, C. (2010). Feedback between dust particles and atmospheric processes over West Africa in March 2006 and June 2007. *Atmospheric Chemistry & Physics Discussions*, *10*(3).
- Stein, T. H., Parker, D., Delanoë, J., Dixon, N., Hogan, R. J., Knippertz, P., Maidment, R. I., & Marsham, J. (2011). The vertical cloud structure of the West African monsoon: A 4 year climatology using CloudSat and CALIPSO. *Journal of Geophysical Research: Atmospheres*, *116*(D22).
- Stephens, G. L., Vane, D. G., Tanelli, S., Im, E., Durden, S., Rokey, M., Reinke, D., Partain, P., Mace, G. G., Austin, R., et al. (2008). Cloudsat mission: Performance and early science after the first year of operation. *Journal of Geophysical Research: Atmospheres*, *113*(D8).
- Stephens, G. L., Winker, D., Pelon, J., Trepte, C., Vane, D., Yuhas, C., L'ecuyer, T., & Lebsock, M. (2018). CloudSat and CALIPSO within the A-Train: Ten years of actively observing the earth system. *Bulletin of the American Meteorological Society*, *99*(3), 569–581.
- Sterl, S., Liersch, S., Koch, H., Van Lipzig, N. P., & Thiery, W. (2018). A new approach for assessing synergies of solar and wind power: Implications for West Africa. *Environmental Research Letters*, *13*(9), 094009.
- Stevens, B., Giorgetta, M., Esch, M., Mauritsen, T., Crueger, T., Rast, S., Salzmann, M., Schmidt, H., Bader, J., Block, K., et al. (2013). Atmospheric component of the MPI-M Earth system model: ECHAM6. *Journal of Advances in Modeling Earth Systems*, *5*(2), 146–172.
- Stocker, T. F., Qin, D., Plattner, G., Tignor, M. M., Allen, S. K., Boschung, J., Nauels, A., Xia, Y., Bex, V., & Midgley, P. M. (2014). *Climate Change 2013: The physical science basis. Contribution of working group I to the fifth*

- assessment report of IPCC the intergovernmental panel on climate change.* Cambridge, United Kingdom, Cambridge University Press.
- Storer, R. L., & Van den Heever, S. C. (2013). Microphysical processes evident in aerosol forcing of tropical deep convective clouds. *Journal of the atmospheric sciences*, *70*(2), 430–446.
- Sulaiman, S. A., Hussain, H. H., Leh, N., Razali, M. S., et al. (2011). Effects of dust on the performance of PV panels. *World Academy of Science, Engineering and Technology*, *58*(2011), 588–593.
- Sultan, B., & Janicot, S. (2000). Abrupt shift of the ITCZ over West Africa and intra-seasonal variability. *Geophysical Research Letters*, *27*(20), 3353–3356.
- Sultan, B., & Janicot, S. (2003). The West African monsoon dynamics. part ii: The preonset and onset of the summer monsoon. *Journal of climate*, *16*(21), 3407–3427.
- Sultan, B., Janicot, S., & Diedhiou, A. (2003). The West African monsoon dynamics. part i: Documentation of intraseasonal variability. *Journal of Climate*, *16*(21), 3389–3406.
- Sun, W., Videen, G., Kato, S., Lin, B., Lukashin, C., & Hu, Y. (2011). A study of subvisual clouds and their radiation effect with a synergy of CERES, MODIS, CALIPSO, and AIRS data. *Journal of Geophysical Research: Atmospheres*, *116*(D22).
- Sundqvist, H. (1978). A parameterization scheme for non-convective condensation including prediction of cloud water content. *Quarterly Journal of the Royal Meteorological Society*, *104*(441), 677–690.
- Sundqvist, H., Berge, E., & KRISTJANSSON, J. (1989). Condensation and cloud parameterization studies with a mesoscale numerical weather prediction model. *Monthly Weather Review*, *117*(8), 1641–1657.
- Supit, I., & Van Kappel, R. (1998). A simple method to estimate global radiation. *Solar Energy*, *63*(3), 147–160.
- Sylla, M., Giorgi, F., Ruti, P., Calmanti, S., & Dell’Aquila, A. (2011). The impact of deep convection on the West African summer monsoon climate: A regional climate model sensitivity study. *Quarterly Journal of the Royal Meteorological Society*, *137*(659), 1417–1430.
- Tan, J., Oreopoulos, L., Jakob, C., & Jin, D. (2018). Evaluating rainfall errors in global climate models through cloud regimes. *Climate Dynamics*, *50*(9), 3301–3314.
- Tanaka, T. Y., Orito, K., Sekiyama, T. T., Shibata, K., Chiba, M., & Tanaka, H. (2003). MASINGAR, a global tropospheric aerosol chemical transport model coupled with MRI/JMA98 GCM: Model description. *Papers in Meteorology and Geophysics*, *53*(4), 119–138.

- Taylor, K. E. (2001). Summarizing multiple aspects of model performance in a single diagram. *Journal of Geophysical Research: Atmospheres*, *106*(D7), 7183–7192.
- Tegen, I., Hollrig, P., Chin, M., Fung, I., Jacob, D., & Penner, J. (1997). Contribution of different aerosol species to the global aerosol extinction optical thickness: Estimates from model results. *Journal of Geophysical Research: Atmospheres*, *102*(D20), 23895–23915.
- Thorncroft, C. D., Nguyen, H., Zhang, C., & Peyrillé, P. (2011). Annual cycle of the West African monsoon: Regional circulations and associated water vapour transport. *Quarterly Journal of the Royal Meteorological Society*, *137*(654), 129–147.
- Tiedtke, M. (1993). Representation of clouds in large-scale models. *Monthly Weather Review*, *121*(11), 3040–3061.
- Tiedtke, M. (1989). A comprehensive mass flux scheme for cumulus parameterization in large-scale models. *Monthly weather review*, *117*(8), 1779–1800.
- Tiyou, T. (2017). *The five biggest solar markets in Africa*. Retrieved December 8, 2020, from <https://blogs.lse.ac.uk/africaatlse/2017/01/18/the-five-biggest-solar-markets-in-africa/>
- Tsujino, H., Nakano, H., Sakamoto, K., Urakawa, S., Hirabara, M., Ishizaki, H., & Yamanaka, G. (2017). Reference manual for the Meteorological Research Institute Community Ocean Model version 4 (MRI. COMv4). *Technical Reports of the Meteorological Research Institute*, *80*, 306.
- Turner, D. D., Vogelmann, A., Austin, R. T., Barnard, J. C., Cady-Pereira, K., Chiu, J. C., Clough, S. A., Flynn, C., Khaiyer, M. M., Liljegren, J., et al. (2007). Thin liquid water clouds: Their importance and our challenge. *Bulletin of the American Meteorological Society*, *88*(2), 177–190.
- UNFCCC. (2015). Paris agreement. *Report of the Conference of the Parties to the United Nations Framework Convention on Climate Change (21st Session, 2015: Paris)*, *4*, 2017. <http://unfccc.int/resource/docs/2015/cop21/eng/109.pdf>
- van den Hurk, B. J., Viterbo, P., Beljaars, A., & Betts, A. (2000). Offline validation of the ERA40 surface scheme.
- van der Linden, R., Fink, A. H., & Redl, R. (2015). Satellite-based climatology of low-level continental clouds in southern West Africa during the summer monsoon season. *Journal of Geophysical Research: Atmospheres*, *120*(3), 1186–1201.
- van der Linden, R., Knippertz, P., Fink, A. H., Ingleby, B., Maranan, M., & Benedetti, A. (2020). The influence of dacciwa radiosonde data on the quality of ecmwf analyses and forecasts over southern west africa. *Quarterly Journal of the Royal Meteorological Society*, *146*(729), 1719–1739.

- Vizy, E. K., & Cook, K. H. (2019). Understanding the summertime diurnal cycle of precipitation over sub-saharan West Africa: Regions with daytime rainfall peaks in the absence of significant topographic features. *Climate Dynamics*, *52*(5-6), 2903–2922.
- Wade, K., & Jennings, M. (2016). The impact of climate change on the global economy. *Schroders Talking Point*.
- Wang, K., Dickinson, R. E., Wild, M., & Liang, S. (2012). Atmospheric impacts on climatic variability of surface incident solar radiation. *Atmospheric Chemistry & Physics Discussions*, *10*, 9581–9592.
- Wang, Q., Danilov, S., Sidorenko, D., Timmermann, R., Wekerle, C., Wang, X., Jung, T., & Schröter, J. (2014). The Finite Element Sea Ice-Ocean Model (FESOM) v. 1.4: formulation of an ocean general circulation model. *Geoscientific Model Development*, *7*(2), 663–693.
- West, M. (1997). Time series decomposition. *Biometrika*, *84*(2), 489–494.
- Wickham, H. (2016). Scales: Scale functions for visualization. *R package version 0.4.0*, URL <https://CRAN.R-project.org/package=scales>.
- Wielicki, B. A., Barkstrom, B. R., Harrison, E. F., Lee III, R. B., Smith, G. L., & Cooper, J. E. (1996). Clouds and the Earth’s Radiant Energy System (CERES): An earth observing system experiment. *Bulletin of the American Meteorological Society*, *77*(5), 853–868.
- Wielicki, B. A., Cess, R. D., King, M. D., Randall, D. A., & Harrison, E. F. (1995). Mission to planet earth: Role of clouds and radiation in climate. *Bulletin of the American Meteorological Society*, 2125–2153.
- Wilberforce, T., Baroutaji, A., Soudan, B., Al-Alami, A. H., & Olabi, A. G. (2019). Outlook of carbon capture technology and challenges. *Science of the Total Environment*, *657*, 56–72.
- Winker, D. M., Vaughan, M. A., Omar, A., Hu, Y., Powell, K. A., Liu, Z., Hunt, W. H., & Young, S. A. (2009). Overview of the CALIPSO mission and CALIOP data processing algorithms. *Journal of Atmospheric and Oceanic Technology*, *26*(11), 2310–2323.
- WorldBank. (2019). *This is what it’s all about: Boosting renewable energy in Africa*. Retrieved February 8, 2020, from <https://www.worldbank.org/en/news/feature/2019/02/26/this-is-what-its-all-about-boosting-renewable-energy-in-africa>
- Wyser, K., Noije, T. v., Yang, S., Hardenberg, J. v., O’Donnell, D., & Döscher, R. (2020). On the increased climate sensitivity in the EC-Earth model from CMIP5 to CMIP6. *Geoscientific Model Development*, *13*(8), 3465–3474.

- Yamasoe, M. A., Do Rosário, N., & Barros, K. M. d. (2017). Downward solar global irradiance at the surface in São Paulo city The climatological effects of aerosol and clouds. *Journal of Geophysical Research: Atmospheres*, *122*(1), 391–404.
- Yang, G.-Y., & Slingo, J. (2001). The diurnal cycle in the tropics. *Monthly Weather Review*, *129*(4), 784–801.
- Yoshimura, H., Mizuta, R., & Murakami, H. (2015). A spectral cumulus parameterization scheme interpolating between two convective updrafts with semi-lagrangian calculation of transport by compensatory subsidence. *Monthly Weather Review*, *143*(2), 597–621.
- Yukimoto, S., Kawai, H., Koshiro, T., Oshima, N., Yoshida, K., Urakawa, S., Tsujino, H., Deushi, M., Tanaka, T., Hosaka, M., et al. (2019). The Meteorological Research Institute Earth System Model version 2.0, MRI-ESM2. 0: Description and basic evaluation of the physical component. *Journal of the Meteorological Society of Japan. Ser. II*.
- Yushchenko, A., De Bono, A., Chatenoux, B., Patel, M. K., & Ray, N. (2018). GIS-based assessment of photovoltaic (PV) and concentrated solar power (CSP) generation potential in West Africa. *Renewable and Sustainable Energy Reviews*, *81*, 2088–2103.
- Zender, C. S. (2008). Analysis of self-describing gridded geoscience data with netcdf operators (NCO). *Environmental Modelling & Software*, *23*(10-11), 1338–1342.
- Zhang, H., Qiao, X., Shen, Y., & Wang, M. (2015). Effect of temperature on the efficiency of organometallic perovskite solar cells. *Journal of energy chemistry*, *24*(6), 729–735.
- Zhang, H., Wang, Z., Wang, Z., Liu, Q., Gong, S., Zhang, X., Shen, Z., Lu, P., Wei, X., Che, H., et al. (2012). Simulation of direct radiative forcing of aerosols and their effects on East Asian climate using an interactive AGCM-aerosol coupled system. *Climate Dynamics*, *38*(7-8), 1675–1693.
- Zhang, M., Wang, Y., Ma, Y., Wang, L., Gong, W., & Liu, B. (2018). Spatial distribution and temporal variation of aerosol optical depth and radiative effect in South China and its adjacent area. *Atmospheric Environment*, *188*, 120–128.
- Zouzoua, M., Lohou, F., Assamoi, P., Lothon, M., Yoboue, V., Dione, C., Kalthoff, N., Adler, B., Babić, K., & Pedruzo-Bagazgoitia, X. (2020). Breakup of nocturnal low-level stratiform clouds during southern West African monsoon season. *Atmospheric Chemistry and Physics Discussions*, 1–39.